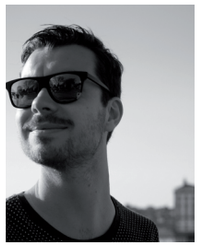

I would like to thank everyone that contributed to this thesis. Either in a scientific way or, foremost, by creating a great atmosphere in the lab.

Furthermore I want to thank everyone that supported me through the tougher times of a PhD. Without all of you, this wouldn't have been possible.

May, 2016

UNIVERSITEIT GENT

Fluorescent Labeling of DNA: Strategies, Pitfalls and Necessity for Fluorescence Microscopy Investigations of Gene Therapy, Koen Rombouts

Fluorescent Labeling of DNA: Strategies, Pitfalls and Necessity for Fluorescence Microscopy Investigations of Gene Therapy

Koen Rombouts

FLUORESCENT LABELING OF DNA: STRATEGIES, PITFALLS AND NECESSITY FOR FLUORESCENCE MICROSCOPY INVESTIGATIONS OF GENE THERAPY

Koen Rombouts

Bio-engineer

Thesis submitted to obtain the degree of

Doctor in the Pharmaceutical Sciences

Proefschrift voorgedragen tot het bekomen van de graad van

Doctor in de Farmaceutische Wetenschappen

2016

Dean

Prof. Dr. Apr. Jan Van Bocxlaer

Promotors

Prof. Dr. Apr. Katrien Remaut

Prof. Dr. Kevin Braeckmans

MEMBERS OF THE EXAM COMMITTEE:

Prof. dr. apr. **Christophe Stove** (Chairman)	Universiteit Gent
dr. **Natalia Beloglazova** (Secretary)	Universiteit Gent
Prof. dr. **Luc Leybaert**	Universiteit Gent
Prof. dr. **Marcel Ameloot**	Universiteit Hasselt
Prof. dr. **Peter Dedecker**	KULeuven

COPYRIGHT STATEMENT

Ghent, 27th of May 2016

The promotors:

Prof. dr. apr. Katrien Remaut

Prof. dr. Kevin Braeckmans

The author:

Ir. Koen Rombouts

TABLE OF CONTENTS

LIST OF ABBREVIATIONS

ATP	Adenosinetriphosphate
bp	base pair
CA	Carboxylic Acid
CCD	Charge-Coupled Device
CD	Cyclodextrin
CDplexes	Cyclodextrin-based complex
Chol	Cholesterol
CLSM	Confocal Laser Scanning Microscopy
CTP	Cytosinetriphosphate
Cy	Cyanine
dATP	deoxyadenosinetriphosphate
dCTP	deoxycytosinetriphosphate
dGTP	deoxyguanosinetriphosphate
DLS	Dynamic Light Scattering
DMEM	Dulbecco's Modified Eagle's Medium
DNA	Deoxyribonucleic Acid
dNTP	deoxynucleotide Triphosphate
dsDNA	double-stranded DNA
dUTP	deoxyuridinetriphosphate
E. coli	*Escherichia coli*
EdU	5' - Ethynyl – 2'- deoxyuridine
EMCCD	Electron Multiplying CCD
FACS	Fluorescence-Associated Cell Sorting

FBS	Fetal Bovine Serum
FCS	Fluorescence Correlation Spectroscopy
FISH	Fluorescence In Situ Hybridization
FLIM	Fluorescence-Lifetime Imaging
FP	Fluorescent Protein
FRET	Fluorescence Resonance Energy Transfer
GFP	Green Fluorescent Protein
GTP	Guanosine Triphosphate
HeLa	cervical cancer cells taken from Henrietta Lacks
HEPES	4-(2-hydroxyethyl)-1-piperazineethanesulfonic acid
kb	Kilobase
kDa	Kilodalton
lipoplex	Liposome-based complex
LNA	Locked nucleic acid
Mal	Maleimide
MB	Molecular Beacon
MEM	Maximum Entropy Method
MFI	Mean Fluorescence Intensity
mRNA	Messenger RNA
MTase	Methyltransferase
mV	milliVolt
NA	Nucleic Acid
NAp	Numerical Aperture
NC	Negative Control

NHS	N-Hydroxysuccinimide
nm	nanometer
N/P ratio	Nitrogen/Phosphate ratio
NTP	Nucleotide Triphosphate
ODN	Oligonucleotide
paCD	Polycationic Amphiphilic Cyclodextrin
PBS	Phosphate Buffered Saline
PC	Positive Control
pCp	Cytidine-5’-phosphate-3’-(6-aminohexyl)phosphate
PCR	Polymerase Chain Reaction
pDNA	Plasmid DNA
PEG	Polyethylene Glycol
PEI	Polyethylenimine
PNA	Peptide Nucleic Acid
polyplex	Polymer-based complex
PS	Phosphatidylserine
QD	Quantum Dot
qPCR	Quantitative PCR
RGD	Arginylglycylaspartic Acid
RICS	Raster Image Correlation Spectroscopy
RNA	Ribonucleic Acid
RT	Room Temperature
SDS	Sodiumdodecylsulphate
SE	Succinimidyl ester

siRNA	small interfering RNA
SFC	Swept Field Confocal
SPAD	Single Photon Avalanche Diode
SPT	Single Particle Tracking
ssDNA	single-stranded DNA
strep	Streptavidin
TdT	Terminal deoxynucleotide Transferase
TCSPC	Time-Correlated Single Photon Counting
UTP	Uridinetriphosphate

GENERAL INTRODUCTION |

Aim and Outline

Research towards the development of medicines that treat genetic diseases, cancer, or viral infections has gained increasing interest over the last decades. Also, progress in the field of genome sequencing and bioinformatics provided information about the genetic origin of many conditions. This knowledge expanded the group of diseases potentially treatable by gene therapy, thereby increasing the interest in this type of treatment even more. In the meantime, it became clear that technology enabling the controlled delivery of nucleic acids would be needed to succeed in the introduction of a therapeutic gene into a mammalian cell.

Both physical and chemical methods have been explored to increase the delivery efficiency of nucleic acids in cells. Physical methods involve the application of an external “physical” trigger to deliver nucleic acids across the cell membrane into the cell’s cytoplasm. Examples of this approach are microinjection, electroporation, sonoporation, photoporation, and biolistic gene delivery (so-called gene gun). A prerequisite for these physical delivery methods to work is that the target tissue should be confined and that it’s accessible by the physical trigger. Chemical delivery methods, on the other hand, have the potential to more easily reach different types of tissues by means of passive or active targeting strategies. Chemical delivery methods typically involve the use of nanomaterials that act as carriers for the therapeutic nucleic acids. Their main task is to protect the nucleic acids and transport them across biological barriers to the target cells. Since these nanocarriers typically need to be injected intravenously, the blood compartment already constitutes a first major barrier. First of all, blood contains nucleases as well as immune cells that can respectively degrade nucleic acids or eliminate exogenous materials. Secondly, contact with blood proteins may lead to nanocarrier aggregation, dissociation of the nucleic acid – nanocarrier complex and loss of targeting functionality. Thirdly, the nanocarriers should be able to extravasate through the endothelial wall toward the target tissue. If all of that is successful, the nanocarriers typically have to cross the extracellular space and reach the target cells. Also on the level of the cell substantial barriers exist, including the plasma membrane, endosomal sequestration following nanoparticle endocytosis, and the nuclear envelope in the case of DNA-based gene therapy. Drug delivery scientists are working hard to design nanomaterials capable of overcoming all of these bio-barriers and bring gene therapy closer to reality.

Synthetic or non-viral vectors that complex nucleic acids are designed to have low immunogenicity and low cytotoxicity. Furthermore, they are easy to manufacture and allow for a broad range of possible chemical modifications. The efficiency of non-viral gene delivery remains, however, relatively low especially when compared to viral vectors. Therefore, fundamental research aimed at obtaining a better understanding of the different extra- and intracellular barriers is necessary to enable further rational optimization of nanocarrier design.

One of the biological barriers that is expected to be responsible for a decrease in efficiency of the nanocarriers in both the extra- and intracellular environment is the degradation of nucleic acids. Nevertheless, only a limited amount of research groups focus on where and how fast plasmid DNA (pDNA) is degraded, especially in living cells. Lechardeur et al. (1999)[1] used fluorescence in situ hybridization (FISH) to visualize degradation after fixation, dual fluorescent labeling was used to visualize degradation in living cells, [2] and atomic force microscopy (AFM) was used to study degradation of pDNA in buffers. [3] This shows that fluorescence microscopy has already proven to be a powerful technique to investigate the interaction of drug delivery nanocarriers with the relevant biological barriers. Especially on the intracellular level it offers detailed insight in the cellular processing of nanocarriers.

The general aim of this thesis was to use advanced fluorescence microscopy methods to study degradation of nucleic acids, which we believe is an important intracellular barrier encountered during the cellular processing of nanocarriers. Fluorescence correlation spectroscopy (FCS) and single particle tracking (SPT) were the advanced microscopy techniques that were used. Both of these techniques give information on the diffusion coefficient (and thus size) and concentration of the fluorescent molecules of interest.

To detect the nucleic acids with these fluorescence-based techniques, evidently they need to be labeled with a fluorescent tag. The design of microscopy experiments, however, often lacks attention to the labeling method. Using the right labeling method to label the carrier or the cargo at the right labeling density is crucial. It is generally accepted that high densities of fluorescent labels alter the intracellular behavior of the labeled molecules. It was, however, not studied how and at which points, interference of the fluorescent labels was significant. For this reason, the first goal of this work was to study the effect the random covalent labeling strategy, that is most often used to

attach fluorophores to pDNA, has on the intracellular processing and the transfection efficiency after lipid-mediated transfection. When a labeling density with minimal interference was found, our second goal was to evaluate two advanced microscopy techniques (FCS and SPT) to follow pDNA degradation in a biological environment. Next, we wanted to investigate if less common alternatives for the fluorescent labeling of nucleic acids showed the same effect on transfection efficiency and could be used for measurements with advanced microscopy techniques. Our final goal was to evaluate a new type of non-viral carrier, based on polycationic amphiphilic β cyclodextrins (paCDs), for the delivery of pDNA or mRNA.

The **first Chapter** gives a detailed overview of the different methods that are available for fluorescence labeling of nucleic acids. Additional to the background and mechanism of each labeling method, a guide for choosing the optimal labeling strategy for intracellular gene trafficking studies is presented. Next, in **Chapter 2** the theoretical background of FCS and SPT is given and the methodology that is used in the rest of the thesis is explained in detail.

Chapter 3 focuses on one of the labeling methods of **Chapter 1**, namely random covalent labeling, and the effect it has on the intracellular trafficking of pDNA that is delivered with a lipid-based carrier. The results showed that the fluorescent labeling influences the transfection capability of the pDNA, even at relatively low labeling densities. This shows that care should be taken when studying the intracellular trafficking of exogenous fluorescent DNA. It also obviates the need for further studies on which intracellular processes are potentially affected by the addition of fluorescent labels. **Chapter 4** describes the evaluation of two advanced microscopy techniques to measure molecular concentration of fluorescently labeled pDNA in biological fluids. We focused on the measurement of pDNA concentration since degradation by enzymes in the extracellular environment, as well as in the cell, leads to a significant loss of pDNA during nucleic acid delivery. Since the regularly used methods at this moment (e.g., agarose gel electrophoresis or quantitative polymerase chain reaction (qPCR)) cannot cope with, for example, the presence of proteins in biologic fluids, purification steps are necessary. For this reason, microscopy measurements directly in the biological fluid would be less labor intensive and faster. The two techniques, FCS and SPT, were evaluated in their ability to measure the concentration of intact pDNA in buffer, in complex mixtures with degraded pDNA, and over time during enzymatic degradation

by the endonuclease DNase I. By increasing the complexity of the medium, it became clear that SPT with concentration analysis was the best technique and that it could show that intracellular degradation after lipofection causes the loss of a significant amount of pDNA even after 8 hours. In **Chapter 5** different possible nucleic acid labeling methods were explored as alternatives to the most commonly used random covalent labeling method. Cyanine dimeric nucleic acid stain TOTO-3, labeling via peptide nucleic acid (PNA) hybridization, methyltransferase (MTase)-mediated enzymatic labeling, and one non fluorescent method were tested with regard to ease-of-use, transfection efficiency, and compatibility with confocal laser scanning microscopy (CLSM), FCS, and SPT.

Newly synthesized carriers are often evaluated using techniques often used in our research group. This expertise was consulted by the research group of Prof. J.M. García Fernández. **Chapter 6** describes the characterization and evaluation of three non-viral nucleic acid carriers consisting of polycationic amphiphilic β cyclodextrins (paCDs) which vary in their polycationic chain. In serum-free medium, the tested paCDs performed almost as well as Lipofectamine 2000 in the transfection of HeLa cells with pDNA and mRNA. However, when serum-containing culture medium is used, the transfection efficiency dropped significantly. We found that uptake of the complexes was affected when the experiments were performed in serum-containing cell culture medium, as well as in the presence of cholesterol. Although further research is needed, it is an indication that CDs need the interaction with cholesterol in the cell membrane to successfully transfect cells and that blocking this mechanism (by the formation of a protein corona in serum, or by saturating the CDs with an excess of free cholesterol) before reaching the cells should be avoided.

REFERENCES

(1) Lechardeur, D., Sohn, K., Haardt, M., Joshi, P., Monck, M., Graham, R., Beatty, B., Squire, J., O'brodovich, H., and Lukacs, G. (1999) Metabolic instability of plasmid DNA in the cytosol: a potential barrier to gene transfer. *Gene therapy 6*, 482-497.

(2) Srinivasan, C., Siddiqui, S., Silbart, L. K., Papadimitrakopoulos, F., and Burgess, D. J. (2008) Dual fluorescent labeling method to visualize plasmid DNA degradation. *Bioconjugate chemistry 20*, 163-169.

(3) Abdelhady, H. G., Allen, S., Davies, M. C., Roberts, C. J., Tendler, S. J., and Williams, P. M. (2003) Direct real-time molecular scale visualisation of the degradation of condensed DNA complexes exposed to DNase I. *Nucleic acids research 31*, 4001-4005.

(4) Slattum, P. (2003) Efficient in vitro and in vivo expression of covalently modified plasmid DNA. *Molecular Therapy 8*.

(5) Ho, Y.-P., Chen, H. H., Leong, K. W., and Wang, T.-H. (2006) Evaluating the intracellular stability and unpacking of DNA nanocomplexes by quantum dots-FRET. *Journal of Controlled Release 116*, 83-89.

CHAPTER 1 |

Fluorescent Labeling of Plasmid DNA and mRNA: Gains and Losses of Current Labeling Strategies

K. Rombouts,[†, ‡] K. Braeckmans,[†, ‡] and K. Remaut[†]. Fluorescent Labeling of Plasmid DNA and mRNA: Gains and Losses of Current Labeling Strategies. *Bioconjugate chemistry*. (2015)

† Laboratory of general biochemistry and physical pharmacy, Faculty of pharmacy

‡ Centre for Nano- and Biophotonics, Ghent University, Ghent 9000, Belgium

TABLE OF CONTENTS

ABSTRACT

Live-cell imaging has provided the life sciences with insights into the cell biology and dynamics. Fluorescent labeling of target molecules proves to be indispensable in this regard. In this chapter, we focus on the current fluorescent labeling strategies for nucleic acids, and in particular mRNA (mRNA) and plasmid DNA (pDNA), which are of interest to a broad range of scientific fields. By giving a background of the available techniques and an evaluation of the pros and cons, we try to supply scientists with all the information needed to come to an informed choice of nucleic acid labeling strategy aimed at their particular needs.

INTRODUCTION

Ever since Robert Hooke and Anton van Leeuwenhoek used a single lens to visualize and describe simple biological samples in the 17th century, scientists relied on advances in technology to reveal more of Nature's details. Image quality was improved in the following two centuries by optimizing lens combinations and progress in glass production, but resolution, contrast, noise, optical aberrations, sensitivity, and specificity were still major problems. Progression toward modern microscopy commenced when halfway through the 19th century, fluorescence was described by Stokes [1] and Von Lommel, creating the awareness that substances could be identified by measuring their specific fluorescence spectrum. Hence, one of the most important principles of fluorescence microscopy was born. Around the same time, Ernst Abbe published his theoretical analysis of the role of diffraction in optical microscopy. [2] It was however only at the start of the 20th century that a prototype of a bright field fluorescence microscope was built at the Carl Zeiss factory. Continuous instrumentation development and fluorescent probe design was conducted over the next 50 years, and with the invention of the beam splitting plate (dichroic mirror), [3] the basis of the fluorescence microscope as we know it today was formed. [4, 5]

The use of fluorophores to color specific substances of interest, has become indispensable in biology. While some molecules have intrinsic fluorescence properties, most biological substances have to be made visible by "labeling" them with specific fluorophores. Once labeled, some molecules can be used as a probe to identify cellular structures, such as for example the use of labeled antibodies to detect protein location. Alternatively, the labeled molecules themselves are the subject of investigation and their intracellular distribution and the biological processes in which they are involved are directly monitored. The choice for a certain fluorophore and an appropriate labeling strategy will greatly depend on the biological process one wishes to study. Ideally, the fluorophores specifically label the molecule of interest without nonspecific binding to other intracellular structures. Also, the fluorophores should have a high brightness and limited photobleaching to allow for imaging of biological processes during a suitable time frame. Finally, the fluorophores should show no or only limited interference with the process one wishes to study, to avoid labeling-induced artifacts. There is a wide variety of fluorophores available with output wavelengths in the blue, green, yellow, orange, red, far-red, or near-infrared

region of the emission spectrum. Obviously, the choice of suitable output wavelengths is strongly dictated by the optics of the available fluorescence microscopes. Also, the labeling strategy itself and the biological application (e.g., live-cell imaging versus fixed samples) will further determine the availability of compatible fluorophores. In Table 1, an overview of common fluorescent molecule families is presented with available functionalities and photophysical properties.

One of the biological processes that is of interest in the field of non-viral nucleic acid delivery, is the hurdles nucleic acids face on their extracellular and intracellular journey. For decades, researchers have fluorescently labeled nucleic acids with a variety of labeling strategies to gain insight in the fate of these nucleic acids. While labeling short interference RNA (siRNA) or antisense oligonucleotides is primarily done during chemical synthesis by the manufacturer, several strategies exist for the labeling of larger polynucleotides, such as plasmid DNA (pDNA) and messenger RNA (mRNA), in a research lab. These polynucleotides are of interest for any biological application in which the expression of proteins is beneficial. The main obstacle to the wide-spread use of these pDNA and mRNA based therapies is the low efficiencies obtained with the current transfection methods. Negatively charged nucleic acids are mostly complexed with positively charged carriers to enhance cellular uptake of the complexes which are formed. Designing new delivery vehicles is crucial for the future success of these treatments. Live-cell imaging will undeniably play an important role in unraveling the different steps of the transfection pathway. [6]

Table 1 Overview of fluorescent molecule classes often used in nucleic acid labeling.

Fluorescent molecule class		Functionalities	Photophysical properties				Supplier
			$\lambda_{Abs.}$ (nm)	$\lambda_{Em.}$ (nm)	Quantum yield	Remarks	
Cyanine (Cy) dyes	Cy3	SE, CA, strep, mal, azide, alkyne, NH_2, UTP, CTP, GTP, ATP, pCp, dUTP, dCTP	550	570	0.15	Broad range of applications, less bright than Alexa Fluor 546	Invitrogen, Jena Bioscience, GE Healthcare Life Sciences, Lumiprobe, …
	Cy5		649	670	0.27	Broad range of applications, less bright than Alexa Fluor 647	
Cyanine dimers	YOYO-1	N/A	491	509	0.38[a], 0.25[b] [7]	Photocleavage of NA and bleaching reported[8]	Molecular Probes
	TOTO-3		642	660	0.06	Bleaches fast (20-30s)[9]	
Ethidium bromide		N/A	285	605	0.20	Especially used for gel staining, but suspected mutagenicity	Invitrogen, Sigma-Aldrich, Bio-Rad, …
Alexa Fluor	Alexa Fluor 488	SE, CA, strep, mal, azide, alkyne, UTP, dUTP	495	519	0.92	Fluorescence output unmatched by any other spectrally similar dye	Molecular Probes
	Alexa Fluor 546		556	573	0.79	Cy3 and TM-Rhodamine substitute	
	Alexa Fluor 594	SE, CA, strep, mal, azide, alkyne, dUTP	590	617	0.66	Bright and photostable	
	Alexa Fluor 647	SE, CA, strep, mal, azide, alkyne, ATP, dUTP, dCTP	650	668	0.33	brighter substitute for Cy5	

ATTO dyes	ATTO 488	SE, CA, strep, mal, azide, alkyne, NH_2, biotin, UTP, ATP, dUTP, dCTP	501	523	0.80	Very high photostability	ATTO-TEC, Sigma-Aldrich, Jena Bioscience
	ATTO 647N		644	669	0.65	Cy5 substitute, high thermal and photostability, exceptionally high stability towards atmospheric ozone	
Fluorescein	FITC (isothiocyanate)	SE, mal, azide, alkyne, UTP, CTP, ATP, dUTP, dCTP, dGTP, dATP	494	518	0.86 (0.1 N NaOH)	pH sensitive, prone to photobleaching	Thermo Scientific, Sigma-Aldrich, Jena Bioscience, …
	5-FAM (carboxylic acid)	SE, azide, alkyne, strep, NH_2, dUTP, dCTP	494	518	0.90	SE form more stable bond with amines compared to FITC-SE	Molecular Probes, Sigma-Aldrich, Jena Bioscience, Lumiprobe, …
TM-Rhodamine	TRITC (isothiocyanate)	SE, strep, mal, azide, dUTP, dCTP	555	580	0.10	Prone to aggregation	Thermo Scientific, Sigma-Aldrich, …
	5-TAMRA (carboxylic acid)	SE, strep, mal, azide, alkyne, NH_2, dUTP, dCTP	555	580	0.10	More stable than TRITC	Molecular Probes, Sigma-Aldrich, AnaSpec.
CX-Rhodamine	5-ROX	SE, mal, azide, alkyne	576	591	0.70 (PO_4 buffer, pH 9)	Unstable compared to other rhodamines	Molecular Probes, Sigma-Aldrich, Jena Bioscience, AnaSpec.
Fluorescent proteins	EGFP	N/A	488	509	0.60	Most used, brighter variants available, no problems with photostability	Thermo Scientific, Sigma-Aldrich,

							BioVision
	mCherry	N/A	587	610	0.22	Superior photostability when compared to other red proteins	BioVision, Abcam
Quantum dots	CdSe-ZnS	CA, strep, mal, azide, alkyne (cyclooctyne), NH_2, biotin			0.20-0.50[c]	Bright, photostable, broad excitation, tunable narrow emission, but concerns about cell toxicity	Molecular Probes, Sigma-Aldrich, Mesolight
Lanthanide chelate	Eu(III)-chelates	SE, CA, strep, mal, azide, alkyne, NH_2, biotin	376	616	~1 (^2H_2O *10*)	Narrow emission peaks, long fluorescence lifetimes, high photostability but often needs a chromophore to transfer absorbed excitation energy to the lanthanide *11*	PerkinElmer,
	Tb(III)-chelates		340	545			Invitrogen, PerkinElmer
Transient metal complexes	Pt(II), Ir(III), Ru(II), Re(I)based	SE, CA, strep, mal, azide, alkyne, NH_2, biotin, dUTP				Long fluorescence lifetimes interesting for FLIM, tunable excitation/emission, high photostability, good quantum yield	Sigma-Aldrich

SE: Succinimidyl ester, CA: carboxylic acid, strep: streptavidin, mal: maleimide, NH_2: amine, FLIM: Fluorescence-Lifetime Imaging Microscopy . [a]: double strand DNA, [b]: single strand DNA, [c]: dependent on shell thickness*12*

This chapter focusses on methods to add fluorescent labels to polynucleotides, with the idea to image these in a biological environment. Labeling strategies which are compatible with live-cell imaging are of particular interest. Both methods that label polynucleotides prior to delivering these to living cells, as well as "in situ" labeling methods will be discussed. Polynucleotides have a well-defined primary and secondary structure, which enables yet another classification of fluorophore interaction which is based on their sequence specificity. Fluorophores that exhibit no sequence specificity interact with polynucleotides in a random fashion and are spread all over the polynucleotide chain. Sequence-specific polynucleotide labeling, on the other hand, only occurs at a predefined primary sequence, enabling control over the exact location of the labels on the target polynucleotide. In this chapter, the current available labeling strategies for DNA-based and RNA-based polynucleotides are classified based on their ability to label the nucleic acids in a random or sequence-specific way, with a special focus on the pros and cons of each labeling method that is being discussed.

AT RANDOM ATTACHMENT OF FLUOROPHORES TO POLYNUCLEOTIDES

In general, at random attachment requires little to no knowledge of the exact primary sequence of the polynucleotide that needs to be labeled. Not surprisingly, it is being used by the oldest, easiest, and most commonly used labeling methods around. Random labeling of polynucleotides can occur based on noncovalent or covalent interactions of the fluorophores with the polynucleotides backbone. Additionally, the random incorporation of fluorescent nucleotides during polynucleotide synthesis will be discussed.

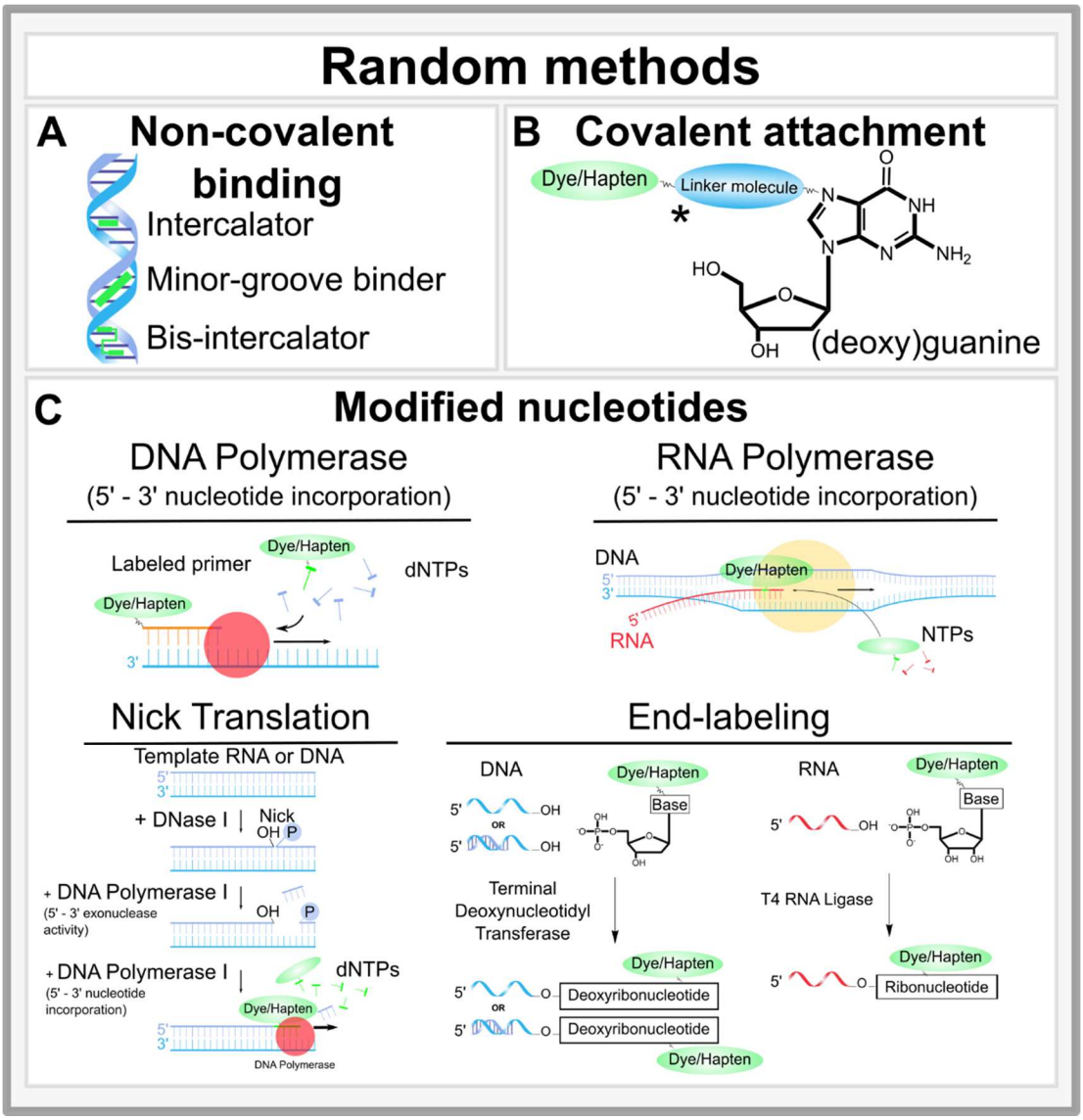

Figure 1 Overview of at random labeling methods. (A) Different modes of intercalation. (B) Schematic overview of random covalent attachment. (C) Different techniques used to incorporate modified nucleotides into DNA and RNA. dNTP: deoxynucleotide triphosphate. NTP: nucleotide triphosphate. *: Linker molecule structures can be found in Slattum (2003)[13] (Mirus kit), Daniel et al. (1998)[14] (FastTag) and van Gijlswijk et al. (2001)[15] (Universal Linkage System)

Noncovalent Nucleic-Acid Binding Dyes

Two modes of random noncovalent interactions with nucleic acids are considered, namely groove binding and insertion of a fluorescent tag between base pairs, which is called intercalation (see Figure 1 A). The family of molecules with nucleic acid-binding properties is fairly large and diverse and binding mechanisms are often not (yet) defined [16], but it is believed most of them exhibit only one of the two binding modes (e.g., YOYO-1 [17]); the combination of both has also been reported for PicoGreen. [18]

Groove binding dyes, as the name indicates, interact with the major or minor groove of a helix structure. In nucleic acids, these grooves are found in the α-helix of double stranded DNA. Reactions in the major groove of DNA are more common for molecules reacting directly with the bases like, for example, the covalent labeling methods which will be discussed later, and proteins. [19] Minor-groove binding dyes are widely used and interact with the DNA in a noncovalent manner. These interactions are based on the shape of the minor groove, which should be accommodating for the dye (see Figure 1 A). A good match will maximize the stability of the van der Waals contacts between target and dye. Next to these contacts, hydrogen bonds and electrostatic stabilizing interactions between the base pairs in the groove floor and the dye are the main contributors to a stable minor-groove binding. Additionally the increase in entropy due to the expulsion of bound water molecules from the minor groove will contribute slightly to the stability. [20] The effect these interactions have on the DNA morphology will differ from dye to dye, but in general an elongation of the total length and persistence length and DNA topology could be observed when using the minor-groove binding dye DAPI. [21]

Intercalation, on the other hand, is generally defined as the reversible insertion of molecules between layered structures. In polynucleotides, these layered structures consist of the stacked base pairs which form the secondary structure of DNA and RNA. Intercalating dyes are often cationic molecules with planar aromatic rings that insert between the base pairs of the helix-structure. During intercalation, π-stack interactions (intercalated moiety), hydrogen-bonding, van der Waals interactions, hydrophobic interactions, and steric hindrance effects all play a role. [22] Most of these will exhibit a strong fluorescence enhancement upon binding. Intercalators can be found either as a monomer (intercalator) or combined in a dimer (bis-intercalation) for stronger binding and higher brightness (see Figure 1 A). Next to this advantage, monomers and dimers will also exhibit a different affinity for a given polynucleotide, such as single stranded vs double stranded DNA or RNA, since intercalation is dependent on the secondary and tertiary structure of the nucleic acid. A good example is the monomer TOPRO-3 which does not stain RNA, while its dimer TOTO-3 does stain RNA. [9]

Like groove binding, the insertion of one (or two) dyes between the stacked bases will induce unwinding and lengthening of the nucleic acid helix structure and may subsequently disturb polynucleotide function. Hence, some intercalating dyes

are potentially mutagenic by interfering with replication, transcription, and DNA repair processes. The best known example is ethidium bromide, which is used for staining of agarose gels and subsequent nucleic acid quantitation. Ethidium bromide is more and more being replaced by less toxic alternatives. Cyanine stains (like the TOTO and TOPRO family of dyes [23])(see Table 1), for example, seem safer but often need cell permeabilization or other membrane disruptive techniques for cell staining. Martin et al. (2005)[9] therefore compared several intercalating labeling methods for their use in staining the nuclei during live-cell imaging (so-called counterstaining). The dyes were scored on cell permeability, live/fixed cell use, RNA staining, and bleaching behavior. They came to the conclusion that the minor-groove binding dyes Hoechst 33258 and DRAQ5 are the most suitable stains for live-cell imaging, wherein the latter dye is reported to have more favorable optical properties. In the search for brighter fluorophores that exhibit better resistance against photobleaching, different metal complexes with intercalating or groove binding properties were considered. Among the elements from the lanthanide group, europium (Eu) (III) and terbium (Tb) (III) are two ions which possess interesting photophysical properties with a large Stokes' shift, long emission lifetimes, interesting for fluorescence-lifetime imaging, and high resistance to photobleaching (see Table 1). [24] When these ions are complexed in a ligand structure, some complexes, like the conjugation of a naphthalene diimide derivative moiety with two luminescent chelates of tetradentate β-diketone-Ru^{3+}, were used to specifically intercalate in double stranded DNA. [25] Similar properties can be found in the transition metal complexes with Pt(II) or d6 metal ion complexes (Ir(III), Ru(II), and Re(I) complexes)(see Table 1). [11, 26] Square planar Pt(II) terpyridyl complexes were first reported to be DNA intercalators in the 1970s. [27] More recently "Ru(II) bisimine complexes" were verified and used as DNA binders. [28] It should be noted that different isomeric forms of the same complex might result in different affinities. Δ-$[Ru(phen)_3]^{2+}$ is, for example, a DNA intercalating complex while the Λ isomer prefers minor-groove binding. [11] Alternatively when one lanthanide complex and two platinum complexes are conjugated in a so-called heterometallic hairpin structure, bis-intercalation is seen. [29]

Next to the use of intercalating dyes for counterstaining of nuclei or staining of dead cells (e.g., propidium iodide), [30] for which they have been known for decades, intercalating dyes are good candidates for super resolution imaging of DNA [31]. The photochemical properties of the minor-groove binding dye Picogreen makes it

possible for direct stochastic optical reconstruction microscopy (dSTORM) to give insight into the dynamics of DNA organization after direct DNA labeling. [32]

Using intercalating dyes is probably the easiest method, since it solely requires mixing a dye with the target polynucleotide. Intercalating dyes are often used in quality control, nucleic acid quantification (e.g., quantitative polymerase chain reaction (PCR)) and as counterstain for the visualization of (live-) cell processes. Due to their interactions with the structure of the polynucleotides, [19, 21, 33, 34] influence on protein-nucleic acid interaction, [35] and low brightness, they are however not used extensively for labeling polynucleotides with the intention of following their intracellular fate in living cells.

Random Covalent Attachment of Fluorophores and Haptens

To prevent possible redistribution of intercalating dyes to non-target nucleic acids, covalently attaching fluorophores to the target nucleic acid is an interesting option. The irreversible binding of an organic dye or hapten to the nucleic acid will secure a stable and bright fluorescent signal. Haptens are defined as small molecules that can be detected by specific antibodies. After binding to nucleic acids, they allow subsequent immunodetection or affinity-base purification. When biotin is used as hapten, any streptavidin or avidin coupled molecule can be coupled to the biotinylated nucleic acids through the strong and specific (strept)avidin-biotin interaction.

One of the most frequently encountered examples of covalent modification of exogenous polynucleotides is the use of the commercially available Label-IT Nucleic Acid Labeling Kit (Mirus bio LLC, Madison, WI, U.S.A.). Slattum (2003)[13] demonstrated that reagents with an aromatic nitrogen mustard reactive center covalently alkylate nucleotides, primarily at the N^7 of (deoxy)guanine residues (see Figure 1 B). The available Label-IT reagents enable the direct coupling of fluorophores to the DNA structure (e.g., Cy3, Cy5, fluorescein, CX-rhodamine, and TM-rhodamine; see Table 1), or the coupling of haptens like biotin that offer the possibility to couple any streptavidin or avidin conjugated molecule in a subsequent labeling reaction. It has been described that the transfection efficiency of pDNA labeled with the Label-IT kit is decreased when compared to unlabeled plasmids in a labeling density dependent manner. [13, 36] For pDNA transfections using liposomal carriers, endosomal escape, DNA dissociation from the carrier, and transcription

were reported to be affected, probably due to the hydrophobicity and steric hindrance of the fluorescent labels. [36] Also, Gasiorowski and Dean (2005)[37] reported that nuclear retention of pDNA was affected by this labeling strategy. The labeling density of the nucleic acids can be controlled by titrating the amount of label-IT reagent for a given amount of nucleic acids. Ideally, the lowest labeling density that is still detectable by the instrumentation used should be preferred. Despite these caveats, this labeling method is useful for, among other things, intracellular tracking of polynucleotides to elucidate cellular mechanisms. Rhodamine labeled pDNA was for example imaged during cytoplasmic transport over the tubulin network after transfection. [38] The labeling of pDNA with Cy3 and Cy5, on the other hand was used to elucidate the cellular internalization mechanisms after transfection with polyethylenimine (PEI). [39] Similarly, Cy5 pDNA was used to image the internalization pathway of bioreducible polymeric nonviral vectors. [40] Furthermore, nonviral nucleic acid carriers like for example cyclic arginylglycylaspartic acid (RGD) peptide-conjugated polyplex micelles, [41] RGD-tagged and non-RGD-tagged PEGylated liposomes, [42] and oligopeptide polyplexes, [43] were tracked and evaluated using labeled polynucleotides. Although most reports make use of fluorescently labeled pDNA, it should be noted also that the fluorescent labeling of mRNA is feasible with the label-IT reagents.

An alternative commercial nucleic acid labeling kit is available from Vector laboratories (Burlingame, CA, U.S.A.). [14] The FastTag Basic Nucleic Acid Labeling Kit is based on aryl-azide chemistry in which the universal disulfide containing FastTag reagent, when exposed to heat or light, becomes activated and attaches onto the nucleic acids without base specificity. In a second step, the disulfide is being reduced after which any sulfhydryl reactive moiety can be coupled. The FastTag system can react with any single- or double-stranded DNA, RNA, or oligonucleotide. For double-stranded nucleic acids, however, light-induced coupling is preferred over heat to avoid denaturation of the double-stranded nucleic acids structure. A wide variety of fluorescent tags and haptens can be added by using this method, mostly using maleimide-derivatives as sulfhydryl reactive moiety (see Table 1). The method is used for the same type of experiments as described for the Label-IT nucleic acid labeling kit, but their broad range of fluorophores, including far-red dyes, makes it possible to extend to *in vivo* applications. A series of poly(glutamic acid)-based peptide coatings were, for example, targeted to the liver, spleen, spine, sternum, and

femur. DNA accumulation in these tissues was confirmed by Alexa Fluor 680 – pDNA. [44] This versatility was also employed to make biotinylated plasmids for *in vivo* transfection with Lac-PEI. Intracellular location was afterward visualized in cryosections by adding streptavidin conjugated dyes. [45]

An older labeling kit is the ULYSIS Nucleic Acid Labeling Kit (Molecular Probes, OR., U.S.A.). Alexa Fluor fluorophores are linked to the bases of DNA, RNA, oligos, and peptide nucleic acids (PNA) through the Universal Linkage System platinum-based chemistry. This system consists of a square planar platinum complex, stabilized by a chelating diamine. One of the two remaining coordination sites of this complex is occupied by a fluorophore, the second one will bind to the N^7 position of (deoxy)guanine. [15] This technique has been used to observe that the rate limiting step in pDNA-PEI transfections is the transfer from the lysosomal compartment to the nucleus. [46] Other carriers like mannosylated dendrimer/α-cyclodextrin conjugates were evaluated [47] to study how, and via which pathway, the DNA of a pathogen (*Cryptococcus neoformans*) stimulates dendritic cells Alexa Fluor 647 was attached using the ULYSIS kit. [48]

In summary, the covalent attachment of haptens and fluorophores offers a lot of benefits when random labeling of exogenous nucleic acids is desired. The different commercially available kits are readily available and easy to use and have already been extensively used for imaging polynucleotides, especially pDNA in living cells. A possible interaction with the system under study, however, should always be kept in mind, as each added fluorophore adds hydrophobicity and steric hindrance to the nucleic acids, when compared to their nonlabeled analogs. Also, the often cationic fluorophores lower the overall negative charge of the polynucleotides, which might interfere with the intracellular migration behavior of nucleic acids, complexation with and dissociation from a cationic carrier.

Incorporation of Modified Nucleotides

Apart from the labeling strategies mentioned above, another popular commercially available option is the *in vitro* incorporation of modified nucleotides into the polynucleotide backbone. The term “modified” stands for a nucleotide that differs from the naturally occurring nucleotides through the addition of a functional moiety. At first, the nucleotides with radioactive atoms (^{32}P, ^{33}P, ^{14}C, ^{3}H, ^{35}S) were used, but nowadays radioactive labels are often replaced by different types of coupling

moieties, fluorescent labels (see Table 1), or haptens (see Table 2). Since the addition or replacement of nucleotides is a phenomenon that occurs constantly in living cells, all these methods are based on naturally occurring enzymatic reactions.

In general, DNA or RNA synthesis is catalyzed respectively by DNA or RNA polymerases that read a DNA template in the 3' to 5' direction. The newly synthesized DNA or RNA molecules are then elongated in the 5' to 3' direction by the coupling of complementary nucleotides at the 3' end. While nucleotide triphosphates (NTPs) are used in RNA molecules, DNA exists of deoxynucleotide triphosphates (dNTPs). In living cells, RNA polymerases are responsible for the transcription of mRNA from the genomic DNA. For labeling purposes, RNA polymerases (T7, SP6, and T3) manage the incorporation of modified NTPs into RNA by *in vitro* transcribing so-called complementary RNA from a provided DNA template. The addition of modified nucleotides in the reaction mixture will therefore result in labeled RNA (see Figure 1 C). [49-51] DNA polymerases are adaptations from the cellular enzymes that take care of DNA replication in every living cell. Also here, modified dNTPs can be incorporated during synthesis of the new DNA strand complementary to the template strand (see Figure 1 C). In other words, both RNA and DNA polymerases act in a template-dependent manner and incorporate modified (deoxy)nucleotides at random over the complete length of the polynucleotide chains.

There is also the possibility to incorporate modified nucleotides in a template-independent manner by using "nick translation". During nick translation, which is based on the cellular DNA repair mechanism, DNA is "nicked" by a DNA endonuclease creating single strand gaps in the nucleotide sequence. A DNA ligase, like DNA polymerase I, will start to repair the polynucleotide starting from this gap by addition of dNTPs supplied in the reaction mixture. Commercially available kits will mostly make use of DNase I as endonuclease which nicks at random, while other sequence specific endonucleases can be bought separately. These endonucleases are derived from existing restriction enzymes, but modified to cut only one strand. When modified nucleotides are used, DNA fragments become fluorescently labeled (see Figure 1 C). [52, 53] By controlling the ratio of modified over nonmodified nucleotides in the reaction mixture, the labeling density of the resulting polynucleotides can be changed. Both methods described above incorporate modified nucleotides all over the polynucleotide chains, thereby achieving internal labeling of pDNA and mRNA. It is therefore to be expected that modified nucleotides

will also be present in the coding region of the pDNA or mRNA molecules. For some applications, this has to be avoided, in which case it is better to add modified nucleotides only to the 3' or 5' end of the polynucleotides.

The addition of nucleotides to the 3' terminus of an existing polynucleotide can occur in a template-independent way by the use of terminal deoxynucleotidyl transferase (TdT). TdT has the strongest affinity for single-stranded DNA or the 3' overhang of double-stranded DNA and is used frequently for adding modified dNTPs to PCR primers or restriction enzyme generated 3' overhangs (see Figure 1 C). [54, 55] An example is the 3' EndTag DNA end labeling kit from Vectorlabs, which couples SH-GTP to the 3' end of DNA molecules. The SH-GTP can subsequently be modified with thiol-reactive molecules such as for example maleimide-coupled dyes. T4 RNA ligase is another enzyme that is able to add modified NTPs to the 3' terminus in a template-independent manner, but only for RNA (see Figure 1 C). It should be noted that a DNA or RNA primer which contains a modified nucleotide at the 3' end (generated using TdT for example) can be used by DNA or RNA polymerases to be further elongated. Hence, internally labeled polynucleotides can also be formed in this way. 5' EndTag nucleic acid labeling kits are another available option from Vectorlabs, using T4 polynucleotide kinase to transfer a thio-phosphate from ATPγS to the 5' end of DNA, RNA, or oligonucleotides. Again, any thiol-reactive molecule can be coupled to the 5' end of these polynucleotides. DNA or RNA primers containing a modified nucleotide at the 5' end can also be used by DNA or RNA polymerases to create longer 5' end labeled polynucleotides (see Figure 1 C). Another interesting enzyme for end-labeling is the DNA polymerase I Klenow Fragment, which lacks 5' to 3' exonuclease activity, but retained its 3' to 5' exonuclease activity and 5' to 3' polymerase activity. The 5' to 3' polymerase activity can be used to fill in 5' overhangs (created for example by restriction enzymes) with dNTPs, leading to labeled fragments when modified nucleotides are used.

As already indicated above, nucleotides can be modified in a broad range of ways (see Table 1). In general, however, they can be classified as (i) containing a fluorophore, (ii) containing a hapten such as biotin or digoxigenin, (iii) being alkyne- or azide-modified for click-chemistry based labeling or (iv) being amine-modified for coupling to NHS-activated molecules (see Table 1). Available fluorescent nucleotides are mostly UTP and CTP and their deoxy-analogues dUTP and dCTP. Alexa Fluor 488 and Alexa Fluor 594-dUTP were used during amplification of linear DNA

fragments which were microinjected in the cytoplasm and nucleus of living cells. Their location and migration was followed using live-cell fluorescence microscopy. [56] Biotinylated nucleotides have been proven useful to conjugate streptavidin-quantum dots to pDNA for live-cell imaging. Biotinylated nucleotides were added in three different ways: nick translation, TdT addition, and by end-filling by the DNA polymerase I Klenow Fragment. [57] The addition of “clickable” nucleotides has been documented as well. Copper-catalyzed click chemistry refers to coupling of an azide-containing molecule A with an alkyne-containing molecule B to form an A-B conjugate. Alkyne- and azide-modified nucleotides can be combined with a wide variety of respectively azide- and alkyne-modified dyes (see Table 1). It should be noted that copper ions damage DNA, resulting in, for example, strand breaks. Therefore, copper(I)-stabilizing ligands should be used, or alternatively, copper-free click reactions involving the coupling of dibenzocyclooctyne (DBCO)-containing molecules to azide-containing molecules could be considered. Attaching fluorophores to nucleotides, added by TdT, has been shown to be feasible via copper-catalyzed azide-alkyne cycloaddition, strain-promoted azide-alkyne cycloaddition, Staudinger ligation, or Diels-Alder reaction with inverse electron demand. [58] Additionally, amine-modified (d)UTP, (d)CTP, and (d)ATP are available, enabling the coupling of NHS-activated fluorophores to, respectively, DNA (dNTPs) and RNA (NTPs) (see Table 1).

In summary, the addition of modified nucleotides is a versatile way of adding radioactive labels, fluorescent labels, or functional moieties to a polynucleotide. The availability of commercial kits also makes them accessible to a broad audience although a well-equipped biotechnology lab and accompanying lab experience is a prerequisite.

LABELING METHODS FOR SEQUENCE-SPECIFIC ATTACHMENT OF FLUOROPHORES TO POLYNUCLEOTIDES

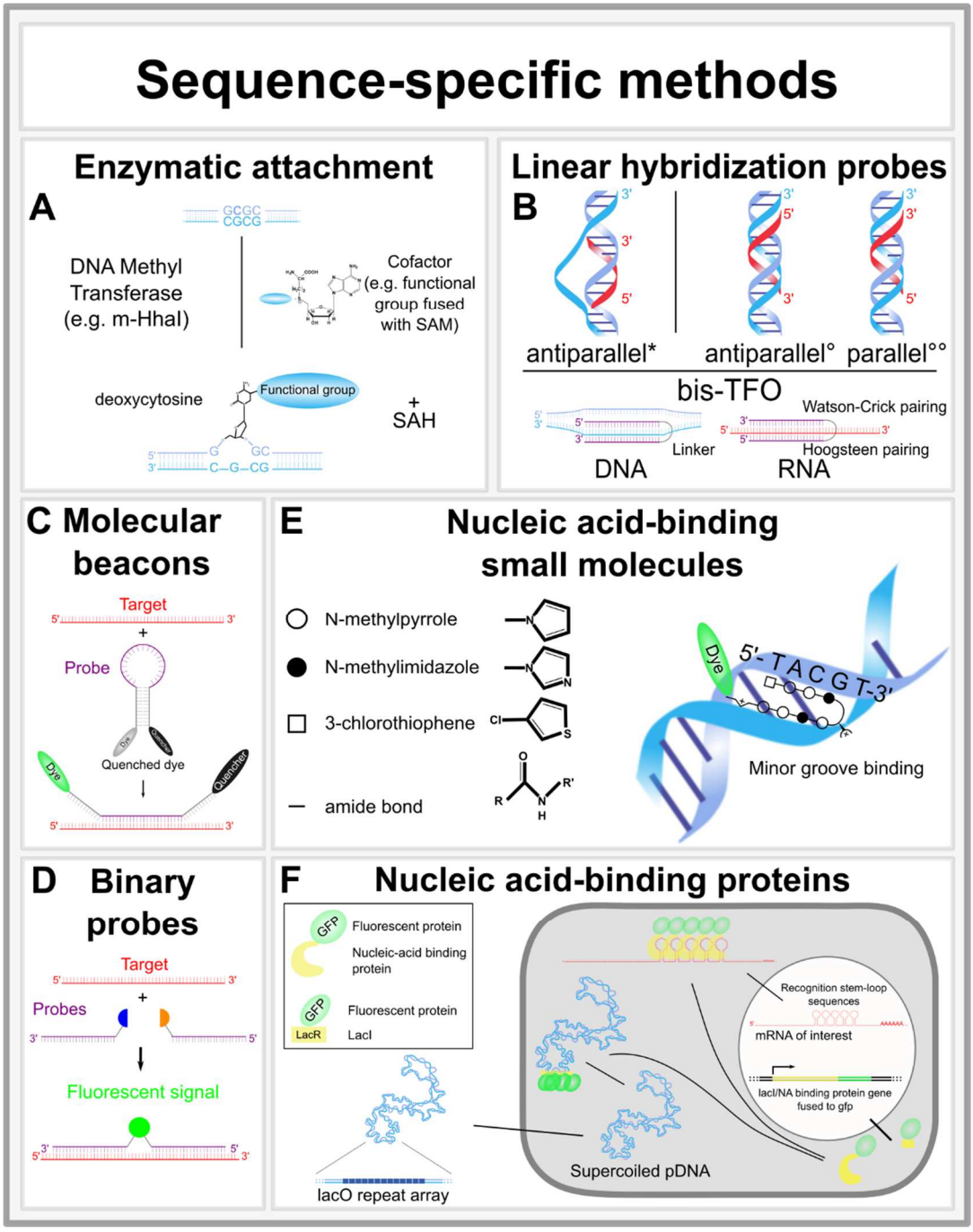

Figure 2 Overview of sequence-specific labeling methods. (A) General principle of MTase directed fluorescent labeling. (B) Schematic of linear hybridization probe interactions and bis-triplex forming oligonucleotides. *: antiparallel interaction following Watson-Crick base pairing. °: antiparallel interaction following reverse Hoogsteen base pairing. °°: parallel interaction following Hoogsteen base pairing. (C) Principle of molecular beacons. (D) Principle of binary probes. (E) Principle of nucleic-acid binding small molecules based on a structure described by Nickols et al. (2007)[59]. (F) Mechanism of GFP-tagged nucleic acid-binding proteins and the lacO/LacI principle. SAM = S-Adenosyl-L-methionine. SAH = S-Adenosyl-L-homocysteine. NA: Nucleic Acid. TFO: Triplex forming oligonucleotide. R and R': functional moieties.

Sequence-specific labeling techniques comprise every method that labels polynucleotides at a predefined primary sequence. The primary sequence of polynucleotides is determined by the particular way in which each of only 4 possible nucleotides is ordered. Targeting specific sequences is beneficial to obtain site-specific labeling, without (much) off-target binding. From a labeling point-of-view this opens up a plethora of opportunities with regard to selectivity, choice of labeling density, and label location. The first technique that is described is remarkably similar to the random covalent attachment methods. The sequence-specificity lies in the fact that an enzymatic reaction is used, instead of the chemical reactions as shown above, adding functional groups only to those sequences that are recognized by the respective enzymes.

Enzymatic Labeling at a Specific Target Sequence

In enzymatic labeling, a functional group (or fluorophore) is added to nucleic acids due to an enzyme-mediated reaction between the nucleic acid and a dedicated cofactor. This direct modification of the chemistry of the nucleobase by the enzyme distinguishes this method from those that use enzymes to incorporate modified nucleotides as mentioned above.

The enzymes used in the so-called sequence-specific methyltransferase-induced labeling (SMILing) method are DNA methyltransferases (MTases). [60] The cytosine-specific DNA MTase from *Haemophilus haemolyticus*, M.HhaI, for example, recognizes the double-strand DNA sequence 5'-G**C**GC-3' and subsequently catalyzes a covalent bond formation between the activated methyl group from a specifically designed cofactor (e.g., S-adenosyl-L-methionine) to the exocyclic amino group of cytosine (see Figure 2 A). The choice of MTase will determine the recognition sequence at which functional groups are attached. At the moment, most recognition sequences exist of 4 to 6 base pairs in which nucleophilic attack will occur on adenine, guanine or cytosine. The cofactor is, however, equally important, as it determines the functional group which is added in the enzymatic reaction. Synthesis of new cofactors determines the range of molecules that can be attached to the activated group. [61] Originally this method was used to add methyl groups, but linear alkyl, alkenyl, and alkynyl functionalization was developed, opening up more possibilities. [60, 62, 63] In the meantime a similar approach was developed for RNA. [64, 65] Based on these techniques the mTAG method was developed, making it possible to

incorporate a primary amine group which can be used for chemoligation reactions with all amine-reactive probes (e.g., NHS coupled-dyes; see Table 1 for examples) onto DNA or RNA. [66] For an in depth overview of the progress in this field the review by Gillingham and Shahid (2015)[67] is recommended.

This enzymatic labeling approach is interesting because it enables labeling polynucleotides internally in a sequence-specific manner. Especially for RNA, which is mostly fluorescently labeled using 3' or 5' end labeling, this might be an interesting opportunity. Labeling density can be easily controlled by designing polynucleotides that contain a fixed number of recognition sequences. Labeling position, on its turn, can be tuned by incorporating recognition sequences side-by-side, for example, flanking the encoding region of the polynucleotide of interest. Also, by combining different enzymes with their own recognition sequence and specific cofactor, dual-labeling of polynucleotides on predefined sites is possible. Despite these interesting features, only a limited amount of studies have employed enzymatic labeling for live-cell imaging applications. Schmidt et al. (2008)[68] evaluated the transfection of enzymatically labeled pDNA with a nonviral carrier. Imaging was, however, performed in fixed cells. Due to the absence of a commercial supplier, follow-up publications in living cells are still lacking. Nevertheless, research is still ongoing to further optimize this labeling method. [69] Neely et al. (2010)[70], for example, adapted this technique to create a DNA fluorocode, making use of the sequence specificity. Fluorophores are added at different locations depending on the location of the recognition sequence which will differ depending on the target nucleic acid. The specific pattern of fluorophores on the target can then be used as a barcode for fast nanometer scale DNA sequence information. [70, 71] Along this line of thought enzymatic labeling is also used for rapid bacteriophage strain typing. [72]

In summary, enzymatic labeling is a promising covalent labeling technique which adds sequence specificity when compared to the random methods. The translation to a broad audience will, however, benefit from the development of a straight-forward labeling kit, ruling out the need for a thorough understanding of the enzymatic reaction before it can be employed.

Nucleic Acid-Based Hybridization Probes

The next method that will be discussed makes use of oligonucleotides which recognize and bind to their nucleic acid target based on sequence complementarity.

Therefore, knowing the exact sequence of the target polynucleotide is key. Sequence complementarity can manifest itself in two types of interactions: antiparallel and parallel to a nucleic acid strand. Antiparallel interactions follow Watson-Crick or reverse Hoogsteen base pairing, while parallel interaction makes use of Hoogsteen base pairing. For single strand DNA and RNA, the complementary oligonucleotides will prefer to follow an antiparallel interaction following Watson-Crick base pairing. For double stranded DNA, antiparallel interactions following Watson-Crick base pairing is also the most common interaction, but it requires the displacement of one strand to form a new oligo-DNA duplex (see Figure 2 B). Oligonucleotides that interact in an antiparallel manner following reverse Hoogsteen base pairing, as well as oligonucleotides interacting in a parallel manner, mainly bind into the major groove of the double helix, creating a triple helix structure at the binding site (see Figure 2 B). [73] These oligonucleotides regardless of their orientation are called triplex forming oligonucleotides.

Linear Oligonucleotide Probes

Already in the late 1970s, it was proposed that antisense oligonucleotides could have a potential in a therapeutic environment. [74] In this method, short DNA or RNA oligonucleotides are designed to bind antiparallel to complementary mRNA sequences inducing downregulation of this specific mRNA. When a fluorescent label is attached to these oligos, this binding could be visualized. A well-known example where the principle of nucleic acid-binding oligonucleotide probes is used is in the cytogenic technique fluorescence in situ hybridization (FISH) where the location of a target DNA or RNA sequence is visualized in fixed and permeabilized cells. [75] This is achieved by the addition of fluorescently labeled oligonucleotide probes, which bind to their complementary sequence and can be visualized by fluorescence microscopy. [76, 77]

This approach was also applied in live cells, but low stability and poor cellular uptake of these DNA and RNA oligonucleotide probes led to the development of modified oligonucleotides. [78] A combination of backbone and sugar moiety modifications proved to be the most interesting, since binding affinity is less affected compared to modifying the bases themselves. [79] Peptide (or polyamide) nucleic acid (PNA) [80, 81], locked nucleic acid (LNA) [82] and 2'-O-methyl and 2'-O-aminoethyl chemistry based nucleic acids [83, 84] are some examples of modified oligonucleotides

used to create a strong and sequence-specific binding to complementary sequences (see Figure 3).

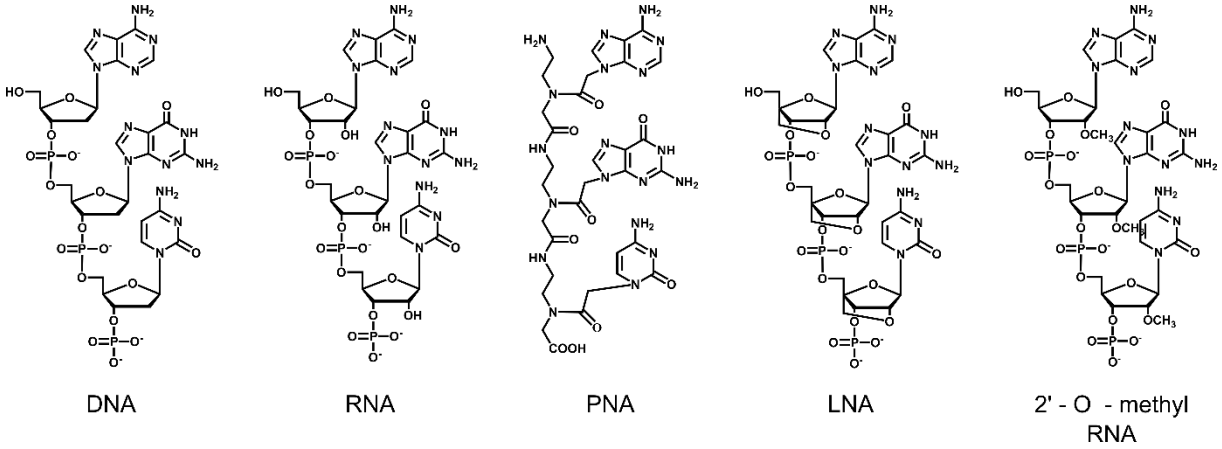

Figure 3 Structures of DNA, RNA, and the backbone-modified oligonucleotides.

Probably the best known modified oligonucleotides are PNAs, where the backbone consists of N-(2-aminoethyl)-glycine units linked by amide bonds. The purine (A, G) and pyrimidine (C, T) bases are attached to the backbone through methylene carbonyl linkages (see Figure 3). [85] This neutral backbone structure leads to a PNA/DNA or PNA/RNA interaction which is stronger than just the DNA/DNA or RNA/RNA interaction. Furthermore, this interaction is also more sequence-specific. Interactions can be either the preferred, antiparallel method, which requires strand displacement and follows Watson-Crick base pairing, or parallel pairing which creates a triple helix. The combination of both can be found in bis-PNA (2 PNA) which is therefore a triple helix forming oligonucleotide (PNA-DNA-PNA) (see Figure 2 B). A bis-PNA – DNA triplex was the first PNA complex described and it is probably the most interesting with regard to labeling. [80] It consists of a Watson-Crick PNA strand coupled with flexible ethylene glycol type linkers to the Hoogsteen PNA strand (see Figure 2 B). Often, the Hoogsteen strand is optimized by replacing cytosine with pseudoisocytosine, eliminating the need for a low pH during hybridization. [86] The versatile use of PNAs has been excellently reviewed by Nielsen and Egholm (1999)[85].

LNA bases are far more identical to DNA (or RNA) bases compared to the modifications seen in PNA bases. The only change from a DNA (or RNA) base is the introduction of an additional 2'-C, 4'-C-oxymethylene linkage that effects conformational fixation of the furanose ring in a C3'-*endo* conformation (see Figure 3). [87, 88] Oligonucleotides consisting of only LNA bases, however, have no double

helix binding capacity. [89, 90] LNA-containing oligonucleotides on the other hand undergo Watson-Crick base pairing resulting in thermostable, 3'-exonucleolytic stable, and sequence-specific double helix interactions with DNA and RNA. [82, 87, 91] Bis-LNA was also developed more recently to bind to supercoiled DNA in a fashion similar to bis-PNA (see Figure 2 B). [92]

2' O-methyl and 2' O-aminoethyl modified RNAs differ only very slightly from regular RNA in that they respectively have a methyl group and a short amino alkyl group attached to the 2' position of the ribose (see Figure 3) which allows, in the case of the aminoethyl group, a specific charge-charge contact of this protonated amino group with a proximal phosphate group of the DNA duplex. This interaction strongly enhances the binding affinity of this oligonucleotide toward double-stranded DNA. [83]

Although originally designed to interfere with the nucleic acid metabolism, similar to antisense oligonucleotides, [93] modified oligonucleotides can be used as a sequence-specific labeling strategy due to their specificity and strong nucleic acid-binding capacity. In general, fluorophores are attached via a linker to the 3' or/and 5' terminus of the oligonucleotide, [94] although fluorophore attachment is reported at all locations of the PNA strand through the use of fluorescently modified nucleotides during synthesis. [95] Other modified oligos can likely be internally labeled in a similar fashion. Early on the potential of PNAs in particular, was seen for detecting single base pair mutations by PNA-directed PCR, facilitating the amplification of mutants due to binding to the native templates and subsequently blocking PCR amplification. [96] PNA strands employing a quencher and fluorescent reporter are also used to perform quantitative PCR (commercially available under the name of PANA qPCR, Panagene, Daejeon, Korea). Their high specificity makes them ideal candidates for multiplexing. As already mentioned, also for FISH, modified oligonucleotides are the ideal candidates. [97, 98]

When we look at live-cell imaging, modified oligonucleotides have been used in very interesting applications. Molenaar et al. (2003)[99], for example, were the first to visualize the spatial localization and dynamics of telomeres in living human osteosarcoma cells, using fluorescently labeled PNA delivered to the cells using glass bead loading. [100] The same research group microinjected 2' O-methyl oligoribonucleotide-RNA probes and used photobleaching techniques to investigate the mobility of poly(A)$^+$ RNA throughout the nucleus. [101] These applications show the potential of modified oligos for intracellular labeling of endogenous nucleic acids in

living cells. However, a major drawback is the background generated by the unbound oligonucleotides. Labeling of exogenously synthesized nucleic acid is also a possibility which does not encounter this problem since a purification step is included before exposure to the cell. Zelphati et al. (1999)[102], for example, followed the nuclear uptake of Rhodamine PNA-labeled nucleic acids and correlated Rhodamine-positive nuclei with green fluorescent protein (GFP) expressing cells. The PNA-based technique for labeling pDNA was also compared with random covalently labeled pDNA with regard to their post-mitotic nuclear retention. It was seen that random covalently labeled pDNA was not retained within the nucleus of the daughter cells after cell division, whereas PNA-labeled pDNA acted as if it were unlabeled pDNA. *37* It was also established via atomic force microscopy and transfection experiments that pDNA labeled with quantum dots via PNAs was still functional. *103* Dual color labeling of one plasmid was later used in combination with confocal time-lapse imaging and intracellular trafficking by the same research group to study the intracellular DNA distribution and degradation after lipofection. *104* For the evaluation of nonviral carriers, PNA labeling is also a good candidate as was shown by testing the effect cell-surface glycosaminoglycans have on the transfection efficiency of mixtures of low-molecular-weight PEI and cationic lipids. *105*

It should be noted that the GeneGrip PNAs and plasmids with corresponding PNA labeling sites (Gene Therapy Systems, U.S.A., now Genlantis, U.S.A.) are no longer commercially available. Obviously it is still possible to design and order vectors and PNAs with the appropriate sequences for site-specific labeling of pDNA. As with any oligonucleotide, however, a careful control of the annealing efficiency and the purification of unbound oligos is necessary to obtain high quality and purified fluorescent nucleic acids.

Related to the direct labeling, as described until now, the concept of complementary sequence recognition by oligonucleotides is also recently used in live-cell RNA expression profiling. So-called Nanoflares (AuraSense, Skokie, IL, U.S.A.) are spherical nanoparticles with a gold core to which oligos complementary to the target RNA are attached. Via a second small oligonucleotide, a dye is bound on the complementary oligo closely to the gold nanoparticle whereafter it is quenched. When the Nanoflare enters the cell after receptor-mediated endocytosis, cytoplasmic target RNA can bind to the complementary oligo, effectively releasing the small oligo with the dye. This release induces unquenching whereafter this signal can be

visualized via live-cell fluorescence microscopy, making it possible to quantify RNA synthesis. [106, 107] Building further on this concept, Briley et al. (2015)[108] designed the so-called sticky flares. Instead of releasing the dye in the cytoplasm, the dye is attached to the target RNA via a long complementary oligo. This oligonucleotide is originally bound to one of the strands attached to the gold nanoparticle. When encountering the target RNA in the cytoplasm, the labeled oligonucleotide will have a higher affinity for the target RNA than for the one bound to the nanoparticle, thus effectively labeling the RNA in situ.

Molecular Beacons

"Molecular beacon" (MB) is a collective term for all probes that recognize and bind to a particular cellular target, enabling visualization. In this chapter, the molecular beacons are an extension on the concept of oligonucleotide probes which are mentioned above. While the "traditional" oligonucleotide probes make use of one fluorescent label, MBs employ two (or more) labels, which are attached at the opposite ends and make use of the fluorescence resonance energy transfer (FRET) principle, a quencher/dye principle or a combination of both (see Table 2 for examples) to ensure that the labels remain in a dark state until they bind to the target hereby guaranteeing a low background signal from unbound probes, which is necessary for live-cell microscopy. The FRET principle makes use of two fluorescent molecules that, when they are in close proximity (tens of nanometers), can transfer energy in a nonradiative way from one (the donor) to the other (the acceptor). To this end, the oligonucleotide is designed in a stem-loop structure which brings both functionalities in close proximity when no target sequence is encountered. Upon binding, the probe's stem-loop structure is stretched and respectively the donor dye (in FRET MBs) or quenched dye will become visible (see Figure 2 C). [109, 110] The concrete implementation of this general principle is variable due to the use of different fluorophores, quencher/dye pairs, oligonucleotide conformations, and number of oligonucleotides used (multiplexing), etc., but all are based on the same concept.

According to Santangelo (2010)[111], a good MB for tracking intracellular RNA should have four characteristics, namely: (i) the importance of delivery to the right cellular compartment, (ii) affinity for the target RNA without disturbing the functionality, (iii) sequence sensitivity and last but not least, (iv) a beacon should be

visible throughout biogenesis, transport, translation, and degradation pathways. These characteristics also pinpoint the four bottlenecks of this labeling method. For labeling intracellular targets, MBs need to be delivered to the cell since they are not taken up spontaneously. The techniques used to deliver MBs, like microinjection, passive uptake, cationic transfection, or reversible cell membrane permeabilization, suffer from low efficiency and a high toxicity to the cells. Also, the stability of the dyes used and the MB over time is important, since most cellular applications need to image the target over a longer period of time without the loss of signal. Despite these challenges, MBs easily found their way in live-cell imaging, but are also used in quantitative PCR. The exonuclease activity of DNA polymerases will cleave the MBs and disconnect the donor/quencher from the acceptor dye/dye, whereupon a fluorescent signal can be detected and correlated to an increase in amplified DNA. [109, 112] In live-cell imaging, MBs are popular for tracking intracellular RNA, [113-115] tracking DNA, [116] and to study protein-DNA interactions. [117, 118]

Similar to MBs, a different type of RNA oligos undergo a conformational change, when they bind to their target sequence. These RNA oligonucleotides, targeting specific RNA sequences (called RNA aptamers), can be integrated and expressed in a stable or transient manner in cells. The induced conformational change upon binding makes them accessible to small fluorescent protein-like molecules, which allow in situ labeling of the target RNA. [119] The design and synthesis of the small dye is crucial for brightness and specificity since it should only be activated by one specific RNA aptamer. Paige et al. (2011)[120] coined the term “Spinach” for their RNA aptamer that in combination with their fluorophore resembled the spectral properties of GFP the most, allowing the localization and tracking of RNA in living cells. Improvements in brightness and specificity on this system have been developed (e.g., Spinach2, [121] RNA mango [122]) and more are under development.

Binary Probes

One of the alternative approaches that combines the structural properties of linear oligos and a light-up principle of MBs is the use of binary probes. In general, this approach makes use of two oligonucleotides which are complementary to adjacent sequences of the target nucleic acid, and each has a different molecule that needs to be joined together to emit fluorescence on their ends (see Figure 2 D). As a standard, this is a fluorescence acceptor and a fluorescence donor which are each

situated at the ends of a oligonucleotide. Only in the presence of the target will the acceptor dye receive the energy with a significant emission. [123] This method has been applied routinely in real-time LightCycler PCR Technology. [124, 125]

Although this method in theory offers improvements on the high signal background signal of linear oligo probes by employing a light-up principle and offers less chance of nonspecific binding by using two independent oligos, some drawbacks should be noted. First of all, the complexity of the design of the probes is even higher than for single linear oligos or MBs. [126] Second, the signal of the acceptor fluorophore might suffer from the noise of the cellular autofluorescence. Additionally, the donor and acceptor fluorophores should be chosen in order to avoid overlap between the spectra of emission of the donor and the acceptor, which would generate false positives. Finally, the hybridization of two separate oligos is from a kinetic and a thermodynamic point of view less favorable. [123] Kolpashchikov (2010)[126] as well as Guo et al. (2012)[123] made overviews of the different approaches that were developed within the concept of binary probes to tackle these issues. The most interesting developments are the use of a ruthenium complex as a fluorescence donor (see Table 1) together with an organic fluorescence acceptor, [127] the creation of a lanthanide chelate (see Table 1), [128, 129] and quenched autoligation [130-132] which was used for live-cell imaging of bacterial strains [133] or to visualize mRNA in living cells. [134]

In summary, oligonucleotide hybridization strategies, as listed above, are a great way of labeling extracellular administered polynucleotides, like those for gene replacement therapy, and intracellular endogenous polynucleotides. Their mechanism however requires a well thought-through design of probes as well as target, ensuring stable and specific labeling of the target sequence with no, to limited, disturbance of its function. To obtain sufficient signal to follow single nucleic acid molecules, for example, not one but an array of recognition sequences is needed. [135] In combination with the initial cost and optimization needed, these methods might not be for every cell biologist who ventures into live-cell imaging, but will remain in specialized laboratories.

Nucleic Acid-Binding Small Molecules

In contrast to the oligonucleotides described above, which are making use of (modified) nucleic acid bases, synthetic small molecules are making use of

polyamides to bind to DNA in a sequence-specific manner. This approach was pioneered by the Dervan group at CalTech who described in detail how the invention of these type of hairpin pyrrole-imidazole polyamides was conceived. [136] Starting from the structure of naturally occurring antibiotics netropsin and actinomycin, which were known to be A/T tract selective DNA minor-groove binders, synthetic hairpin polyamides were developed which showed minor-groove binding and a high sequence specificity (see Figure 2 E). Originally, this approach was aimed at creating synthetic molecules for therapeutic gene expression regulation. However, conjugations of these polyamides to fluorescent dyes were developed and shown to be effective in binding double stranded DNA [137] and in intracellular localization, [138] due to their uptake in living cells. [139] Vaijayanthi et al. (2012)[140] assembled practical information about dye-polyamide conjugates and summarized the progress in this field based on the fluorescent dye used. Most notably was the increase of biological information obtained due to the overlap of the biological activity of the polyamides in gene expression regulation and the monitoring of the fluorescent signal in real time. [140] The sequence specificity made them ideal candidates for following DNA repeats in genomes of eukaryotic cells. [141, 142] Furthermore, FRET was observed when combining two polyamide conjugates with either Cy3 or Cy5, opening the door to the study of DNA-protein interactions by the gain or loss of the FRET signal. [143]

In summary, conjugates of hairpin pyrrole-imidazole polyamides and fluorophores have found applications as sequence-specific nuclear stains. Due to their gene regulatory properties in which interest was shown as a therapeutic, [144] these minor-groove binders can aid in the study of the mechanism of these therapeutics. The chemical synthesis, design and cost might be a hurdle to the application by a broader cell biology community and remains for specialized laboratories.

Nucleic Acid-Binding Proteins

Most labeling techniques discussed so far, with the exception of the molecular beacons, the binary probes, and polyamide conjugates, are employed to label exogenous DNA and RNA prior to delivering them to the target cells. In situ labeling of polynucleotides is however an interesting option in those cases in which only nucleic acids that are present in the cytoplasm or nucleus of the cells should be detected. The main principle of in situ labeling is that the target cells express

(fluorescently tagged) proteins that bind specifically to DNA or RNA sequences. An advantage of this method is that the polynucleotides are not modified during the early steps of the transfection pathway, ruling out potential label-induced artifacts until cytoplasmic or nuclear entry. This implies that information on the steps in the transfection pathway before endosomal escape is lacking when using in situ labeling of nucleic acids.

In the informative review by Tyagi (2009)[113], an overview is presented of the methods that are available to track intracellular RNA. The nucleic acid binding methods: MS2 system, [145] Bg1 system, [146] the λN system, [147] poly(A)-binding proteins, [148] and PUMILIO1 [149], are all systems that share the same basic principle. [113, 150] A fluorescent protein (most often GFP; see Table 1) is fused to an RNA-binding protein which has a strong affinity for a certain RNA motif or sequence, which is mostly incorporated in the target RNA sequence as a stem-loop structure. This binding of the GFP-tagged protein makes it possible to visualize RNA molecules intracellularly and can be used for endogenous mRNA tracking (see Figure 2 F) (e.g., ref. [151]), as well as for exogenously delivered RNA. Especially in the field of RNA viruses, these techniques have proven to be valuable. [146, 152]

A similar approach is available for DNA. A well-known example is the Lac operon/Lac repressor (lacO/LacI) system in which the LacI-GFP protein binds to the lacO sequence (see Figure 2 F). [153] Annibale and Gratton (2015)[154] used the lacO/LacI-GFP approach to visualize DNA, while the MS2 system was used to visualize the transcriptional kinetics of the produced mRNA. Apart from using GFP-fusion proteins, two methods are commercially available that attach a protein tag to the target sequence of a nucleic acid. When a fluorescently labeled ligand is added, it binds the protein tag resulting in a fluorescently labeled protein. Both the SNAP tag method [155] by New England Biolabs (cited by 798 papers (Google Scholar, September 2015)) and the HaloTag technology [156] by Promega (cited by 472 papers (Google Scholar, September 2015)) make use of this principle. These methods have the advantage of a broad range of cell-permeable organic fluorophores that can be utilized in comparison with the fusion of, traditionally less bright, fluorescent proteins to the DNA-binding protein of interest. Nevertheless, the option of directly fusing a fluorescent protein to the DNA-binding protein might be preferred in cases where, for example, unwanted binding events in the nucleus are observed when using the commercially available methods. [157] This was also a concern when Shimizu et al.

(2005)[56] microinjected DNA into the cytoplasm and nucleus of cells. That is why, next to the use of modified nucleotides to detect the short DNA fragments, they worked with lacO arrays to visualize their long DNA fragments.

Apart from the lacO/LacI system, other naturally occurring transcription factors like zinc-finger nucleases, CRISPR/Cas-based methods, and transcription activator-like effectors (TALEs) are used. This last type can be designed to recognize very specific DNA sequences, which makes them great tools for labeling. [158, 159] Their specificity made it, for example, possible to track major satellite DNA throughout the cell cycle. [160] The use of these rather complex techniques is up to this point not routinely utilized in live-cell imaging.

In summary, nucleic acid-binding proteins are an interesting option in the range of labeling techniques available to researchers (see Table 2), but are certainly not the most straightforward. The availability of commercial options relieves this partly, but the need for a stable or transient expression of the fluorescent protein-tagged proteins poses an extra hurdle which lowers efficiency. Furthermore, the need for a well-designed target also complicates the experimental design.

LIGHTING UP THE INTRACELLULAR DELIVERY PATH OF PDNA AND MRNA POLYNUCLEOTIDES

The choice of an optimal labeling strategy to visualize nucleic acids in living cells will greatly depend on the specific research questions. The labeling of native DNA and RNA in the context of analyzing gene expression profiles, elucidating primary and secondary structure, and following epigenetic modifications and visualizing interactions with other cell components has been nicely reviewed by Boutorine et al. (2013)[161]. Here, we aim to overview the labeling choices which are available for fluorescent labeling of pDNA and mRNA, in the context of following their intracellular uptake, endosomal escape, mobility, stability, and distribution in living cells.

Table 2 Advantages and disadvantages of the different labeling methods.

labeling method	pros	cons	ideal for:	available functional groups	key ref.
Intercalating dyes	+ Easy to use kits available + Fast + Large scale reactions + Light-up principle	- Off-target interactions - Negative effects on NA conformation - Low efficiency dyes	Counterstaining Quantification of cellular uptake	Possibilities all over the visual spectrum (e.g. YOYO-1, TOTO-3)	[19], [22], [9]
Covalent attachment	+ Easy to use kits available + Fast + Large scale reactions + Strong covalent attachment	- Negative effects on transfection at high labeling density	Polynucleotide tracking Random labeling	Label-IT: DIG, biotin, DNP, Cy3, fluorescein, Cy5, TM-Rhodamine, CX-Rhodamine FastTag: thiol-reactive reagents ULYSIS: Alexa Fluor 488-546-594-647	[13], [36], [14], [15]
Modified nucleotides	+ Kits available + Broad range of possible methods + End labeling possible	- Prior knowledge of labeling mechanism - Labor intensive - Expensive modified nucleotides	End labeling Random labeling	NHS ester + primary amine Maleimide + thiol Azide + Alkyne Biotin + streptavidin Intrinsically fluorescent labeled nucleotides (see Table 1)	[50], [52], [55]
Enzymatic labeling	+ Sequence-specific (4 to 6 bp recognition sequence) + Easy to use + Strong covalent attachment + Fast	- No individual components for reaction commercially available - Extensive knowledge of chemistry of co-factors necessary - Small scale reaction - Expensive enzymes and co-factors	Polynucleotide tracking	All NHS ester-dyes and haptens (e.g. NHS ester-Alexa Fluor 488, NHS ester-Alexa Fluor 647, NHS ester-biotin)	[66], [68]
Linear oligos	+ Highly sequence-specific + Strong attachment + Fast + Large-scale reactions + Low cost per reaction + Multiplexing possible	- No kit available (anymore) - Needs sequence information of target - Needs knowledge of oligo design - Optimization needed - High initial price of nucleotides	Polynucleotide tracking	Same options as for modified nucleotides (see Table 1)	[79], [81], [85]
MBs	+ Highly sequence-specific	- No kit available - Intracellular delivery needed	Intracellular	Virtually all commercial organic quencher-dye pairs	[109], [111]

	+ Strong attachment + In situ labeling possible + Light-up principle + Versatile	- Sequence information on target needed - Custom oligo design - Optimization needed - High initial price of (modified) probe	detection of specific polynucleotides	available (e.g. TAMRA – 5'-FAM, Quasar 670 – Cy 5)	
Binary probes	+ Highly sequence-specific + Strong attachment + In situ labeling + Light-up principle + Versatile + Reduction of background	- No kit available - Intracellular delivery needed - Sequence information on target needed - Custom design for two adjacent oligos - Optimization needed - High initial price of (modified) probe	Intracellular detection of specific polynucleotides	Virtually all commercial quencher-dye pairs available (e.g. TAMRA – 5'-FAM, Quasar 670 - Cy5, Ru(II) – Cy5)	*123, 126*
NA-binding small molecules	+ Sequence-specific + In situ labeling possible + Spontaneous uptake by cells + Versatile	- No kit available - Sequence information on target needed - Not all sequences can be targeted - Extensive knowledge of polyamide conjugate chemistry necessary - Expensive	Intracellular detection of specific polynucleotides	Same options as for modified nucleotides (see Table 1)	
NA-binding proteins	+ Kits available + Sequence-specific + In situ labeling + Cell compartment specific labeling possible	- Extensive knowledge of FP-tagged proteins needed - Adaption of target with recognition sequences to facilitate binding of proteins - Stable or transient expression of FP-tagged protein in cell needed - Labor intensive - Expensive - Optical properties of FP	Intracellular detection of specific polynucleotides in specific cell compartment	All available fluorescent proteins. Mostly (E)GFP	*113*, *150*

Polynucleotides such as pDNA and mRNA are prominently negative due to the anionic charge at the phosphate group of each nucleotide in the polymer sequence. Polynucleotides can be directly delivered into the cytoplasm or nucleus of the cells by microinjection or electroporation. They are however most frequently complexed with positively charged carriers to enable cellular uptake of the (net positive) complexes that are formed. These complexes are taken up by endocytosis, after which they should escape the endosomal compartment to prevent lysosomal degradation. Finally, the complexes should release their cargo into the cytoplasm (mRNA) or nucleus (pDNA) of the cells. [162, 163]

The different steps of the intracellular delivery path contribute to the overall observation that polynucleotide delivery is rather inefficient, especially when nonviral nucleic acid delivery is concerned. Therefore, each step of the intracellular trafficking has been the subject of intensive investigation over the past years. Hereby, fluorescence microscopy remains the most widely applied tool to gather information, going from more common wide field or confocal fluorescence microscopy setups to more advanced instrumentation such as spinning disk microscopy, single particle tracking, fluorescence correlation spectroscopy and super resolution microscopy. [164-167]

The choice of labeling technique needs to be incorporated early in experimental design, at the same time the microscopy method, cell line, transfection method, and type of polynucleotide (mRNA or pDNA) are chosen. Several aspects have to be considered when choosing a labeling strategy for mRNA and pDNA, such as the need for single versus dual color labeling, random versus sequence-specific labeling, labeling of the polynucleotides during *in vitro* synthesis, or intracellular (in situ) labeling. The ease and cost of the labeling procedure is also a factor to consider.

When complexing fluorescently labeled polynucleotides with nonlabeled carriers, for example, single-colored complexes are formed. These single-colored complexes can be used to follow, for example, intracellular uptake and endosomal escape, as well as the intracellular location of the (fluorescent) nucleic acids. Also, the colocalization of (e.g. red) complexes with GFP-tagged (green) endosomal vesicles could be performed. [40, 165] One should always keep in mind, however, that the fate of the nonlabeled complexation partner cannot be followed in this experimental setup. Moreover, certain carriers such as PEI have the tendency to

quench fluorescence upon complexation. In that case, fluorescence will only return once the polynucleotides have dissociated from their carrier. This principle was elegantly explored to develop an endosomal escape assay based on the (de)quenching of small oligonucleotide fragments. [168] By simultaneously labeling different types of endosomal vesicles, the specific type of endosomes from which complexes are preferentially released has been recently identified. [169] Apart from single color-labeling, both the carrier and nucleic acids can be labeled with spectrally separated fluorophores to obtain dual-colored complexes. [170] In this way, both parts of the delivery complex can be tracked before and after dissociation of the nucleic acids from the carriers. Dual-labeling of the polynucleotides themselves is also an interesting option to monitor their stability in the intracellular environment, as discussed below.

The choice between random and sequence-specific labeling of polynucleotides will largely depend on the biological application under investigation. Random labeling frequently results in more fluorophores per polynucleotide, generating brighter polynucleotides and complexes (until quenching occurs) suited for use with basic fluorescence microscopes. The two fast and easy options for random labeling are intercalation and covalent attachment of probes. After endosomal escape, however, intercalating dyes hold the risk of redistribution to endogenous nucleic acids in the cytoplasm or nucleus of the cells. Random covalent attachment of fluorophores to polynucleotides, on the other hand, has been proven to interfere with the endosomal escape and transcription/translation properties of the labeled polynucleotides themselves. Therefore, both labeling methods are best suited to follow the first two steps (cellular uptake and identification of endosomal vesicles) of the transfection pathway.

Whenever the random presence of dyes on the polynucleotide backbone holds a risk of disturbing the natural function of the polynucleotides, sequence-specific labeling can be preferred. Both for mRNA and pDNA, target sequences can be chosen outside the coding region. While linear oligos, MBs and binary probes can in theory make use of the natural primary sequence of the polynucleotides, plasmids for sequence-specific labeling are mostly designed to contain a known number of target repeats to ensure sufficient and specific binding. Alternatively, recognition site arrays for enzymatic labeling can be incorporated at the location of choice. An elegant application of sequence-specific labeling of polynucleotides is the spatially separated

double labeling. [104] This allows the coding region to be flanked with, for example, a green and a red fluorophore, which can be of interest to monitor the stability of polynucleotides. Indeed, as long as the polynucleotides remain intact, the green and red color will colocalize. As soon as backbone degradation occurs the colocalization is expected to disappear. Despite many possible experimental designs, the disadvantage of the sequence-specific labeling methods remains the need to custom order and design your polynucleotide of interest. This requires the preparation, isolation, and quality control of cloned pDNA vectors, which might be a challenge for researchers with a limited biotechnology background. It should be noted that, for mRNA stability testing, 5' and 3' end labeling of the synthesized mRNA can also be considered, overcoming the need to incorporate recognition sequences into the template DNA used to prepare mRNA.

The labeling of polynucleotides during synthesis is an option that is of interest when fluorescently labeled mRNA molecules are desired. Indeed, the *in vitro* synthesis of mRNA is a routine method to prepare mRNA from a DNA template. Nonmodified NTPs are frequently replaced by modified nonfluorescent NTPs in the reaction mixture to yield more stable and less immunogenic mRNA. [171] The addition of labeled NTPs to prepare fluorescent mRNA is thus a slight and easy adaptation of the normal protocols. Also, fluorescent cap analogues are available for 5' end labeling. [172] 3' End labeling, on the other hand, would require fluorophore addition to the mRNA poly-A tail.

A final consideration to be made is the added value of using an in situ labeling method. For the detection of endogenously synthesized polynucleotides, in situ labeling is obviously the only suitable method to ensure intracellular detection. In situ labeling of exogenously delivered polynucleotides could also be an interesting option to visualize the polynucleotides only after reaching the cytoplasm or nucleus of the cells. This would allow detection of endosomal escape events of initially nonlabeled polynucleotides, ensuring that the labeling strategy cannot interfere with the escape process. The three possible methods for in situ labeling are the use of molecular beacons, nucleic acid-binding small molecules, or the nucleic acid binding proteins. Molecular beacons have the advantage of employing a light-up principle, thereby limiting any fluorescent background signal. The use of organic dyes also increases their brightness and photostability, compared to fluorescent proteins. A substantial disadvantage of these molecular beacons is the need for a delivery method since

they are essentially (modified) oligonucleotides, which will not spontaneously reach the cytoplasm of cells. Mechanical methods like microinjection, electroporation, and bioballistics as well as chemical methods like toxin-mediated cell membrane permeabilization, liposomes, and polyplexes are possible strategies. [173-175] The nucleic-acid binding small molecules have the advantage of MBs in their use of organic dyes while being spontaneously taken up by cells. The need for an in depth knowledge of the polyamide conjugate chemistry, cost, and the limitations in sequences that can be specifically recognized limits their application by a broader audience. For in situ labeling with nucleic acid-binding proteins, the fact that one molecule of coding DNA/mRNA leads to multiple functional proteins is an advantage when compared to the large amount of MBs and polyamide conjugates that need to be present for a good reporter signal. To accomplish this, however, the target cells need a transient or stable expression of nucleic-acid binding proteins, which might be experimentally challenging. Furthermore, extra toxicity or cell stress that might influence the intracellular path of the polynucleotides under investigation might be induced.

It should be noted that apart from coupling fluorophores and haptens to polynucleotides, the label-free detection of polynucleotides is also gaining attention. The biggest advantage is that the use of bulky fluorophores or haptens is avoided, by employing the molecule's own chemical fingerprint for visualization. Interestingly, label-free detection can occur over a long time, since photobleaching, which is an important bottleneck in live-cell imaging, is no issue anymore. Raman scattering is one of those promising techniques that might be used to visualize nucleic acids. [176] Alkyne-bearing nucleotides were, for example, used to visualize DNA and RNA synthesis *in vivo* by stimulated Raman spectroscopy. [177] This principle might be extended to a priori labeling, making this an interesting option for the future.

CONCLUSION

In this chapter, we aimed for an overview of different labeling strategies for adding fluorophores or haptens to polynucleotides such as pDNA and mRNA. Also, some considerations on how to evaluate the compatibility of a certain labeling technique for tracking polynucleotides in the context of nonviral gene delivery were made. It is clear that more than one labeling strategy might be suited for a given application. Then, ease of operation, cost, and compatibility of the possible fluorophores with the research instrumentation will be valuable extra concerns to determine the preferred labeling option. Obviously, one should always carefully evaluate if the labeling method and labeling density of choice is not interfering with the process under investigation, relative to a nonlabeled control. It is expected that the continuous development of advanced microscopy methods will further shape the future of polynucleotide labeling strategies. One exciting new application, for example, is the label-free detection of molecules, which is being explored in a broad range of fields. Undeniably, live cell imaging will continue to play an important role in unraveling intracellular mysteries, creating a step-by-step insight in (and possible optimization of) the polynucleotide delivery pathways.

REFERENCES

(1) Stokes, G. G. (1852) On the Change of Refrangibility of Light. *Philosophical Transactions of the Royal Society of London 142*, 463-562.

(2) Abbe, E. (1873) Beiträge zur Theorie des Mikroskops und der mikroskopischen Wahrnehmung. *Archiv für mikroskopische Anatomie 9*, 413-418.

(3) Ploem, J. (1967) The use of a vertical illuminator with interchangeable dichroic mirrors for fluorescence microscopy with incident light. *Zeitschrift fur wissenschaftliche Mikroskopie und mikroskopische Technik 68*, 129-142.

(4) Kasten, F. H. (1989) The origins of modern fluorescence microscopy and fluorescent probes. *Cell structure and function by microspectrofluorometry*, 3-50.

(5) Masters, B. R. (2001) The Development of Fluorescence Microscopy, in *eLS*, John Wiley & Sons, Ltd.

(6) Vercauteren, D., Rejman, J., Martens, T., Demeester, J., De Smedt, S., and Braeckmans, K. (2012) On the cellular processing of non-viral nanomedicines for nucleic acid delivery: mechanisms and methods. *Journal of Controlled Release 161*, 566-581.

(7) Cosa, G., Focsaneanu, K. S., McLean, J. R. N., McNamee, J. P., and Scaiano, J. C. (2001) Photophysical Properties of Fluorescent DNA-dyes Bound to Single- and Double-stranded DNA in Aqueous Buffered Solution¶. *Photochemistry and Photobiology 73*, 585-599.

(8) Kanony, C., Åkerman, B., and Tuite, E. (2001) Photobleaching of Asymmetric Cyanines Used for Fluorescence Imaging of Single DNA Molecules. *Journal of the American Chemical Society 123*, 7985-7995.

(9) Martin, R. M., Leonhardt, H., and Cardoso, C. M. (2005) DNA labeling in living cells. *Cytometry Part A 67A*, 45-52.

(10) Selvin, P. R., and Hearst, J. E. (1994) Luminescence energy transfer using a terbium chelate: improvements on fluorescence energy transfer. *Proceedings of the National Academy of Sciences 91*, 10024-10028.

(11) Fernández-Moreira, V., Thorp-Greenwood, F. L., and Coogan, M. P. (2010) Application of d6 transition metal complexes in fluorescence cell imaging. *Chemical Communications 46*, 186-202.

(12) Grabolle, M., Ziegler, J., Merkulov, A., Nann, T., and Resch-Genger, U. (2008) Stability and fluorescence quantum yield of CdSe–ZnS quantum dots—influence of the thickness of the ZnS shell. *Annals of the New York Academy of Sciences 1130*, 235-241.

(13) Slattum, P. (2003) Efficient in vitro and in vivo expression of covalently modified plasmid DNA. *Molecular Therapy 8*.

(14) Daniel, S. G., Westling, M. E., Moss, M. S., and Kanagy, B. D. (1998) FastTag nucleic acid labeling system: a versatile method for incorporating haptens, fluorochromes and affinity ligands into DNA. *RNA and oligonucleotides. Biotechniques 24*, 484-489.

(15) van Gijlswijk, R. P. M., Talman, E. G., Janssen, P. J. A., Snoeijers, S. S., Killian, J., Tanke, H. J., and Heetebrijl, R. J. (2001) Universal Linkage System: versatile nucleic acid labeling technique. *Expert Review of Molecular Diagnostics 1*, 81-91.

(16) Mukherjee, A., Lavery, R., Bagchi, B., and Hynes, J. T. (2008) On the Molecular Mechanism of Drug Intercalation into DNA: A Simulation Study of

the Intercalation Pathway, Free Energy, and DNA Structural Changes. *Journal of the American Chemical Society 130*, 9747-9755.

(17) Murade, C., Subramaniam, V., Otto, C., and Bennink, M. L. (2009) Interaction of oxazole yellow dyes with DNA studied with hybrid optical tweezers and fluorescence microscopy. *Biophysical journal 97*, 835-843.

(18) Dragan, A. I., Casas-Finet, J. R., Bishop, E. S., Strouse, R. J., Schenerman, M. A., and Geddes, C. D. (2010) Characterization of PicoGreen Interaction with dsDNA and the Origin of Its Fluorescence Enhancement upon Binding. *Biophysical Journal 99*, 3010-3019.

(19) Armitage, B. (2005) Cyanine Dye–DNA Interactions: Intercalation, Groove Binding, and Aggregation, in *DNA Binders and Related Subjects* pp 55-76, Springer Berlin Heidelberg.

(20) Nelson, S. M., Ferguson, L. R., and Denny, W. A. (2007) Non-covalent ligand/DNA interactions: Minor groove binding agents. *Mutation Research/Fundamental and Molecular Mechanisms of Mutagenesis 623*, 24-40.

(21) Japaridze, A., Benke, A., Renevey, S., Benadiba, C., and Dietler, G. (2015) Influence of DNA Binding Dyes on Bare DNA Structure Studied with Atomic Force Microscopy. *Macromolecules 48*, 1860-1865.

(22) Neto, B., and Lapis, A. (2009) Recent Developments in the Chemistry of Deoxyribonucleic Acid (DNA) Intercalators: Principles, Design, Synthesis, Applications and Trends. *Molecules 14*, 1725.

(23) Rye, H. S., Yue, S., Wemmer, D. E., Quesada, M. A., Haugland, R. P., Mathies, R. A., and Glazer, A. N. (1992) Stable fluorescent complexes of double-stranded DNA with bis-intercalating asymmetric cyanine dyes: properties and applications. *Nucleic Acids Research 20*, 2803-2812.

(24) Montgomery, C. P., Murray, B. S., New, E. J., Pal, R., and Parker, D. (2009) Cell-Penetrating Metal Complex Optical Probes: Targeted and Responsive Systems Based on Lanthanide Luminescence. *Accounts of Chemical Research 42*, 925-937.

(25) Nojima, T., Kondoh, Y., Takenaka, S., Ichihara, T., Takagi, M., Tashiro, H., and Matsumoto, K. (2001) in *Nucleic acids symposium series* pp 105-106, Oxford University Press.

(26) Baggaley, E., Weinstein, J. A., and Williams, J. A. G. (2012) Lighting the way to see inside the live cell with luminescent transition metal complexes. *Coordination Chemistry Reviews 256*, 1762-1785.

(27) Jennette, K. W., Lippard, S. J., Vassiliades, G. A., and Bauer, W. R. (1974) Metallointercalation Reagents. 2-Hydroxyethanethiolato(2,2′,2″-terpyridine)-platinum(II) Monocation Binds Strongly to DNA By Intercalation. *Proceedings of the National Academy of Sciences of the United States of America 71*, 3839-3843.

(28) Lincoln, P., and Nordén, B. (1998) DNA Binding Geometries of Ruthenium(II) Complexes with 1,10-Phenanthroline and 2,2‘-Bipyridine Ligands Studied with Linear Dichroism Spectroscopy. Borderline Cases of Intercalation. *The Journal of Physical Chemistry B 102*, 9583-9594.

(29) Glover, P. B., Ashton, P. R., Childs, L. J., Rodger, A., Kercher, M., Williams, R. M., De Cola, L., and Pikramenou, Z. (2003) Hairpin-Shaped Heterometallic Luminescent Lanthanide Complexes for DNA Intercalative Recognition. *Journal of the American Chemical Society 125*, 9918-9919.

(30) Sanchez, E. L., Carroll, P. A., Thalhofer, A. B., and Lagunoff, M. (2015) Latent KSHV Infected Endothelial Cells Are Glutamine Addicted and Require Glutaminolysis for Survival. *PLoS Pathogens 11*, e1005052.
(31) Flors, C. (2011) DNA and chromatin imaging with super-resolution fluorescence microscopy based on single-molecule localization. *Biopolymers 95*, 290-297.
(32) Benke, A., and Manley, S. (2012) Live-Cell dSTORM of Cellular DNA Based on Direct DNA Labeling. *ChemBioChem 13*, 298-301.
(33) Åkerman, B., and Tuite, E. (1996) Single- and Double-Strand Photocleavage of DNA by YO, YOYO and TOTO. *Nucleic Acids Research 24*, 1080-1090.
(34) Kundukad, B., Yan, J., and Doyle, P. S. (2014) Effect of YOYO-1 on the mechanical properties of DNA. *Soft Matter 10*, 9721-9728.
(35) Meng, X., Cai, W., and Schwartz, D. C. (1996) Inhibition of Restriction Endonuclease Activity by DNA Binding Fluorochromes. *Journal of Biomolecular Structure and Dynamics 13*, 945-951.
(36) Rombouts, K., Martens, T. F., Zagato, E., Demeester, J., De Smedt, S. C., Braeckmans, K., and Remaut, K. (2014) Effect of Covalent Fluorescence Labeling of Plasmid DNA on Its Intracellular Processing and Transfection with Lipid-Based Carriers. *Molecular Pharmaceutics 11*, 1359-1368.
(37) Gasiorowski, J. Z., and Dean, D. A. (2005) Postmitotic nuclear retention of episomal plasmids is altered by DNA labeling and detection methods. *Molecular therapy 12*, 460-467.
(38) Akita, H., Enoto, K., Tanaka, H., and Harashima, H. (2013) Particle Tracking Analysis for the Intracellular Trafficking of Nanoparticles Modified with African Swine Fever Virus Protein p54-derived Peptide. *Molecular Therapy 21*, 309-317.
(39) von Gersdorff, K., Sanders, N. N., Vandenbroucke, R., De Smedt, S. C., Wagner, E., and Ogris, M. (2006) The Internalization Route Resulting in Successful Gene Expression Depends on both Cell Line and Polyethylenimine Polyplex Type. *Molecular Therapy 14*, 745-753.
(40) Vercauteren, D., Piest, M., van der Aa, L. J., Al Soraj, M., Jones, A. T., Engbersen, J. F., De Smedt, S. C., and Braeckmans, K. (2011) Flotillin-dependent endocytosis and a phagocytosis-like mechanism for cellular internalization of disulfide-based poly(amido amine)/DNA polyplexes. *Biomaterials 32*, 3072-3084.
(41) Oba, M., Fukushima, S., Kanayama, N., Aoyagi, K., Nishiyama, N., Koyama, H., and Kataoka, K. (2007) Cyclic RGD Peptide-Conjugated Polyplex Micelles as a Targetable Gene Delivery System Directed to Cells Possessing αvβ3 and αvβ5 Integrins. *Bioconjugate Chemistry 18*, 1415-1423.
(42) Majzoub, R. N., Chan, C.-L., Ewert, K. K., Silva, B. F. B., Liang, K. S., Jacovetty, E. L., Carragher, B., Potter, C. S., and Safinya, C. R. (2014) Uptake and transfection efficiency of PEGylated cationic liposome–DNA complexes with and without RGD-tagging. *Biomaterials 35*, 4996-5005.
(43) Seow, W. Y., Yang, Y.-Y., and George, A. J. T. (2009) Oligopeptide-mediated gene transfer into mouse corneal endothelial cells: expression, design optimization, uptake mechanism and nuclear localization. *Nucleic Acids Research 37*, 6276-6289.
(44) Harris, T. J., Green, J. J., Fung, P. W., Langer, R., Anderson, D. G., and Bhatia, S. N. (2010) Tissue-specific gene delivery via nanoparticle coating. *Biomaterials 31*, 998-1006.

(45) Grosse, S., Thévenot, G., Aron, Y., Duverger, E., Abdelkarim, M., Roche, A.-C., Monsigny, M., and Fajac, I. (2008) In vivo gene delivery in the mouse lung with lactosylated polyethylenimine, questioning the relevance of in vitro experiments. *Journal of Controlled Release 132*, 105-112.

(46) Bieber, T., Meissner, W., Kostin, S., Niemann, A., and Elsasser, H.-P. (2002) Intracellular route and transcriptional competence of polyethylenimine–DNA complexes. *Journal of Controlled Release 82*, 441-454.

(47) Arima, H., Chihara, Y., Arizono, M., Yamashita, S., Wada, K., Hirayama, F., and Uekama, K. (2006) Enhancement of gene transfer activity mediated by mannosylated dendrimer/α-cyclodextrin conjugate (generation 3, G3). *Journal of Controlled Release 116*, 64-74.

(48) Nakamura, K., Miyazato, A., Xiao, G., Hatta, M., Inden, K., Aoyagi, T., Shiratori, K., Takeda, K., Akira, S., Saijo, S., et al. (2008) Deoxynucleic Acids from Cryptococcus neoformans Activate Myeloid Dendritic Cells via a TLR9-Dependent Pathway. *The Journal of Immunology 180*, 4067-4074.

(49) Studier, F. W., and Moffatt, B. A. (1986) Use of bacteriophage T7 RNA polymerase to direct selective high-level expression of cloned genes. *Journal of Molecular Biology 189*, 113-130.

(50) Melton, D., Krieg, P., Rebagliati, M., Maniatis, T., Zinn, K., and Green, M. (1984) Efficient in vitro synthesis of biologically active RNA and RNA hybridization probes from plasmids containing a bacteriophage SP6 promoter. *Nucleic Acids Research 12*, 7035-7056.

(51) Milligan, J. F., Groebe, D. R., Witherell, G. W., and Uhlenbeck, O. C. (1987) Oligoribonucleotide synthesis using T7 RNA polymerase and synthetic DNA templates. *Nucleic acids research 15*, 8783-8798.

(52) Rigby, P. W. J., Dieckmann, M., Rhodes, C., and Berg, P. (1977) Labeling deoxyribonucleic acid to high specific activity in vitro by nick translation with DNA polymerase I. *Journal of Molecular Biology 113*, 237-251.

(53) Luzzietti, N., Knappe, S., Richter, I., and Seidel, R. (2012) Nicking enzyme-based internal labeling of DNA at multiple loci. *Nature Protocols 7*, 643-653.

(54) Roychoudhury, R., Jay, E., and Wu, R. (1976) Terminal labeling and addition of homopolymer tracts to duplex DNA fragments by terminal deoxynucleotidyl transferase. *Nucleic Acids Research 3*, 863-878.

(55) Kumar, A., Tchen, P., Roullet, F., and Cohen, J. (1988) Nonradioactive labeling of synthetic oligonucleotide probes with terminal deoxynucleotidyl transferase. *Analytical Biochemistry 169*, 376-382.

(56) Shimizu, N., Kamezaki, F., and Shigematsu, S. (2005) Tracking of microinjected DNA in live cells reveals the intracellular behavior and elimination of extrachromosomal genetic material. *Nucleic acids research 33*, 6296-307.

(57) Kim, J., Lim, S., Lee, Y., Shin, Y., Chung, C., Yoo, J., and Chang, J. (2004) in *Proceedings of the NSTI Nanotechnology Conference and Trade Show* pp 379-382.

(58) Winz, M.-L., Linder, E. C., André, T., Becker, J., and Jäschke, A. (2015) Nucleotidyl transferase assisted DNA labeling with different click chemistries. *Nucleic Acids Research gkv544*.

(59) Nickols, N. G., Jacobs, C. S., Farkas, M. E., and Dervan, P. B. (2007) Improved nuclear localization of DNA-binding polyamides. *Nucleic Acids Research 35*, 363-370.

(60) Pljevaljčić, G., Schmidt, F., and Weinhold, E. (2004) Sequence-specific Methyltransferase-Induced Labeling of DNA (SMILing DNA). *ChemBioChem*.
(61) Pljevaljcic, G., Pignot, M., and Weinhold, E. (2003) Design of a New Fluorescent Cofactor for DNA Methyltransferases and Sequence-Specific Labeling of DNA. *Journal of the American Chemical Society 125*, 3486-3492.
(62) Dalhoff, C., Lukinavicius, G., Klimasauskas, S., and Weinhold, E. (2006) Direct transfer of extended groups from synthetic cofactors by DNA methyltransferases. *Nature Chemical Biology 2*, 31-32.
(63) Lukinavičius, G., Lapinaitė, A., Urbanavičiūtė, G., Gerasimaitė, R., and Klimašauskas, S. (2012) Engineering the DNA cytosine-5 methyltransferase reaction for sequence-specific labeling of DNA. *Nucleic Acids Research 40*, 11594-11602.
(64) Motorin, Y., Burhenne, J., Teimer, R., Koynov, K., Willnow, S., Weinhold, E., and Helm, M. (2011) Expanding the chemical scope of RNA:methyltransferases to site-specific alkynylation of RNA for click labeling. *Nucleic Acids Research 39*, 1943-1952.
(65) Plotnikova, A., Osipenko, A., Masevičius, V., Vilkaitis, G., and Klimašauskas, S. (2014) Selective Covalent Labeling of miRNA and siRNA Duplexes Using HEN1 Methyltransferase. *Journal of the American Chemical Society 136*, 13550-13553.
(66) Lukinavičius, G., Lapienė, V., Staševskij, Z., Dalhoff, C., Weinhold, E., and Klimašauskas, S. (2007) Targeted Labeling of DNA by Methyltransferase-Directed Transfer of Activated Groups (mTAG). *Journal of the American Chemical Society 129*, 2758-2759.
(67) Gillingham, D., and Shahid, R. (2015) Catalysts for RNA and DNA modification. *Current Opinion in Chemical Biology 25*, 110-114.
(68) Schmidt, F. H. G., Hüben, M., Gider, B., Renault, F., Teulade-Fichou, M.-P., and Weinhold, E. (2008) Sequence-specific Methyltransferase-Induced Labelling (SMILing) of plasmid DNA for studying cell transfection. *Bioorganic & Medicinal Chemistry 16*, 40-48.
(69) Ramadan, M., Bremner-Hay, N. K., Carlson, S. A., and Comstock, L. R. (2014) Synthesis and evaluation of N6-substituted azide- and alkyne-bearing N-mustard analogs of S-adenosyl-l-methionine. *Tetrahedron 70*, 5291-5297.
(70) Neely, R. K., Dedecker, P., Hotta, J.-i., Urbanaviciute, G., Klimasauskas, S., and Hofkens, J. (2010) DNA fluorocode: A single molecule, optical map of DNA with nanometre resolution. *Chemical Science 1*, 453-460.
(71) Vranken, C., Deen, J., Dirix, L., Stakenborg, T., Dehaen, W., Leen, V., Hofkens, J., and Neely, R. K. (2014) Super-resolution optical DNA Mapping via DNA methyltransferase-directed click chemistry. *Nucleic Acids Research 42*, e50.
(72) Grunwald, A., Dahan, M., Giesbertz, A., Nilsson, A., Nyberg, L. K., Weinhold, E., Ambjörnsson, T., Westerlund, F., and Ebenstein, Y. (2015) Bacteriophage strain typing by rapid single molecule analysis. *Nucleic Acids Research*.
(73) Buske, F. A., Mattick, J. S., and Bailey, T. L. (2011) Potential in vivo roles of nucleic acid triple-helices. *RNA Biology 8*, 427-439.
(74) Zamecnik, P. C., and Stephenson, M. L. (1978) Inhibition of Rous sarcoma virus replication and cell transformation by a specific oligodeoxynucleotide. *Proceedings of the National Academy of Sciences 75*, 280-284.
(75) Langer-Safer, P. R., Levine, M., and Ward, D. C. (1982) Immunological method for mapping genes on Drosophila polytene chromosomes.

Proceedings of the National Academy of Sciences of the United States of America 79, 4381-4385.

(76) Gozzetti, A., and Le Beau, M. M. (2000) Fluorescence in situ hybridization: Uses and limitations. *Seminars in Hematology 37*, 320-333.

(77) Jensen, E. (2014) Technical Review: In Situ Hybridization. *The Anatomical Record 297*, 1349-1353.

(78) Milligan, J. F., Matteucci, M. D., and Martin, J. C. (1993) Current concepts in antisense drug design. *Journal of medicinal chemistry 36*, 1923-1937.

(79) De Mesmaeker, A., Altmann, K.-H., Waldner, A., and Wendeborn, S. (1995) Backbone modifications in oligonucleotides and peptide nucleic acid systems. *Current Opinion in Structural Biology 5*, 343-355.

(80) Nielsen, P., Egholm, M., Berg, R., and Buchardt, O. (1991) Sequence-selective recognition of DNA by strand displacement with a thymine-substituted polyamide. *Science 254*, 1497-1500.

(81) Egholm, M., Buchardt, O., Nielsen, P. E., and Berg, R. H. (1992) Peptide nucleic acids (PNA). Oligonucleotide analogs with an achiral peptide backbone. *Journal of the American Chemical Society 114*, 1895-1897.

(82) K. Singh, S., A. Koshkin, A., Wengel, J., and Nielsen, P. (1998) LNA (locked nucleic acids): synthesis and high-affinity nucleic acid recognition. *Chemical Communications*, 455-456.

(83) Cuenoud, B., Casset, F., Hüsken, D., Natt, F., Wolf, R. M., Altmann, K.-H., Martin, P., and Moser, H. E. (1998) Dual Recognition of Double-Stranded DNA by 2′-Aminoethoxy-Modified Oligonucleotides. *Angewandte Chemie International Edition 37*, 1288-1291.

(84) Puri, N., Majumdar, A., Cuenoud, B., Natt, F., Martin, P., Boyd, A., Miller, P. S., and Seidman, M. M. (2001) Targeted Gene Knockout by 2′-O-Aminoethyl Modified Triplex Forming Oligonucleotides. *Journal of Biological Chemistry 276*, 28991-28998.

(85) Nielsen, P. E., and Egholm, M. (1999) An introduction to peptide nucleic acid. *Current Issues in Molecular Biology*.

(86) Egholm, M., Christensen, L., Dueholm, K. L., Buchardt, O., Coull, J., and Nielsen, P. E. (1995) Efficient pH-independent sequence-specific DNA binding by pseudoisocytosine-containing bis-PNA. *Nucleic Acids Research 23*, 217-222.

(87) Koshkin, A. A., Rajwanshi, V. K., and Wengel, J. (1998) Novel convenient syntheses of LNA [2.2.1]bicyclo nucleosides. *Tetrahedron Letters 39*, 4381-4384.

(88) Obika, S., Nanbu, D., Hari, Y., Andoh, J., Morio, K., Doi, T., and Imanishi, T. (1998) Stability and structural features of the duplexes containing nucleoside analogues with a fixed N-type conformation, 2'-O,4'-C-methyleneribonucleosides. *Tetrahedron Letters 39*, 5401-5404.

(89) Obika, S., Uneda, T., Sugimoto, T., Nanbu, D., Minami, T., Doi, T., and Imanishi, T. (2001) 2′-O,4′-C-methylene bridged nucleic acid (2′,4′-BNA): synthesis and triplex-forming properties1. *Bioorganic & Medicinal Chemistry 9*, 1001-1011.

(90) Koizumi, M., Morita, K., Daigo, M., Tsutsumi, S., Abe, K., Obika, S., and Imanishi, T. (2003) Triplex formation with 2′-O,4′-C-ethylene-bridged nucleic acids (ENA) having C3′-endo conformation at physiological pH. *Nucleic Acids Research 31*, 3267-3273.

(91) Brunet, E., Alberti, P., Perrouault, L., Babu, R., Wengel, J., and Giovannangeli, C. (2005) Exploring Cellular Activity of Locked Nucleic Acid-modified Triplex-forming Oligonucleotides and Defining Its Molecular Basis. *Journal of Biological Chemistry 280*, 20076-20085.

(92) Moreno, P. M. D., Geny, S., Pabon, Y. V., Bergquist, H., Zaghloul, E. M., Rocha, C. S. J., Oprea, I. I., Bestas, B., Andaloussi, S. E., Jørgensen, P. T., et al. (2013) Development of bis-locked nucleic acid (bisLNA) oligonucleotides for efficient invasion of supercoiled duplex DNA. *Nucleic Acids Research 41*, 3257-3273.

(93) Knauert, M. P., and Glazer, P. M. (2001) Triplex forming oligonucleotides: sequence-specific tools for gene targeting. *Human Molecular Genetics 10*, 2243-2251.

(94) Seitz, O., Bergmann, F., and Heindl, D. (1999) A Convergent Strategy for the Modification of Peptide Nucleic Acids: Novel Mismatch-Specific PNA-Hybridization Probes. *Angewandte Chemie International Edition 38*, 2203-2206.

(95) Englund, E. A., and Appella, D. H. (2005) Synthesis of γ-Substituted Peptide Nucleic Acids: A New Place to Attach Fluorophores without Affecting DNA Binding. *Organic Letters 7*, 3465-3467.

(96) Ørum, H., Nielsen, P. E., Egholm, M., Berg, R. H., Buchardt, O., and Stanley, C. (1993) Single base pair mutation analysis by PNA directed PCR clamping. *Nucleic Acids Research 21*, 5332-5336.

(97) Lansdorp, P. M., Verwoerd, N. P., van de Rijke, F. M., Dragowska, V., Little, M.-T., Dirks, R. W., Raap, A. K., and Tanke, H. J. (1996) Heterogeneity in Telomere Length of Human Chromosomes. *Human Molecular Genetics 5*, 685-691.

(98) Silahtaroglu, A. N., Tommerup, N., and Vissing, H. (2003) FISHing with locked nucleic acids (LNA): evaluation of different LNA/DNA mixmers. *Molecular and Cellular Probes 17*, 165-169.

(99) Molenaar, C., Wiesmeijer, K., Verwoerd, N. P., Khazen, S., Eils, R., Tanke, H. J., and Dirks, R. W. (2003) Visualizing telomere dynamics in living mammalian cells using PNA probes. *22*, 6631-6641.

(100) McNeil, P. L., and Warder, E. (1987) Glass beads load macromolecules into living cells. *Journal of Cell Science 88*, 669-678.

(101) Molenaar, C., Abdulle, A., Gena, A., Tanke, H. J., and Dirks, R. W. (2004) Poly(A)(+) RNAs roam the cell nucleus and pass through speckle domains in transcriptionally active and inactive cells. *The Journal of Cell Biology 165*, 191-202.

(102) Zelphati, O., Liang, X., Hobart, P., and Felgner, P. L. (1999) Gene Chemistry: Functionally and Conformationally Intact Fluorescent Plasmid DNA. *Human Gene Therapy 10*, 15-24.

(103) Srinivasan, C., Lee, J., Papadimitrakopoulos, F., Silbart, L. K., Zhao, M., and Burgess, D. J. (2006) Labeling and Intracellular Tracking of Functionally Active Plasmid DNA with Semiconductor Quantum Dots. *Molecular Therapy 14*, 192-201.

(104) Srinivasan, C., Siddiqui, S., Silbart, L. K., Papadimitrakopoulos, F., and Burgess, D. J. (2009) Dual Fluorescent Labeling Method to Visualize Plasmid DNA Degradation. *Bioconjugate Chemistry 20*, 163-169.

(105) Lampela, P., Soininen, P., Puttonen, K. A., Ruponen, M., Urtti, A., Männistö, P. T., and Raasmaja, A. (2004) Effect of cell-surface glycosaminoglycans on

cationic carrier combined with low-MW PEI-mediated gene transfection. *International Journal of Pharmaceutics 284*, 43-52.
(106) Seferos, D. S., Giljohann, D. A., Hill, H. D., Prigodich, A. E., and Mirkin, C. A. (2007) Nano-Flares: Probes for Transfection and mRNA Detection in Living Cells. *Journal of the American Chemical Society 129*, 15477-15479.
(107) Briley, W. E., Halo, T. L., Randeria, P. S., Alhasan, A. H., Auyeung, E., Hurst, S. J., and Mirkin, C. A. (2012) Biochemistry and Biomedical Applications of Spherical Nucleic Acids (SNAs), in *Nanomaterials for Biomedicine* pp 1-20, American Chemical Society.
(108) Briley, W. E., Bondy, M. H., Randeria, P. S., Dupper, T. J., and Mirkin, C. A. (2015) Quantification and real-time tracking of RNA in live cells using Sticky-flares. *Proceedings of the National Academy of Sciences 112*, 9591-9595.
(109) Tyagi, S., and Kramer, F. R. (1996) Molecular Beacons: Probes that Fluoresce upon Hybridization. *Nature biotechnology 14*, 303-308.
(110) Wang, K., Tang, Z., Yang, C. J., Kim, Y., Fang, X., Li, W., Wu, Y., Medley, C. D., Cao, Z., Li, J., et al. (2009) Molecular Engineering of DNA: Molecular Beacons. *Angewandte Chemie International Edition 48*, 856-870.
(111) Santangelo, P. J. (2010) Molecular beacons and related probes for intracellular RNA imaging. *Wiley Interdisciplinary Reviews: Nanomedicine and Nanobiotechnology 2*, 11-19.
(112) Ortiz, E., Estrada, G., and Lizardi, P. (1998) PNA molecular beacons for rapid detection of PCR amplicons. *Molecular and cellular probes 12*, 219-226.
(113) Tyagi, S. (2009) Imaging intracellular RNA distribution and dynamics in living cells. *Nature Methods 6*, 331-338.
(114) Santangelo, P. J., Nix, B., Tsourkas, A., and Bao, G. (2004) Dual FRET molecular beacons for mRNA detection in living cells. *Nucleic Acids Research 32*, e57.
(115) Okamoto, A. (2011) ECHO probes: a concept of fluorescence control for practical nucleic acid sensing. *Chemical Society Reviews 40*, 5815-5828.
(116) Kuhn, H., Demidov, V. V., Coull, J. M., Fiandaca, M. J., Gildea, B. D., and Frank-Kamenetskii, M. D. (2002) Hybridization of DNA and PNA molecular beacons to single-stranded and double-stranded DNA targets. *Journal of the American Chemical Society 124*, 1097-1103.
(117) Heyduk, T., and Heyduk, E. (2002) Molecular beacons for detecting DNA binding proteins. *Nature biotechnology 20*, 171-176.
(118) Li, J. J., Fang, X., Schuster, S. M., and Tan, W. (2000) Molecular beacons: a novel approach to detect protein–DNA interactions. *Angewandte Chemie International Edition 39*, 1049-1052.
(119) Sato, S. i., Watanabe, M., Katsuda, Y., Murata, A., Wang, D. O., and Uesugi, M. (2015) Live-Cell Imaging of Endogenous mRNAs with a Small Molecule. *Angewandte Chemie 127*, 1875-1878.
(120) Paige, J. S., Wu, K. Y., and Jaffrey, S. R. (2011) RNA Mimics of Green Fluorescent Protein. *Science 333*, 642-646.
(121) Strack, R. L., Disney, M. D., and Jaffrey, S. R. (2013) A superfolding Spinach2 reveals the dynamic nature of trinucleotide repeat-containing RNA. *Nature Methods 10*, 1219-1224.
(122) Dolgosheina, E. V., Jeng, S. C. Y., Panchapakesan, S. S. S., Cojocaru, R., Chen, P. S. K., Wilson, P. D., Hawkins, N., Wiggins, P. A., and Unrau, P. J. (2014) RNA Mango Aptamer-Fluorophore: A Bright, High-Affinity Complex for RNA Labeling and Tracking. *ACS Chemical Biology 9*, 2412-2420.

(123) Guo, J., Ju, J., and Turro, N. J. (2012) Fluorescent hybridization probes for nucleic acid detection. *Analytical and bioanalytical chemistry 402*, 3115-3125.
(124) Wittwer, C. T., Herrmann, M. G., Moss, A. A., and Rasmussen, R. P. (1997) Continuous fluorescence monitoring of rapid cycle DNA amplification. *Biotechniques 22*, 130-139.
(125) Lyon, E., and Wittwer, C. T. (2009) LightCycler technology in molecular diagnostics. *The Journal of Molecular Diagnostics 11*, 93-101.
(126) Kolpashchikov, D. M. (2010) Binary probes for nucleic acid analysis. *Chemical reviews 110*, 4709-4723.
(127) Marti, A. A., Puckett, C. A., Dyer, J., Stevens, N., Jockusch, S., Ju, J., Barton, J. K., and Turro, N. J. (2007) Inorganic-organic hybrid luminescent binary probe for DNA detection based on spin-forbidden resonance energy transfer. *Journal of the American Chemical Society 129*, 8680-8681.
(128) Kitamura, Y., Ihara, T., Tsujimura, Y., Tazaki, M., and Jyo, A. (2005) DNA-templated cooperative formation of the luminous lanthanide complex and its analytical application to gene detection. *Chemistry Letters 34*, 1606-1607.
(129) Kitamura, Y., Ihara, T., Tsujimura, Y., Osawa, Y., Sasahara, D., Yamamoto, M., Okada, K., Tazaki, M., and Jyo, A. (2008) Template-directed formation of luminescent lanthanide complexes: Versatile tools for colorimetric identification of single nucleotide polymorphism. *Journal of inorganic biochemistry 102*, 1921-1931.
(130) Silverman, A. P., and Kool, E. T. (2006) Detecting RNA and DNA with templated chemical reactions. *Chemical reviews 106*, 3775-3789.
(131) Silverman, A. P., and Kool, E. T. (2007) Oligonucleotide Probes for RNA-Targeted Fluorescence In Situ Hybridization. *Advances in clinical chemistry 43*, 79-115.
(132) Kleinbaum, D. J., and Kool, E. T. (2010) Sandwich probes: two simultaneous reactions for templated nucleic acid detection. *Chemical Communications 46*, 8154-8156.
(133) Franzini, R. M., and Kool, E. T. (2009) Efficient Nucleic Acid Detection by Templated Reductive Quencher Release. *Journal of the American Chemical Society 131*, 16021-16023.
(134) Pianowski, Z., Gorska, K., Oswald, L., Merten, C. A., and Winssinger, N. (2009) Imaging of mRNA in Live Cells Using Nucleic Acid-Templated Reduction of Azidorhodamine Probes. *Journal of the American Chemical Society 131*, 6492-6497.
(135) Zhang, X., Zajac, A. L., Huang, L., Behlke, M. A., and Tsourkas, A. (2014) Imaging the Directed Transport of Single Engineered RNA Transcripts in Real-Time Using Ratiometric Bimolecular Beacons. *PLoS ONE 9*, e85813.
(136) Dervan, P. B. (2001) Molecular recognition of DNA by small molecules. *Bioorganic & Medicinal Chemistry 9*, 2215-2235.
(137) Rucker, V. C., Foister, S., Melander, C., and Dervan, P. B. (2003) Sequence Specific Fluorescence Detection of Double Strand DNA. *Journal of the American Chemical Society 125*, 1195-1202.
(138) Crowley, K. S., Phillion, D. P., Woodard, S. S., Schweitzer, B. A., Singh, M., Shabany, H., Burnette, B., Hippenmeyer, P., Heitmeier, M., and Bashkin, J. K. (2003) Controlling the intracellular localization of fluorescent polyamide analogues in cultured cells. *Bioorganic & Medicinal Chemistry Letters 13*, 1565-1570.

(139) Nishijima, S., Shinohara, K.-i., Bando, T., Minoshima, M., Kashiwazaki, G., and Sugiyama, H. (2010) Cell permeability of Py–Im-polyamide-fluorescein conjugates: Influence of molecular size and Py/Im content. *Bioorganic & Medicinal Chemistry 18*, 978-983.
(140) Vaijayanthi, T., Bando, T., Pandian, G. N., and Sugiyama, H. (2012) Progress and Prospects of Pyrrole-Imidazole Polyamide–Fluorophore Conjugates as Sequence-Selective DNA Probes. *ChemBioChem 13*, 2170-2185.
(141) Nakamura, A., Takigawa, K., Kurishita, Y., Kuwata, K., Ishida, M., Shimoda, Y., Hamachi, I., and Tsukiji, S. (2014) Hoechst tagging: a modular strategy to design synthetic fluorescent probes for live-cell nucleus imaging. *Chemical Communications 50*, 6149-6152.
(142) Nozeret, K., Loll, F., Escudé, C., and Boutorine, A. S. (2015) Polyamide Fluorescent Probes for Visualization of Repeated DNA Sequences in Living Cells. *ChemBioChem 16*, 549-554.
(143) Han, Y.-W., Tsunaka, Y., Yokota, H., Matsumoto, T., Kashiwazaki, G., Morinaga, H., Hashiya, K., Bando, T., Sugiyama, H., and Harada, Y. (2014) Construction and characterization of Cy3-or Cy5-conjugated hairpin pyrrole–imidazole polyamides binding to DNA in the nucleosome. *Biomaterials Science 2*, 297-307.
(144) Gottesfeld, J. M., Neely, L., Trauger, J. W., Baird, E. E., and Dervan, P. B. (1997) Regulation of gene expression by small molecules. *Nature 387*, 202-205.
(145) Bertrand, E., Chartrand, P., Schaefer, M., Shenoy, S. M., Singer, R. H., and Long, R. M. (1998) Localization of ASH1 mRNA Particles in Living Yeast. *Molecular Cell 2*, 437-445.
(146) Chen, J., Nikolaitchik, O., Singh, J., Wright, A., Bencsics, C. E., Coffin, J. M., Ni, N., Lockett, S., Pathak, V. K., and Hu, W.-S. (2009) High efficiency of HIV-1 genomic RNA packaging and heterozygote formation revealed by single virion analysis. *Proceedings of the National Academy of Sciences of the United States of America 106*, 13535-13540.
(147) Daigle, N., and Ellenberg, J. (2007) [lambda]N-GFP: an RNA reporter system for live-cell imaging. *Nature Methods 4*, 633-636.
(148) Calapez, A., Pereira, H. M., Calado, A., Braga, J., Rino, J., Carvalho, C., Tavanez, J. P., Wahle, E., Rosa, A. C., and Carmo-Fonseca, M. (2002) The intranuclear mobility of messenger RNA binding proteins is ATP dependent and temperature sensitive. *The Journal of Cell Biology 159*, 795-805.
(149) Ozawa, T., Natori, Y., Sato, M., and Umezawa, Y. (2007) Imaging dynamics of endogenous mitochondrial RNA in single living cells. *Nature Methods 4*, 413-419.
(150) Bann, D. V., and Parent, L. J. (2012) Application of Live-Cell RNA Imaging Techniques to the Study of Retroviral RNA Trafficking. *Viruses 4*, 963-979.
(151) Lange, S., Katayama, Y., Schmid, M., Burkacky, O., Bräuchle, C., Lamb, D. C., and Jansen, R.-P. (2008) Simultaneous Transport of Different Localized mRNA Species Revealed by Live-Cell Imaging. *Traffic 9*, 1256-1267.
(152) Boireau, S., Maiuri, P., Basyuk, E., de la Mata, M., Knezevich, A., Pradet-Balade, B., Bäcker, V., Kornblihtt, A., Marcello, A., and Bertrand, E. (2007) The transcriptional cycle of HIV-1 in real-time and live cells. *The Journal of Cell Biology 179*, 291-304.
(153) Robinett, C. C., Straight, A., Li, G., Willhelm, C., Sudlow, G., Murray, A., and Belmont, A. S. (1996) In vivo localization of DNA sequences and visualization

of large-scale chromatin organization using lac operator/repressor recognition. *The Journal of Cell Biology 135*, 1685-1700.
(154) Annibale, P., and Gratton, E. (2015) Single cell visualization of transcription kinetics variance of highly mobile identical genes using 3D nanoimaging. *Scientific Reports 5*, 9258.
(155) Keppler, A., Gendreizig, S., Gronemeyer, T., Pick, H., Vogel, H., and Johnsson, K. (2003) A general method for the covalent labeling of fusion proteins with small molecules in vivo. *Nature biotechnology 21*, 86-89.
(156) Los, G. V., Encell, L. P., McDougall, M. G., Hartzell, D. D., Karassina, N., Zimprich, C., Wood, M. G., Learish, R., Ohana, R. F., Urh, M., et al. (2008) HaloTag: A Novel Protein Labeling Technology for Cell Imaging and Protein Analysis. *ACS Chemical Biology 3*, 373-382.
(157) Gebhardt, J. C. M., Suter, D. M., Roy, R., Zhao, Z. W., Chapman, A. R., Basu, S., Maniatis, T., and Xie, X. S. (2013) Single-molecule imaging of transcription factor binding to DNA in live mammalian cells. *Nature Methods 10*, 421-426.
(158) Bogdanove, A. J., and Voytas, D. F. (2011) TAL Effectors: Customizable Proteins for DNA Targeting. *Science 333*, 1843-1846.
(159) Gaj, T., Gersbach, C. A., and Barbas, C. F. (2013) ZFN, TALEN, and CRISPR/Cas-based methods for genome engineering. *Trends in biotechnology 31*, 397-405.
(160) Thanisch, K., Schneider, K., Morbitzer, R., Solovei, I., Lahaye, T., Bultmann, S., and Leonhardt, H. (2014) Targeting and tracing of specific DNA sequences with dTALEs in living cells. *Nucleic Acids Research 42*, e38.
(161) Boutorine, A. S., Novopashina, D. S., Krasheninina, O. A., Nozeret, K., and Venyaminova, A. G. (2013) Fluorescent probes for nucleic acid visualization in fixed and live cells. *Molecules 18*, 15357-15397.
(162) Wang, T., Upponi, J. R., and Torchilin, V. P. (2012) Design of multifunctional non-viral gene vectors to overcome physiological barriers: Dilemmas and strategies. *International Journal of Pharmaceutics 427*, 3-20.
(163) Lam, A., and Dean, D. (2010) Progress and prospects: nuclear import of nonviral vectors. *Gene therapy 17*, 439-447.
(164) Remaut, K., Lucas, B., Raemdonck, K., Braeckmans, K., Demeester, J., and De Smedt, S. (2007) Can we better understand the intracellular behavior of DNA nanoparticles by fluorescence correlation spectroscopy? *Journal of Controlled Release 121*, 49-63.
(165) Vercauteren, D., Deschout, H., Remaut, K., Engbersen, J. F., Jones, A. T., Demeester, J., De Smedt, S. C., and Braeckmans, K. (2011) Dynamic colocalization microscopy to characterize intracellular trafficking of nanomedicines. *ACS Nano 5*, 7874-7884.
(166) Sandin, P., Fitzpatrick, L. W., Simpson, J. C., and Dawson, K. A. (2012) High-speed imaging of Rab family small GTPases reveals rare events in nanoparticle trafficking in living cells. *ACS nano 6*, 1513-1521.
(167) Thomsen, P., Roepstorff, K., Stahlhut, M., and Van Deurs, B. (2002) Caveolae are highly immobile plasma membrane microdomains, which are not involved in constitutive endocytic trafficking. *Molecular biology of the cell 13*, 238-250.
(168) Rehman, Z. u., Hoekstra, D., and Zuhorn, I. S. (2013) Mechanism of Polyplex- and Lipoplex-Mediated Delivery of Nucleic Acids: Real-Time Visualization of Transient Membrane Destabilization without Endosomal Lysis. *ACS Nano 7*, 3767-3777.

(169) Wittrup, A., Ai, A., Liu, X., Hamar, P., Trifonova, R., Charisse, K., Manoharan, M., Kirchhausen, T., and Lieberman, J. (2015) Visualizing lipid-formulated siRNA release from endosomes and target gene knockdown. *Nature biotechnology 33*, 870-876.

(170) Ruponen, M., Rönkkö, S., Honkakoski, P., Pelkonen, J., Tammi, M., and Urtti, A. (2001) Extracellular glycosaminoglycans modify cellular trafficking of lipoplexes and polyplexes. *Journal of Biological Chemistry 276*, 33875-33880.

(171) Sahin, U., Karikó, K., and Türeci, Ö. (2014) mRNA-based therapeutics [mdash] developing a new class of drugs. *Nature Reviews Drug Discovery*.

(172) Ziemniak, M., Szabelski, M., Lukaszewicz, M., Nowicka, A., Darzynkiewicz, E., Rhoads, R. E., Wieczorek, Z., and Jemielity, J. (2013) Synthesis and evaluation of fluorescent cap analogues for mRNA labelling. *RSC advances 3*, 20943-20958.

(173) Leonetti, J. P., Mechti, N., Degols, G., Gagnor, C., and Lebleu, B. (1991) Intracellular distribution of microinjected antisense oligonucleotides. *Proceedings of the National Academy of Sciences 88*, 2702-2706.

(174) Spiller, D. G., Giles, R. V., Grzybowski, J., Tidd, D. M., and Clark, R. E. (1998) Improving the intracellular delivery and molecular efficacy of antisense oligonucleotides in chronic myeloid leukemia cells: a comparison of streptolysin-O permeabilization, electroporation, and lipophilic conjugation. *Blood 91*, 4738-4746.

(175) Nitin, N., Santangelo, P. J., Kim, G., Nie, S., and Bao, G. (2004) Peptide-linked molecular beacons for efficient delivery and rapid mRNA detection in living cells. *Nucleic Acids Research 32*, e58-e58.

(176) Zhang, X., Roeffaers, M. B. J., Basu, S., Daniele, J. R., Fu, D., Freudiger, C. W., Holtom, G. R., and Xie, X. S. (2012) Label-Free Live-Cell Imaging of Nucleic Acids Using Stimulated Raman Scattering Microscopy. *ChemPhysChem 13*, 1054-1059.

(177) Wei, L., Hu, F., Shen, Y., Chen, Z., Yu, Y., Lin, C.-C., Wang, M. C., and Min, W. (2014) Live-cell imaging of alkyne-tagged small biomolecules by stimulated Raman scattering. *Nature Methods 11*, 410-412.

CHAPTER 2 |

Fluorescence Correlation Spectroscopy and Single Particle Tracking: Theory and Methodology

K. Rombouts[†, ‡], K. Braeckmans[†, ‡] and K. Remaut[†]

† Laboratory of general biochemistry and physical pharmacy, Faculty of pharmacy

‡ Centre for Nano- and Biophotonics, Ghent University, Ghent 9000, Belgium

TABLE OF CONTENTS

INTRODUCTION

Next to the use of fluorescence microscopy to visualize the behavior of fluorescently labeled molecules or particles in a biological environment, studying the dynamic properties of these labeled particles has gained importance for many research areas. In the context of this thesis, especially the mobility studies of molecules associated with gene delivery capabilities, like non-viral carriers or nucleic acids, is of interest. These mobility studies have provided information on the capability of non-viral gene carriers to move, for example, through sputum [1] and vitreous, [2] but also surface modifications of non-viral carriers to protect the therapeutic molecules against enzymatic degradation were evaluated. [3]

A collection of advanced fluorescence microscopy methods have been developed over the years to study the mobility of particles at extremely low concentrations. Fluorescence correlation spectroscopy (FCS) and single particle tracking (SPT) are the relevant techniques for this thesis, but also fluorescence recovery after photobleaching is a technique that can be used to this end.

FCS is a fluorescence microscopy-based technique that was developed in the 1970's as a special case of relaxation analysis to measure diffusion and chemical dynamics of DNA-drug intercalation via the temporal autocorrelation of fluctuations in fluorescence emission. [4, 5] The fluctuations are caused by the entrance and the exit of fluorescent molecules in and out of the observational volume. The technique was refined by reducing the observational volume and concentration of the molecules of interest, while increasing the sensitivity to detect fluorescence. By the combination of FCS with confocal detection, the current form of the technique was established. [6] Rigler and Elson (2012)[7] bundled an extensive overview describing the technique and most interesting applications. In our lab, the technique was used to study the complexation and dissociation of antisense oligonucleotides and short interference RNA (siRNA) from non-viral complexes and the *in vitro* and *in vivo* stability of these nucleic acids. [8-11]

SPT on the other hand is a fluorescence microscopy-based method that obtains spatio-temporal information on individual moving fluorescent molecules or particles. To this end, movies are recorded inside a solution with a low concentration of the particles of interest. The movement of the particles during the movie is then used to calculate

the distribution of the diffusion coefficients of the particles and a number concentration.[12-15] Zagato et al. (2014)[16] provided an interesting overview of how single particle tracking (SPT) has been used in the field of drug delivery. In our lab, this method has been used to study the mobility of carriers within environments that form a barrier for the delivery of non-viral vectors, like sputum and the vitreous. [1, 2]

In this chapter, FCS and SPT are described with regards to their principle, instrumentation, and particular analysis methods that were used throughout this thesis. This should enable a better understanding of all the terms and analysis methods that are being used in the following chapters of this thesis.

FLUORESCENCE CORRELATION SPECTROSCOPY

Fluorescence correlation spectroscopy is a fluorescence microscopy-based method that, rather than making use of the fluorescence emission intensity, makes use of spontaneous fluorescence intensity fluctuations to analyze low concentrated biomolecules by high-resolution spatial and temporal analysis. These fluctuations stem primarily from the movement of fluorescently labeled particles in and out of the detection volume, (Figure 1 A) but also conformational changes and chemical or photophysical reactions (e.g., blinking, photobleaching, …) induce fluorescence intensity fluctuations. The fluorescence intensities ($F(t)$) are recorded over time and displayed in so-called time traces (Figure 1 B). Based on these traces an autocorrelation curve ($G(\tau)$) is calculated, (Figure 1 C) which can be fitted by a mathematical model (*vide infra*). From these calculations, most importantly for this thesis, local concentrations and diffusion coefficients can be retrieved. [4, 17] To achieve this, the fluorescence intensity is measured in a confocal observation volume (~1 fl) in a solution with a nanomolar concentration of fluorescently labeled molecules, to assure that every fluorescent molecule contributes significantly to the fluorescent signal.

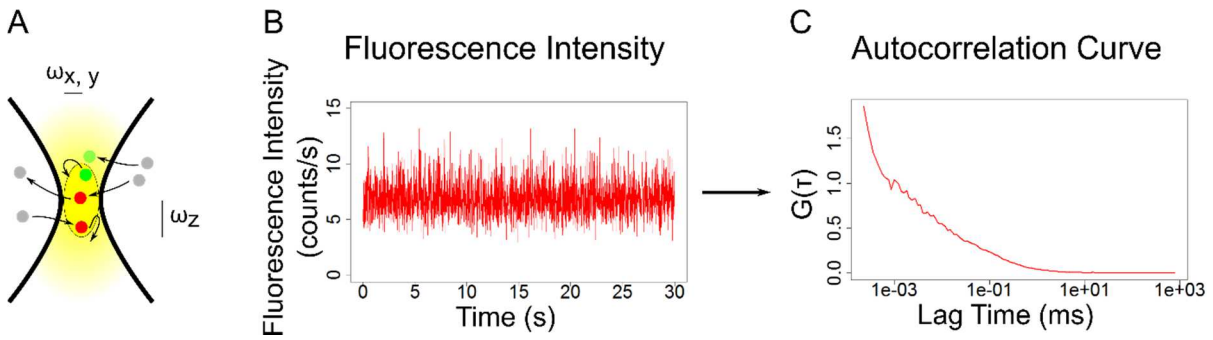

Figure 1 (A) Schematic representation of the detection volume with fluorescently labeled particles moving in and out of the focus. $\omega_{x,y}$ and ω_z are respectively the radial and the axial radius of the focal volume. Plots of the (B) fluorescence intensity time trace and (C) autocorrelation curve.

Instrumentation

A FCS setup to simultaneously detect fluorescence fluctuations of two colors needs at least four important components, namely: laser excitation, a high numerical aperture (NAp) objective, emission filters, and single molecule sensitive detectors. These requirements allow the integration of this setup with a standard confocal microscope. In Figure 2, the setup at our facility is schematically represented. The Compact FLIM and FCS Upgrade Kit for LSMs (PicoQuant, Berlin, Germany) is, in our case, added to a Nikon EZC1-si setup (Nikon Instruments Europe B.V., Brussels, Belgium). In practice this means that from a laser box with solid state lasers of 488 nm and 636 nm, laser light is sent through an excitation pinhole toward a dichroic mirror, which directs this excitation light to a 60x water immersion (WI) objective (Nikon Plan Apo VC 60x WI DIC N2, NAp 1.2). This objective focuses the excitation beam into a sample which is contained in a glass bottom 96 well plate (Greiner Bio-One, Vilvoorde, Belgium) and simultaneously collects the fluorescence emission. This emission light passes through the dichroic mirror and excitation pinhole after which the light is focused on the τ-single photon avalanche diode (τ-SPAD) detectors. The PicoQuant detector box consists of a 50/50 beam splitter guiding the emission light via a 520/35 nm bandpass filter or a 690/70 nm bandpass filter towards two detectors which detect photons to address them respectively to the green channel or the red channel. The electronic signal from the detectors is finally sent to the Time-Correlated Single Photon Counting (TCSPC) module to assign arrival times to the fluorescence intensities. This data is synced with the SymphoTime software (FCS package) to perform the analysis.

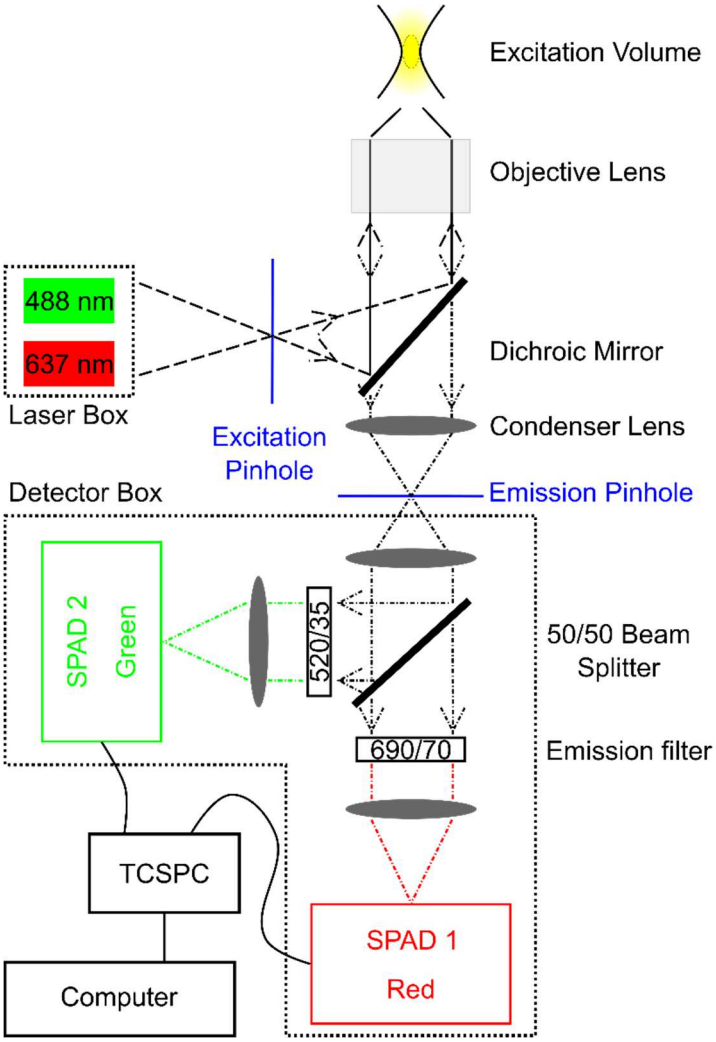

Figure 2 Setup of a (dual) color FCS instrument. For single color FCS, the emission light is guided to only one detector. SPAD = Single Photon Avalanche Diode, TCSPC = Time-Resolved Single Photon Counter. Dashed line: excitation light, dashed and dotted line: emission light

Autocorrelation Analysis

As mentioned above, fluorescence intensity fluctuations can be quantified by temporally autocorrelating the intensity signal ($F(t)$). This measure of self-similarity of the time signal can then further be used to extract time constants of underlying physical processes. [4] For the theoretical derivation to be correct, a couple of assumptions about the data acquisition should be made. The laser power, effective volume and temperature are assumed to be constant during the measurement and the dynamic processes observed are caused by free diffusion.

During the recording process the fluorescence intensity from the fluorescent molecules inside the detection volume is recorded photon by photon. The fluctuations

of the fluorescence signal $\delta F(t)$ are defined as the deviation of this signal to the average signal $\langle F(t)\rangle$ over the time frame of the measurement.

$$\delta F(t) = F(t) - \langle F(t)\rangle$$

$$\langle F(t)\rangle = \frac{1}{T}\int_0^T F(t)dt$$

Eq. 1

The correlation function is then obtained by calculating the self-similarity of fluctuations after lag time τ. The normalized autocorrelation curve is then calculated by:

$$\boldsymbol{G}(\tau) = \frac{\langle \delta F(t) \times \delta F(t+\tau)\rangle}{\langle F(t)\rangle^2}$$

Eq. 2

This function is plotted in function of τ to give rise to a graph depicting the experimental autocorrelation curve (cf. Figure 1 C).

Since the goal of the FCS experiments in this thesis is to extract information on concentration (N) and the diffusion time (τ_D), the experimental autocorrelation curve needs to be fitted with a mathematical model. The SymphoTime fitting software requires some parameters, describing the effective volume and the ratio of the axial over the lateral radius of the detection volume (V_{eff} and κ), to be able to retrieve meaningful values for N and τ_D. The structural parameter κ (defined in Eq. 3) was calibrated and is fixed at 6 for the red channel and 9 for the green channel for all the fits. V_{eff} of the detection volume (see Figure 1 A and Figure 2) is experimentally obtained by measuring a rhodamine green solution with a known diffusion coefficient and solving the equations in Eq. 3 based on the obtained correlation curve.

$$D = \frac{{\omega_{x,y}}^2}{4\tau_D}$$

$$V_{eff} = \pi^{3/2}\,{\omega_{x,y}}^2\,\omega_z$$

$$\kappa = \frac{\omega_z}{\omega_{x,y}}$$

Eq. 3

The model that is used throughout this thesis to fit the autocorrelation curves, is the predefined triplet-state model from the SymphoTime software. This model adjusts the general model for free diffusion to compensate for triplet blinking, which arises from the transition of fluorophores to the first excited triplet state. The number of species can be adjusted by varying the n in Eq. 4.

$$G(\tau) = \left[1 - T + Te^{\left(-\frac{\tau}{\tau_T}\right)}\right] \sum_{i=1}^{n} \rho_i \left(1 + \frac{\tau}{\tau_i}\right)^{-1} \left(1 + \frac{\tau}{\tau_i \kappa^2}\right)^{-1/2} \quad \textbf{Eq. 4}$$

with:

T = % fluorophores in triplet state

n = number of species

$\sum_{i=1}^{n} \rho_i = \frac{1}{\langle N \rangle}$

τ_T = triplet state time

τ_i = diffusion time for species i

κ = see Eq. 3

In this thesis, most of the time, a two species fit was used to analyze the autocorrelation curves of the pDNA solutions. Next to the structural parameters V_{eff} and κ, the dynamic parameters σ_{D1}, τ_{D1}, σ_{D2}, τ_{D2}, T, and τ_T can be provided by the user. By fixing one of the two diffusion times, while leaving the other dynamic parameters free, the presence of fast species, like free dye, labeled hybridization probes, or degraded DNA fragments with a pre-defined diffusion time, can be taken into account (illustrated in Figure 3). This leads to a better fit of the data which returns better values for the parameters of the slow species.

A

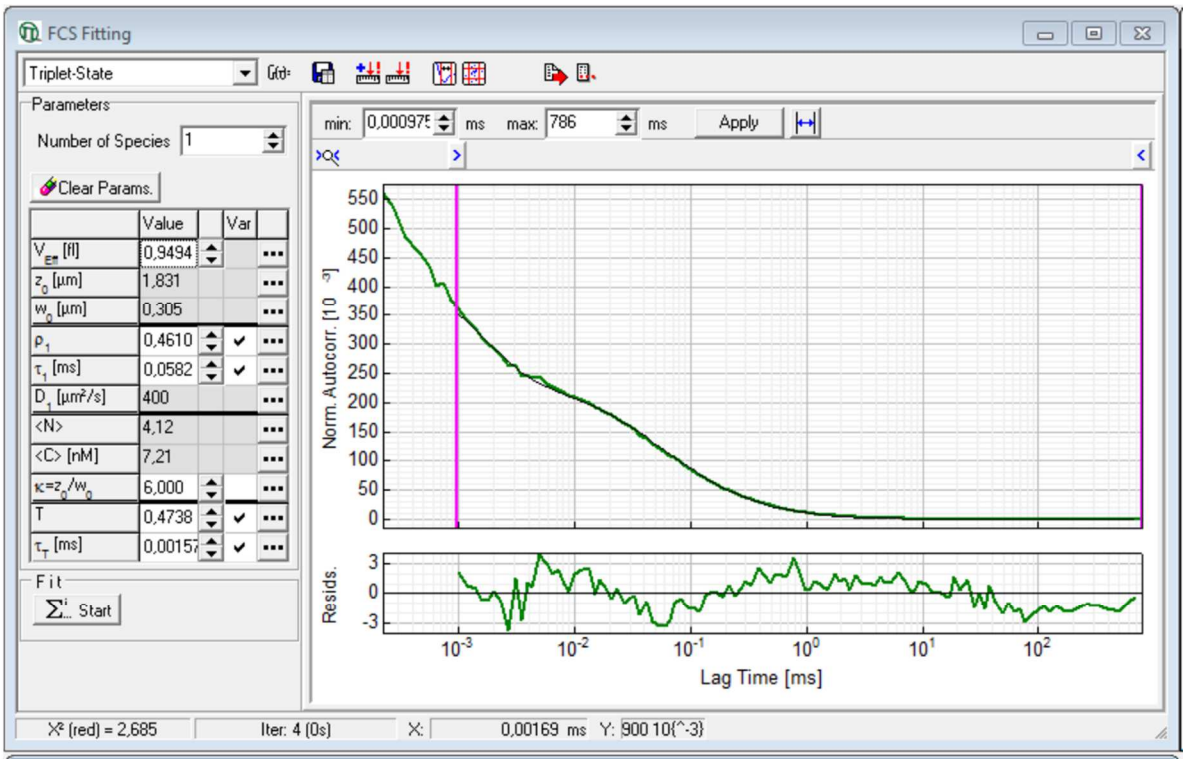

B

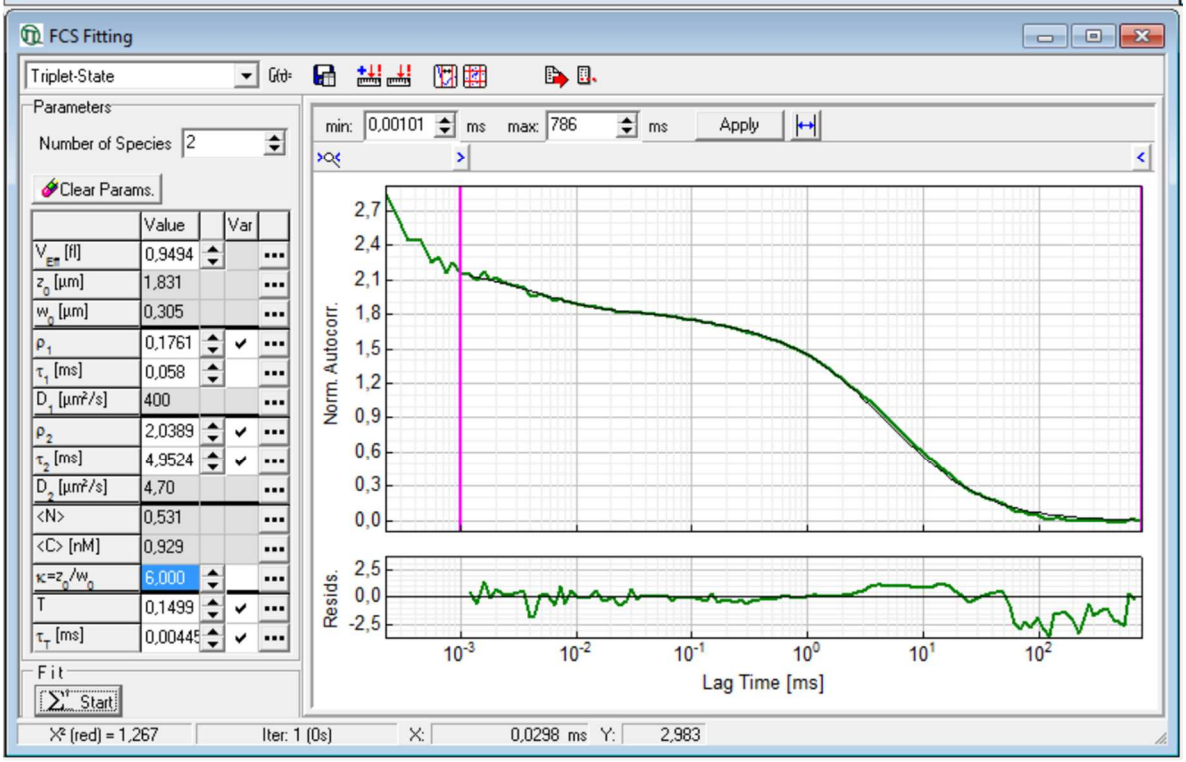

Figure 3 FCS analysis window in the SymphoTime software (A) for calibration and (B) for a sample with supercoiled pDNA. The sample in (A) is free dye with a known D of 400 µm²/s. The K value is fixed at 6 and the V_{eff} is calculated and fixed. The obtained τ_D can then be used as a measure for the fast component in (B). In (B) the correlation curve of supercoiled pDNA is fitted with the two species triplet-state model. V_{eff}, K, and τ_{D1} are fixed based on (A). A diffusion coefficient is then calculated from the fit for the second species.

Peak Number Analysis

Alternatively to autocorrelation analysis, the total number of peaks, present in the time trace, was also used as a measure for the concentration of pDNA (see Chapter 3). This is possible due to the observation that in the low concentration solutions that are used for these experiments, a large, slow moving fluorescently labeled pDNA molecule gives rise to a high intensity value when it passes through the detection volume, (Figure 4 A) while small, fast moving DNA fragments generate only small fluctuations around the average fluorescence intensity when passing through the detection volume (Figure 4 B). These so-called high intensity peaks are quantified in the "burst size histogram" window of the SymphoTime software. This analysis counts a peak when the fluorescence intensity increases to a value higher than the threshold and returns back to a lower value. To obtain a number of peaks, a threshold is determined and fixed, based on the baseline of the fast moving fragments (see Supplementary data of **Chapter 3** and **4** for a practical example). The threshold is chosen to be above the maximum fluorescence intensity seen in these samples, since no large pDNA should be present (see Figure 4 B). This baseline is then fixed for all other samples (see Figure 4 A) and a number of peaks is calculated in the software for every time trace.

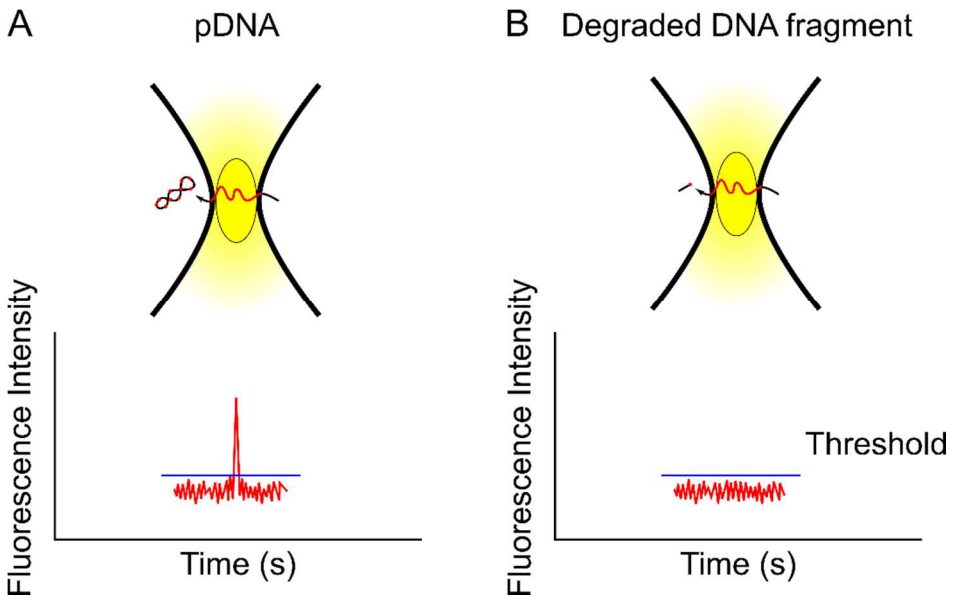

Figure 4 Schematic representation of a fluorescence intensity peak rising from (A) fluorescently labeled pDNA and (B) a degraded DNA fragment migrating through the detection volume. Blue line indicates the threshold which is chosen based on the maximum value on the right.

SINGLE PARTICLE TRACKING

Single particle tracking (SPT) is the second fluorescence microscopy-based method that was used throughout this thesis. It enables the study of the movement of individual fluorescently labeled particles or molecules in time and in space with nanometer precision. [13] This is achieved by a multiple step process as depicted in Figure 5. First, images are recorded in solutions with a concentration that is low enough to avoid the presence of more than one particle per diffraction-limited spot. For a high NA objective, this means that there should be a distance of at least 500 nm between each particle. [12] Then, trajectories are calculated based on image processing of the recorded movies. Finally, these trajectories are analyzed in a quantitative manner to obtain information on the mobility and concentration of the particles in solution. The instrumentation used in this thesis and the analysis methods will now further be discussed in more details in the following paragraphs.

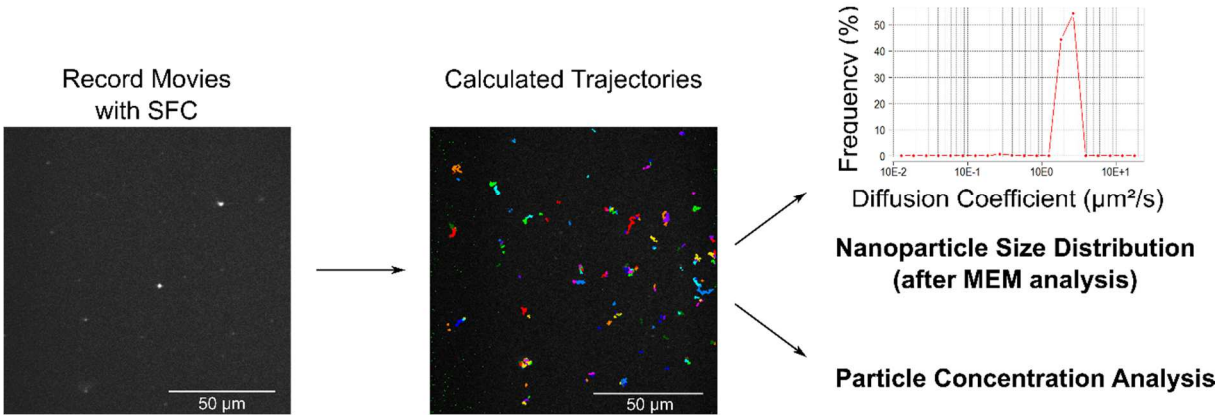

Figure 5 Schematic overview of a typical workflow when performing SPT for sizing and concentration analysis on the swept-field confocal (SFC) microscope. MEM: Maximum Entropy Method which is used to refine the obtained distribution of diffusion coefficients.

Instrumentation

The equipment that is typically used to record movies of moving fluorescent particles for SPT is an epi-fluorescence microscope which is adjusted to allow widefield laser illumination and detection with a fast and sensitive charge-coupled device (CCD) camera. In this thesis however, a swept-field confocal (SFC) microscope (Nikon LiveScan attached to a Nikon Eclipse Ti-E inverted microscope (Nikon Instruments Europe B.V., Brussels, Belgium)) is used to record the movies. The SFC microscope setup makes use of a four line solid-state laser box of which either the 488 nm laser or

the 640 nm were used in this thesis depending on the type of fluorescent label. From there on, the laser light is sent to the SFC scan head (Figure 6 A), which guides the light via a pinhole array/slit aperture (Figure 6 B) and a scanning galvanometer mirror toward the sample. This pinhole array/slit aperture allows for pinhole imaging at a high-resolution or high-speed slit imaging. In this work, the microscope was always used in slit mode (50 µm slit), which uses a single slit for sweeping the sample and allows for high-speed imaging at a lower excitation power. This, however, leads to a slightly diminished spatial resolution and optical sectioning, when compared to the pinhole imaging, since confocality is only created in axis (perpendicular on the slit) and out of focus light has a higher contribution to the emitted signal on the other axis. [18] The scanning galvanometer mirror then guides the light via the dichroic mirror toward the same 60x high NAp WI objective that is described for FCS, which focuses the light inside the sample, which is placed in a glass-bottom 96 well plate. The excitation light from the fluorescent particles is then returned onto the dichroic mirror, where the beam is sent back over the scanning galvanometer mirror through the emission aperture slit. Via a mirror, the scanning galvanometer mirror again directs the light through an emission filter onto the electron multiplying CCD (EMCCD) camera. The NIS elements software (Nikon Instruments Europe B.V., Brussels, Belgium) then displays the recorded images. To ensure the acquisition of high quality images, all the different components are synchronized by a SFC controller module.

Two imaging parameters always need to be known for a correct SPT analysis: the frame rate and the pixel size. These parameters are checked via the NIS software, where the scanning and acquisition parameters are set to the needs of the experiment. Very fast acquisition can be obtained by synchronizing the exposure time with the maximum acquisition rate of the camera. With our setup this gives rise to a maximum frame rate of 37.4 frames per second at a full frame (512 x 512 pixels). This is ideal for very bright, fast moving particles. For the imaging of slower moving particles, as is the case for pDNA, slower acquisition rates can be used (e.g., throughout this thesis an exposure time of 100 ms was used, giving rise to a frame rate of around 8-9 frames per second). This frame rate should always be checked during the analysis. The pixel size on the other hand is a parameter that is determined by the camera and the optical configuration of the microscope. Since the full surface of the camera's detector was always used, it has a fixed number of pixels. Only the optical configuration will then

contribute to a change in image pixel size. Apart from the objective lens, our setup has two additional magnification steps which influence the pixel size. The first additional magnification is incorporated into the microscope body and makes it possible to add an optional extra 1.5x magnification. An additional adjustable magnification, between 1x and 2.25x, is introduced in the emission pathway of our setup between the dichroic mirror and the EMCCD camera. For the experiments further in this thesis, the total extra magnification was set at 1.5x. For our camera with 16 µm pixels and the 60x WI objective this resulted in an image pixel size of $\frac{16\ \mu m}{(60\times1.5)} = 0.18\ \mu m/pixel$.

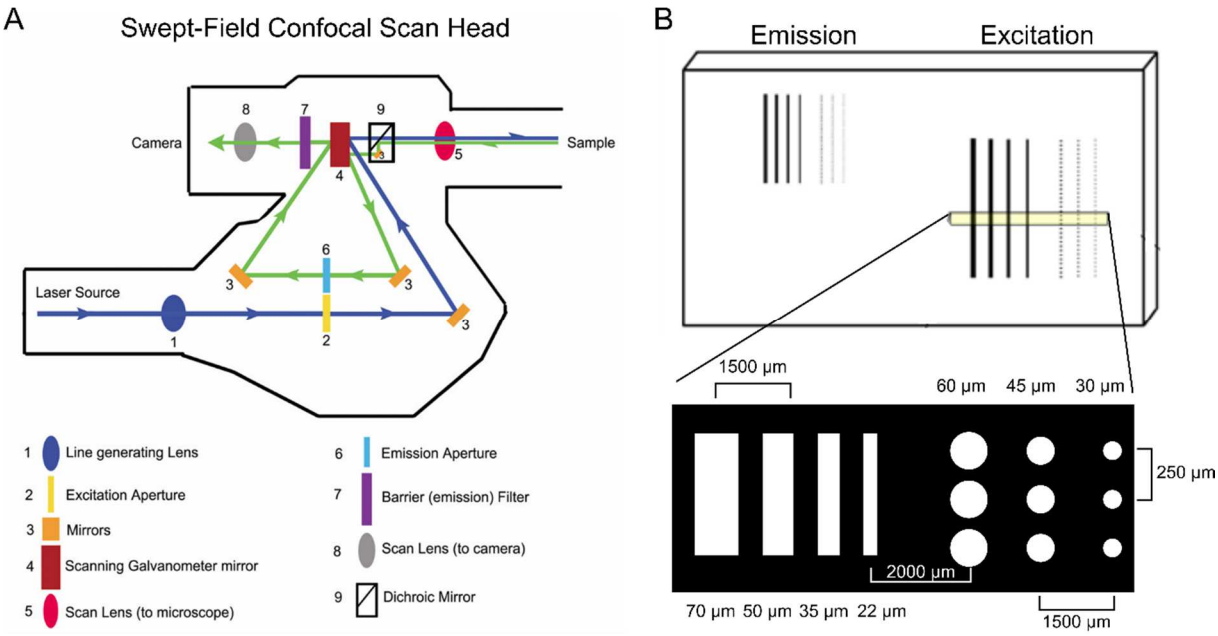

Figure 6 Schematic representation of (A) the SFC scan head and (B) the slit apertures and pinhole arrays of the LiveScan system. Blue line: excitation light. Green line: emission light. Part (A) adapted from Castellano-Muñoz et al. (2012)[18]

Calculation of Trajectories

After the movies are recorded, two analysis steps need to be performed to calculate the trajectories (or tracks) of each particle that provide information on the mobility and concentration of the particles. First, the location of the particles is determined and the center location is calculated for each frame of the movie via the centroid algorithm.[12] Next the locations belonging to the same particle should be linked together via a suitable nearest neighbor algorithm.

When we take a look at these steps in more detail, we see that in the first step, the locations of particles in all the SPT images should be found. This can be done by

a variety of methods, such as a Gaussian fit, centroid identification or a pattern-recognition method. [19, 20] Since all the work in this thesis is analyzed on our proprietary software, the analysis will be explained by the algorithms used for the image processing, which were described by Braeckmans et al. (2010)[12], Deschout et al. (2012)[14], and Forier et al. (2012)[1]. First, a background correction is performed with an unsharp filter, to remove a nonuniform background. In the filtered image F with a more uniform background, a first selection of possible particles can then be made by means of intensity thresholding. Since most of the pixels belong to the background, while the particles give rise to considerably less pixels (with higher intensities), the intensity histogram will consist of a Gaussian-like peak around the intensity of the background with a long tail for the higher intensities, stemming from the particles. The threshold should be set at an intensity that separates the background intensity from the particle intensity. This intensity threshold T is based on an algorithm that fits a Gaussian distribution to the intensity histogram and can be calculated as:

$$T = \mu + N \times \sigma \qquad \textbf{Eq. 5}$$

with mean value μ, standard deviation σ and N a user-defined parameter to fine-tune the threshold for a particular series of experiment. A binary image F_b can now be created where all the pixels below intensity T have an intensity equal to zero and values above or equal to T as one.

From F_b the contours of the objects can be determined which delineate potential particles in the original image I. These contours allow for the calculation of object properties, but most importantly allow for the calculation of the center location. This is calculated as the intensity-weighted center of the object pixels or 'centroid' given by coordinates x_c and y_c which are defined as:

$$x_c = \frac{\sum_{i \in S} x_i \times (I_i - BG)}{\sum_{i \in S}(I_i - BG)},\ y_c = \frac{\sum_{i \in S} y_i \times (I_i - BG)}{\sum_{i \in S}(I_i - BG)} \qquad \textbf{Eq. 6}$$

With S the set of all pixels with coordinates (x_i, y_i) and intensities I_i. BG is the local background calculated from the mean pixel value along a contour drawn close around the object contour. Based on the object properties, a final selection is performed by the user, to retain only the objects that are coming from the particles of interest. It should be noted that although most of the particles that are imaged for SPT are smaller than

the resolution of the microscope (<250 nm), SPT can obtain subresolution accuracy on the location of a particle by calculating the centroid of the diffraction-limited spot. [21]

Based on these particle locations the trajectories can be calculated by deciding, via a suitable algorithm, which particles in subsequent frames should be linked. In our work we used a nearest neighbor algorithm that connects positions of particles that are closest to each other in subsequent frames. In order not to connect particles that are too far from each other, the maximum distance that a particle can travel over the time between two subsequent frames needs to be taken into account. In the case of free diffusion, this maximum step size can be estimated according to the exponential distribution given by the following equation: [22]

$$P(\xi) = \frac{1}{4Dt} e^{-\xi/4Dt} d\xi \qquad \textbf{Eq. 7}$$

with $\xi = r^2$ the distance squared that a particle can travel after a time t due to free diffusion. This exponential distribution has the cumulative distribution function:

$$F(x) = 1 - e^{-x/4Dt} \qquad \textbf{Eq. 8}$$

This equation represents the probability that a particle with a diffusion coefficient D traveled a square distance within the interval $[0\ \ x]$ after a time t. This means that the particle will not have moved further than a distance $r = \sqrt{x} = \sqrt{4Dt\ ln(1/(1-p))}$ with a probability p.The maximum step size can thus be calculated for a certainty level when the diffusion coefficient D and time between two subsequent frames (t) is given.

Once this maximum step size is fixed, the nearest neighbor algorithm will connect the nearest particle positions in subsequent frames within the maximum search distance to obtain tracks. The algorithm used also takes the disappearance of particles, due to photophysical causes or due to movement out of the focus, and the appearance of new particles during the acquisition into account. For details on this the interested reader is referred elsewhere. [12]

Analysis of the Mobility

Once the trajectories are calculated, information on the mobility can be obtained. This is usually done by mean square displacement (MSD) analysis (Figure 7). For a trajectory that is N steps long (thus $N+1$ locations), the time between subsequent steps is t, which is in fact the time between two consecutive frames in the SPT movies which we from now on call the first time-lag. This first time-lag is related to the so-called first step, which is the distance $r_{1,t}$ between the first two points. The distance between the second and third point is then given by $r_{2,t}$ (see Figure 7). The MSD for the first time-lag is then given by:

$$\langle r^2 \rangle_t = \frac{\sum_{i=1}^{N} r_{i,t}^2}{N} \qquad \textbf{Eq. 9}$$

This MSD can be calculated for longer time-lags ($2t$, $3t$, …, nt) with $n = 1, 2, \ldots, N$. In general, the MSD for time-lag nt can be defined as:

$$\langle r^2 \rangle_{nt} = \frac{\sum_{i=1}^{N-n+1} r_{i,nt}^2}{N-n+1} \qquad \textbf{Eq. 10}$$

When the MSD is plotted against the time-lag, the diffusion coefficient can be calculated by fitting the experimental data. For free 2-D diffusion, the MSD is described by:

$$\langle r^2 \rangle = 4\,Dt - {}^{4}/_{3}\,D\Delta t + 4\sigma^2(D, \Delta t) \qquad \textbf{Eq. 11}$$

with t the time-lag, Δt the acquisition time, and σ the localization precision which is dependent on the diffusion coefficient D and the acquisition time.

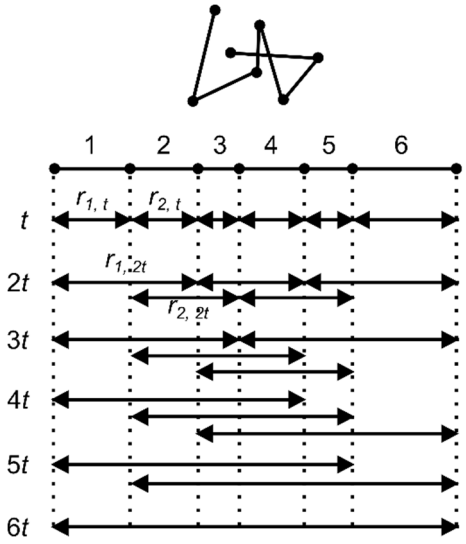

Figure 7 The principle behind the MSD analysis of a trajectory consisting of six steps. For the first time-lag (t), the MSD is calculated from six distances. For the second time-lag ($2t$), only five distances are retrieved from this trajectory for the calculation of the MSD. The last time-lag has only one distance contributing to the MSD.

To obtain a correct calculation for the diffusion coefficient two things should be noted. First, the number of distances, from which the MSD is calculated, decreases for increasing values of t. This leads to an increase of the uncertainty of the obtained values. This increase is visualized in Figure 8. Therefore, it is suggested that the longest time-lag for which the MSD is calculated should be at most 25% of the length of the longest time-lag or a weighted fit should be used. [12]

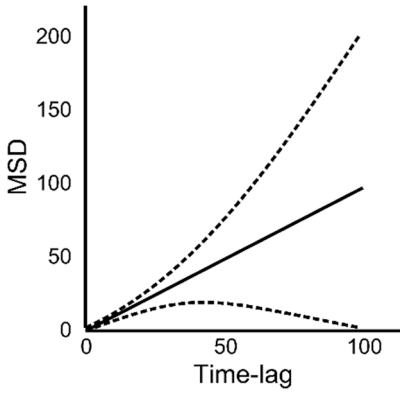

Figure 8 The relation between the MSD for free diffusion and the time-lag (as a solid line) for a trajectory of 100 steps. The dashed lines represent the positive and negative standard deviation on the MSD at time-lag nt, which increases for larger lag-times

Secondly, the localization precision value σ can, in its most simple form, be determined by recording a movie of a sample with stationary particles in the same

imaging conditions as the samples, building the trajectories and taking the standard deviation of the calculated positions. Deschout et al. (2012)[14], however, described that the value will deviate from this standard deviation due to 3-D movement of a particle during the acquisition. This alternative calculation method assumes that the average localization precision of diffusing particles is equal to the localization precision for a point spread function blurred by the average diffusion. *[14]* This was experimentally proven to be a more accurate description of the localization precision and it is therefore used in our program.

By incorporating all these parameters in the fit, described by Eq. 11, to the MSD from the individual trajectories, a distribution of diffusion coefficients is calculated. This distribution is then even more refined by a maximum-entropy analysis (MEM). Via this method, the noise that is not statistically warranted is removed resulting in a more precise distribution of the diffusion coefficients. *[13]*

Concentration Analysis

The concentration analysis that is used within this thesis has been developed and described in detail in Röding et al. (2013)[15] and Röding et al. (2013)[23]. The analysis starts from a file containing information on the trajectories in a movie. Based on the data from the tracks, this method calibrates the volume of the detection region which makes it possible to calculate absolute number concentrations in a highly accurate fashion. Furthermore, these results were shown to be independent of particle brightness, instrumental settings and the image processing parameters.

First, the volume of the detection region is determined by modeling the distribution of trajectory lengths within the detection region, which is shaped as a rectangular box. The lateral dimensions of this box can be obtained by calibration, but the axial dimension is unknown and should be derived from the measurements. Since the lateral size is typically much larger than the axial size, the model is simplified by assuming that a particle can only enter or leave the detection region via axial diffusion. By doing this, the 3-D problem is reduced to a one-dimensional problem. *[15]* For a monodisperse sample, it is assumed that the particles are uniformly distributed within the sample. This means that the position of a particle in the next time step is the current position plus a Gaussian increment. From this, the conditional probability density of the position of a particle that has just entered the detection region can be defined. This

probability density is then used to compute the probability distribution of the trajectory length once a particle enters the detection region. This probability distribution for a trajectory length K was shown to be implicitly a function of the axial size of the detection region and the diffusion coefficient of the particles.

The distribution of trajectory lengths can be obtained from the experiment, while the diffusion coefficient can also be determined from the analysis of mobility (*vide supra*). A maximum likelihood estimate of the axial size ($\hat{a}$) is then obtained by fitting the theoretical trajectory length distribution to the experimental trajectory length distribution. This axial size estimate is thereafter used to calculate the absolute number concentration (Eq. 12). It is important to note here that a minimal track length threshold is imposed, since shorter track lengths are more likely to be false positives, caused by errors in the localization. In this thesis, this minimum track length is kept at 4.

Next, the number concentration is given by:

$$\hat{c} = \frac{\bar{N}}{8\hat{a}a_x a_y \times 10^{-12}} \text{ particles/ml} \qquad \textbf{Eq. 12}$$

with 2 a_x and 2 a_x the lateral dimensions of the detection region in µm and $\bar{N}$ the mean number of particles per frame. This value can be estimated by:

$$\bar{N} = \frac{1}{\hat{p}_{obs}} \frac{1}{n} \sum_{k \geq k_{min}} n\, N_k \qquad \textbf{Eq. 13}$$

with n the number of frames, k the track length, k_{min} the minimum track length (as discussed before), N_k the number of tracks of length k and $\hat{p}_{obs}$ a correction factor to compensate for the underestimation that is introduced by omitting shorter track lengths than k_{min}. It's defined by the estimated probability of a random particle position within the detection region to be observed with $k \geq k_{min}$. [15]

The standard error on the concentration estimate is calculated using bootstrapping on the level of the movie, since the movies can be considered to be independent measurements. Röding et al. (2013)[15] showed by simulation experiments that 50 bootstrap samples returned standard errors which were very close to the actual standard errors.

In practice the parameters that need to be provided by the user of the concentration analysis are the dimensions of the field of view (512 x 512 pixels in our case), the pixel size (0.18 µm/pixel), and the time between two consecutive frames. Based on the provided movies, 10 movies per sample in this thesis, the analysis will return a number concentration expressed in particles/ml.

REFERENCES

(1) Forier, K., Messiaen, A.-S., Raemdonck, K., Deschout, H., Rejman, J., De Baets, F., Nelis, H., De Smedt, S. C., Demeester, J., Coenye, T., et al. (2012) Transport of nanoparticles in cystic fibrosis sputum and bacterial biofilms by single-particle tracking microscopy. *Nanomedicine 8*, 935-949.

(2) Martens, T. F., Vercauteren, D., Forier, K., Deschout, H., Remaut, K., Paesen, R., Ameloot, M., Engbersen, J. F., Demeester, J., and De Smedt, S. C. (2013) Measuring the intravitreal mobility of nanomedicines with single-particle tracking microscopy. *Nanomedicine 8*, 1955-1968.

(3) Remaut, K., Sanders, N., N., De Geest, B., G., Braeckmans, K., Demeester, J., and De Smedt, S., C. . (2007) Nucleic acid delivery: Where material sciences and bio-sciences meet. *Materials Science and Engineering: R: Reports 58*.

(4) Bacia, K., and Schwille, P. (2007) Fluorescence correlation spectroscopy, in *Lipid rafts* pp 73-84, Springer.

(5) Magde, D., Elson, E., and Webb, W. W. (1972) Thermodynamic fluctuations in a reacting system—measurement by fluorescence correlation spectroscopy. *Physical Review Letters 29*, 705.

(6) Rigler, R., Mets, Ü., Widengren, J., and Kask, P. (1993) Fluorescence correlation spectroscopy with high count rate and low background: analysis of translational diffusion. *European Biophysics Journal 22*, 169-175.

(7) Rigler, R., and Elson, E. S. (2012) *Fluorescence correlation spectroscopy: theory and applications*, Vol. 65, Springer Science & Business Media.

(8) Buyens, K., Lucas, B., Raemdonck, K., Braeckmans, K., Vercammen, J., Hendrix, J., Engelborghs, Y., De Smedt, S. C., and Sanders, N. N. (2008) A fast and sensitive method for measuring the integrity of siRNA-carrier complexes in full human serum. *Journal of Controlled Release 126*, 67-76.

(9) Buyens, K., Meyer, M., Wagner, E., Demeester, J., De Smedt, S. C., and Sanders, N. N. (2010) Monitoring the disassembly of siRNA polyplexes in serum is crucial for predicting their biological efficacy. *Journal of Controlled Release 141*, 38-41.

(10) Raemdonck, K., Remaut, K., Lucas, B., Sanders, N. N., Demeester, J., and De Smedt, S. C. (2006) In situ analysis of single-stranded and duplex siRNA integrity in living cells. *Biochemistry 45*, 10614-10623.

(11) Remaut, K., Lucas, B., Raemdonck, K., Braeckmans, K., Demeester, J., and De Smedt, S. (2007) Can we better understand the intracellular behavior of DNA nanoparticles by fluorescence correlation spectroscopy? *Journal of Controlled Release 121*, 49-63.

(12) Braeckmans, K., Vercauteren, D., Demeester, J., and De Smedt, S. C. (2010) Single Particle Tracking, in *Nanoscopy and Multidimensional Optical Fluorescence Microscopy* pp 5.1-5.17, Chapman and Hall.

(13) Braeckmans, K., Buyens, K., Bouquet, W., Vervaet, C., Joye, P., De Vos, F., Plawinski, L., Doeuvre, L., Angles-Cano, E., Sanders, N., et al. (2010) Sizing nanomatter in biological fluids by fluorescence single particle tracking. *Nano letters 10*, 4435-4442.
(14) Deschout, H., Neyts, K., and Braeckmans, K. (2012) The influence of movement on the localization precision of sub-resolution particles in fluorescence microscopy. *Journal of biophotonics 5*, 97-109.
(15) Röding, M., Deschout, H., Braeckmans, K., and Rudemo, M. (2013) Measuring absolute nanoparticle number concentrations from particle count time series. *Journal of microscopy 251*, 19-26.
(16) Zagato, E., Forier, K., Martens, T., Neyts, K., Demeester, J., Smedt, S. D., Remaut, K., and Braeckmans, K. (2014) Single-particle tracking for studying nanomaterial dynamics: applications and fundamentals in drug delivery. *Nanomedicine 9*, 913-927.
(17) Schwille, P. (2001) Fluorescence correlation spectroscopy and its potential for intracellular applications. *Cell Biochemistry and Biophysics 34*, 383-408.
(18) Castellano-Muñoz, M., Peng, A. W., Salles, F. T., and Ricci, A. J. (2012) Swept field laser confocal microscopy for enhanced spatial and temporal resolution in live-cell imaging. *Microscopy and Microanalysis 18*, 753-760.
(19) Cheezum, M. K., Walker, W. F., and Guilford, W. H. (2001) Quantitative comparison of algorithms for tracking single fluorescent particles. *Biophysical journal 81*, 2378-2388.
(20) Levi, V., Serpinskaya, A. S., Gratton, E., and Gelfand, V. (2006) Organelle Transport along Microtubules in Xenopus Melanophores: Evidence for Cooperation between Multiple Motors. *Biophysical Journal 90*, 318-327.
(21) Deschout, H., Zanacchi, F. C., Mlodzianoski, M., Diaspro, A., Bewersdorf, J., Hess, S. T., and Braeckmans, K. (2014) Precisely and accurately localizing single emitters in fluorescence microscopy. *Nature methods 11*, 253-266.
(22) Qian, H., Sheetz, M., and Elson, E. (1991) Single particle tracking. Analysis of diffusion and flow in two-dimensional systems. *Biophysical journal 60*, 910-921.
(23) Röding, M., Deschout, H., Braeckmans, K., Särkkä, A., and Rudemo, M. (2013) Self-calibrated concentration measurements of polydisperse nanoparticles. *Journal of microscopy 252*, 79-88.

CHAPTER 3 |

Effect of Covalent Fluorescence Labeling of Plasmid DNA on its Intracellular Processing and Transfection with Lipid-Based Carriers

K. Rombouts[†, ‡], T. F. Martens[†, ‡], E. Zagato[†, ‡], J. Demeester[†], S. C. De Smedt[†], K. Braeckmans[†, ‡] and K. Remaut[†]. Effect of Covalent Fluorescence Labeling of Plasmid DNA on its Intracellular Processing and Transfection with Lipid-Based Carriers. *Molecular Pharmaceutics.* (2014)

† Laboratory of general biochemistry and physical pharmacy, Faculty of pharmacy

‡ Centre for Nano- and Biophotonics, Ghent University, Ghent 9000, Belgium

TABLE OF CONTENTS

ABSTRACT

The development of biotechnological pharmaceutics, like macro and nanocarriers, can benefit greatly from studying their characteristics in situ using advanced fluorescence microscopy methods. While choosing the optimal labeling method for visualizing the carrier or its cargo is crucial, it seldom receives attention. The possibility that high labeling densities alter the intracellular processing of the molecule is considered, but how and at which point this interference happens is not yet studied. The aim of this study was to elucidate the effect of labeling density on the cellular trafficking of labeled plasmid DNA (pDNA). Due to the drastic effect on expression levels for higher labeling densities, we tried to determine at which steps in the intracellular processing labeled pDNA behaves different than its nonlabeled counterpart. Therefore, different labeling densities, up to the manufacturer's recommended density, were tested. It was found that the cellular uptake remains unaffected, while the affinity for lipids is increased, which affects dissociation from the lipid-based complex and may affect endosomal escape. Also, nuclear injections clearly demonstrated that transcription is affected. The information and methodology, included in this work, could be helpful in determining if the labeling method and density used yields biologically relevant results for the intended research question.

INTRODUCTION

The administration of plasmid DNA (pDNA) is frequently used to introduce protein expression inside living cells. [1] pDNA has the advantage that it is easily produced and has great modulation possibilities. Virtually any protein of interest can be incorporated in the expression cassette. The delivery of pDNA, however, remains an important bottleneck. As naked nucleic acids are poorly taken up by cells, they need a delivery system for efficient intracellular delivery. While some successes have been obtained with viral vectors, [2-4] safety issues have stimulated the development of non-viral vectors for delivery of DNA therapeutics. [5, 6] In the research and development of non-viral therapeutics, the main goal is to find ways to make the transfection efficiency up to par with viral vectors. In order to optimize non-viral carriers, studies are conducted to obtain a better understanding of the intracellular barriers that are encountered during the transfection process. [7-10] When reaching the target cells, pDNA gene complexes are typically internalized through endocytosis. Then, the pDNA needs to escape the endosomal compartment into the cytosol, dissociate from its carrier and travel toward the nucleus. During the entire transfection process degradation of the pDNA should be avoided.

Advanced fluorescence microscopy methods are increasingly being used to get a better understanding of the intracellular processing of gene complexes in cells. [11-20] This requires that the gene complexes are fluorescently labeled, either by fluorescent labeling of the carrier material, or by fluorescent labeling of the cargo, i.e., the pDNA in this case. Labeled DNA can be obtained through a variety of techniques. Covalent labeling, enzymatic labeling, intercalating dyes, and peptide nucleic acid (PNA) clamps are all commonly used techniques. [8] Due to the simple nature of the protocols, methods that label the molecules in a random fashion, e.g., intercalating and most covalent binding labels, are used extensively.

A systematic study of labeled pDNA and its effect on the intracellular processing of gene complexes is currently missing. Yet this is required to correctly interpret microscopy-based intracellular trafficking studies. The aim of this study was to investigate the effect of labeling density of covalently labeled plasmids on the various steps of the intracellular processing and the final transfection efficiency of gene complexes containing labeled pDNA. As a case study, gene complexes

prepared from Cy5 labeled pDNA and the frequently used transfection agent Lipofectamine 2000 were investigated. It was found that for these gene complexes the cellular uptake and the intrinsic ability of lipoplexes to enable endosomal escape remains unaffected by the labeling of the pDNA, while other steps in the transfection pathway like dissociation from the complex and nuclear transcription are strongly inhibited at higher labeling densities which resemble the manufacturer's recommended amount of pDNA over volume labeling reagent of 1:1 (w:v).

These results clearly show that a good balance between fluorescent signal and labeling density of the pDNA is crucial in order to reliably study pDNA labeled gene lipoplexes during the different steps of the intracellular transfection pathway by means of fluorescence based techniques. The assays and protocols presented in this study could easily be used to evaluate the effect of labeling on the performance of other nucleic acid/carrier combinations and labeling techniques.

MATERIAL AND METHODS

Cell Culture

A HeLa cell line was maintained at 37°C (5% CO_2) in Dulbecco's modified Eagle's medium supplemented with growth factor F12 (DMEM:F12 (1:1)), 10% heat inactivated fetal bovine serum (FBS), 2 mM L-glutamine and 100 µg/ml penicillin/streptomycin. All cell culture reagents were purchased from GibcoBRL (Merelbeke, Belgium).

Plasmid DNA Preparation and Fluorescent Labeling of Plasmid DNA

gWIZ-GFP plasmids were purchased from Genlantis (San Diego, USA). The plasmids, expressing green fluorescent protein (GFP), were amplified in E. coli and isolated from a bacteria suspension using a Purelink HiPure Plasmid DNA Gigaprep kit K2100 (Invitrogen, Merelbeke, Belgium). Plasmid concentration measurements at a wavelength of 260 nm were performed on a NanoDrop 2000c (Thermo Fisher Scientific, Rockford, IL, USA) . The A_{260}/A_{280} ratio was measured to assess the purity. 25 µl aliquots at 1 µg/µl were prepared and stored at -20°C.

Covalent labeling of Cy5 molecules to the plasmids was performed according to the protocol provided by the manufacturer (Label IT kit, Mirus Bio Corporation, WI, USA). Briefly, Label IT reagent, the volume depending on the labeling density, was

mixed with 12 µl of pDNA and 5 µl 10 x Reaction buffer and subsequently adjusted with nuclease free water to a reaction volume of 50 µl. The reaction mixture was incubated overnight in the dark at room temperature. DNA:Cy5 ratios of 1:1, 2:1, 4:1, 6:1, 10:1, 20:1, 50:1 and 100:1 (w:v) were prepared. In Slattum (2003)[21], it is stated that a 1:1 (w:v) labeling density labels on average one base every 60 base pairs. We therefore assumed the previous mentioned ratios to be corresponding with on average 100, 50, 25, 16.7, 10, 5, 2 and 1 label per plasmid. Ethanol precipitation was used for DNA extraction and the precipitated DNA was reconstituted in HEPES buffer (20 mM HEPES, pH 7.2).

The intercalating dimeric cyanine nucleic acid stain TOTO-3 was used, as an alternative labeling method, according to manufacturer's instructions (Invitrogen, Molecular Probes, Merelbeke, Belgium). TOTO-3 iodide (1 mM in DMSO) was added to the pDNA and incubated overnight at room temperature in the dark. The fluorescently labeled DNA was then recovered using ethanol precipitation and reconstituted in HEPES buffer.

Liposome and Lipoplex Preparation

Lipoplexes were obtained by mixing Lipofectamine 2000 (Invitrogen, Merelbeke, Belgium) and pDNA in a Lipofectamine - DNA ratio of 5:1 (v:w) in HEPES buffer according to the protocol (Invitrogen, Merelbeke, Belgium). A DNA concentration of 0.02 µg/µl complex was used throughout the experiments.

Anionic liposomes were obtained by mixing phosphatidyl choline, DOPE and phosphatidyl serine (PS) in a 6/3/1 molar ratio in a chloroform/methanol solution (50:50). A lipid film is obtained by drying under vacuum. 1 ml of HEPES (20 mM HEPES, pH 7.2) was subsequently added for re-suspension and the mixture was vortexed for uniformity.

Transfection

HeLa cells were plated 1 day before transfection in 6 or 12 well plates at respectively 230.000 and 100.000 cells/well. Incubation of the cells with the lipoplexes prepared with pDNA at various labeling densities was done at 1 µg of DNA per well (in 500 µl lipoplex solution, prepared as described above) for 4 hours at 37°C. Afterwards, the cells were washed with phosphate buffered saline (PBS) and fresh medium was added for overnight incubation. After 24 hours, the cells were

trypsinized and examined by flow cytometry (FACSCalibur, BD Biosciences Benelux N.V., Erembodegem, Belgium).

Cellular Uptake

HeLa cells were plated 1 day prior transfection in 6 or 12 well plates at respectively 230.000 and 100.000 cells/well. Lipoplexes were prepared as described above and incubated for 4 hours at 37°C, analogous to a transfection. The cells were washed with PBS, trypsinized and suspended in flow buffer (1% bovine serum albumin in PBS). The red fluorescence from the plasmids was measured by FACS. Alternatively, the cells were analyzed after 4 hours by confocal laser scanning microscopy (Nikon EZC1-si, Nikon Instruments Europe B.V., Brussels, Belgium). Bright field images were recorded of the cells in combinations with red fluorescent images obtained by excitation at 636 nm and emission captured with a 660 nm long pass filter.

Dissociation from the Lipoplex

Lipoplexes were prepared as described above. 10 µl of a lipoplex solution (0.02 µg DNA/µl) was incubated for 20' at room temperature with different concentrations of sodium dodecyl sulphate (SDS) to obtain a total volume of 20 µl. A 50% sucrose loading buffer was added and the mixture was loaded on a 1% agarose gel in 1 x TBE buffer (90 mM Tris-base/90 mM Borate/2 mM EDTA). The gel was run for 50' at 100 V, stained with ethidium bromide and imaged.

Anionic Vesicle-Induced DNA Release

Lipoplexes and anionic liposomes were prepared as described above. Quant-iT PicoGreen reagent (Molecular Probes, Eugene, OR, USA) was 200-fold diluted in 1 x TE buffer (10 mM TRIS-HCl, 1 mM EDTA, pH 7.2). After initial fluorescence measurements, to determine the starting value, a 5-fold molar excess of anionic liposomes was added. The fluorescence emission (PerkinElmer 2104 EnVision, λex. 492 nm, λem. 535 nm), indicating the amount of accessible DNA, was followed for at least 15'.

Oligonucleotide Leakage Assay

HeLa cells were plated 1 day prior transfection in CELLview glass-bottom dishes (Greiner Bio-One GmbH, Frickenhausen, Germany). Lipoplexes were

prepared as described above, but to the solution of plasmid DNA (unlabeled, 10 labels/plasmid and 100 labels/plasmid), 5 µl of Cy5-labeled oligonucleotides (ODNs) at 2 µM was added before complexation. The cells were incubated with these complexes for 8 hours at 37°C and 5% CO_2. Images were recorded by confocal laser scanning microscopy and fluorescence fluctuations for fluorescence correlation spectroscopy (FCS) were recorded with a Compact FCS Upgrade Kit (PicoQuant GmbH, Berlin, Germany) on the Nikon EZC1-si confocal laser scanning microscope setup. Cells were imaged with bright field microscopy to determine locations for intranuclear FCS measurements. For every condition three 60 s FCS measurements were performed in three different nuclei. Autocorrelation curves were calculated from time traces with a binning time of 1000 µs and analyzed by a single species fit with the triplet-state model incorporated in the SymPhotime Software (PicoQuant GmbH, Berlin, Germany) with κ value fixed at 6 for the red channel and 9 for the green channel (see **Chapter 2** for a more detailed explanation of this model). All microscopy images were processed with ImageJ. [22]

Polymerase Chain Reaction

In vitro amplification of labeled plasmids, was performed using the GoTaq Flexi DNA Polymerase protocol (Promega Corporation, WI, USA, revision 03/08) using a Polymerase Chain Reaction (PCR) nucleotide mix from Promega Corporation (WI, USA). 5'-tggctagcaaaggagaagaac-3' was used as a forward primer and 5'-tcatccatgccatgtgtaatc-3' as the reverse primer. A reaction volume of 50 µl was prepared with an initial DNA concentration of 0.2 µg/50 µl. The PCR program consisted of 2' at 95°C, 25 cycles of 45 s at 95°C - 45 s at 59°C – 45 s at 72°C and as a final extension step 5' at 72°C.

10 µl of PCR product was loaded on a 1% agarose gel prepared in 1 x TBE buffer, ran for 50' at 100 V, stained with ethidium bromide, imaged and analyzed with ImageJ. [22]

Nuclear Microinjection

Microinjection experiments were performed with a Femtojet microinjector and an Injectman NI 2 micromanipulator (Eppendorf, Hamburg, Germany) coupled to an EZC1-si confocal laser scanning microscope. 24 hour prior to injection, HeLa cells, suspended in DMEM F12 phenol red-free cell medium containing 10% FBS, were

plated in CELLview glass-bottom dishes (Greiner Bio-One GmbH, Frickenhausen, Germany). The dish was placed in a stage top CO_2 incubator at 37°C and 5% CO_2 (Tokai Hit Co., Shizuoka, Japan). Injections, in the nuclei of 50 HeLa cells, were performed using non-labeled pDNA and labeled pDNA at labeling densities of 10 and 100 labels/plasmid at a concentration of 10 ng/µl in water. 2h post-injection, confocal images were captured in the transmission, green (excitation with 488 nm) and red (excitation with 633 nm) channel.

RESULTS

Transfection

pDNA encoding GFP was covalently labeled with Cy5 using the commercially available Mirus kit. The labeling density was varied between 0 and 100 labels on average per plasmid. Then, labeled plasmids were delivered to HeLa cells using the cationic lipid vector Lipofectamine 2000. Transfection efficiency was quantified by flow cytometry using the expressed GFP signal.

Figure 1 A shows the percentage of cells expressing GFP in function of the pDNA labeling density. Up to 5 labels per plasmid no significant decrease ($p < 0.01$) in transfection efficiency can be observed when compared to non-labeled pDNA. However, a significant decrease ($p < 0.05$) in transfection efficiency was present starting from 10 labels per plasmid. The decrease in transfection efficiency became even more pronounced for higher labeling densities. The samples with the highest labeling intensities (50 and 100 labels per plasmid) did not show any significant transfection ($p < 0.01$) as compared to the non-transfected control cells (NC).

The same experiment was repeated using an intercalating fluorescent dye, rather than a covalently coupled one. Figure 1 B shows transfection efficiencies in HeLa cells transfected with pDNA labeled with TOTO-3. It can be seen that with this intercalating dye markedly different results were obtained, with transfection levels that are independent from the labeling density. Since we do see an effect of the covalent labeling method on transfection, we wanted to know the reason behind this observation. To elucidate this, the effect of fluorescent labeling of pDNA on the different steps of the transfection process was investigated, as discussed below.

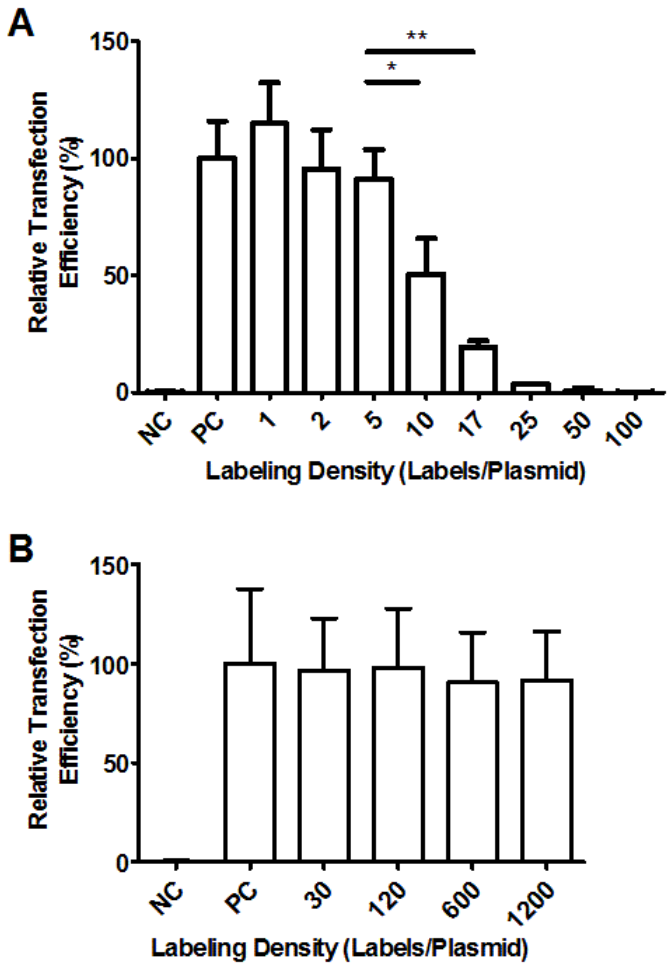

Figure 1 Relative transfection efficiency in function of labeling density, where cells transfected with unlabeled pDNA represent 100% transfection efficiency. (A) Relative transfection efficiency for the covalent labeled plasmids and (B) for the dimeric cyanine-labeled plasmids (TOTO-3). HeLa cells were incubated with lipoplexes (Lipofectamine/pDNA 5:1) for 4 hours, and green fluorescence was measured 24 hours post-transfection with flow cytometry. NC: Negative Control: no plasmids were added. PC: Positive Control: unlabeled plasmids; *: $p < 0.05$, **:$p < 0.01$. All averages obtained from 3 independent transfection experiments with three repetitions with error bars representing the standard deviation.

Cellular Uptake

The first important step in the transfection pathway is the cellular entry of the complexes. Thus, it is of importance to investigate if cellular internalization is impeded. Cellular uptake was quantified by determination of the number of cells containing lipoplexes (with red fluorescently labeled pDNA) using flow cytometry. In Figure 2 A it can be seen that almost 100% of cells contain lipoplexes irrespective of the labeling density. Figure 2 B shows the average fluorescence intensity per cell.

The linear increase in fluorescence intensity as a function of labeling density, can most likely be attributed to the increasing number of labels per plasmid. Confocal images (Figure 2 C-D.) confirm that lipoplexes are effectively internalized into the HeLa cells (rather than sticking to the outer plasma membrane). Taken together, these results show no substantial effect on the cellular uptake of lipoplexes prepared with covalently labeled plasmids, regardless of the labeling density.

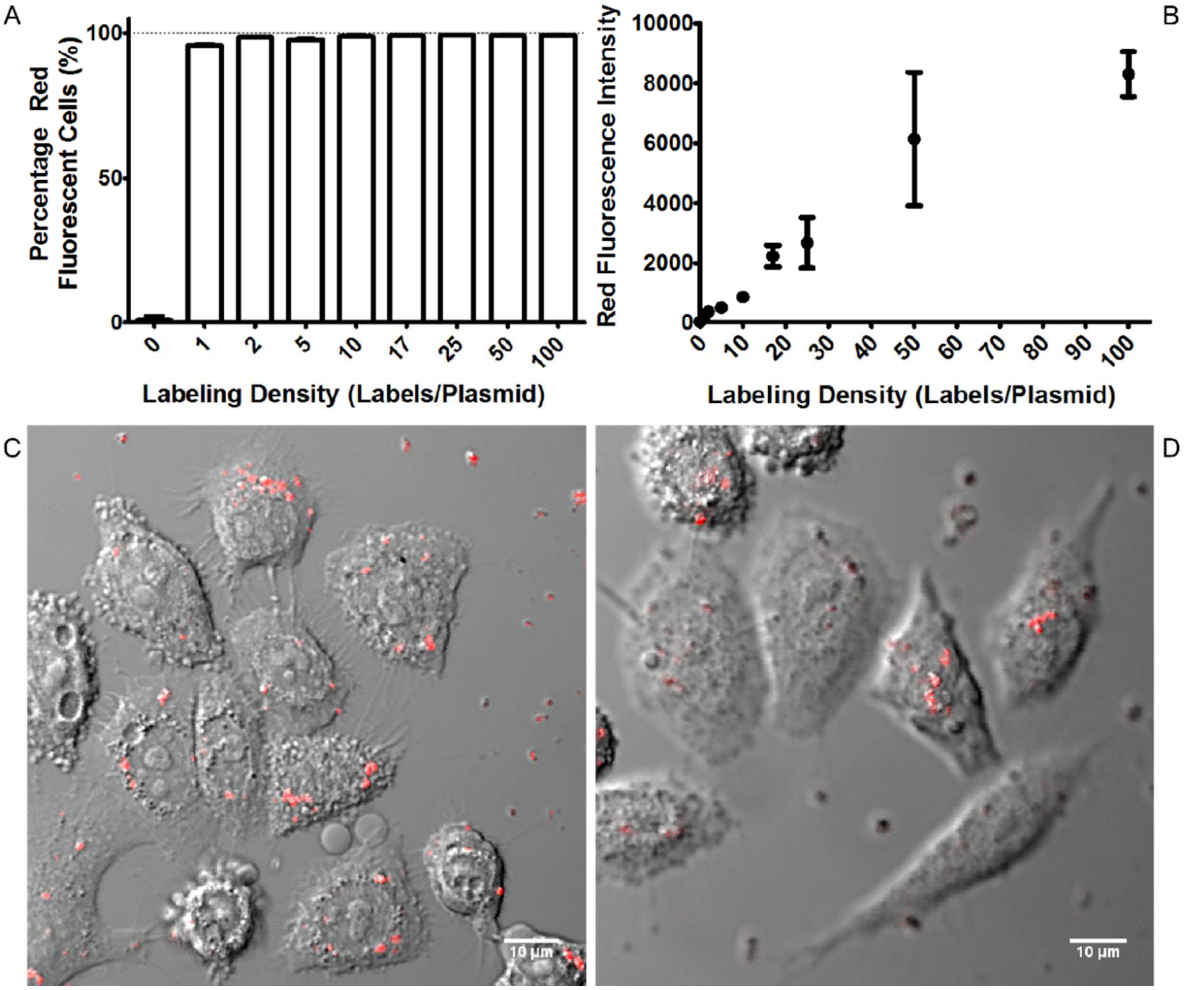

Figure 2 Cellular uptake measured by the percentage of red fluorescence positive cells, red fluorescence intensity, and confocal imaging. HeLa cells were incubated for 4 hours with lipoplexes (Lipofectamine/pDNA 5:1) and measured with flow cytometry. (A) Percentage of red fluorescent cells was measured in the function of labeling density. The percentage represents the relative amount of cells which are associated with labeled pDNA. (B) Red fluorescence intensity was measured with FACS in the function of labeling density expressed as labels per plasmid. (C,D) Superposition of bright field and confocal images of HeLa cells after 4 hour incubation with lipoplexes containing pDNA with, respectively, 100 and 10 labels per plasmid. (A) and (B) depict the average values of 3 independent experiments with 3 repetitions. Error bars represent the standard deviation on the averages.

Dissociation from the Lipoplexes and Implications for Endosomal Escape

After cellular uptake, which typically proceeds through endocytosis, lipoplexes are present in the endosomal compartment. Since the dissociation of pDNA from the lipoplex is essential to have free plasmids that potentially induce the expression of the target protein, the ability of pDNA to dissociate from a lipid environment was investigated using two assays. First, we tested the ability of pDNA to dissociate from lipoplexes by the addition of the surfactant SDS, which induces the rupture of lipoplexes. pDNA release was measured by agarose gel electrophoresis and ethidium bromide staining. Unlabeled pDNA was found to be released from the lipoplexes at a concentration of 5 mg/l SDS (Figure 3 A). While the same result was found for pDNA with 10 labels per plasmid (Figure 3 B), also intact lipoplexes were observed at all concentrations of SDS, indicating that not all DNA dissociated from the complexes. At 100 labels per plasmid, no dissociation from the lipoplex was observed, not even for SDS concentrations up to 3 g/l (Figure 3 C). It should be noted that the same results were obtained when another lipid based carrier such as DOTAP/DOPE liposomes were used to complex the plasmid DNA.

Next, the ability of pDNA to release from lipoplexes upon addition of anionic lipids with an endosomal mimicking composition was measured. It is generally accepted that the mixing of the lipids from the lipoplexes with the lipid bilayer of the endosome is responsible for the release of the cargo in the cytosol. [23-25] Therefore, this DNA release assay is generally used to get an insight into the ability of lipoplexes to undergo lipid mixing, which is essential for a successful endosomal escape. [7, 26] Lipoplexes are mixed with anionic liposomes in a solution containing PicoGreen, a compound that becomes green fluorescent when intercalated in the DNA double strand. When present in a lipoplex, DNA is not accessible and will not contribute to the fluorescent signal. However, as the pDNA is displaced from the lipoplexes upon adding the “artificial endosomes”, the fluorescent signal is expected to increase. As can be seen in Figure 4, the rate and the extent to which DNA is released clearly differs for different labeling densities. About 15 min after addition of the anionic liposomes, we observed around 70% release for unlabeled pDNA, 60% for pDNA with 10 labels per plasmid, and only around 20% for pDNA with 100 labels per plasmid when compared to the signal expected for free pDNA of the same labeling density.

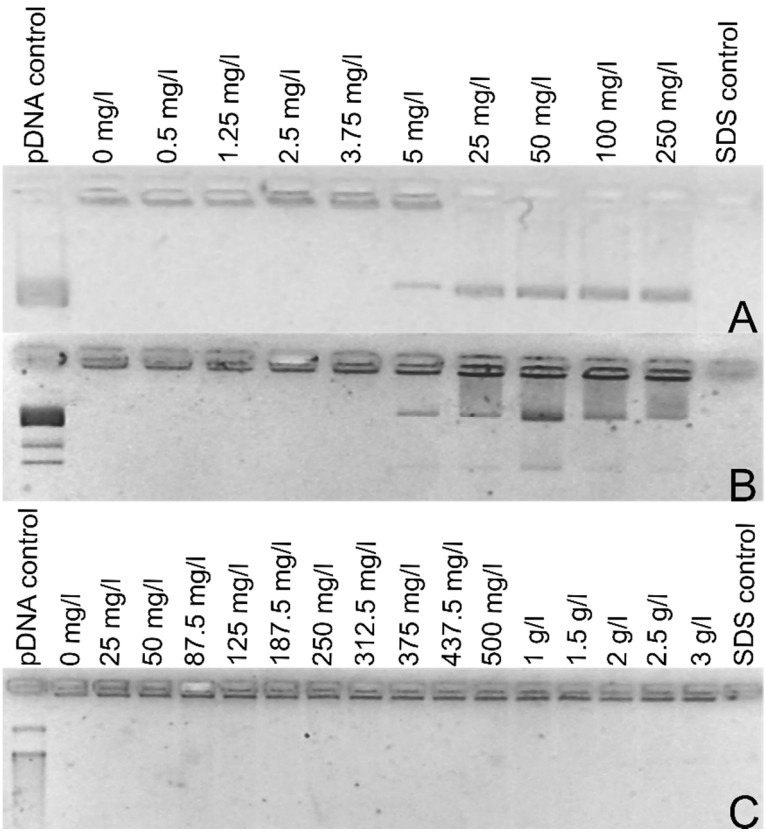

Figure 3 Image of the 1% agarose gel of lipoplexes (Lipofectamine/pDNA 5:1) after addition of SDS and incubation for 20 min at room temperature. (A) Unlabeled pDNA. (B) pDNA containing 10 labels per plasmid. (C) pDNA containing 100 labels per plasmid. pDNA control: pDNA diluted with HEPES buffer. SDS control: 500 mg/l of SDS in HEPES. Representive image of three independent experiments.

To investigate if the lipoplexes are still able to interact with the endosomes and release cargo, an ODN leakage assay was performed. [27] Unlike pDNA, free ODNs are known to rapidly accumulate in the cell nucleus. [28, 29] The presence of ODNs in the nucleus of the cell thus indicates that endosomal escape and release of the ODNs from the liposomes has taken place. pDNA and labeled ODNs were co-complexed and incubated on cells for 8 hours. Confocal images (Figure 5) showed that independent of the labeling density of the co-complexed pDNA, most of the cells displayed a uniform red signal in the nucleus. This indicates that labeled nucleic acids are able to escape the lipoplex as well as the endosomal compartment for all plasmid labeling densities.

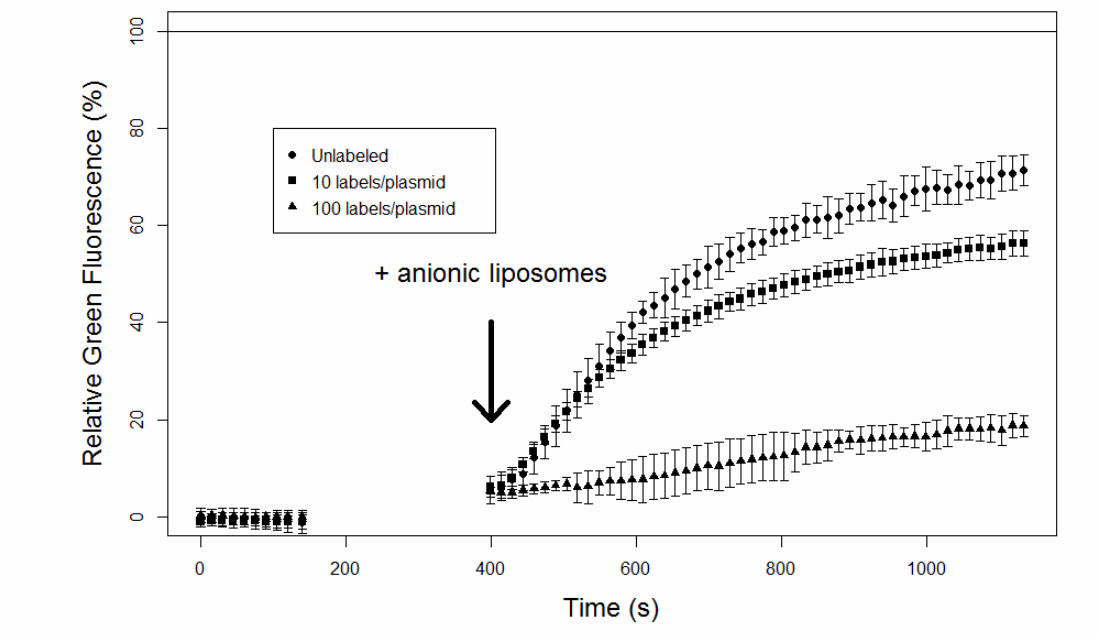

Figure 4 Accessibility of pDNA toward PicoGreen in lipoplexes after addition of an anionic lipid mixture at t = 400 s. pDNA was complexed with Lipofectamine (LF/DNA, 5:1 (v/w)). The anionic lipid mixture was composed of Phosphatidyl Choline/DOPE/PS (6:3:1 molar ratio) and added to the liposomes in a 5-fold molar excess, as indicated with the arrow. Results are shown relative to the green fluorescence measured for free pDNA of the same labeling density. (●) unlabeled pDNA. (■) labeled pDNA containing 10 labels per plasmid. (▲) labeled pDNA containing 100 labels per plasmid. Averages are calculated based on three independent experiments with three repetitions. Error bars are the standard deviation on the average.

The diffusion coefficients of the red signal, as investigated by FCS, for the samples with 10 and 100 labels per plasmid, at respectively 7.88 ± 2.89 µm²/s and 8.07 ± 2.09 µm²/s, were in accordance with the unlabeled pDNA sample, where only the ODNs were labeled, at 8.32 ± 3.36 µm²/s (Figure 6). This confirms that only released ODNs are responsible for this red fluorescent signal in the nucleus, since the presence of pDNA would induce a decrease in diffusion coefficient. As FCS can also detect the expressed GFP, also green autocorrelation curves were recorded in the nuclei of the transfected cells. In agreement with Figure 1, only the non-labeled plasmid DNA and the plasmid containing on average 10 labels were able to induce GFP expression (Figure 6).

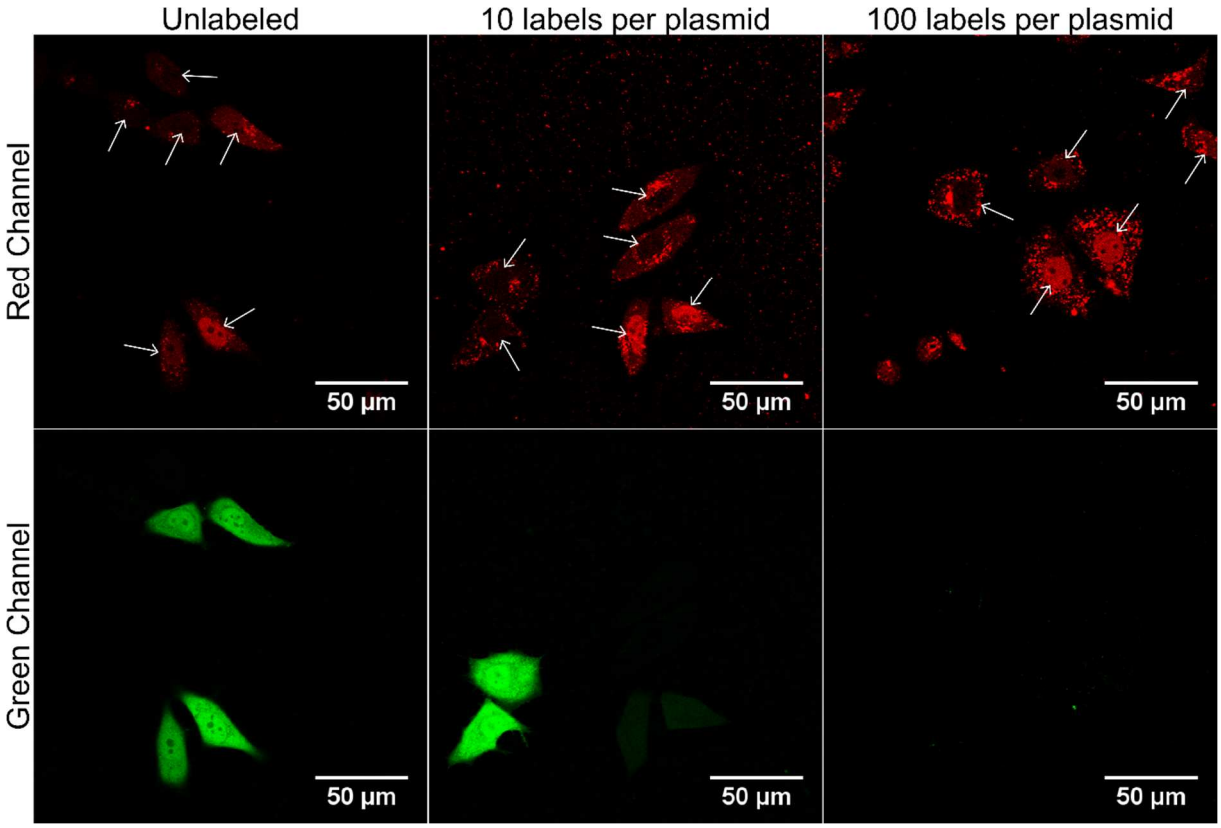

Figure 5 Cy5-labeled oligonucleotide leakage assay. HeLa cells were incubated during 8 hours with lipoplexes containing Cy5-ODNs mixed with plasmids which are unlabeled, contain 10 labels per plasmid, or contain 100 labels per plasmid. (Red channel) Cy5-ODNs and Cy5-pDNA signal. Only free ODNs accumulate in the nuclei of the cells. Nuclei are indicated with white arrows. (Green channel) GFP expression of the corresponding formulations.

Taken together, our experiments indicate that labeled plasmid DNA has a higher affinity for lipid structures resulting in the inhibition of pDNA release from these structures, but without disturbing the intrinsic capabilities of the lipoplex to promote endosomal escape. Upon interaction of the lipoplexes with the endosomal membrane, however, pDNA with a higher labeling density will most likely not be released from the lipoplexes, in contrast to pDNA with lower labeling density or the shorter ODNs.

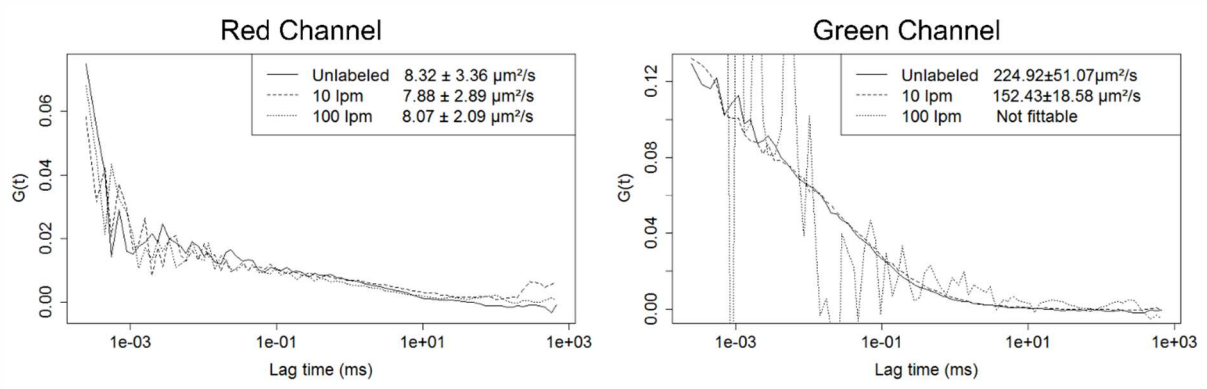

Figure 6 Representative autocorrelation curves derived from intranuclear FCS measurements. Left: derived from red fluorescent fluctuations. Right: derived from green fluorescent fluctuations. Diffusion coefficients calculated based on three measurements in three separate nuclei.

Transcription

To verify the effect of the labeling on the transcription properties of pDNA, in living cells, 50 nuclei of HeLa cells were microinjected with pDNA encoding for GFP. Confocal images were acquired immediately and 2 hours post-injection (Figure 7 A-C.). In 90% of the cells injected with non-labeled plasmids, expression of GFP was observed after 2 hours. pDNA labeled with a density of 10 labels per plasmid showed green fluorescent protein expression in 50% of the injected cells after 2 hours, whereas in the case of 100 labels per plasmid expression of GFP was never observed, not even 24 hours after injection. These microinjection experiments clearly demonstrate the impairment of transcription by the random covalent attachment of labels to plasmids. It should be noted that the results obtained with microinjection are closely related to the results obtained from the transfection experiments.

As an alternative technique, *in vitro* amplification of the plasmids was performed using semi-quantitative PCR. In Figure 7 D, the amplification is shown in relation to the labeling density of pDNA relative to unlabeled pDNA. A significant decrease is found starting from 25 labels per plasmid. All labeling densities, however, retain at least 30% of their amplification properties. Thus, although PCR acts as a fast assay to observe changes in the availability to transcriptionally active enzymes, like polymerase, it underestimates the effect of the labeling in living cells, when compared to nuclear injections.

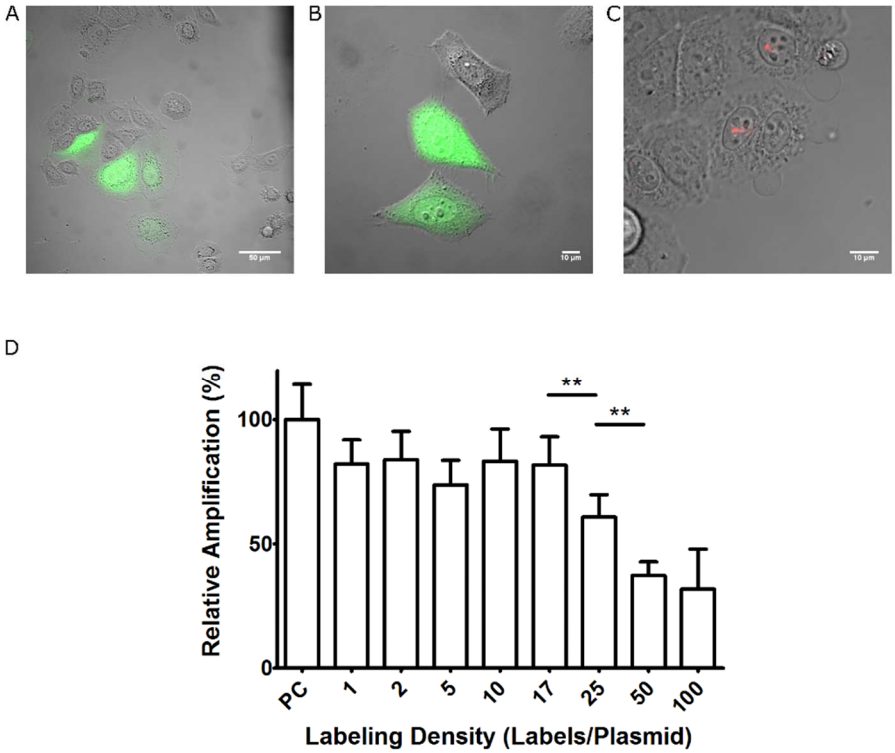

Figure 7 Transcription of the labeled green fluorescent protein construct was tested by nuclear microinjection and a PCR assay was used to check for availability to transcriptionally active enzymes. (A–C) Confocal images of HeLa cells 2 hour after nuclear injection with (A) non-labeled pDNA, (B) pDNA containing 10 labels per plasmid and (C) pDNA containing 100 labels per plasmid. Green: GFP expression. Red: fluorescently labeled plasmids. (D) Relative amplification in a PCR reaction of pDNA at different labeling densities. PC: Positive Control: Unlabeled pDNA. ** $p < 0.01$. Averages in (D) are based on three independent experiments with error bars depicting the standard deviation on the average.

DISCUSSION

The administration of pDNA to cells to induce protein expression is used in a variety of applications. In non-viral gene delivery, cationic polymers or liposomes are used to deliver the nucleic acids to the cells. Then, different extra- and intracellular barriers need to be overcome before protein expression is obtained. Fluorescent labeling of pDNA is frequently done, as fluorescence microscopy based techniques are widely used with respect to understanding the intracellular processing in drug delivery. The effect of the labeling itself on the intracellular behavior is however often overlooked. In this study the effect of random covalently attaching Cy5 fluorophores to pDNA on the transfection efficiency with lipid-based carriers in HeLa cells is assessed. The main questions raised in this work are: which labeling densities of plasmid DNA are still representative for the native pDNA molecule and at which point

in the transfection pathway do the used labeling densities start to alter the intracellular processing of gene complexes prepared with labeled pDNA and liposomes. To answer these questions, we performed a series of assays that mimic the different steps of the intracellular processing. Cy5 labeled pDNA, complexed with Lipofectamine 2000 as a carrier, was used throughout this study.

We found that for labeling densities assumed to be lower than 10 labels on average per plasmid, the transfection pathway of lipoplexes can be considered unaffected (Figure 1 A). Transfection efficiency was affected dramatically, however, for a labeling density starting from 10 labels per plasmid. Since the average length of the pDNA used was about 5800 base pairs, this implies that on average one fluorophore every 580 base pairs already influences the intracellular processing of the pDNA when complexed in lipoplexes.

Several experiments were conducted to verify which critical points in the transfection pathway with lipid-based carriers were affected at these higher labeling densities. The first step in the transfection pathway is the cellular uptake, which could be measured using flow cytometry. In case of the Lipofectamine complexes, uptake was not affected for any labeling density as more than 90% of the cells take up the plasmid DNA (Figure 2). This most likely can be explained by the fact that the plasmids, and thus the fluorophores, are inside the lipoplexes, covered by one or more lipid layers. Evidently, this might be different for other types of lipo or polyplexes and needs to be investigated on a case-by-case basis. A control by confocal microscopy was added to verify if all complexes are effectively internalized, rather than being bound to the outer plasma membrane. It should be noted here that no nuclear or cellular membrane stain was used in this microscopy experiment, so based on these images, we cannot be sure that the lipoplexes are inside the cells. Figure 5 confirms however that the lipoplexes with labeled pDNA are indeed inside of the cell.

When the lipoplex is taken up by the cell, it is entrapped in the endosomal compartment. Without endosomal escape, the contents of the endosomes will eventually be digested by lysosomal degradation of the cell. It has been suggested that lipid-based carriers escape from the endosomal compartment by lipid mixing with the endosomal membrane, thereby releasing free pDNA in the cytoplasm of the cells. [23-25] To ensure release, the affinity of pDNA for the lipids should not be too high. We

found however, that dissociation of plasmids containing 100 fluorophores per plasmid from the lipoplexes, after addition of SDS (Figure 3) and anionic lipids (Figure 4), is not as efficient as for plasmids bearing 10 or no labels per plasmid. A possible reason for this impaired release can most likely be found in the increase of hydrophobicity of the labeled pDNA compared to unlabeled pDNA. As each fluorophore introduces a certain level of hydrophobicity, the affinity of the plasmid for the lipids (either those of the liposomes or the endosomal membrane) increases. Therefore, the ability to escape lipid structures like liposomes and endosomes can be challenging for labeled plasmids.

In 2013, endosomal escape events in living cells were observed directly for the first time for gene complexes using state of the art microscopy equipment and a specific labeling method. [27] Here the complexes were prepared by a mixture of PEI and fluorescently labeled ODNs. As long as the endosome was intact, ODN fluorescence was quenched. When endosomal escape occurs, a burst in fluorescence is observed due to dequenching of the fluorescence. In the case of lipid-based carriers, this quenching does not occur, but released ODNs gradually accumulated in the nuclei of the cells, demonstrating their endosomal escape and release from the lipoplexes. Using this methodology, in living cells we found that regardless of the labeling density of the co-complexed plasmid DNA, all formulations showed fluorescent nuclei, demonstrating that lipid mixing, and thus release of cargo out of the lipoplex, can still occur (Figure 5). This indicates that the first step of endosomal escape, namely lipid mixing with the endosomal membrane, is most likely not affected. The higher affinity of the labeled pDNA for the lipid vesicles may lead, however, to a decreased or inhibited release into the cytosol during this endosomal escape event. As the amount of free pDNA in the cytoplasm most likely relates to the obtained transfection efficiencies, [30, 31] the higher affinity for lipid structures could be attributing to the decreased transfection efficiencies observed in Figure 1.

The assay which induces dissociation of pDNA from the liposomes by SDS can be modified for polyplexes. The adjuvant used must then be selected based on the dissociation mechanism of the polyplexes. The anionic lipid release assay was used as an *in vitro* DNA release assay to study the lipid mixing and ability to release free pDNA of a carrier which, for lipid-based carriers, could give an indirect indication of endosomal escape properties. Live intracellular measurements, like the ODN

release assay, give additional insight into the cellular endosomal escape. One should keep in mind, however, that it is the escape of small ODNs that is observed, rather than the pDNA itself. Other options like dual-color colocalization of pDNA with the endosomal membrane, [32] are potentially interesting, but again imply the labeling of the pDNA itself. Therefore, this method was not applicable to compare both the labeled and non-labeled plasmid DNA that was used in this study. It should also be noted that the co-complexation was not verified, meaning that we are not sure that all lipoplexes contain both pDNA and ODNs. The fluorescent signal in the nucleus could therefore be coming from lipoplexes that only contain ODNs. The co-complexation could be checked by using red labeled pDNA and green labeled ODNs and inspecting the colocalization via confocal microscopy or FCS.

The final step in a successful transfection pathway is the transcription of the plasmids in the nucleus of the cells. The *in vitro* amplification of pDNA with higher labeling densities was affected, suggesting there might be hindrance of the enzymatic interaction between DNA polymerase and the DNA backbone. It should however be noted that PCR is an assay for DNA amplification, rather than investigating the transcription process. Therefore nuclear injections of non-labeled and labeled pDNA were performed, directly following transcription in living cells (Figure 7 A-C). While 90% of cells injected with non-labeled pDNA expressed GFP, the levels decrease to 50% and 0% when plasmids with respectively 10 and 100 labels attached were used. Transcription is thus clearly impaired when using higher labeling densities. It should be noted that the percentages of GFP positive cells found, corresponded well to the levels observed in Figure 1. These results point out that independent from the used carrier – pDNA combination, covalent labeled Cy5 pDNA that reaches the nucleus will never be efficiently transcribed, when high labeling densities are used.

Another factor that can lower the transfection efficiency is the fact that labeled plasmids are excluded from the nucleus of the daughter cells after mitosis, as was observed by Gasiorowski and Dean [10], thereby limiting the time frame in which they can be transcribed. Although we cannot exclude that nuclear entry of labeled pDNA is also impaired, several authors have seen that nuclear inclusion of labeled pDNA did not seem to be a problem. [8, 33]

As shown in this study, the highest labeling density of pDNA, which is the recommended density by the manufacturer, can only be used to follow the first step in the transfection pathway, namely cellular uptake. Trying to tackle for example the question of where and when endosomal escape of these labeled pDNA molecules takes place, is however impossible. This could explain why the mechanism of endosomal escape has never been clearly visualized in literature before, as the affinity of the labeled pDNA for the endosomal membranes may prevent these endosomal escape events, which do occur for non-labeled pDNA molecules.

Interference of your DNA labeling with the intracellular trafficking might be prevented in a number of ways. Other means of fluorescent labeling, such as intercalating dyes could be a valuable alternative [34] next to PNA clamp linked fluorophores, [8, 35, 36] chemical labeling, [37] enzymatic labeling, [38] etc. Another option is label-free imaging, which however still comes with some problems. [39] It should be noted that intercalating dyes had no effect on the level of transfection (Figure 1). This non-covalent labeling method has, however, as a drawback that the label can redistribute and integrate aspecifically into other DNA present in the cell. Therefore, intercalating dyes are not an option for intracellular trafficking applications.

Apart from alternative labeling techniques, also lowering the labeling density of the pDNA could be an option for intracellular studies, provided that the fluorescence microscopy techniques used are sensitive enough to visualize the labeled pDNA. Fluorescence Correlation Spectroscopy and Single Particle Tracking (SPT) are promising techniques for this purpose (see **Chapter 2** for a background on both techniques). [40] We have shown previously that FCS in combination with confocal microscopy could be used to follow the delivery and degradation of antisense oligonucleotides. [41] Also the dissociation of oligonucleotides from their carrier could be studied. [42] It should be noted that in both cases lipid-based carriers were used to deliver fluorescently labeled short antisense oligonucleotides. A deterioration in the dissociation from the lipid carrier was however not observed. Therefore, the effect of labeling will depend both on the type of DNA, the fluorescent labels and the delivery carrier used.

CONCLUSION

We found that covalent attachment of Cy5 fluorophores to pDNA affects the transfection efficiency of lipid-based carriers on different levels, including an increased affinity for lipids, which may have implications for the dissociation from the lipoplex and endosomal compartment and most importantly a lowered intrinsic ability of the labeled pDNA to be transcribed in the nucleus of the cells. An increase in hydrophobicity and steric hindrance of the attached labels may be responsible for the quantifiable decrease in transfection efficiency. This points out that when designing an experiment where fluorescent microscopy is used to follow biomolecules intracellularly, one must balance fluorescent signal strength against the effect of the labeling on the cellular processing to prevent biased conclusions. The series of experiments that were used in this study to evaluate the intracellular processing of pDNA can easily be extrapolated to other labeling techniques and other nucleic acid/carrier combinations. Therefore, when one aims to follow fluorescently labeled biomolecules intracellular, we strongly recommend to study the effect of the labeling on the cellular processing to prevent biased conclusions.

REFERENCES

(1) Chen, C., and Okayama, H. (1987) High-efficiency transformation of mammalian cells by plasmid DNA. *Molecular and cellular biology 7*, 2745-2752.

(2) Hacein-Bey-Abina, S., von Kalle, C., Schmidt, M., Le Deist, F., Wulffraat, N., McIntyre, E., Radford, I., Villeval, J.-L., Fraser, C., Cavazzana-Calvo, M., et al. (2003) A serious adverse event after successful gene therapy for X-linked severe combined immunodeficiency. *The New England journal of medicine 348*, 255-256.

(3) Alexander, B. L., Ali, R. R., Alton, E. W., Bainbridge, J. W., Braun, S., Cheng, S. H., Flotte, T. R., Gaspar, H. B., Grez, M., Griesenbach, U., et al. (2007) Progress and Prospects: Gene Therapy Clinical Trials (Part 1). *Gene Therapy 14*, 1439-1447.

(4) Edelstein, M., Abedi, M., and Wixon, J. (2007) Gene therapy clinical trials worldwide to 2007--an update. *The journal of gene medicine 9*, 833-842.

(5) Boulaiz, H., Marchal, J., Prados, J., Melguizo, C., and Aránega, A. (2005) Non-viral and viral vectors for gene therapy. *Cellular and Molecular Biology 51*, 3-22.

(6) Wang, T., Upponi, J., and Torchilin, V. (2012) Design of multifunctional non-viral gene vectors to overcome physiological barriers: dilemmas and strategies. *International journal of pharmaceutics 427*, 3-20.

(7) Xu, Y., and Szoka, F. (1996) Mechanism of DNA release from cationic liposome/DNA complexes used in cell transfection. *Biochemistry 35*, 5616-5623.

(8) Zelphati, O., Liang, X., Hobart, P., and Felgner, P. (1999) Gene chemistry: functionally and conformationally intact fluorescent plasmid DNA. *Human gene therapy 10*, 15-24.

(9) Ludtke, J., Sebestyén, M., and Wolff, J. (2002) The effect of cell division on the cellular dynamics of microinjected DNA and dextran. *Molecular Therapy 5*, 579-588.

(10) Gasiorowski, J., and Dean, D. (2005) Postmitotic nuclear retention of episomal plasmids is altered by DNA labeling and detection methods. *Molecular Therapy 12*, 460-467.

(11) Watson, P., Jones, A., and Stephens, D. (2005) Intracellular trafficking pathways and drug delivery: fluorescence imaging of living and fixed cells. *Advanced drug delivery reviews 57*, 43-61.

(12) De Smedt, S., Remaut, K., Lucas, B., Braeckmans, K., Sanders, N., and Demeester, J. (2005) Studying biophysical barriers to DNA delivery by advanced light microscopy. *Advanced Drug Delivery Reviews 57*, 191-210.

(13) Lang, P., Yeow, K., Nichols, A., and Scheer, A. (2006) Cellular imaging in drug discovery. *Nature reviews. Drug discovery 5*, 343-356.

(14) Remaut, K., Lucas, B., Raemdonck, K., Braeckmans, K., Demeester, J., and De Smedt, S. (2007) Can we better understand the intracellular behavior of DNA nanoparticles by fluorescence correlation spectroscopy? *Journal of Controlled Release 121*, 49-63.

(15) Braeckmans, K., Buyens, K., Bouquet, W., Vervaet, C., Joye, P., De Vos, F., Plawinski, L., Doeuvre, L., Angles-Cano, E., Sanders, N., et al. (2010) Sizing nanomatter in biological fluids by fluorescence single particle tracking. *Nano letters 10*, 4435-4442.

(16) Vercauteren, D., Deschout, H., Remaut, K., Engbersen, J., Jones, A., Demeester, J., De Smedt, S., and Braeckmans, K. (2011) Dynamic colocalization microscopy to characterize intracellular trafficking of nanomedicines. *ACS Nano 5*, 7874-7884.

(17) Suh, J., Dawson, M., and Hanes, J. (2005) Real-time multiple-particle tracking: applications to drug and gene delivery. *Advanced drug delivery reviews 57*, 63-78.

(18) Bausinger, R., von Gersdorff, K., Braeckmans, K., Ogris, M., Wagner, E., Bräuchle, C., and Zumbusch, A. (2006) The transport of nanosized gene carriers unraveled by live-cell imaging. *Angewandte Chemie (International ed. in English) 45*, 1568-1572.

(19) Lai, S., Hida, K., Chen, C., and Hanes, J. (2008) Characterization of the intracellular dynamics of a non-degradative pathway accessed by polymer nanoparticles. *Journal of Controlled Release 125*, 107-111.

(20) Ruthardt, N., de Bruin, K., Braeckmans, K., Wagner, E., and Bräuchle, C. (2010) Live-cell imaging and single-particle tracking of polyplex internalization. *Drug Discovery Today 15*.

(21) Slattum, P. (2003) Efficient in vitro and in vivo expression of covalently modified plasmid DNA. *Molecular Therapy 8*.

(22) Rasband, W. S. (1997-2012) ImageJ. *U. S. National Institutes of Health, Bethesda, Maryland, USA*.

(23) Wasungu, L., and Hoekstra, D. (2006) Cationic lipids, lipoplexes and intracellular delivery of genes. *Journal of Controlled Release 116*, 255-264.

(24) Elouahabi, A., and Ruysschaert, J.-M. (2005) Formation and intracellular trafficking of lipoplexes and polyplexes. *Molecular Therapy 11*, 336-347.

(25) Zuhorn, I., Bakowsky, U., Polushkin, E., Visser, W., Stuart, M., Engberts, J., and Hoekstra, D. (2005) Nonbilayer phase of lipoplex-membrane mixture determines endosomal escape of genetic cargo and transfection efficiency. *Molecular Therapy 11*, 801-810.

(26) Rejman, J., Wagenaar, A., Engberts, J., and Hoekstra, D. (2004) Characterization and transfection properties of lipoplexes stabilized with novel exchangeable polyethylene glycol-lipid conjugates. *Biochimica et biophysica acta 1660*, 41-52.

(27) ur Rehman, Z., Hoekstra, D., and Zuhorn, I. (2013) Mechanism of polyplex- and lipoplex-mediated delivery of nucleic acids: real-time visualization of transient membrane destabilization without endosomal lysis. *ACS nano 7*, 3767-3777.

(28) Chin, D. J., Green, G. A., Zon, G., Szoka, F. C., Jr., and Straubinger, R. M. (1990) Rapid nuclear accumulation of injected oligodeoxyribonucleotides. *New Biol 2*, 1091-100.

(29) Vivès, E., Dell'Aquila, C., Bologna, J.-C., Morvan, F., Rayner, B., and Imbach, J.-L. (1999) Lipophilic pro-oligonucleotides are rapidly and efficiently internalized in HeLa cells. *Nucleic Acids Research 27*, 4071-4076.

(30) Symens, N., Rejman, J., Lucas, B., Demeester, J., De Smedt, S. C., and Remaut, K. (2013) Noncoding DNA in Lipofection of HeLa Cells—A Few Insights. *Molecular Pharmaceutics 10*, 1070-1079.

(31) Symens, N., Soenen, S., Rejman, J., Braeckmans, K., De Smedt, S., and Remaut, K. (2012) Intracellular partitioning of cell organelles and extraneous nanoparticles during mitosis. *Advanced drug delivery reviews 64*, 78-94.

(32) Deschout, H., Martens, T., Vercauteren, D., Remaut, K., Demeester, J., De Smedt, S., Neyts, K., and Braeckmans, K. (2013) Correlation of Dual Colour Single Particle Trajectories for Improved Detection and Analysis of Interactions in Living Cells. *International Journal of Molecular Sciences 14*, 16485-16514.

(33) Dean, D., Strong, D., and Zimmer, W. (2005) Nuclear entry of nonviral vectors. *Gene therapy 12*, 881-890.

(34) Rye, H., Yue, S., Wemmer, D., Quesada, M., Haugland, R., Mathies, R., and Glazer, A. (1992) Stable fluorescent complexes of double-stranded DNA with bis-intercalating asymmetric cyanine dyes: properties and applications. *Nucleic acids research 20*, 2803-2812.

(35) Svahn, M., Lundin, K., Ge, R., Törnquist, E., Simonson, E., Oscarsson, S., Leijon, M., Brandén, L., and Smith, C. (2004) Adding functional entities to plasmids. *The journal of gene medicine 6 Suppl 1*, 44.

(36) Srinivasan, C., Siddiqui, S., Silbart, L., Papadimitrakopoulos, F., and Burgess, D. (2009) Dual fluorescent labeling method to visualize plasmid DNA degradation. *Bioconjugate chemistry 20*, 163-169.

(37) Proudnikov, D., and Mirzabekov, A. (1996) Chemical methods of DNA and RNA fluorescent labeling. *Nucleic acids research 24*, 4535-4542.

(38) Schmidt, F., Hüben, M., Gider, B., Renault, F., Teulade-Fichou, M.-P., and Weinhold, E. (2008) Sequence-specific Methyltransferase-Induced Labelling (SMILing) of plasmid DNA for studying cell transfection. *Bioorganic & medicinal chemistry 16*, 40-48.

(39) Parekh, S., Lee, Y., Aamer, K., and Cicerone, M. (2010) Label-free cellular imaging by broadband coherent anti-Stokes Raman scattering microscopy. *Biophysical journal 99*, 2695-2704.

(40) Braeckmans, K., Buyens, K., Naeye, B., Vercauteren, D., Deschout, H., Raemdonck, K., Remaut, K., Sanders, N., Demeester, J., and De Smedt, S. (2010) Advanced fluorescence microscopy methods illuminate the transfection pathway of nucleic acid nanoparticles. *Journal of Controlled Release 148*, 69-74.

(41) Remaut, K., Lucas, B., Braeckmans, K., Sanders, N., Demeester, J., and De Smedt, S. (2006) Delivery of phosphodiester oligonucleotides: can DOTAP/DOPE liposomes do the trick? *Biochemistry 45*, 1755-1764.

(42) Lucas, B., Remaut, K., Sanders, N., Braeckmans, K., De Smedt, S., and Demeester, J. (2005) Towards a better understanding of the dissociation behavior of liposome-oligonucleotide complexes in the cytosol of cells. *Journal of Controlled Release 103*, 435-450.

CHAPTER 4 |

Advanced microscopy methods for detecting plasmid DNA degradation in a biological environment

K. Rombouts,[†, ‡] K. Braeckmans,[†, ‡] and K. Remaut[†].

† Laboratory of general biochemistry and physical pharmacy, Faculty of pharmacy

‡ Centre for Nano- and Biophotonics, Ghent University, Ghent 9000, Belgium

This manuscript is in preparation for submission

TABLE OF CONTENTS

ABSTRACT

Degradation of plasmid DNA (pDNA) in the extracellular and intracellular environment is a significant barrier in gene replacement therapy. Viral and nonviral carriers can be used to protect the nucleic acids from degradation before they reach the cells, but enzymatic degradation in the cytoplasm of the cell may decrease the number of functional pDNA molecules that reach the nucleus. Fluorescence correlation spectroscopy (FCS) and single particle tracking (SPT) are both microscopy-based methods that give information on the diffusion and concentration of fluorescently labeled molecules in a solution. Here, we evaluate the use of these two advanced microscopy methods to detect the degradation of fluorescently labeled pDNA in a cellular environment. pDNA degradation results in a decrease in the concentration of intact pDNA, while the concentration of smaller fragments increases. Both techniques could be successfully used to measure the concentration of intact pDNA in a buffer solution. However, when pDNA degradation was induced by adding DNase I, FCS was not capable of retrieving the correct percentages of intact pDNA, while SPT could. SPT was finally used to follow plasmid degradation in a cellular environment. Fluorescently labeled pDNA was first delivered into cells by lipofection. Next, cell lysate was obtained at different time points and the concentration of intact pDNA was determined by SPT. The results showed that pDNA is significantly degraded already 8 hour after lipofection and is almost fully degraded after 24 hour. These results indicate that SPT is well-suited to investigate the degradation of pDNA in biological media like cell lysates.

INTRODUCTION

Plasmid DNA (pDNA) is a large, circular double-stranded DNA molecule with the potential to induce protein expression when delivered to the nucleus of living cells. As DNA by itself does not efficiently cross the cell membrane, it is mostly complexed with a cationic delivery system to guide the pDNA into the intracellular environment. Apart from cellular uptake, the carrier system also offers protection to the pDNA against degradation. As pDNA degradation abolishes the possibility to transcribe the pDNA sequence into the corresponding mRNA and thus the further translation into proteins, it is clear that pDNA degradation should be avoided during each step of the delivery process. Surprisingly, there are only very few techniques that can measure the degradation of pDNA during its extracellular and intracellular journey. To date, the stability of pDNA and pDNA complexes is mostly studied by gel electrophoresis. This technique, however, does not allow to measure degradation of pDNA directly in complex biologic environments. The presence of free DNA and other biomolecules in these environments will generate a background in which the pDNA's signal is lost. Hence, there is a need for more advanced methods to follow the degradation of large nucleic acids such as pDNA in complex biological fluids and living cells. It should be noted that progress in quantitative polymerase chain reaction (qPCR) methods allow measurements in undiluted biological samples after an adjustment of the reaction conditions. [1]

Since its introduction, traditional fluorescence microscopy has raised itself as a cornerstone in life science research. Fluorescence microscopy employs cell staining and labeling of molecules to visualize cell morphology, or 2D (and 3D) structure. The most commonly found microscopy setups are wide field and confocal scanning laser microscopes. Due to the limited resolution of optical microscopy, however, direct visualization of the degradation of a 200 – 400 nm sized plasmid is virtually impossible. Instead, these microscopy techniques can be used to determine the size of molecules indirectly by diffusion measurements. [2] In particular, we evaluated fluorescence correlation spectroscopy (FCS) and single particle tracking (SPT) for their potential to follow the degradation of pDNA molecules in a complex biological fluid, by studying the dynamics of single fluorescently labeled pDNA molecules and their degradation products.

In FCS, a temporal correlation is measured between fluctuations in fluorescence intensities coming from molecules moving into and out of a confocal detection volume (~1 fl). From these fluctuations, the dynamic properties of the fluorescent molecules in solution can be obtained, including the concentration and the diffusion coefficient (which is inversely proportional to the molecule's hydrodynamic size) (see **Chapter 2**). [3, 4] FCS has proven to be a valuable tool to follow the degradation of small antisense oligonucleotides, both in buffer and in living cells. [5] Hence, we were interested to know whether it is possible to study the degradation of larger nucleic acids such as pDNA by FCS. Theoretically, the degradation of pDNA into shorter fragments should lead to an increase of the average diffusion coefficient in function of time, as well as a decrease in the concentration of intact pDNA.

Apart from FCS, also SPT was evaluated for its potential to follow pDNA degradation. In SPT, as the name indicates, single particles are tracked in microscopy video recordings (see **Chapter 2**). [2] The recorded movies are analyzed to determine the motion trajectories of the fluorescent particles. [6, 7] Based on these trajectories, the diffusion coefficients [8] and, via the Stokes-Einstein equation, the hydrodynamic diameter can be measured on a single particle level. [9-11] In addition, the nanoparticle concentration can be accurately determined as our group has recently demonstrated. [12-14] For speed and sensitivity SPT is typically performed on a wide field laser microscope with a fast and sensitive camera (e.g. EMCCD). We recently demonstrated, however, that SPT concentration measurements are better performed with a microscope configuration that avoids out of focus fluorescence. [15] Therefore, in this work we have performed SPT experiments on a swept-field confocal microscope (SFC), which offers excellent speed and sensitivity while reducing out-of-focus light.

The ability of FCS and SPT to measure molecular concentrations and dynamics in complex biological fluids makes both of them interesting for a broad range of applications in life sciences. [16, 17] In this paper, we investigate the use of FCS and SPT to study degradation of pDNA in a biological environment. pDNA degradation is one of the potential bottlenecks to efficient gene therapy. Our results show that SPT is the most suited to measure the concentration of intact pDNA in a

biological environment. We demonstrate that the degradation of pDNA can be accurately measured by SPT after it was delivered into cells by lipofection.

MATERIALS AND METHODS

Cell Culture

A HeLa cell line was cultured at 37°C and 5% CO_2 in Dulbecco's modified Eagle's Medium and growth factor F12 (1:1 DMEM:F12) supplemented with 10% heat-inactivated fetal bovine serum (FBS), 100 µg/ml penicillin/streptavidin and 2 mM L-glutamine. All cell culture reagents were ordered at GibcoBRL (Merelbeke, Belgium).

Plasmid DNA Preparation

gWIZ-GFP plasmids, expressing the green fluorescent protein (GFP) were purchased from Genlantis (San Diego, CA, U.S.A.). The plasmids were amplified in *Escherichia coli* and isolated from the bacteria suspension using the Qiafilter Plasmid Giga Kit (Qiagen, Venlo, The Netherlands). DNA concentration and purity was determined by UV absorption at 260/280 nm using the NanoDrop 2000c (Thermo Fisher Scientific, Rockford, IL, USA). The plasmids were suspended and stored in 20 mM HEPES buffer (pH 7.2) at a final concentration of 1 µg/µl. Fluorescent labeling with Cy5 was performed using the Label-IT nucleic acid labeling kit (Mirus Bio LLC, Madison, WI, U.S.A.) at a pDNA to Label-IT reagent ratio of 10:1 (w:v). Free label was removed via ethanol precipitation. Briefly, 2.5 volumes of ice-cold ethanol and 0.1 volume of 5 M NaCl were added to the labeled pDNA and kept at -80°C for 30'. The samples were centrifuged at 18000 x g at 4°C for 30'. The pellet is washed with 70% ethanol and centrifuged again at maximum speed for 10'. Labeled plasmids were resuspended in 20 mM HEPES buffer (pH 7.2) and the concentration and purity was determined by UV absorption at 260/280 nm.

Plasmid DNA Standard Curve

A standard array of concentrations between 0 and 33 ng/µl was obtained by diluting the stock solution of Cy5-pDNA in 20 mM HEPES buffer (pH 7.2). From this array 50 µl was used for either gel electrophoresis or FCS and SPT, as advanced microscopy methods. For FCS, (PicoQuant, Berlin, Germany) 10 different spots in the solution were measured for 60 seconds and analyzed for each measurement.

The analysis was performed in the FCS software (SymPhoTime, PicoQuant, Berlin, Germany) and consists of the calculation of an autocorrelation curve for every recording. The obtained autocorrelation curves are then fitted with the correlation model: “Triplet-state” as described in **Chapter 2** and the diffusion coefficient is fixed at 3.23 $\mu m^2/s$ for intact pDNA and 120 $\mu m^2/s$ for degraded pDNA. This fit returns values for the molecular concentration of each species in the solution during the measurement. Alternatively peak analysis was performed directly on the fluorescence intensity fluctuations recorded over time. Intact pDNA shows high intensity peaks, when passing through the detection volume. The number of times a signal, higher than the baseline, is detected, can be correlated with the concentration of intact pDNA in the solution. The baseline is set just above the maximal value for the fully degraded pDNA sample.

For SFC (Nikon Instruments Europe B.V., Brussels, Belgium) 10 movies of 200 frames were captured and analyzed in three steps using proprietary software in Matlab (The MathWorks, Inc., Natick, Massachusetts, U.S.A.). First, for every frame contours are plotted to identify fluorescent labeled pDNA molecules. Secondly, tracks are created for every movie, based on the calculated contours. Lastly, based on these tracks, concentrations in particles/ml were calculated according to the method described by Röding et al. (2011)[12]. Both analysis methods have been described in detail in **Chapter 2**.

Measuring Intact Plasmid DNA

Cy5 pDNA was fully degraded by the addition of DNase I (2 U/µl) (Invitrogen, Merelbeke, Belgium) and a 1 x degradation buffer during 30’ at 37°C, according to the manufacturer’s protocols. Mixtures of non-degraded (intact) and fully degraded Cy5 pDNA were prepared to have 0/100, 20/80, 40/60, 50/50, 80/20 and 100/0% of intact/degraded pDNA for FCS measurements and 0/100, 10/90, 25/75, 40/60, 50/50, 60/40, 75/25, 90/10 and 100/0% of intact/degraded pDNA, for SFC recordings. Every sample was subsequently measured as described for the standard curve.

DNase I Plasmid DNA Degradation Experiment

First, DNase I (2 U/µl) (Invitrogen, Merelbeke, Belgium) was diluted in a 1 x degradation buffer (Invitrogen, Merelbeke, Belgium) in Nuclease-Free water (Ambion, Merelbeke, Belgium) to a concentration of 0.06 U/µl. Secondly, a 100 ng/µl Cy5

labeled pDNA solution was prepared in the same 1 x degradation buffer and thermostated in a heat block (VWR International, Leuven, Belgium) at 37°C.

The DNase I solution was subsequently added to the pDNA solution resulting in 0.03 U/µg of pDNA. To follow the degradation in function of time, 10 µl of this solution was added to 40 µl of DNase I inhibitor solution (0.1 M Iodoacetate, 10 mM Tris-HCl, 50 mM EDTA, pH 7.4) on ice at time points 0', 1', 2', 5', 10', 15', 20', and 30'. 2 µl of these solutions was mixed with 3 µl of gel loading buffer (Ambion, Merelbeke, Belgium) and loaded onto a 1% agarose gel (UltraPure™ agarose, Invitrogen, Merelbeke, Belgium) supplemented with GelRed (Biotium, Hayward, CA, U.S.A.). After running the gel 50' at 100 V, a picture of the gel was taken under UV light and analyzed using ImageJ. [18] FCS measurements and SFC microscopy were performed on the remaining 48 µl of the pDNA solutions, like described above.

Intracellular Degradation

Two 6 well plates were seeded with HeLa cells at 150,000 cells/well and the cells were allowed to grow overnight. The next day, complexes were prepared with Cy5-pDNA in 20 mM HEPES buffer (pH 7.2) and Lipofectamine 2000 in a 3:1 ratio (v:w) (Lipofectamine:pDNA). These complexes were then diluted in optiMEM and added to the cells at a concentration of 500 ng pDNA/50,000 cells and the plates were incubated at 37°C in an incubator for 4 hours. After 4 hours all cells were washed with Phosphate Buffered Saline (PBS) (-/-) and cell lysate was prepared from two wells of each plate with RIPA buffer (Sigma Aldrich, Bornem, Belgium) as described in the protocol. Briefly, cells were trypsinized for 5' whereafter fresh cell medium was used to inhibit trypsin. Cells were collected by centrifugation at 1800 x g for 5', the pellet was washed with PBS (-/-) and again spun down at 1800 x g. The supernatant was removed and the cells were resuspended in 1 ml of ice-cold RIPA buffer and incubated for 30' on ice. After 30', the solution was forced through a 20 gauge needle to further break up the cells and placed back on ice. After 30' the solution was spun down for 10' at 10,000 x g and at 4°C. The supernatant can be stored at -80°C until microscopy measurements. The cell lysate obtained from the first two wells serves as the 4 hour time point. To obtain the 8 hour and 24 hour time point to follow plasmid DNA degradation, fresh medium was supplied to the remaining wells and one series of samples was kept on ice, from this point, in order to induce low enzymatic activity, while the other samples were incubated again at

37°C which should yield normal enzyme activity. After 8 hours and 24 hours, cell lysate was collected from two wells of each plate and stored at -80°C until the samples were measured. For all cell lysates, protein concentration was measured using the Pierce™ BCA protein assay kit (Thermo Scientific, Erembodegem, Belgium) to compensate for the amount of cells the cell lysate originated from. The intact plasmid concentration was measured in each cell lysate by agarose gel and SPT. pDNA concentrations were compensated for the amount of cells in the sample by equalizing to the measured total protein concentrations.

RESULTS

Figure 1 shows FCS and SPT measurements on fully intact and fully degraded pDNA solutions. The intact pDNA used in this study, was fluorescently labeled with the Mirus kit at a labeling density of 10 fluorophores per plasmid, which means on average one fluorophore per 600 base pairs. [19] After degradation, we expect that single labeled degradation fragments are formed. FCS measurements on the intact pDNA show high intensity fluorescence peaks each time a plasmid passes the confocal detection volume. Autocorrelation analysis gives a diffusion coefficient of 3.23 ± 0.92 µm²/s, which corresponds to particles with on average a hydrodynamic size of 68 nm. When pDNA was degraded by the addition of DNase I, the highly intense fluorescence peaks disappeared as expected. Autocorrelation of these fluorescence fluctuations confirmed the presence of faster (i.e. smaller) degradation products, with an average diffusion coefficient of 120 ± 36 µm²/s, corresponding to molecules with on average a size of 1.8 nm. Also SPT was able to distinguish fully intact from fully degraded pDNA molecules. Intact pDNA was bright enough to be seen as individual particles. SPT diffusion analysis revealed an average diffusion coefficient of 2.29 ± 0.42 µm²/s. On the SPT image of degraded pDNA, however, no individual particles could be seen any more so that diffusion analysis was no longer possible.

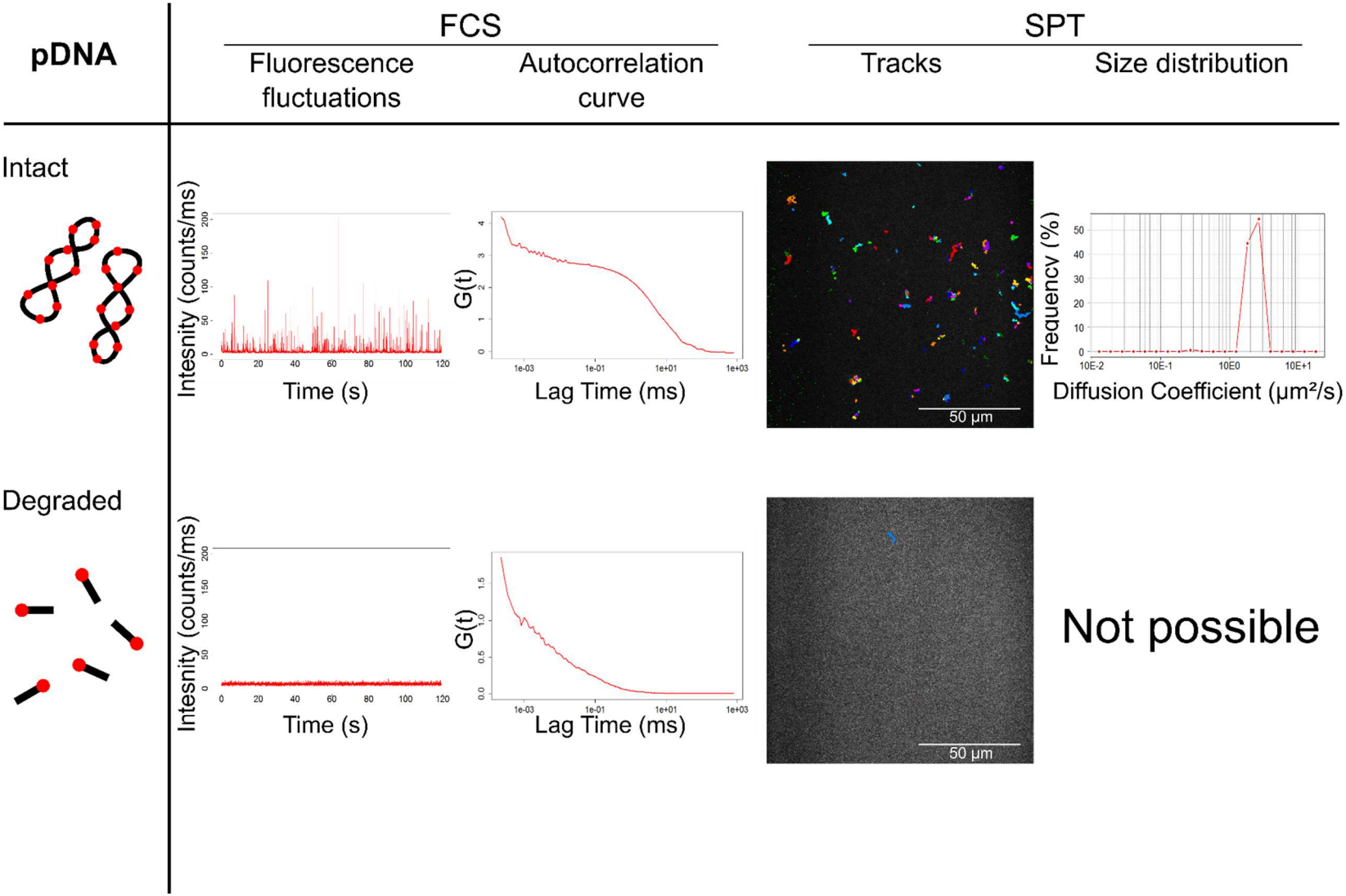

Figure 1 Overview of FCS and SPT measurements for intact and degraded pDNA. For FCS, fluorescence intensity fluctuations and autocorrelation curves are shown. For SPT, an overlay of tracks on a still from a movie and the distribution of diffusion coefficients are shown.

Standard Curves for Intact Plasmid DNA Solutions with Known Concentration

Having shown that both FCS and SPT can detect intact pDNA, the next step is to evaluate their potential to measure the concentration of intact pDNA. A concentration series was prepared from a stock solution of intact pDNA from 0 to 33 ng/µl. For FCS, the concentration of intact pDNA was determined by analyzing the autocorrelation curves with a single species fit in which the diffusion coefficient of the single species was fixed to 3.23 µm²/s according to the measurements on intact pDNA (*vide supra*). For SPT, the number concentration of intact pDNA molecules was calculated following the method of Röding et al. (2011)[12] (see **Chapter 2**). Figure 2 shows that SPT yields a slightly better correlation for the trend line (R = 0.98) when compared to FCS (R = 0.94).

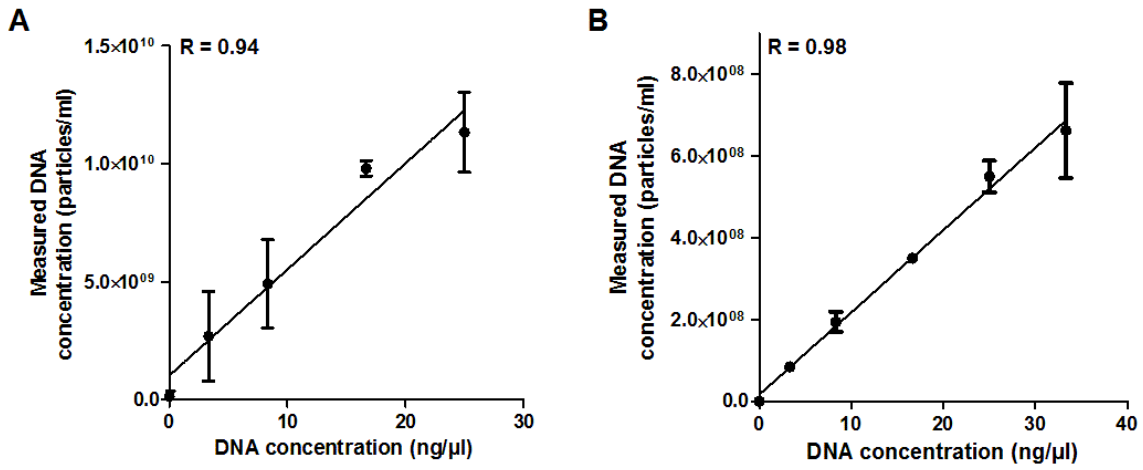

Figure 2 (A) Standard curve of measured DNA concentration in particles/ml derived from the autocorrelation curve after FCS measurement. Averages were based on two independent experiments with ten repetitions per sample. Error bars depict the standard deviation on the average. (B) Standard curve of measured concentration in particles/ml with SPT. Averages were based on three independent experiments with ten repetitions per sample. Error bars depict the standard deviation on the average.

Measuring the Fraction of Intact Plasmid DNA in Mixed Intact/Degraded pDNA Solutions

The standard curves above demonstrate that it is possible to measure the concentration of pDNA in a solution containing only intact pDNA. When pDNA degrades, however, smaller fragments will arise as well. To determine whether FCS

and SPT are still able to detect the amount of intact pDNA in these more complex solutions, we prepared mixtures of intact and degraded pDNA at known ratios. The FCS data was analyzed in two ways, i.e. by autocorrelation analysis and by peak analysis. For autocorrelation analysis a 2 species fit was performed, for which the diffusion coefficients of 100% intact pDNA and fully degraded pDNA were fixed to 3.23 $\mu m^2/s$ and 120 $\mu m^2/s$, as determined before. The autocorrelation fit then returns the relative fractions of both components. In Suppl. Figure 1, the autocorrelation curves are depicted. From Figure 3 A it is clear that this procedure leads to an overestimation of intact pDNA. In the analysis method in the FCS software, the intensity of the particles could not be taken into account. This potentially contributes to the overestimation of the intact plasmids. As an alternative to autocorrelation analysis, we analyzed the number of intense peaks in the FCS time traces, which correspond to the diffusion of intact pDNA through the detection volume (cf. Figure 1). Interestingly, fluorescence peaks do not appear in the fluorescence fluctuations recorded from a fully degraded pDNA sample. To calculate the percentage of intact pDNA from the fluorescence fluctuations profile, the baseline was set above the maximum fluorescence intensity obtained for fully degraded pDNA. Then, the number of peaks arising above this baseline was determined relative to the number of peaks in the intact sample. Figure 3 A shows that calculating the number of peaks clearly produces better results than autocorrelation analysis which could be fitted with a high correlation by a linear trend line ($R = 0.99$). In parallel we performed SPT analysis, which is based on the assumption that only intact pDNA will be bright enough to be visible as individual particles. Figure 3 B shows that the measured amount of intact pDNA molecules corresponds well with the expected values in the intact/degraded pDNA mixtures. A linear trend was also found here ($R = 0.97$), although it is clear that at lower intact pDNA concentrations, the experimental values become less accurate. This is likely due to the fact that a high concentration of degradation fragments gives rise to a higher background intensity and, therefore, a lower signal to noise ratio of intact pDNA. This makes it more difficult to reliably track the remaining intact pDNA molecules.

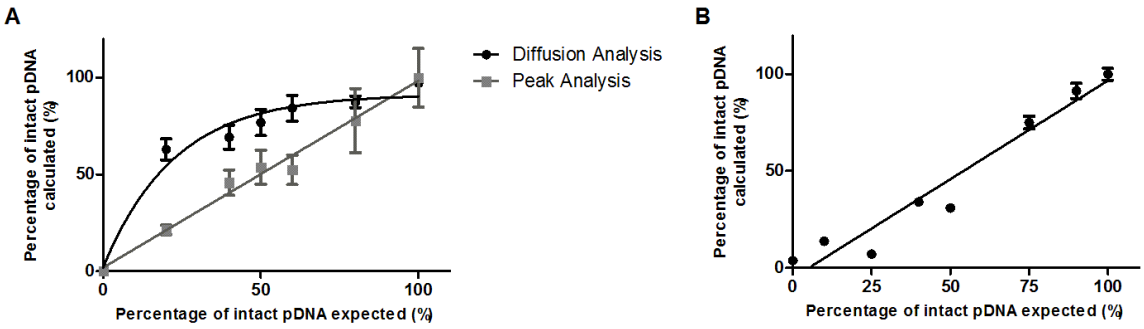

Figure 3 Percentage of intact pDNA calculated using (A) the ratio of slow moving components (intact pDNA) and fast moving components (degraded) after analysis of the autocorrelation curve and analysis of the number of peaks in the intensity fluctuations obtained with FCS. and (B) concentration analysis after SPT. Averages were based on ten repetitions per sample. Error bars depict the standard deviation on the average.

Enzymatic Degradation of Plasmid DNA in Function of Time

The experiments above demonstrate that peak analysis by FCS and concentration measurements of intact pDNA by SPT seem adequate to determine the concentration of intact pDNA in a solution containing varying ratios of intact/degraded pDNA. These solutions, however, contain only two pDNA degradation states (non-degraded versus fully degraded) and are not representative for the different lengths of degradation fragments that are expected to be formed during the actual enzymatic degradation of pDNA in function of time. Therefore, as a next step, we evaluated the potential of FCS and SPT to follow the amount of intact pDNA in the presence of degradation products of varying lengths formed during the enzymatic degradation of pDNA over time after the addition of DNase I. The DNase I enzyme is an endonuclease that nonspecifically cleaves DNA to oligonucleotides of four base pairs and smaller.

As a reference, gel electrophoresis was used to visualize degradation fragments which are formed when the DNase I enzyme cuts the pDNA molecules into smaller pieces. It can be clearly seen that the pDNA indeed degrades into a wide variety of shorter DNA fragments, which appear as a smear on the gel (Figure 4 A). The supercoiled form of the pDNA is no longer detectable on the gel starting from 10 minutes onwards. The graph shows the percentage of intact pDNA as determined from the gel images. The amount of intact pDNA decreases rapidly and reaches a plateau around 0% after 10 minutes. Figure 4 B shows the percentage of intact pDNA

as measured by FCS peak analysis. The time traces can be seen in Suppl. Figure 2. Here, intact pDNA is seen to be fully degraded within the first 2 minutes. After 20-30', however, the apparent amount of intact pDNA increases again, although the gel confirms that these mixtures no longer contain intact pDNA. Therefore, FCS peak analysis as carried out by the provided tools in the SymphoTime software seems less suitable to detect the amount of intact pDNA in solutions which contain a high concentration of smaller degradation fragments. We do not exclude the possibility, however, that peak analysis with custom-made algorithms would yield a more acceptable result to follow pDNA degradation.

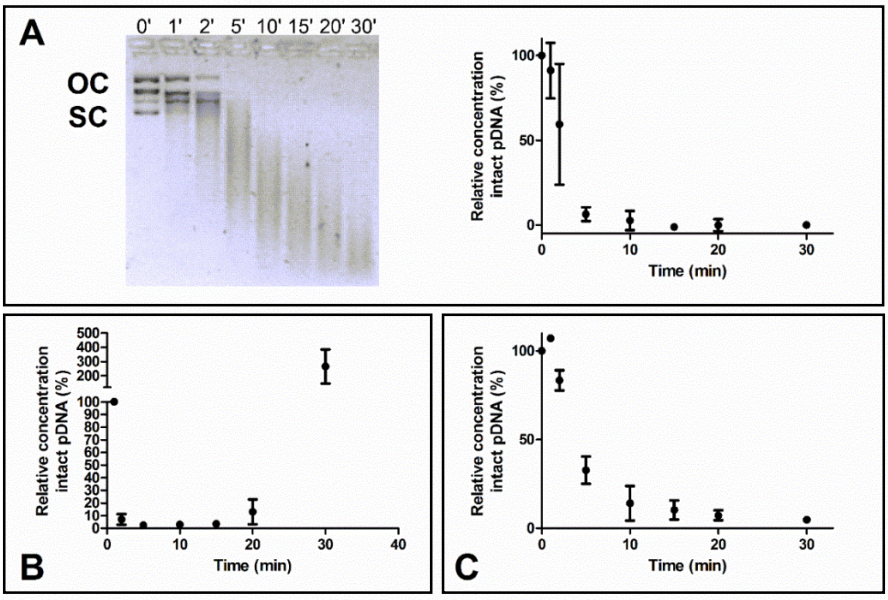

Figure 4 Raw data and relative percentage of concentration of intact pDNA compared to t = 0. (A) Example photograph and results of gel electrophoresis. Averages were based on three independent experiments with ten repetitions per sample. Error bars depict the standard deviation on the average. (B) Results of FCS with peak analysis. Averages were based on ten repetitions per sample. Error bars depict the standard deviation on the average. (C) Results of SPT analysis. Averages were based on three independent experiments with ten repetitions per sample. Error bars depict the standard deviation on the average.

Finally, Figure 4 C shows the amount of intact pDNA as determined by SPT. Here, a gradual decrease in the percentage of intact pDNA is found which closely resembles the data from gel electrophoresis. It should be noted that the number of intact pDNA molecules seems to increase in the first minute after adding the DNase I enzyme (cf. second data point in Figure 4 C). This is likely due to bigger fragments at early time points that are still detectable as single particles. In any case, based on

these results, SPT seems the most reliable to detect the amount of intact pDNA in more complex mixtures containing a broad range of degradation fragments.

SPT to Follow Intracellular Degradation of Plasmid DNA

As a final proof of principle that SPT is useful to measure pDNA concentrations in more complex biological environments, we followed the degradation of plasmid DNA in cell lysate obtained from transfected HeLa cells after different time points. pDNA was delivered in the cells by lipofection. After 4 hours at 37°C, uptake is complete, so the collected cell lysate of these samples was used as a reference of the total amount of pDNA present in the cell. An agarose gel was ran with the cell lysate, but as shown in Figure 5 A no single bands were seen making it impossible to determine pDNA concentration. Figure 5 B shows the percentages of pDNA measured with SPT after 8 hours and 24 hours at 4°C (black bars) and 37°C (white bars) compared to this reference. After the uptake was complete after 4 hours, half of the samples were incubated at 4°C, which lowers the activity of the enzymes responsible for pDNA degradation, while the remaining samples were incubated at 37°C. Figure 5 B demonstrates that at the 8 hour time point, the concentration of intact pDNA dropped significantly for the 37°C samples, while the 4°C control doesn't differ significantly ($p < 0.05$) compared to the initial amount of intact pDNA that was taken up in the cells during the first 4 hours. After 24 hour, the concentration of intact pDNA in cell lysate from the 37°C samples dropped even further, demonstrating that enzymatic degradation of pDNA has proceeded. The amount of intact pDNA detected in the cell populations incubated at 4°C, also decreased when compared to the 8 hour time point. When compared to the concentration of the 37°C samples at the 24 hour time point, however, the concentration in the 4°C treated cells was still significantly higher ($p < 0.1$). Taken together, we conclude that intracellular degradation is a fast process that decreases the amount of functional pDNA available for transfection significantly, compared to the total amount of pDNA delivered to the cell. This indicates that loss of pDNA is an important barrier to efficient gene delivery.

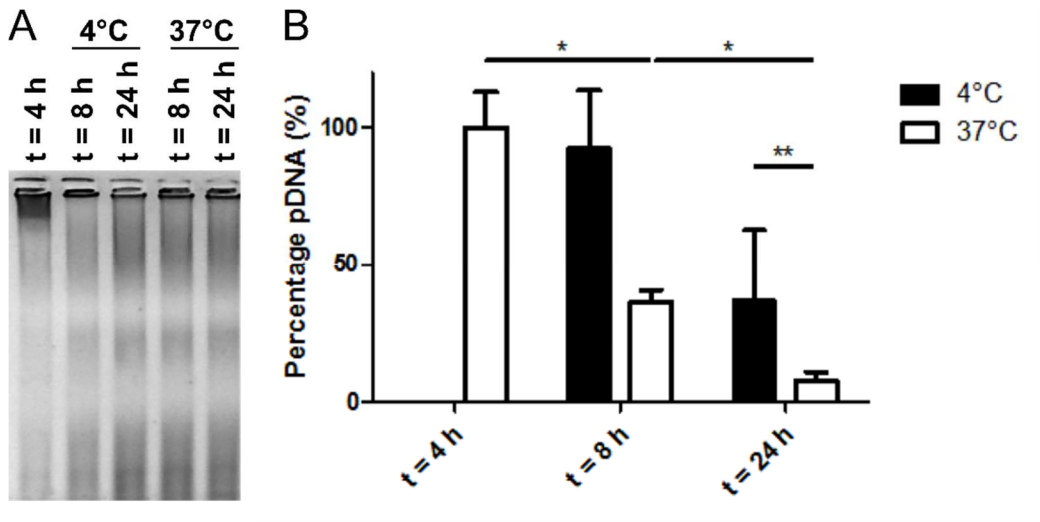

Figure 5 Agarose gel of cell lysate (A) and percentage of pDNA from SPT measurements (B) in cell lysate 4, 8 and 24 hours after Cy5-pDNA lipofection. Percentages are relative to the concentration measured at t = 4 hours. All results were compensated for the amount of cells by taking total protein concentration into account. Both samples were incubated at 37°C up to the 4 hour time point. Black bars: 4°C. White bars: 37°C. *: $p < 0.05$, **: $p < 0.1$. Averages were based on four independent experiments with two repetitions per sample. Error bars depict the standard deviation on the average.

DISCUSSION

Measuring the concentration of macromolecules in complex biological media is interesting in a range of applications from disease diagnostics to evaluation of administered drugs. In the case of gene therapy, for example, the macromolecule of interest is plasmid DNA, a large, double stranded circular DNA molecule administered with the aim to induce protein expression in living cells. Concentration measurements of pDNA in buffer and other simple solutions are routine practice. The fastest method is probably measuring the absorption at 260 nm. Another method that is often used is measuring the fluorescence after addition of an intercalating dye which can be performed in buffer or on agarose gel. The intensity of the signal can then be correlated when using a standard curve. For the detection of very low concentrations, qPCR is used. One of the biggest disadvantages of these techniques is that most of the times it needs a purification step, in which DNA is isolated from the medium prior to the quantification. DNA concentration in blood was for example compared between healthy patients and patients suffering from prostate cancer. It was seen that the cancer patients exhibited a higher amount of circulating DNA, caused by a decreased DNase activity compared to healthy individuals. [20] The same

was done for lung cancer patients, where circulating plasma DNA levels were investigated as a biomarker for lung cancer. [21] DNA concentration in blood and target organs was also detected in the evaluation of a gene therapy treatment. In blood, the pDNA had a half time of less than 5 min, while pDNA could be detected for longer using southern blot and qPCR in the lung, spleen, liver, heart, kidney, marrow, and muscle up to 24 hours postinjection. [22]

When pDNA is used as a therapeutic to induce protein expression in living cells, it is of interest to understand where and when the pDNA molecule is actually delivered. Also, as the pDNA sequence should be intact to obtain protein expression, degradation of pDNA should be avoided during each step of the delivery pathway. Surprisingly, there are only a few methods that allow to follow the degradation of pDNA in the extracellular or intracellular environment. Both Lechardeur et al. (1999)[23] and Pollard et al. (2001)[24], employed fluorescence in situ hybridization (FISH) and quantitative single-cell fluorescence video imaging to measure total fluorescence intensity per cell and estimated an average half-life of 50-90 minutes. A two-step fluorescence resonance energy transfer (FRET) approach was able to monitor complexation and degradation of quantum dot (QD) labeled pDNA in a non-invasive way in living cells. [25] This approach has the disadvantage that at least two different fluorescent molecules need to be added to the pDNA. In this study, we evaluated two single molecule microscopy methods in their ability of measuring concentrations of intact pDNA with only one type of fluorescent label in complex biological media. This approach minimizes the effect of the fluorescent labels on the intracellular processing. More importantly, the use of measurements directly in a complex medium eliminates the need for purification of the samples before measurements, which on itself could potentially influence the obtained concentrations. [26] The first technique that was evaluated was fluorescence correlation spectroscopy (FCS) (see **Chapter 2** for more detailed background). FCS has already proven to be able to detect the degradation of small nucleic acids such as oligonucleotides and small interfering RNA. [5, 27] It has however not been evaluated before to detect degradation of larger macromolecules such as pDNA.

FCS was very well able to determine the concentration of intact pDNA in a simple dilution series based on single species autocorrelation analysis. However, it did not perform well in mixtures of intact pDNA and fully (DNase I) degraded pDNA.

Using two component autocorrelation analysis with fixed diffusion coefficients for intact and degraded pDNA, the fraction of intact pDNA molecules was over-estimated (see Figure 3 A). This might be caused by the fluorescence intensity of the intact molecules which is obviously higher than that of the fully degraded plasmids and will therefore contribute more to the fluorescence fluctuations than the smaller degraded fragments. By taking this difference in fluorescence intensity between the two fractions into account, this potentially could be solved. This was however not an option in our analysis software. Peak analysis of the FCS data, which counts the number of "peaks" above a baseline determined by the fully degraded sample, turned out to perform much better in this case (see Figure 3 B). This approach is based on the assumption that each peak which arises above the baseline intensity level can be attributed to intact pDNA. Unfortunately, peak analysis proved to be less successful in retrieving the percentages of intact pDNA (see Figure 4 B) in more complex mixtures where enzymatic degradation of pDNA was followed in function of time. The number of intact plasmids was underestimated at early time points, while overestimated after longer degradation times. A closer look at the corresponding fluorescence fluctuations shows that the peaks originate from a slight shift in the baseline fluorescence, and not from actual peaks (see Suppl. Figure 2). This means that peak analysis has difficulties to cope with the more complex mixture of DNA during enzymatic degradation, in which a large variety of pDNA fragments are formed with different sizes and fluorescence intensities.

Apart from FCS, also SPT was evaluated as a technique to measure intact pDNA concentrations. As SPT relies on the visibility of individual fluorescent particles, only intact pDNA will be visible. Smaller - and thus faster - fragments which have less labels per molecule and which are present at higher degraded pDNA concentrations cannot be discerned as individual objects. Instead they contribute to the overall background signal. We used a previously published method (described in **Chapter 2**) to accurately determine particle number concentration measurements from SPT data to determine the concentration of intact pDNA. [12-14] Counting the number of intact pDNA molecules seemed feasible both in solutions containing only intact pDNA as well as in mixtures with fully degraded pDNA fragments. Also, the determination of the concentration of intact pDNA was possible after nuclease activity. The enzymatic degradation creates an even more complex mixture of labeled

fragments, distributed between fully intact and fully degraded pDNA. SPT showed an estimation of intact pDNA that matched closely with the data obtained with gel electrophoresis.

In the end, the real advantage of using these microscopy technique compared to the established techniques as described before, lies in the possibility to measure in more complex environments. Here we measured pDNA degradation in cells after it has been delivered by lipofection. Cells were treated with pDNA-lipoplexes and cell lysates were prepared at distinct time points afterwards. SPT could show that the concentration of intact pDNA decreases gradually over time (Figure 5). After 24 hours, only a small fraction of the originally delivered amount is still intact. Our measurements would put the half-life of the pDNA present after cellular uptake at 4 hours in the range of 3 to 4 hours, which is longer than the 50 – 90 minutes reported for naked pDNA in the cytoplasm by Lechardeur et al. (1999)[23]. This shows that the complexation delays the degradation of the pDNA. As could be expected, putting the cells at 4°C did slow down the degradation process.

While both FCS and SPT eliminate the need for purification of the pDNA from biological samples, which is needed for gel electrophoresis (Figure 5 A) and qPCR, both microscopy-based approaches require that the pDNA is fluorescently labeled. Obviously, this extra step does diminish the advantage in simplicity this microscopy techniques has over a purification step and subsequent measurement, but is still more representative for the situation encountered in the cell.

In conclusion, the SPT technique presented in this paper shows potential to measure intact pDNA concentrations both in buffer and in more complex biological environments such as cell lysate obtained from living cells. In future experiments, SPT can also be used to determine the protection of non-viral gene delivery carriers towards pDNA, by measuring the amount of intact pDNA that can be retrieved after incubation of the complexes in different extracellular or intracellular environments. As SPT relies on the measurement of fluorescently labeled molecules, one should take care to investigate that the labeling method does not interfere with the process under investigation, such as the degradation of pDNA in this manuscript. When taking into account the appropriate controls, however, SPT proves to be a reliable method to measure the amount of intact pDNA in varying environments.

CONCLUSIONS

In this chapter, two advanced microscopy techniques, FCS and SPT were compared with regards to their ability to measure the concentration of intact pDNA. Both techniques are suited to measure intact pDNA in buffer, but when a more complex environment with different smaller sized fragments is created, either by mixing intact pDNA with fully degraded pDNA or by following the process of degradation, SPT proves to be more suited than FCS to estimate the amount of intact pDNA molecules. The power of SPT was confirmed by following degradation of pDNA after lipofection in the cell extract of HeLa cells. These experiments show the power of this technique to study these types of phenomena which include the measurement of DNA in more complex biological media.

REFERENCES

(1) Bu, Y., Huang, H., and Zhou, G. (2008) Direct polymerase chain reaction (PCR) from human whole blood and filter-paper-dried blood by using a PCR buffer with a higher pH. *Analytical Biochemistry 375*, 370-372.

(2) Braeckmans, K., Vercauteren, D., Demeester, J., and De Smedt, S. C. (2010) Single particle tracking, in *Nanoscopy multidimensional optical fluorescence microscopy.* , Taylor and Francis Group.

(3) Thompson, N. L. (1999) Fluorescence correlation spectroscopy, in *Topics in fluorescence spectroscopy* pp 337-378, Springer.

(4) Bacia, K., and Schwille, P. (2007) Fluorescence correlation spectroscopy, in *Lipid Rafts* pp 73-84, Springer.

(5) Remaut, K., Lucas, B., Braeckmans, K., Sanders, N., De Smedt, S., and Demeester, J. (2005) FRET-FCS as a tool to evaluate the stability of oligonucleotide drugs after intracellular delivery. *Journal of controlled release 103*, 259-271.

(6) Cheezum, M. K., Walker, W. F., and Guilford, W. H. (2001) Quantitative Comparison of Algorithms for Tracking Single Fluorescent Particles. *Biophysical Journal 81*, 2378-2388.

(7) Thompson, R. E., Larson, D. R., and Webb, W. W. (2002) Precise nanometer localization analysis for individual fluorescent probes. *Biophysical Journal 82*, 2775-2783.

(8) Qian, H., Sheetz, M. P., and Elson, E. L. (1991) Single particle tracking. Analysis of diffusion and flow in two-dimensional systems. *Biophysical journal 60*, 910.

(9) Saxton, M. J. (1997) Single-particle tracking: the distribution of diffusion coefficients. *Biophysical Journal 72*, 1744.

(10) Saxton, M. J., and Jacobson, K. (1997) Single-particle tracking: applications to membrane dynamics. *Annual review of biophysics and biomolecular structure 26*, 373-399.

(11) Suh, J., Dawson, M., and Hanes, J. (2005) Real-time multiple-particle tracking: applications to drug and gene delivery. *Advanced drug delivery reviews 57*, 63-78.

(12) Röding, M., Deschout, H., Braeckmans, K., and Rudemo, M. (2011) Measuring absolute number concentrations of nanoparticles using single-particle tracking. *Physical Review E 84*, 031920.

(13) Röding, M., Deschout, H., Braeckmans, K., Särkkä, A., and Rudemo, M. (2013) Self-calibrated concentration measurements of polydisperse nanoparticles. *Journal of Microscopy 252*, 79-88.

(14) Röding, M., Deschout, H., Braeckmans, K., and Rudemo, M. (2013) Measuring absolute nanoparticle number concentrations from particle count time series. *Journal of Microscopy 251*, 19-26.

(15) Deschout, H., Raemdonck, K., Stremersch, S., Maoddi, P., Mernier, G., Renaud, P., Jiguet, S., Hendrix, A., Bracke, M., and Van den Broecke, R. (2014) On-chip light sheet illumination enables diagnostic size and concentration measurements of membrane vesicles in biofluids. *Nanoscale 6*, 1741-1747.

(16) Braeckmans, K., Buyens, K., Bouquet, W., Vervaet, C., Joye, P., Vos, F. D., Plawinski, L., Doeuvre, L., Angles-Cano, E., and Sanders, N. N. (2010) Sizing

nanomatter in biological fluids by fluorescence single particle tracking. *Nano letters 10*, 4435-4442.

(17) Bulseco, D. A., and Wolf, D. E. (2003) Fluorescence correlation spectroscopy: molecular complexing in solution and in living cells. *Methods in cell biology 72*, 465-498.

(18) Schneider, C. A., Rasband, W. S., and Eliceiri, K. W. (2012) NIH Image to ImageJ: 25 years of image analysis. *Nature Methods 9*, 671-675.

(19) Rombouts, K., Martens, T. F., Zagato, E., Demeester, J., De Smedt, S. C., Braeckmans, K., and Remaut, K. (2014) Effect of Covalent Fluorescence Labeling of Plasmid DNA on Its Intracellular Processing and Transfection with Lipid-Based Carriers. *Molecular Pharmaceutics 11*, 1359-1368.

(20) Cherepanova, A. V., Tamkovich, S. N., Bryzgunova, O. E., Vlassov, V. V., and Laktionov, P. P. (2008) Deoxyribonuclease activity and circulating DNA concentration in blood plasma of patients with prostate tumors. *Annals of the New York Academy of Sciences 1137*, 218-221.

(21) Yoon, K.-A., Park, S., Lee, S. H., Kim, J. H., and Lee, J. S. (2009) Comparison of Circulating Plasma DNA Levels between Lung Cancer Patients and Healthy Controls. *The Journal of Molecular Diagnostics 11*, 182-185.

(22) Lew, D., Parker, S. E., Latimer, T., Abai, A. M., Kuwahara-Rundell, A., Doh, S. G., Yang, Z.-Y., Laface, D., Gromkowski, S. H., and Nabel, G. J. (1995) Cancer gene therapy using plasmid DNA: pharmacokinetic study of DNA following injection in mice. *Human gene therapy 6*, 553-564.

(23) Lechardeur, D., Sohn, K., Haardt, M., Joshi, P., Monck, M., Graham, R., Beatty, B., Squire, J., O'brodovich, H., and Lukacs, G. (1999) Metabolic instability of plasmid DNA in the cytosol: a potential barrier to gene transfer. *Gene Therapy 6*, 482-497.

(24) Pollard, H., Toumaniantz, G., Amos, J. L., Avet-Loiseau, H., Guihard, G., Behr, J. P., and Escande, D. (2001) Ca2+-sensitive cytosolic nucleases prevent efficient delivery to the nucleus of injected plasmids. *The Journal of Gene Medicine 3*, 153-164.

(25) Chen, H. H., Ho, Y.-P., Jiang, X., Mao, H.-Q., Wang, T.-H., and Leong, K. W. (2009) Simultaneous non-invasive analysis of DNA condensation and stability by two-step QD-FRET. *Nano Today 4*, 125-134.

(26) Lahiri, D. K., and Schnabel, B. (1993) DNA isolation by a rapid method from human blood samples: effects of MgCl2, EDTA, storage time, and temperature on DNA yield and quality. *Biochemical Genetics 31*, 321-328.

(27) Raemdonck, K., Remaut, K., Lucas, B., Sanders, N. N., Demeester, J., and De Smedt, S. C. (2006) In situ analysis of single-stranded and duplex siRNA integrity in living cells. *Biochemistry 45*, 10614-10623.

SUPPLEMENTARY DATA

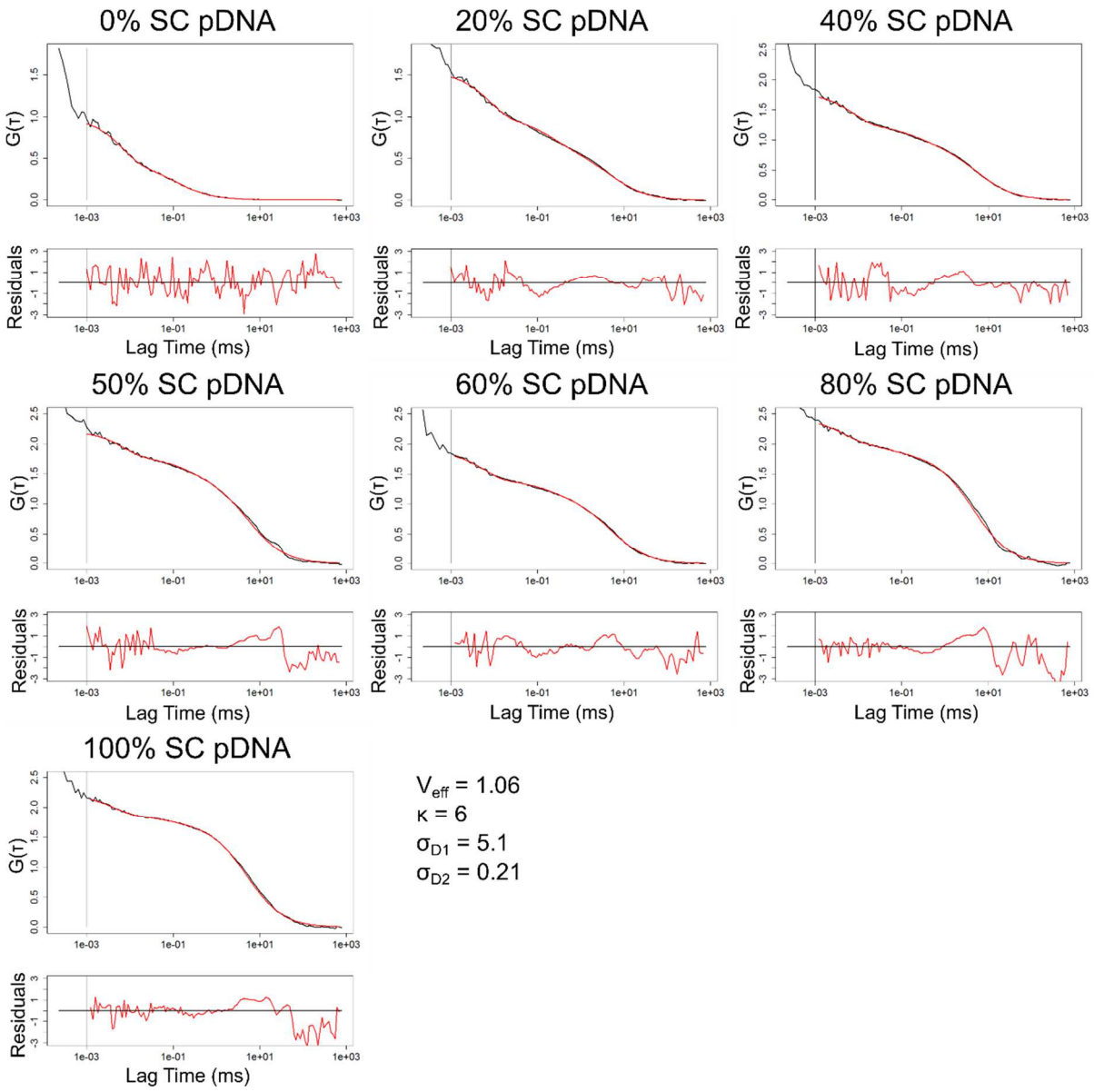

Suppl. Figure 1 Representative autocorrelation curves (black), fitting curves (red) and residuals of the fit for the calculated ratios of Figure 3. Laser power = 10% ~0.05 mW. Triplet model, two species fit with fixed parameters: V_{eff} = 1.06, κ = 6, σ_{D1}= 5.1, σ_{D2} = 0.21

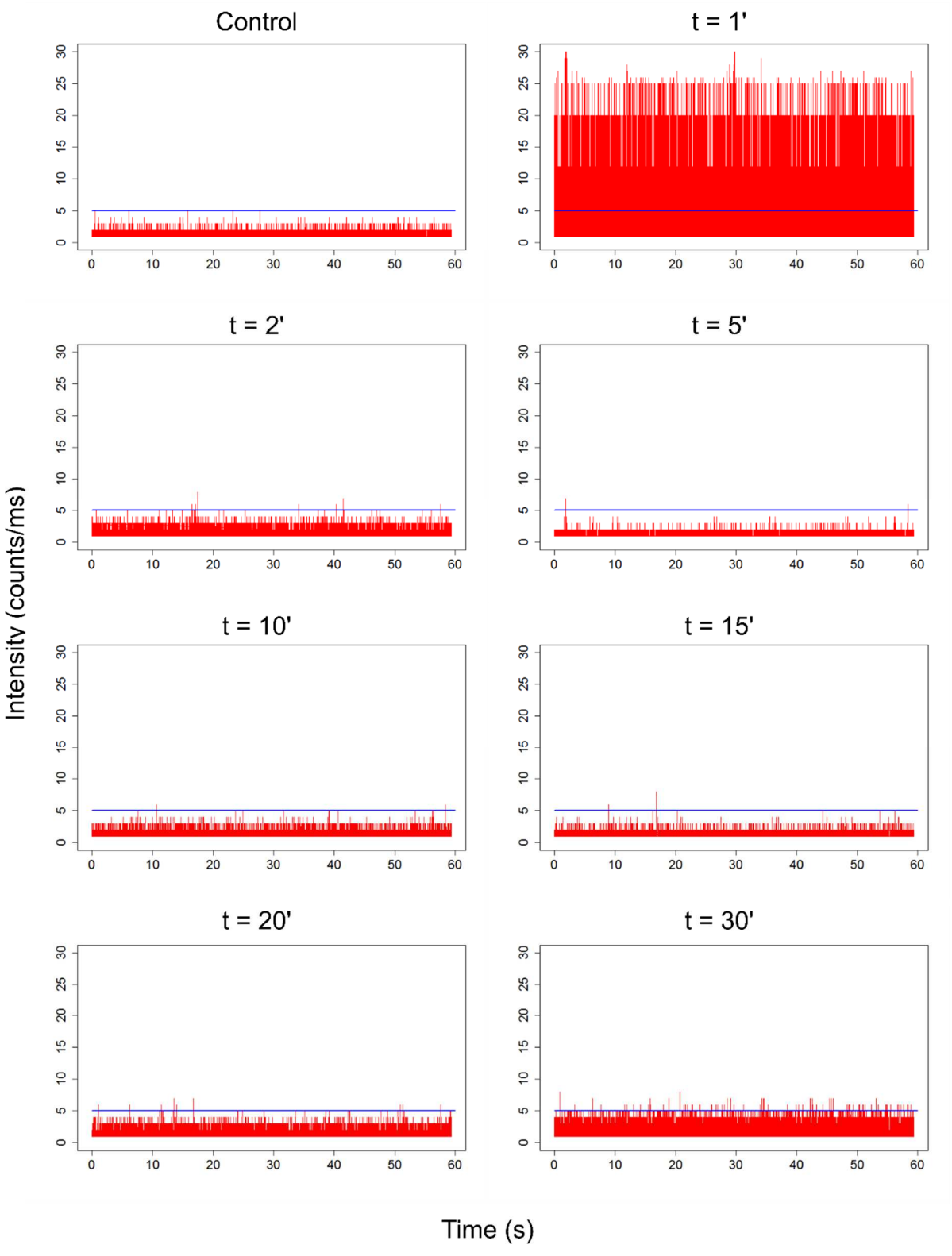

Suppl. Figure 2 Representative time traces for the degradation experiment depicted in Figure 4 B. Binning time = 1000 µs, laser power = 1% ~ 0.0029 mW, threshold at 5 counts/ms, based on the control, which is fully degraded pDNA.

CHAPTER 5 |

Evaluation of Alternative Nucleic Acid Labeling Methods

K. Rombouts[†], R. Neely[‡], V. Leen[‡], J. Hofkens[‡], K. Braeckmans[†], K. Remaut[†]

† Laboratory of general biochemistry and physical pharmacy, Faculty of pharmacy, Ghent University, Belgium

‡ Molecular Design and Synthesis, Faculty of Chemistry, KU Leuven, Belgium

This chapter contains unpublished results.

TABLE OF CONTENTS

ABSTRACT

Advanced fluorescence microscopy methods are great techniques to study the characteristics of nucleic acid delivery inside living cells. To follow the intracellular journey of nanoparticles, the nanoparticles should be made visible, which can be achieved by labeling the carriers themselves or by labeling the nucleic acids they carry. A wide variety of labeling methods are available to attach (mostly fluorescent) tags to nucleic acids. It has, however, already been demonstrated that random covalent attachment of a high density of fluorophores to plasmid DNA (pDNA) by the widely used Mirus nucleic acid labeling kit can negatively influence the intracellular processing of the pDNA. In this study, we aimed to evaluate alternative labeling strategies to label pDNA, and to evaluate their effect on the natural behavior of pDNA. As labeling strategies, the intercalating cyanine dimeric nucleic acid stain TOTO-3, the sequence-specific hybridization of fluorescently labeled peptide nucleic acid (PNA) probes, a sequence-specific methyltransferase (MTase) mediated enzymatic labeling, and a nonfluorescent method were evaluated. The potential of labeled pDNA to generate an efficient transfection after lipid-mediated transfection was evaluated. Also, the suitability of fluorescent pDNA to be measured by two advanced microscopy techniques, namely fluorescence correlation microscopy (FCS) and single particle tracking (SPT), was investigated. We found that all three fluorescent labeling techniques generated labeled pDNA that showed only a limited decrease in the transfection efficiency when compared to non-labeled pDNA. For the nonfluorescent labeling method, however, transfection efficiency was seriously hampered. With regard to the dynamic properties of the pDNA, all fluorescent labeled pDNA molecules showed acceptable diffusion coefficients as retrieved from the FCS and SPT measurements. In applications measuring the degradation of pDNA, however, none of the alternative labeling techniques proved to be more reliable than the previous results obtained with the Mirus kit labeling. In conclusion, although the alternative fluorescent labeling methods are promising, the ease of use and the reproducability of the diffusion coefficients retrieved by advanced microscopy methods still favor the use of the Mirus nucleic acid labeling kit when high labeling densities of pDNA are avoided.

INTRODUCTION

The study of nucleic acids as a potential gene replacement therapy, has, despite being around for more than 40 years, [1] not yet resulted in a widely applied therapy. One of the big hurdles that needs to be tackled, is the design of nanocarriers that are stable in the hostile extracellular environment in the body, yet are efficient at delivering their cargo to the right cell compartment. To understand the individual barriers that reduce the intracellular delivery, (advanced) fluorescent microscopy methods are invaluable. [2, 3] Attaching the fluorescent label to the carrier is one way of enabling detection by fluorescence microscopes, but this approach might perturb the interactions between the delivery vehicle and the cell. For this purpose, fluorescent labeling of the cargo, which is encapsulated inside the nanoparticles formed with the carrier, might be more useful. In **Chapter 1**, an overview was presented of the available labeling techniques that can be utilized to attach fluorescent moieties to nucleic acids. We have observed, however, in **Chapter 3** that some labeling methods might interfere with the biological activity of the nucleic acids under investigation. We hypothesized that the random labeling methods used before, hinders the transcription of the labeled plasmid DNA due to the presence of fluorophores in the coding region of the pDNA. To overcome this limitation of the widely applied Mirus kit labeling method, in this chapter we evaluated the potential of alternative labeling techniques to label plasmid DNA without interfering with its functionality. Cyanine dimeric nucleic acid stains, peptide nucleic acid (PNA) hybridization and enzymatic labeling were the three alternative labeling methods that were considered.

The basic principle behind the first labeling strategy that was evaluated, the cyanine dimeric nucleic acid stains, is the mechanism of bis-intercalation. Each of the monomers, that make up the dimer, will undergo intercalation with the DNA, which is the insertion between the base pairs of the helix-structure. During intercalation, π-stack interactions, hydrogen-bonding, van der Waals interactions, hydrophobic interactions, and steric hindrance effects all play a role [4] (see **Chapter 1** for a more detailed explanation). The binding of the stains at random locations of the plasmid increase the fluorophore's brightness, which enables visualization of the nucleic acid with a fluorescence microscope.

As a second pDNA labeling strategy, PNA probes that hybridize in a sequence-specific manner to nucleic acids were evaluated for the labeling of pDNA. The PNA probes used in this chapter, consist of two linear probes made up by nucleotides linked by a peptide-modified backbone. The two probes are linked to each other with a flexible spacer and are therefore called bis-PNA probes. [5] During hybridization, one of the linear probes is undergoing Watson-Crick base pairing, while the second probe undergoes Hoogsteen base pairing with their specific recognition sequence, resulting in a strong PNA-DNA-PNA triple helix structure. [6] When multiple recognition sequences are grouped in an array, several labeled PNA probes can hybridize in this region, creating a strong fluorescently labeled molecule. Plasmids can be designed to incorporate these arrays in a selected region, eliminating possible interference between the labels and the coding region. The GeneGrip gWIZ-GFP pDNA (Genlantis, San Diego, CA, U.S.A.) used throughout this thesis, for example, has two different arrays built into its sequence, outside the coding region of the pDNA.

The third labeling method that has been evaluated is the enzymatic labeling with DNA methyltransferases (MTases). The MTases (M.TaqI) used in this chapter catalyze a covalent bond formation between the activated primary amine from a specifically designed co-factor (e.g. S-adenosyl-L-methionine) to the exocyclic amino group of guanine in the 4 base sequence: 5' – TCGA - 3'. [7] By conjugating a functional group with a NHS ester-linker to the cofactor, the functional group can be attached to the DNA. [8] Choosing a different MTase will change the recognition sequence at which functional groups are attached. At the moment, most recognition sequences consist of 4 to 6 base pairs in which the nucleophilic attack will occur. This sequence specificity can be used to quickly make a "fluorocode". The positions of the fluorescent labels will be unique for every species, enabling recognition of the origin of unknown DNA [9]. For the labeling of pDNA, the enzymatic labeling can also be used to label the naturally occurring recognition sequences in the plasmid or to label plasmids with a custom designed recognition sequence array. In this chapter, the enzymatic labeling method was applied to couple two types of functional moieties to the plasmid DNA. In one set of experiments, a fluorophore was coupled to obtain fluorescently labeled pDNA. Alternatively, the enzymatic labeling method was applied to couple poly-ethylene-glycol (PEG) chains to the pDNA. PEG is hypothesized to

increase the mobility of pDNA in the intracellular environment by hindering non-specific protein binding. Therefore, a PEGylated DNA molecule could potentially be more potent to induce transfection efficiency, due to an increased intracellular mobility and decreased recognition by proteins of the intracellular innate immunity pathway.

Apart from the alternative labeling methods based on the addition of fluorescent molecules, we also evaluated a nonfluorescent nucleic acid labeling method. This was achieved by making a modified plasmid in which a portion of the thymine residues were replaced by an alkyne-tagged deoxyuridine: 5' – ethynyl – 2' - deoxyuridine (EdU). These alkyne groups can be visualized in a living cell by stimulated Raman spectroscopy, as has already been shown by Wei et al. (2014)[10]. In this paper, EdU was supplied to the cell's growth medium and incorporated by the cell during de novo DNA synthesis. This allowed the imaging of this process by stimulated Raman spectroscopy of the EdU containing DNA in real time. [10] In this chapter, an EdU modified pDNA was tested, to examine the potential of this nonfluorescent labeling technique for following extracellular DNA in their journey through the cell.

All mentioned labeling techniques were evaluated in terms of transfection efficiency, as well as their suitability for use in (advanced) microscopy methods (e.g., fluorescence correlation spectroscopy (FCS) and single particle tracking (SPT) to measure pDNA diffusion properties and/or degradation of labeled pDNA (cf. **Chapter 4**). Briefly, both microscopy methods can determine the hydrodynamic diameter and concentration of fluorescently labeled molecules in solution by diffusion analysis. In the case of FCS, diffusion analysis is based on the autocorrelation of fluorescence fluctuations over time, while for SPT individual fluorescent particles are tracked in time-lapse movies.

In summary, this chapter deals with the search for an alternative for the Mirus labeling kit, which is currently the standard labeling technique in our and many other laboratories. The alternative labeling techniques all make use of different methods of fluorescent labeling. While intercalating dyes and EdU incorporation result in random labeling of the entire pDNA molecule, PNA probes and enzymatic labeling result in sequence-specific labeling enabling the researcher to control the location of the fluorescent labels on the nucleic acid. The latter could potentially be important to

minimize the effect of the chosen labeling method on the intracellular path of the labeled nucleic acids for gene replacement therapy.

MATERIALS AND METHODS

Cyanine Dimeric Nucleic Acid Staining

The intercalating dimeric cyanine nucleic acid stains YOYO-1 (λabs. 491 nm, λem. 509 nm) and TOTO-3 (λabs. 642 nm, λem. 660 nm) were used according to the manufacturer's instructions (Invitrogen, Molecular Probes, Merelbeke, Belgium). The stock iodide (1 mM in DMSO) was diluted in TE buffer (10 mM Tris-base, 1 mM EDTA, pH 8.0) and added to the DNA in molar ratios pDNA over TOTO-3 of 200:1, 50:1, 10:1, 5:1, assumed to be corresponding to labeling densities of respectively 30, 120, 500, and 1000 TOTO-3 labels per pDNA molecule. This assumption was based on the protocol provided by the manufacturer. These solutions were incubated overnight at room temperature in the dark. The fluorescently labeled pDNA was then recovered using ethanol precipitation and reconstituted in HEPES buffer (20 mM, pH 7.2).

Peptide Nucleic Acid Hybridization

The gWIZ-GFP plasmid has been designed with two PNA recognition sequence arrays by Genlantis (San Diego, CA, U.S.A.). Two PNA sequences were ordered at Panagene (Daejeon, Korea). One sequence was a 5' – Alexa Fluor 647-OO-TCTCTCTC-(AEEA)-(AEEA)-(AEEA)-CTCTCTCT-(AEEA)-(AEEA)-3' (λex. 650 nm, λem. 665 nm) and the second PNA sequence was 5' – Alexa Fluor 488-OO-CCTTCCTT-(AEEA)-(AEEA)-(AEEA)-TTCCTTCC-(AEEA)-(AEEA) – 3' (λex. 490 nm, λem. 525 nm) with O, E and A as linker molecules. To label the plasmids, a 30 molar excess of PNA molecules was added to finally obtain a labeling density of maximal 10 PNA molecules per plasmid. Therefore, PNAs and pDNA were mixed in a hybridization buffer (50 mM Tris-HCl, pH 8) after which the mixture was incubated for 2h at 55°C. To recover labeled DNA, ethanol precipitation was performed and the DNA was reconstituted in HEPES buffer. Alternatively, size exclusion spin column chromatography was performed to remove unbound PNA molecules.

Methyl Transferase Mediated Enzymatic Labeling

Enzymatic Atto647N (λex. 644 nm, λem. 669 nm) labeled pDNA was directly obtained from the collaborating laboratory of Prof. Hofkens at the KULeuven, or labeled by a three step labeling kit provided by the laboratory of Prof. Hofkens. In the first step, a functional NHS ester is coupled to the amine-cofactor in the presence of "Buffer 1". This reaction is mixed and left for reaction on ice. After 20', the first reaction is quenched completely by addition of "Buffer 2" and incubation during 1' on ice. In the meantime, a separate tube is prepared with the target DNA and the MTase: M.TaqI, which specifically targets the 4 base sequence 5' - TCGA – 3'. This mixture is added to the tube containing the cofactor and is incubated at 60°C for 1h. The labeled DNA is then recovered via ethanol precipitation and the pellet is resuspended in HEPES buffer.

5-Ethynyl-2'-deoxyuridine Incorporation

The modified nucleotide EdU is incorporated via nick translation, according to the protocol provided by the manufacturer (Nick translation system, Invitrogen, Merelbeke, Belgium). Briefly, the dNTP mix (0.2 mM each of dATP, dCTP, dGTP, 500 mM Tris-HCl, pH 7.8, 50 mM $MgCl_2$, 100 mM 2-mercaptoethanol), DNA, the modified nucleotide (EdU), and water were mixed in a tube. To this tube the DNase I/Polymerase I mixture was added, mixed thoroughly, and incubated at 15°C. After 1h the reaction was stopped by addition of a Stop buffer (0.5 M EDTA, pH 8.0). Ethanol precipitation was used to recover the modified DNA in HEPES buffer.

Plasmid Preparation

gWIZ-GFP plasmids were purchased from Genlantis (San Diego, CA, U.S.A.). The plasmids, that express GFP, were amplified in *Escherichia coli* and isolated from a bacteria suspension using a PurelinkHiPure Plasmid DNA Gigaprep kit K2100 (Invitrogen, Merelbeke, Belgium). Plasmid concentration measurements at a wavelength of 260 nm were performed on a NanoDrop 2000c (Thermo Fisher Scientific, Rockford, IL, USA). The A260/A280 ratio was measured to assess the purity of the pDNA. Twenty-five microliter aliquots at 1 µg/µL were prepared and stored at −20 °C.

Gel Electrophoresis

An agarose gel was prepared by adding 1% agarose (UltraPore™ agarose, Invitrogen, Merelbeke, Belgium) to a 1 x TBE buffer (90 mM Tris base/90 mM borate/2 mM EDTA) supplemented with GelRed (Biotum, Hayward, CA, U.S.A.). Gel loading buffer (Ambion, Merelbeke, Belgium) was mixed with the samples and this mixture was loaded onto the agarose gel. After running the gel for 50' at 100 V, a picture was taken under UV light.

Cell Culture

A HeLa cell line was maintained at 37 °C (5% CO2) in Dulbecco's modified Eagle's medium supplemented with growth factor F12 (1:1 DMEM/F12), 10% heat inactivated fetal bovine serum (FBS), 2 mM L-glutamine, and 100 µg/mL penicillin/streptomycin. All cell culture reagents were purchased from GibcoBRL (Merelbeke, Belgium).

Transfection

HeLa cells were plated 1 day prior to transfection in 12 or 24-well plates at, respectively, 100 000 and 50 000 cells/well. Incubation of the cells with the Lipofectamine 2000 (Invitrogen, Merelbeke, Belgium) complexes (3:1 volume:weight ratio of Lipofectamine:pDNA), prepared with labeled or unlabeled pDNA, was done at 1 µg of DNA per 100 000 cells (in 500 µL lipoplex solution per well) for 4 h at 37 °C. At this point, the cells were washed with phosphate buffered saline (PBS), and fresh medium was added for overnight incubation. After 24 h, the cells were trypsinized and examined by flow cytometry (FACSCalibur, BD Biosciences Benelux N.V., Erembodegem, Belgium) to detect the GFP expressing cells.

Degradation of Plasmid DNA

Two degradation experiments were performed. In the DNase I degradation experiment, DNase I (2 U/µl) (Invitrogen, Merelbeke Belgium) was added to a 0.1 µg/µl solution of labeled pDNA prepared in a 1 x degradation buffer kept at 37°C. After different time points a sample was taken out of the reaction mixture and added to a DNase I inhibitor solution (0.1 M Iodoacetate, 10 mM Tris-HCl, 50 mM EDTA, pH 7.4) on ice. These samples were then measured using FCS as described in **Chapter 2**.

In the second type of experiment, labeled pDNA was fully degraded by the addition of DNase I (2 U/µl) (Invitrogen, Merelbeke, Belgium) and a 1 x degradation buffer and incubation over 30' at 37°C, according to the manufacturer's protocols. Mixtures of non-degraded (or intact) and fully degraded Cy5-pDNA were prepared to have 0/100, 20/80, 40/60, 50/50, 80/20 and 100/0 % of intact/degraded pDNA for FCS measurements (cf. **Chapter 4**) and 0/100, 10/90, 25/75, 40/60, 50/50, 60/40, 75/25, 90/10 and 100/0% of intact/degraded pDNA for SFC recordings. Ten movies of 200 frames were subsequently recorded for every sample with SFC microscopy (cf. **Chapter 4**) and diffusion coefficients or number concentrations were obtained as described in **Chapter 2**.

RESULTS

Cyanine Dimeric Nucleic Acid Stains

YOYO-1 and TOTO-3 are two of the cyanine dimeric nucleic acid stains which were evaluated for their use as fluorescent pDNA labels. YOYO-1 was used by multiple colleagues (e.g., Vercauteren et al. (2011)[11]) to quantify cellular uptake of the resulting green fluorescently labeled pDNA with flow cytometry. Here, we evaluated TOTO-3, which results in red fluorescent labeling of the pDNA upon intercalation. Red fluorescent labeled pDNA was chosen as the detection does not interfere with the possible expression of GFP which is detected in the green channel. Since it is known that these cyanine dimeric stains have an influence on DNA conformation and integrity, [12-15] the effect of the stain on the transfection efficiency was tested. To examine the compatibility of the stain with FCS, experiments on degradation of pDNA were also performed.

Transfection Efficiency of TOTO-3 Labeled Plasmid DNA

Results from **Chapter 3** indicated that transfection with lipid-based carriers can be hampered by the labeling density of pDNA, upon the at random labeling by covalent attachments of fluorophores using the Mirus kit. Therefore, we were interested to see if the transfection efficiency of TOTO-3 labeled pDNA would also be hampered. The percentages of GFP positive cells resulting from transfection with pDNA labeled with TOTO-3 at different labeling densities were compared to the positive control, which is the lipofection with unlabeled plasmids. As can be seen in Figure 1 A, the transfection efficiencies of the pDNA, containing different labeling

densities of the intercalating dye TOTO-3, are not significantly different ($p < 0.01$) to the positive control, containing unlabeled pDNA. The mean fluorescence intensity (MFI) was, however, lower for the higher labeling densities. This indicates that the intercalating dyes have some influence on the potential of the cellular machinery to transcribe the fluorescent pDNA into mRNA and the translation into the corresponding GFP molecules, but not significant enough to decrease the transfection efficiency. The red fluorescence intensity and % red fluorescent cells inside the cell increased, as expected, with an increasing labeling density (Figure 1 B).

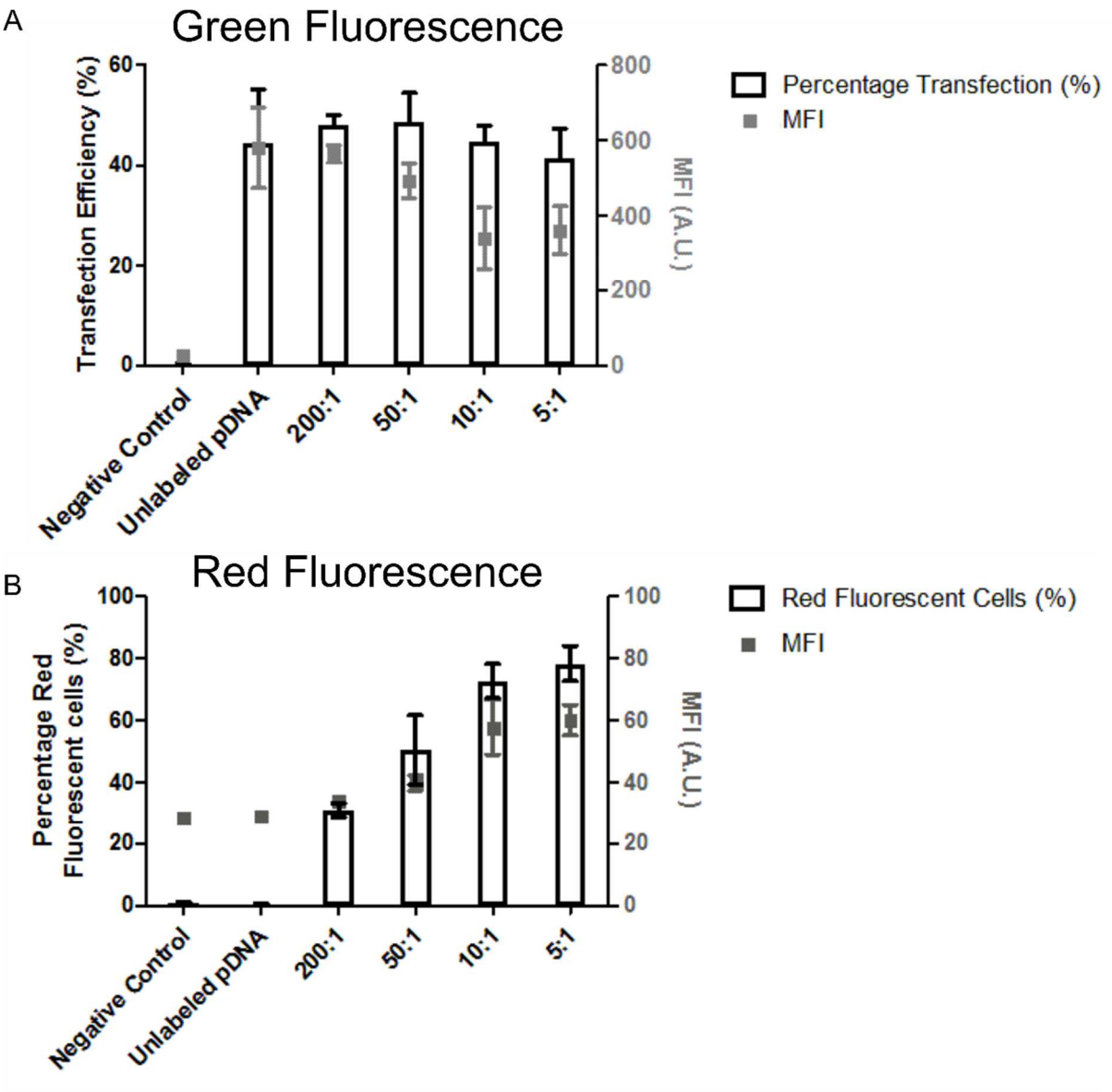

Figure 1 (A) Percentage GFP expressing cells and (B) percentage red fluorescent cells following lipofection with pDNA in function of the labeling density with TOTO-3, expressed as the ratio between mol pDNA : mol TOTO-3 and mean fluorescence intensity (MFI) (grey) of

respectively the (A) GFP fluorescent signal and (B) the TOTO-3 signal per cell. Negative Control = no pDNA. The average depicted is based on one representative experiment with three repetitions. Error bars are standard deviation on the average.

Fluorescence Correlation Spectroscopy

In **Chapter 4**, FCS measurements were performed on pDNA labeled with the Mirus kit. In this chapter, we evaluated if pDNA labeled with the TOTO-3 dye can be detected by FCS as well. FCS autocorrelation analysis resulted in a diffusion coefficient of 3.81 ± 0.86 µm²/s, which is comparable with the diffusion coefficient of 3.23 ± 0.92 µm²/s that was measured in **Chapter 4** for Mirus Kit labeled pDNA.

In a next set of experiments, the endonuclease activity of the enzyme DNase I was followed by measuring TOTO-3 labeled pDNA with FCS in function of time. In parallel, agarose gel electrophoresis was performed to visualize the degradation of pDNA. As expected, the DNA concentration diminishes in function of the reaction time and after 30', almost all DNA is degraded (Figure 2). To follow the degradation of pDNA with FCS, peak analysis on fluorescence intensities over time was performed to determine the concentration of intact pDNA. The intensity threshold to determine the peaks is set just above the maximum intensity recorded for a fully degraded sample. This was 12.5 counts/ms (see Suppl. Figure 1 for the time traces).

Initially, the number of peaks decreases, in comparison to the number of peaks counted at t = 0', during the first 2 minutes of reaction with the DNase I enzyme. After 5 minutes, however, the number of peaks reaches a constant percentage around 70% although the agarose gel clearly demonstrates further degradation of the pDNA. Therefore it seems that peak analysis of pDNA fluorescently labeled with intercalating dyes such as TOTO-3 is not suited to follow the pDNA degradation over time. As intercalating dyes are spread throughout the DNA backbone, also smaller degradation fragments are expected to contain more than 1 dye molecule. Therefore, it is possible that the number of peaks does not decrease significantly when smaller degradation products are being formed. Although the average fluorescence intensity is expected to decrease for shorter pDNA fragments, the peak analysis will consider a fluorescent peak as a single event as soon as it rises above the background level, irrespective of the absolute intensity value of the peaks. This could explain why the peak analysis was less suitable to

follow TOTO-3 labeled pDNA, when compared to the Mirus kit labeled pDNA used in **Chapter 4**.

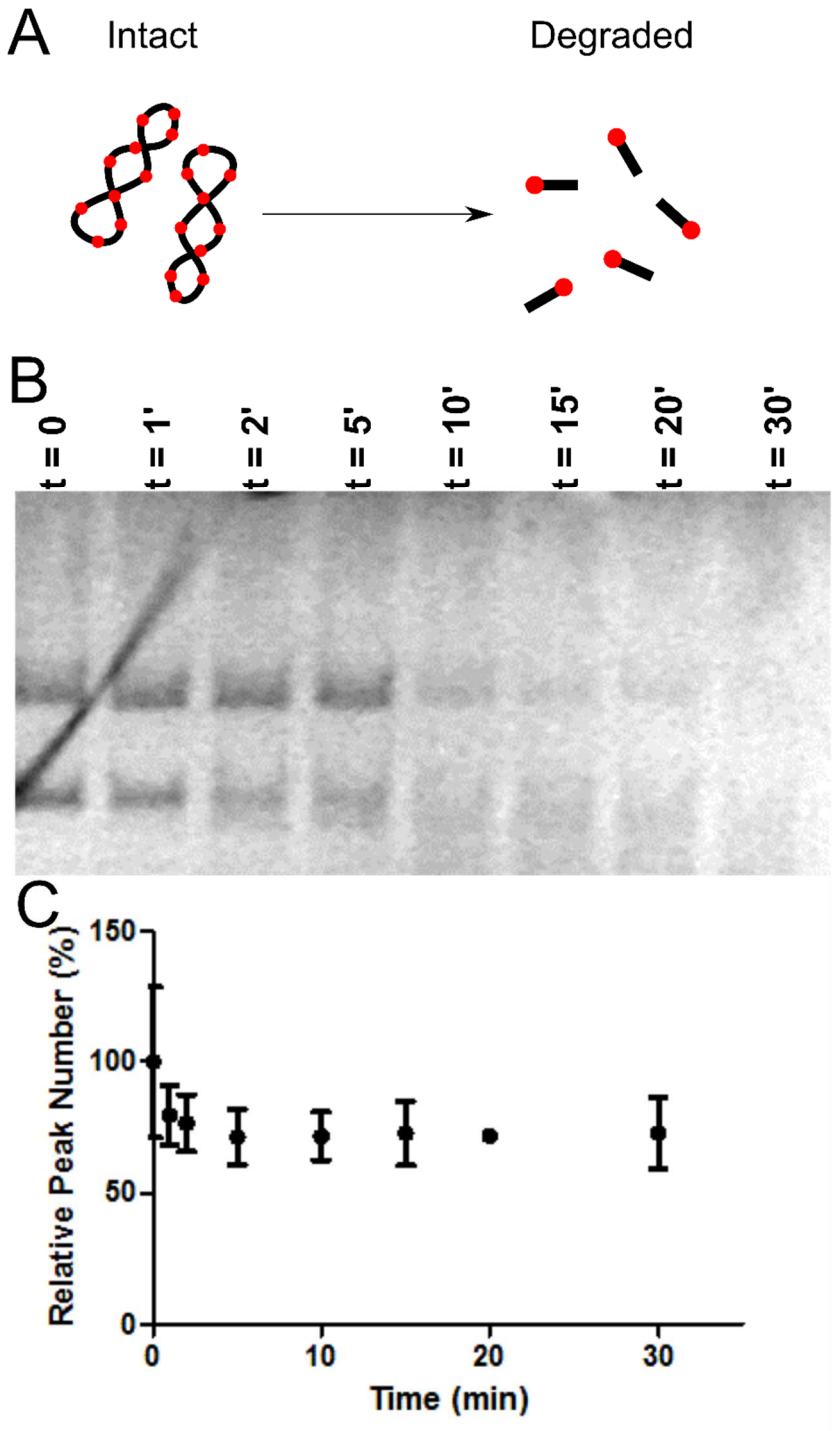

Figure 2 Degradation of TOTO-3 labeled pDNA by DNase I. (A) Graphic representation of degradation of TOTO-3 labeled pDNA. (B) Image of agarose gel. (C) Peak analysis after FCS measurements. Data points are averages from a single experiment with five repetitions per sample. Error bars are standard deviation on the average.

Peptide Nucleic Acid Hybridization

The second labeling strategy evaluated in this chapter is the sequence-specific labeling of pDNA by fluorescent PNA clamps, complementary to a pre-designed recognition site in the pDNA. The gWIZ-GFP plasmid that is used throughout this work was originally designed to include two so-called GeneGrip sites. These sites are recognition sequence arrays, aimed at the hybridization of PNA probes. The labeling technique in itself is based on PNA-DNA-PNA triple-helix formation. As 10 PNA recognition sites are positioned one after the other in an array on the pDNA, up to 10 fluorophores can be attached to the pDNA by hybridization with fluorescently labeled PNA probes. A PNA probe with Alexa Fluor 488 was designed and ordered to fit the plasmid recognition site 2. Incubation of the pDNA with the PNA clamp will result in the fluorescent labeling with one type of fluorophore. The transfection efficiency of this fluorescent labeled pDNA was checked, as well as the potential of PNA clamp labeled pDNA for use in FCS and SPT experiments.

Transfection Efficiency of PNA-Labeled Plasmid DNA

Chapter 3 learned us that the random labeling of pDNA, by using the Mirus labeling kit, interfered with the potential of pDNA to be transcribed, due to the presence of fluorophores that are covalently attached to nucleotides in the coding region of the pDNA. Zelphati et al. (1999)[16] described PNA-labeled plasmids as being functional, while the conformation is preserved. We in turn evaluated the transfection efficiency of PNA clamp labeled pDNA as an indicator for the functionality of the labeled pDNA. Figure 3 demonstrates that the single-color PNA-labeled pDNA reaches the same transfection efficiency as unlabeled pDNA upon delivery with Lipofectamine. Therefore, we could demonstrate that pDNA that carries fluorescent labels outside the coding region does not suffer from a decrease in transfection efficiency and, in other words, is still transcriptionally active.

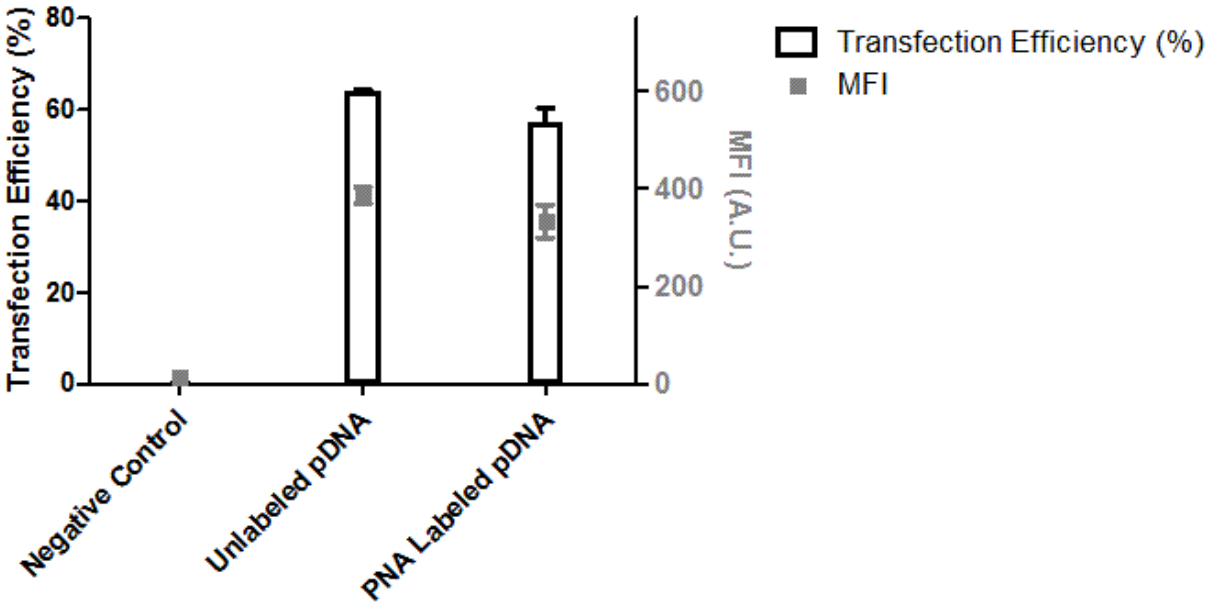

Figure 3 Percentage GFP expressing cells following lipofection of unlabeled and PNA labeled pDNA and mean fluorescence intensity (MFI) (grey) of GFP fluorescent signal. Negative control = no pDNA. The average depicted is based on one representative experiment with three repetitions. Error bars are standard deviation on the average.

Fluorescence Correlation Spectroscopy

In a first set of experiments, the diffusion coefficients of the free PNA probes and PNA labeled plasmids were characterized. Then, we evaluated the potential to use PNA-labeled pDNA to study degradation of the pDNA molecules

In PNA-labeled pDNA, all the fluorescent labels are concentrated at the recognition sequence array. During the labeling procedure, fluorescently labeled PNA clamps are incubated with pDNA to allow hybridization to the recognition sequence. Unbound PNA probes are removed via ethanol precipitation, but a small fraction remains in the solution. To take these free fluorescent labeled probes into account, autocorrelation curves are always fitted with a two species fit with fixed diffusion coefficients for PNA probes and intact pDNA as described in **Chapter 2** (respectively 193.47 ± 5.47 µm²/s and 3.44 ± 1.24 µm²/s). This diffusion coefficient for intact pDNA corresponds to the diffusion coefficient of Mirus kit labeled pDNA as measured in **Chapter 4**.

Now that the diffusion coefficient of intact PNA labeled pDNA is determined, this knowledge can be used to follow degradation. Degradation by endonuclease

activity of DNase I shortens the DNA strands, which should produce faster moving labeled DNA fragments since all the fluorescent labels are located in one short sequence. As depicted in Figure 4 A, the fluorescent fragments are becoming smaller, but the number of fluorophores will be more or less the same. This means the small fragments are still detectable whereas these small fragments did not emit enough signal to be detectable in the case of the random labeling techniques (e.g., Figure 2 A).

Due to the formation of smaller fluorescent degradation fragments, we expected that the diffusion coefficient of the slow component (originally corresponding to intact pDNA) should increase until degradation is complete. The fast components was therefore fixed. DNase I was added to a mixture of intact pDNA and samples were collected at different time points. These samples were in parallel run on an agarose gel and measured with FCS. The agarose gel in Figure 4 B shows how the amount of intact pDNA decreases with increasing incubation times. At t = 20' all DNA is degraded. This was reflected in the FCS measurement, where a gradual increase in the diffusion coefficient of the slow component is found over time.

Single Particle Tracking

Next to FCS, SPT analysis is a technique that can provide information on the dynamic properties of fluorescently labeled molecules and their concentration. We evaluated whether SPT was suitable to follow the degradation of PNA labeled pDNA over time, as was reported for Mirus kit labeled pDNA in **Chapter 4**.

Starting with intact PNA labeled pDNA in a buffer solution, a diffusion coefficient of 1.94 ± 0.19 $\mu m^2/s$ was found. This diffusion coefficient is lower than the one obtained by FCS, but comparable to the diffusion coefficient found for Mirus labeled pDNA with SPT (see Figure 10 B). Next, similar to what was done in **Chapter 4**, mixtures of intact and fully degraded pDNA were made. Based on the concentration algorithm, the percentage of intact pDNA from these mixtures was calculated, and compared to the known amount of intact pDNA present in the solutions. This approach is based on the fact that degraded pDNA fragments are too fast to successfully be imaged by the microscope. Therefore, degraded pDNA will not result in analyzable tracks and only contribute to the background signal.

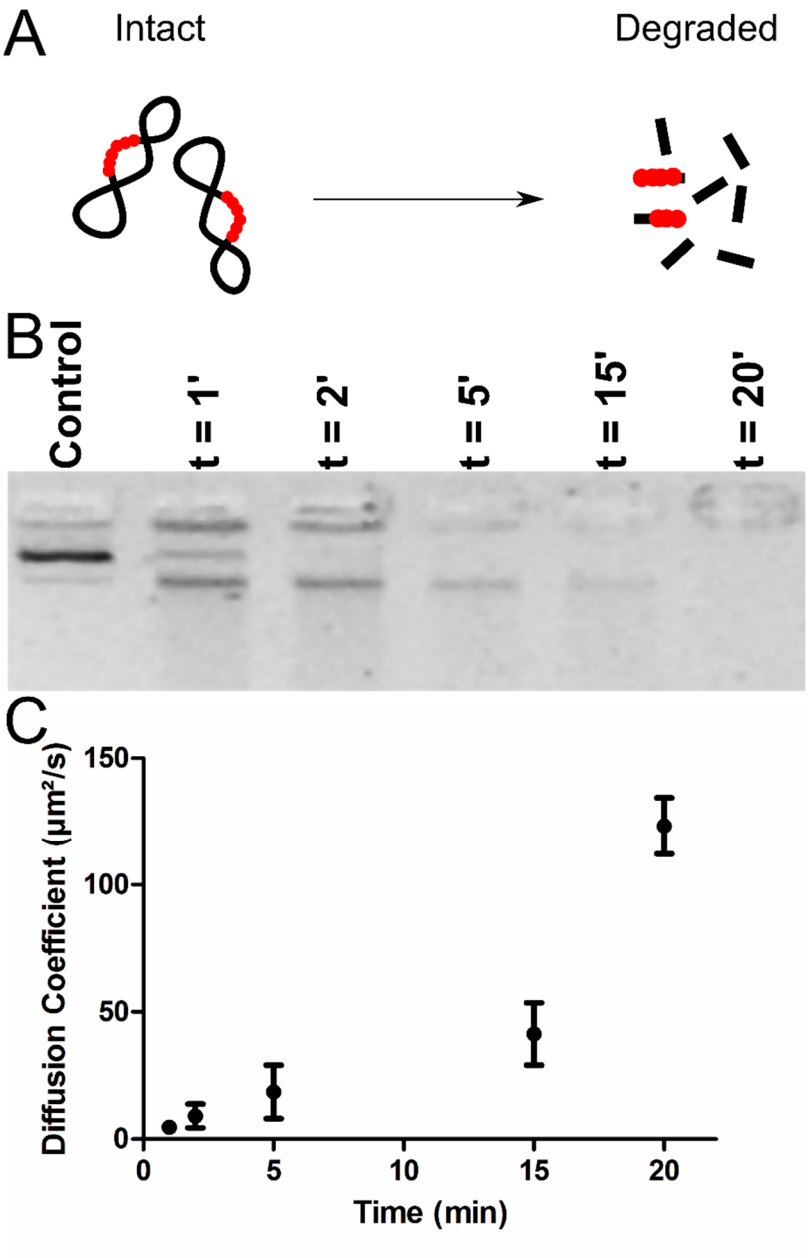

Figure 4 DNase I degradation of labeled pDNA over time.(A) Graphic representation of degradation of PNA labeled pDNA. (B) Agarose gel. (C) Diffusion coefficients over time measured with FCS on the degrading pDNA solutions. Average diffusion coefficient based on ten repetitions from one experiment. Error bars are the standard deviation on the average.

As can be seen in Figure 5, a slight underestimation of the amount of intact pDNA was found for all mixtures. It should be noted that when PNA labeled pDNA degrades, the fluorescence intensity of the degradation products will only decrease when the degradation occurs at the PNA recognition sequence. In all other cases, shorter pDNA fragments are formed, which still bear a maximum of 10 fluorescent labels at the PNA recognition site (see Figure 4 A). This is a clear difference when compared to the random fluorescent labeling method evaluated in **Chapter 4**, where

almost each cut in the pDNA molecules results in shorter degradation fragments that contain less fluorophores since there is on average only one fluorophore about every 600 base pairs. Possibly, this difference in fluorescent labeling of the degradation fragments that are formed, could explain why SPT could more reliably measure the amount of intact pDNA in **Chapter 4**, where the degradation products are more rapidly falling under the detection limit of the SFC microscope while the small fragments in this chapter, with a high amount of fluorescent labels, contribute more to the background signal, making it harder to detect intact pDNA.

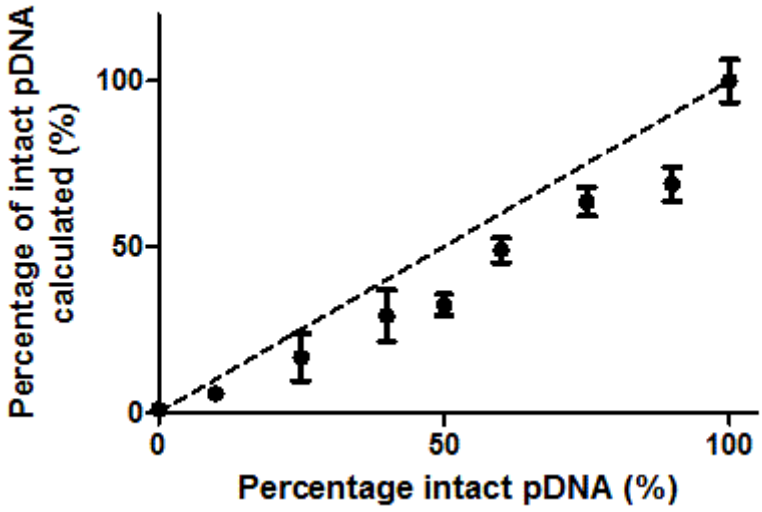

Figure 5 Percentage of intact pDNA retrieved by concentration analysis in function of known percentage intact pDNA. Dashed line indicates the theoretical expected values. Averages calculated from ten movies of the same sample. Error bars are the standard deviation on the average.

Sequence-Specific Enzymatic Labeling of pDNA

As an alternative for PNA probe mediated site-specific labeling of pDNA, in collaboration with the research group of Prof. Hofkens at the KU Leuven, a newly developed labeling kit was tested. This labeling kit (called “Chrometra”) is derived from the technique used to produce a fluorocode as described in Neely et al. (2010)[9] and provides sequence specific attachment of fluorescent labels to DNA (also see **Chapter 1**, for a more detailed explanation). It makes use of the DNA methyltransferase TaqI (mTaqI) which targets the four base sequence 5’ – TCGA – 3’ where it attaches the label via a covalent bond formation between the activated methyl group from a specifically designed cofactor to the exocyclic amino group of

the nucleobase. In case of the gWIZ-GFP vector, which is used throughout this thesis, this enzymatic labeling results in the attachment of a fluorophore to nine recognition sites which are naturally present in the pDNA sequence. Two of those are present in the coding region of the pDNA (see Figure 6). In a first set of experiments, we evaluated the enzymatic attachment of the Atto647N dye to the pDNA. The labeling procedure was evaluated by a number of experiments. The transfection efficiency was compared to unlabeled pDNA. Also, detection of the fluorescent pDNA was performed with advanced microscopy techniques like FCS and SPT. Apart from the fluorescent labeling, also the potential of adding polyethylene glycol (PEG) chains to the pDNA (also called PEGylating) by enzymatic labeling was evaluated, with the aim to improve intracellular mobility of the pDNA and potentially limit the recognition of PEGylated pDNA by the key players of the innate intracellular immunity pathways.

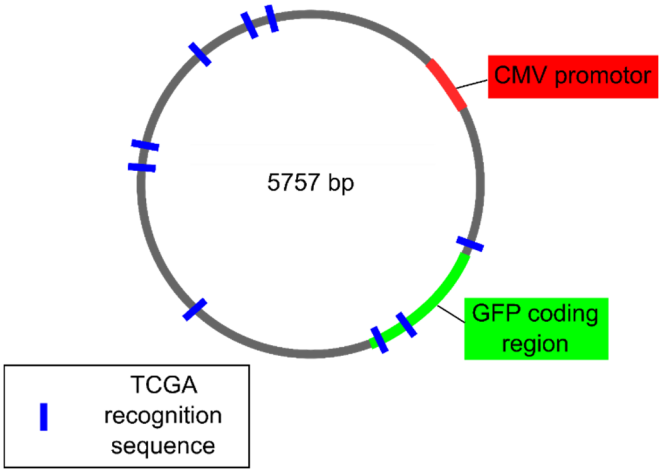

Figure 6 Graphic map of gWIZ-GFP vector with the nine mTaqI recognition sites (5' - TCGA - 3') indicated in blue. CMV promotor is indicated in red. The sequence coding for GFP is indicated in green.

Transfection Efficiency of Enzymatic Labeled Plasmid DNA

One of the factors of the enzymatic labeling kit that needed to be optimized, was the use of the cofactor in the labeling reaction. Therefore, different cofactors were compared to see if there was a difference in labeling efficiency, and to evaluate the influence of the cofactors on the conformation and functionality of the labeled pDNA. A transfection of HeLa cells was performed using Lipofectamine. The positive control consists of complexes with unlabeled pDNA and the negative control lacks pDNA. In Figure 7 A, it can be seen that the transfection efficiency of the enzymatic labeling for pDNA obtained with the cofactors MTC-3 and MTC-6 is slightly lower

than the positive control ($p < 0.05$). The MTC-7 cofactor seemed to result in labeled pDNA with a lower transfection efficiency than the positive control and also slightly lower than the transfection efficiency obtained from pDNA labeled with the other cofactors ($p < 0.05$). A look at the red fluorescence signal showed that the % of red fluorescent cells is lower (around 15% red fluorescence cells), compared to ~99% seen for the other cofactors, indicating that cellular uptake is probably less efficient or that the pDNA is not labeled efficiently and the fraction of pDNA that is labeled is degraded before reaching the cell. Therefore, it seems that the cofactors MTC-3 and MTC-6 are most suitable for enzymatic labeling of the pDNA, with MTC-6 leading to a higher red fluorescence signal per cell compared to MTC-3, which is probably due to a more efficient labeling process that leads to more labels per plasmid (Figure 7 B). Hereafter, MTC-6 is always used as the cofactor.

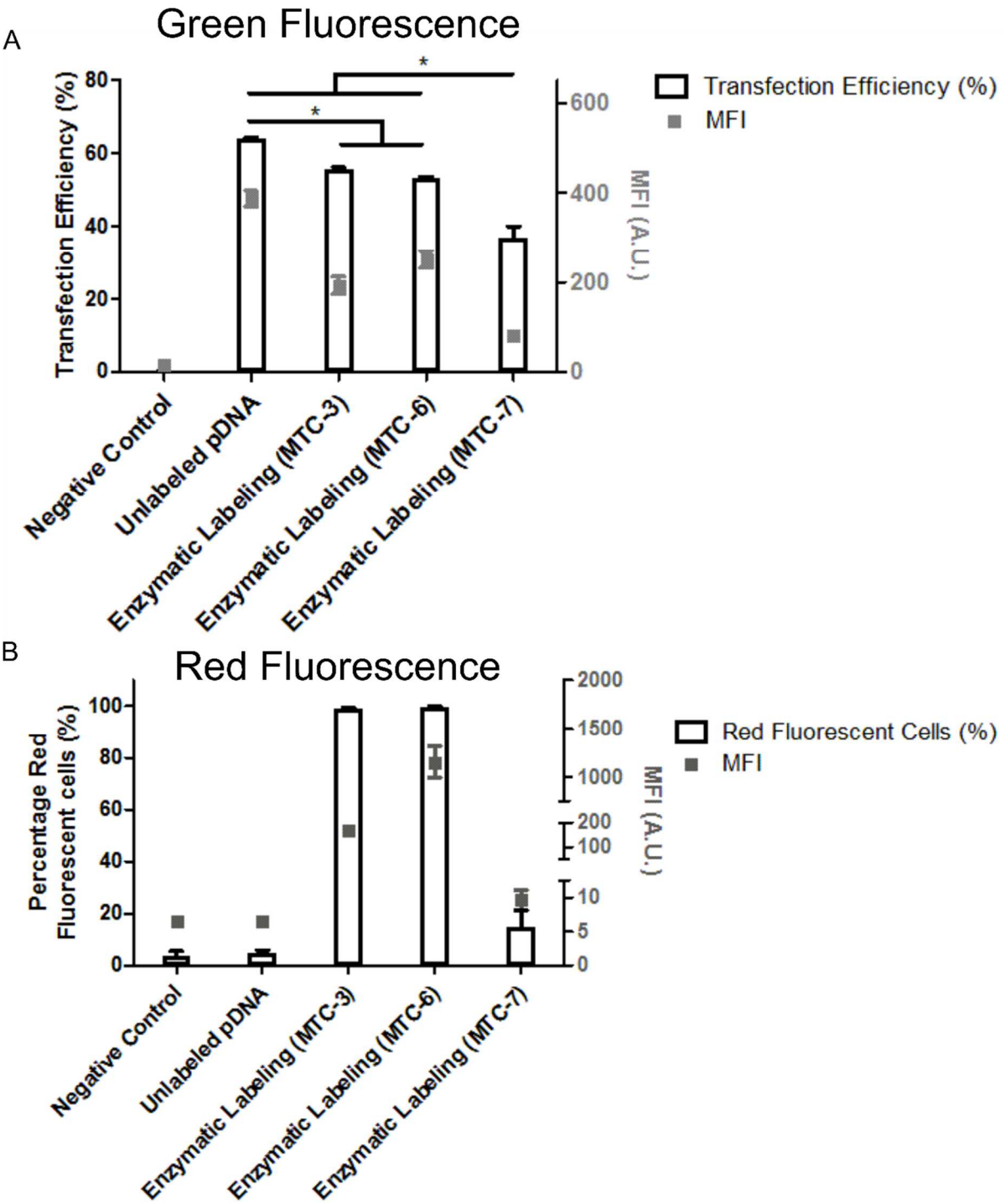

Figure 7 (A) Percentage GFP expressing cells and (B) percentage red fluorescent cells following lipofection with of unlabeled and enzymatic labeled pDNA and mean fluorescence intensity (MFI) (grey) of respectively the (A) GFP fluorescent signal and (B) the Atto647N signal per cell. The right y-axis of (B) is truncated. Negative control = no pDNA. MTC-3, MTC-6 and MTC-7 are different cofactors used in the mTaqI-mediated labeling reaction. *: $p < 0.05$. The average depicted is based on one representative experiment with three repetitions. Error bars are standard deviation on the average.

Diffusional Properties Measured with Fluorescence Correlation Spectroscopy and Swept Field Confocal with Single Particle tracking

When the diffusion coefficient of the enzymatically labeled pDNA was measured by FCS, a diffusion coefficient of 2.64 ± 0.21 μm²/s was found which is a bit lower than what is seen with the PNA clamp labeling, or the Mirus kit labeling. This value, however, falls into the expected range of diffusion coefficients for a 6000 bp plasmid DNA, demonstrating the enzymatic labeling of pDNA results in labeled pDNA that can reliably be detected by FCS.

Also SPT proved to be able to detect the motion of enzymatically labeled pDNA in buffer. A diffusion coefficient of 2.08 ± 0.50 μm²/s was obtained, which is in line with the value obtained with SPT for the PNA labeled plasmids and the Mirus kit labeling.

PEGylation of Plasmid DNA

Experiments in which plasmids were labeled with PEG-2000, making use of the enzymatic labeling technique, were conducted to see if PEGylation of plasmids could potentially increase the transfection efficiency, by increasing the mobility of pDNA in the intracellular environment and limiting interactions with intracellular compartments. In drug delivery, PEGylation is often used to increase mobility of nanoparticles and to reduce aggregation. [17] Whether or not PEGylated would also be beneficial for increasing the diffusion of PEGylated pDNA, however, remains unclear. Transfection efficiency of the PEGylated pDNA was compared to the transfection with unlabeled pDNA, both complexed with Lipofectamine. In Figure 8, it can be seen that transfection efficiency of PEGylated pDNA decreased in comparison with the lipofection of unlabeled pDNA. The drop in transfection efficiency was slightly larger than the one seen in Figure 7 A, when the same cofactor (MTC-6) was used to couple the fluorescent dye Atto647N instead of the PEG-2000 chains. Therefore, it seems that PEGylation has a more pronounced (negative) influence of the transfection efficiency of enzymatic labeled pDNA, when compared to the smaller Atto dyes.

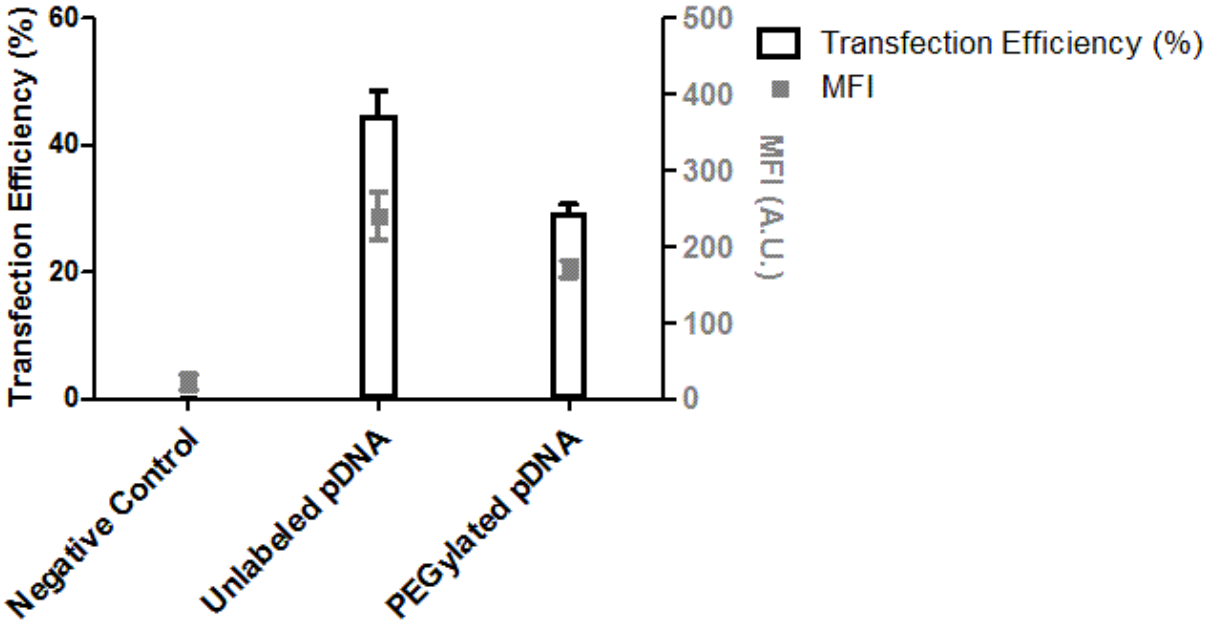

Figure 8 Lipofection of unlabeled and enzymatic PEGylated pDNA and mean fluorescence intensity (MFI) (grey) of the GFP fluorescent signal. Negative control = no pDNA. The average is based on one experiment with three repetitions. Error bars are standard deviation on the average.

5-Ethynyl-2'-Deoxyuridine

A final method that was evaluated in this chapter was the nonfluorescent nucleic acid labeling method. These methods are gaining more and more interest among researchers who were previously relying solemnly on fluorescent labeling techniques. [18] Since DNA is present throughout the cell, a modification should be implemented to the DNA molecule under investigation, to allow specific imaging of the target DNA molecules. A possible modification is the introduction of an alkyne-bearing nucleotide analog, [10] which was already known for its use in the fluorescent labeling with click-chemistry. [19] The detection of the modified pDNA is then possible using Raman spectroscopy. To obtain this pDNA, the modified nucleotide EdU was incorporated into the pDNA via nick translation. As a first test to examine if this method of labeling holds promise, transfection efficiency of the modified pDNA was assessed. As can be seen in Figure 9, the transfection efficiency of EdU modified pDNA dropped to a negligible percentage, indicating that functionality is disrupted. Since the interest of our research group revolves around following the progress of functional nucleic acids through the cell, this fluorescent label free modification of pDNA was not considered for further evaluation.

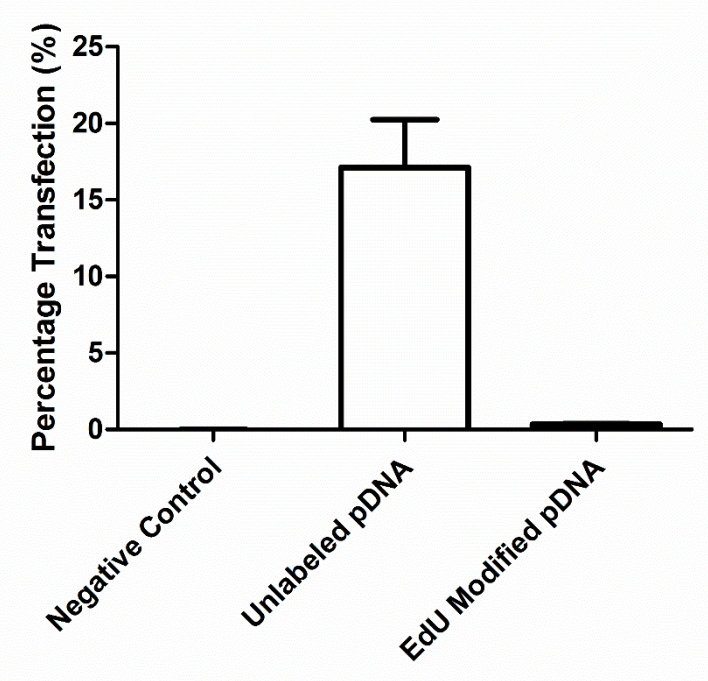

Figure 9 Lipofection of unlabeled and EdU modified pDNA. Negative control = no pDNA. The average depicted is based on one experiment with three repetitions. Error bars are standard deviation on the average.

DISCUSSION

In **Chapter 1**, an overview is presented of the most interesting nucleic acid labeling strategies that are currently available. In **Chapter 3** and **4**, the covalent fluorescent labeling kit of the Mirus Bio company was used for all experiments. Despite the use in those papers, **Chapter 3** clearly indicated that the Mirus labeling kit should be used with care for intracellular processing studies. Therefore, different alternative strategies were compared to the Mirus kit and their potential to be used in cell studies and for microscopy based degradation studies (cf. **Chapter 4**). Cyanine dimeric nucleic acid stains, PNA hybridization, and enzymatic labeling were the alternative fluorescent labeling methods that were considered.

From a user perspective, all labeling methods were relatively easy to perform. For the Mirus labeling kit and the cyanine stains, the commercial kit can be readily used. This is somewhat different for PNA probes and the enzymatic labeling method. Both sequence-specific labeling approaches need to be specifically tailored for the used target DNA. Especially PNA probes need to be designed and ordered to fit a specific sequence. These design steps require knowledge of the exact sequence and of the hybridization mechanism. When a recognition sequence array (36 bp per

probe) is not built into the plasmids on purpose, the chance that significant labeling of a random plasmid will take place is slim. This decreases the interchangeability between different plasmids. The enzymatic labeling approach is in this regard more flexible, since the sequence specificity is limited to a four to six base sequence which is most likely found by chance at least once in every plasmid. The MTase and cofactor, however, need to be synthesized and optimized, which needs an extensive knowledge of protein production. Of course this problem will be alleviated as soon as the optimized labeling kit will be commercially available.

The applications tested within this chapter are analogous to the ones described in **Chapter 2** and performed in **Chapters 3** and **4**. A labeling method therefore should be compatible with the advanced microscopy techniques, while the pDNA's functionality is not disturbed. In Figure 10, a short resume is presented of the obtained results for the transfection efficiency and the diffusion coefficient measured throughout this chapter.

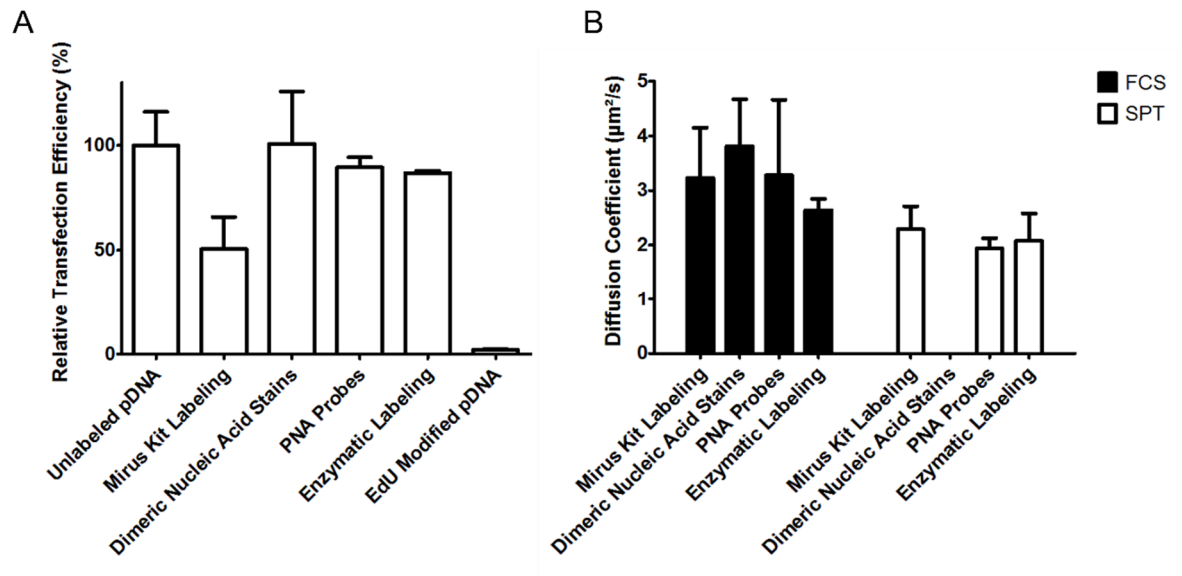

Figure 10 Summary of the (A) transfection efficiencies and (B) the obtained diffusion coefficients with FCS (black bars) and SPT (white bars) for the labeling strategies discussed.

By studying the transfection efficiency, the functionality of the pDNA (e.g., expression of GFP), as well as the ability of the (red or green) labeled pDNA to enter the cells can be measured by flow cytometry. This last parameter is evaluated by looking at the red fluorescent signal. These results are presented visually in Figure 1 B and Figure 7 B, but are due to absence of red fluorescent labels not available for the PNA, PEGylation and EdU transfections. With regard to functionality, TOTO-3

and PNA labeled pDNA do not seem to be affected by the attachment of fluorescent labels (Figure 10 A). In the case of TOTO-3, DNA binding enzymes, responsible for the transcription, may be able to (temporarily) detach the intercalator to interact with the DNA strands. [20] The PNA probes on the other hand, are located outside of the coding region of the plasmids. No interference with the DNA binding enzymes is to be expected. A small difference between the PNA probe labeled pDNA and unlabeled pDNA could be observed. Hydrophobicity of the fluorescent labels probably might come into play at this point, increasing the affinity of the pDNA to "stick" to cellular lipid structures. [21] Enzymatic labeled pDNA showed a lower transfection efficiency than unlabeled pDNA. In Figure 6, the location of each of the nine fluorescent recognition sites is indicated. It can be seen that three of them are within or near the coding region of GFP. This could disturb interactions with transcriptional proteins, which might explain the reduction in transfection efficiency. When instead of fluorescent labels, PEG chains are attached, the percentage of transfection drops further, which is probably because PEG chains induce more steric hindrance and can block protein interactions.

FCS is a valuable microscopy technique to study the mobility of fluorescent labeled molecules. [3] In **Chapter 4**, FCS is used to study the concentration and degradation of pDNA in buffer systems. In this chapter, degradation was looked at in more detail, for the different labeling strategies. First of all, labeled pDNA needs to be characterized, which means that the diffusion coefficient needs to be determined. This was feasible for all labeling strategies and results were more or less comparable, indicating that FCS could be performed (Figure 10 B). Degradation was studied for the TOTO-3 stained pDNA as well as for the PNA probe labeled pDNA. In the case of TOTO-3, the results of the FCS data analysis didn't match the trend that became apparent in the agarose gel. This peak number method for counting the number of intact pDNA molecules has also been used in **Chapter 4**, but it could not retrieve the amount of degradation, while still keeping a high number of detectable peaks (see Suppl. Figure 1). This happens even when all DNA seems to be degraded. This last observation can probably be attributed to the labeling method. The dimeric labels will redistribute over the remaining larger fragments, giving rise to smaller peaks, which are still detectable. In the case of the PNA labeled pDNA, the average diffusion coefficient of the "slow" moving fraction was taken as a measure for

degradation since the pDNA molecules are becoming shorter, and thus more mobile. The results represent the degradation in a sufficient manner, although the standard deviation becomes larger at long degradation times. This is probably due to the influence of single intact DNA molecules. If these, at this point, rare molecules pass through the focal volume a high intensity peak is registered. These high intensities influence the autocorrelation curve and the subsequent fitting, leading to a higher variation between measurements with and without the presence of a large molecule. For an agarose gel, stained with GelRed, these concentrations of molecules are below the limit of detection.

SPT has become an invaluable technique in our laboratory. Mobility has been studied in biofilms [22], in the vitreous of the eye, [23] and in much more applications. [2] Being able to visualize, localize, and track labeled plasmids is a prerequisite for the correct determination of diffusion coefficients and subsequently the size. This proved to be no problem for Mirus kit labeled pDNA, PNA probe labeled pDNA, or enzymatic labeled pDNA. Furthermore, the diffusion coefficients seem to be consistent between the labeling methods (Figure 10 B). PNA labeled pDNA was also used in an experiment which tests if the correct amount of intact pDNA can be retrieved from a mixture of intact and fully degraded pDNA. It was observed that the amount of intact pDNA was underestimated for all samples. In **Chapter 4**, this experiment was performed with Mirus labeled pDNA and in contrast with the results presented in this chapter, percentages of intact pDNA could be retrieved. This might be due to the presence of a strong background signal, in the case of PNA labeled pDNA, caused by the presence of small labeled DNA fragments and free PNA probes. Some intact plasmids may therefore not be recognized by the localization software as particles. In the case of the Mirus labeling, only very fast moving fluorescent linker molecules are present, which probably contribute less to the background fluorescence.

Additionally, two completely different approaches were included with the test of the EdU modification of pDNA and the PEGylation of pDNA via enzymatic labeling. The nonfluorescent labeling approach may potentially be the future in nucleic acid labeling, but in this work, it was seen that the potential to transfect HeLa cells was lost when the modification was implemented. Also the PEGylation of pDNA did not result in the increase in transfection efficiency that was hoped for.

CONCLUSIONS

Three alternative labeling methods were compared to the frequently used Mirus nucleic acid labeling kit since there are issues with this labeling method at higher labeling densities. Furthermore, sequence-specific labeling enables the researcher to adjust the labeling to the needs of the experiment. This could, for example, potentially be of interest for transfections when the coding region can be left untouched. The different alternative approaches and especially the PNA labeling method seem the most promising for further use in the lab, but in applications the results obtained with the Mirus kit labeled plasmids (described in **Chapter 4**) proved to be more accurate. The enzymatic labeling could be the perfect cross between the Mirus kit and the PNA probe labeling, but proprietary plasmids should be designed to combine the advantages of both.

Without much success, less common approaches were tested by PEGylating plasmids and a small venture into a nonfluorescent approach, but they did not deliver the hoped results.

Although all tested labeling methods could be interesting for the use within our research field, the ease of use and the results in advanced microscopy experiments show that the Mirus kit labeling is still the best choice when the labeling density is kept low enough.

REFERENCES

(1) Friedmann, T., and Roblin, R. (1972) Gene Therapy for Human Genetic Disease? *Science 175*, 949-955.

(2) Zagato, E., Forier, K., Martens, T., Neyts, K., Demeester, J., Smedt, S. D., Remaut, K., and Braeckmans, K. (2014) Single-particle tracking for studying nanomaterial dynamics: applications and fundamentals in drug delivery. *Nanomedicine 9*, 913-927.

(3) Schwille, P. (2001) Fluorescence correlation spectroscopy and its potential for intracellular applications. *Cell biochemistry and biophysics 34*, 383-408.

(4) Neto, B., and Lapis, A. (2009) Recent Developments in the Chemistry of Deoxyribonucleic Acid (DNA) Intercalators: Principles, Design, Synthesis, Applications and Trends. *Molecules 14*, 1725.

(5) Nielsen, P., Egholm, M., Berg, R., and Buchardt, O. (1991) Sequence-selective recognition of DNA by strand displacement with a thymine-substituted polyamide. *Science 254*, 1497-1500.

(6) Egholm, M., Buchardt, O., Nielsen, P. E., and Berg, R. H. (1992) Peptide nucleic acids (PNA). Oligonucleotide analogs with an achiral peptide backbone. *Journal of the American Chemical Society 114*, 1895-1897.

(7) Lukinavičius, G., Lapinaitė, A., Urbanavičiūtė, G., Gerasimaitė, R., and Klimašauskas, S. (2012) Engineering the DNA cytosine-5 methyltransferase reaction for sequence-specific labeling of DNA. *Nucleic acids research 40*, 11594-11602.

(8) Pljevaljcic, G., Pignot, M., and Weinhold, E. (2003) Design of a New Fluorescent Cofactor for DNA Methyltransferases and Sequence-Specific Labeling of DNA. *Journal of the American Chemical Society 125*, 3486-3492.

(9) Neely, R. K., Dedecker, P., Hotta, J.-i., Urbanaviciute, G., Klimasauskas, S., and Hofkens, J. (2010) DNA fluorocode: A single molecule, optical map of DNA with nanometre resolution. *Chemical Science 1*, 453-460.

(10) Wei, L., Hu, F., Shen, Y., Chen, Z., Yu, Y., Lin, C.-C., Wang, M. C., and Min, W. (2014) Live-cell imaging of alkyne-tagged small biomolecules by stimulated Raman scattering. *Nature Methods 11*, 410-412.

(11) Vercauteren, D., Piest, M., van der Aa, L. J., Al Soraj, M., Jones, A. T., Engbersen, J. F., De Smedt, S. C., and Braeckmans, K. (2011) Flotillin-dependent endocytosis and a phagocytosis-like mechanism for cellular internalization of disulfide-based poly(amido amine)/DNA polyplexes. *Biomaterials 32*, 3072-3084.

(12) Armitage, B. (2005) Cyanine Dye–DNA Interactions: Intercalation, Groove Binding, and Aggregation, in *DNA Binders and Related Subjects* pp 55-76, Springer Berlin Heidelberg.

(13) Åkerman, B., and Tuite, E. (1996) Single- and Double-Strand Photocleavage of DNA by YO, YOYO and TOTO. *Nucleic acids research 24*, 1080-1090.

(14) Kundukad, B., Yan, J., and Doyle, P. S. (2014) Effect of YOYO-1 on the mechanical properties of DNA. *Soft Matter 10*, 9721-9728.

(15) Japaridze, A., Benke, A., Renevey, S., Benadiba, C., and Dietler, G. (2015) Influence of DNA Binding Dyes on Bare DNA Structure Studied with Atomic Force Microscopy. *Macromolecules 48*, 1860-1865.

(16) Zelphati, O., Liang, X., Hobart, P., and Felgner, P. L. (1999) Gene Chemistry: Functionally and Conformationally Intact Fluorescent Plasmid DNA. *Human Gene Therapy 10*, 15-24.

(17) Jokerst, J. V., Lobovkina, T., Zare, R. N., and Gambhir, S. S. (2011) Nanoparticle PEGylation for imaging and therapy. *Nanomedicine 6*, 715-728.
(18) Freudiger, C. W., Min, W., Saar, B. G., Lu, S., Holtom, G. R., He, C., Tsai, J. C., Kang, J. X., and Xie, X. S. (2008) Label-free biomedical imaging with high sensitivity by stimulated Raman scattering microscopy. *Science 322*, 1857-1861.
(19) Salic, A., and Mitchison, T. J. (2008) A chemical method for fast and sensitive detection of DNA synthesis in vivo. *Proceedings of the National Academy of Sciences 105*, 2415-2420.
(20) Biebricher, A. S., Heller, I., Roijmans, R. F. H., Hoekstra, T. P., Peterman, E. J. G., and Wuite, G. J. L. (2015) The impact of DNA intercalators on DNA and DNA-processing enzymes elucidated through force-dependent binding kinetics. *Nature Communications 6*.
(21) Rombouts, K., Martens, T. F., Zagato, E., Demeester, J., De Smedt, S. C., Braeckmans, K., and Remaut, K. (2014) Effect of Covalent Fluorescence Labeling of Plasmid DNA on Its Intracellular Processing and Transfection with Lipid-Based Carriers. *Molecular Pharmaceutics 11*, 1359-1368.
(22) Forier, K., Messiaen, A.-S., Raemdonck, K., Deschout, H., Rejman, J., De Baets, F., Nelis, H., De Smedt, S. C., Demeester, J., and Coenye, T. (2013) Transport of nanoparticles in cystic fibrosis sputum and bacterial biofilms by single-particle tracking microscopy. *Nanomedicine 8*, 935-949.
(23) Martens, T. F., Vercauteren, D., Forier, K., Deschout, H., Remaut, K., Paesen, R., Ameloot, M., Engbersen, J. F., Demeester, J., and De Smedt, S. C. (2013) Measuring the intravitreal mobility of nanomedicines with single-particle tracking microscopy. *Nanomedicine 8*, 1955-1968.

SUPPLEMENTARY DATA

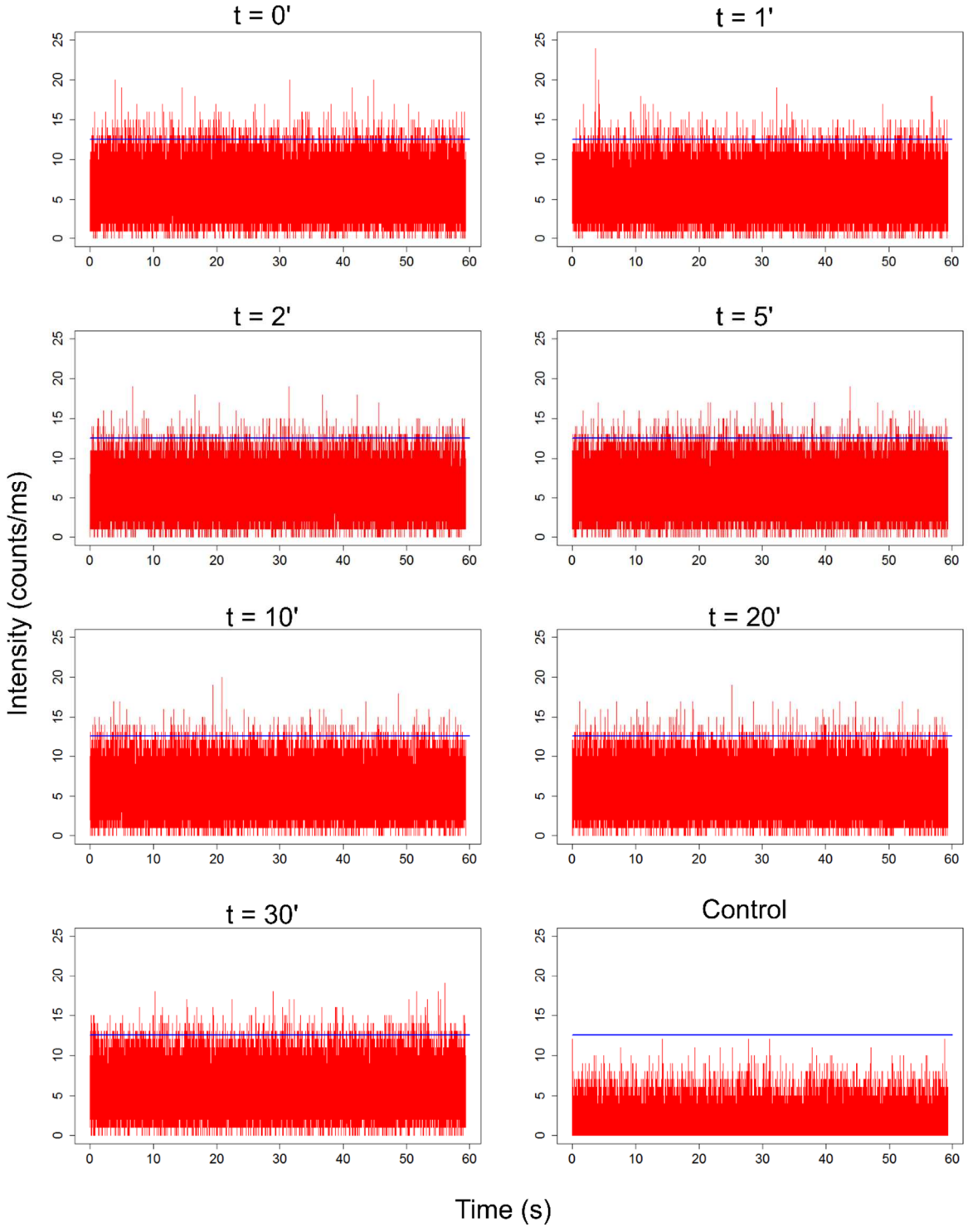

Suppl. Figure 1 Representative time traces for the degradation experiment with TOTO-3 depicted in Figure 2. Binning time = 1000 µs, laser power = 1% ~ 0.0029 mW, threshold at 12.5 counts/ms.

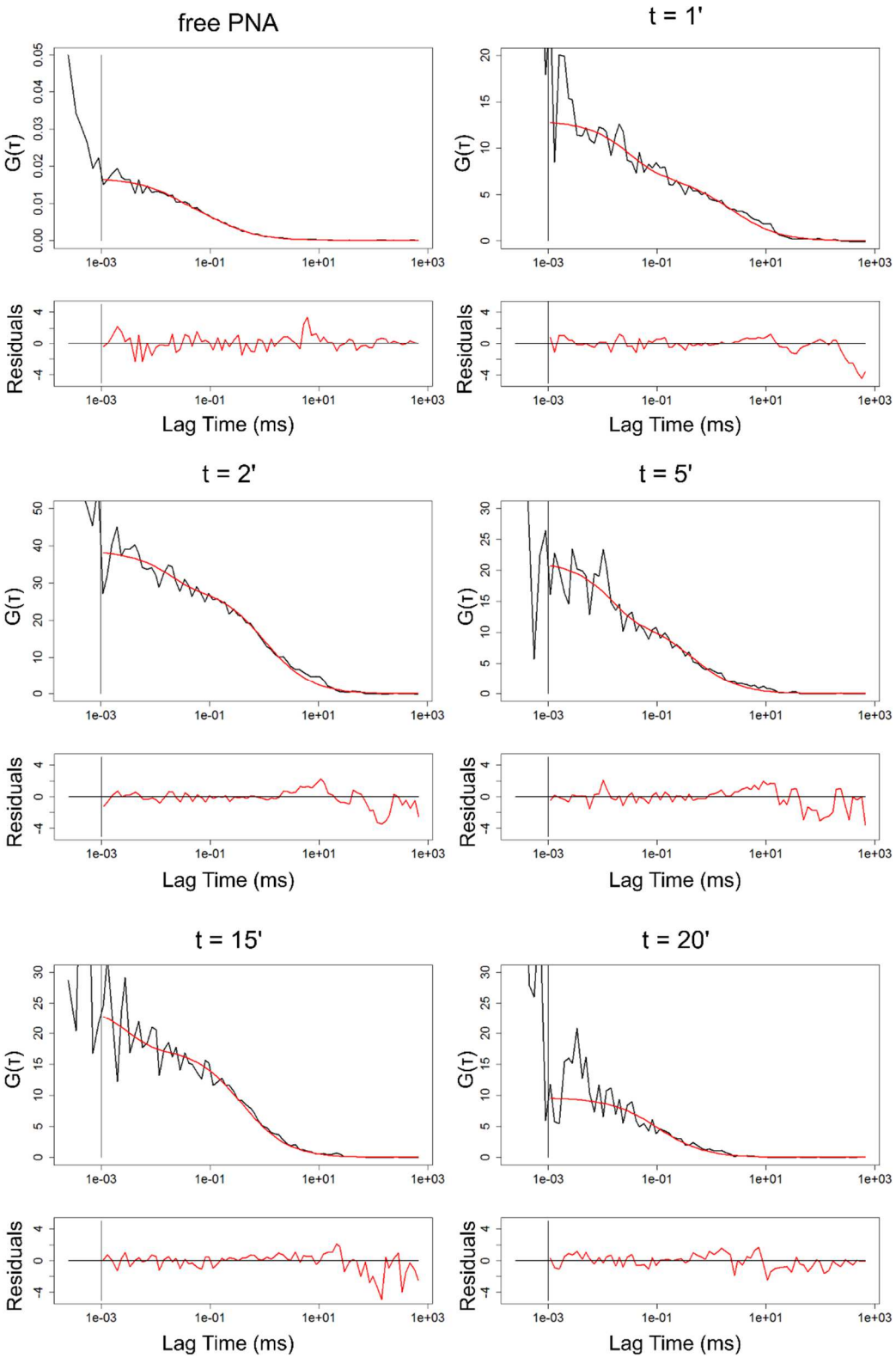

Suppl. Figure 2 Representative autocorrelation curves (black line), fitting curves (red line) and residuals (bottom) in function of the lag time for the different degradation times corresponding with Figure 4. Laser power = 0.5% ~ 0.0578 mW. Fixed values in triplet model fit (see Chapter 2: V_{eff} = 0.55, κ = 9, τ_{D2}= 0.09.

CHAPTER 6 |

Evaluation of Cationic Amphiphilic β-Cyclodextrins for Gene Delivery

K. Rombouts[†], C. F. C. Costa, J.M. García Fernández[‡], K. Remaut[†]

† Laboratory of general biochemistry and physical pharmacy, Faculty of pharmacy, Ghent University, Belgium

‡ Instituto de Investigaciones Químicas, CSIC – Universidad de Sevilla, Spain

This chapter contains unpublished results.

TABLE OF CONTENTS

ABSTRACT

Polycationic amphihilic β cyclodextrins (paCDs) are a versatile family of molecules, which are promising candidates for the delivery of nucleic acids for gene therapy. In this study, three different modified paCDs were investigated as carriers for plasmid DNA (pDNA) as well as messenger RNA (mRNA). Complexation, stability and transfection efficiency were assessed in both serum free and in serum-containing environments. While transfection efficiency of paCDs in serum-free conditions was only slightly lower than for the Lipofectamine-based transfections, the presence of serum completely abolished the expression of the reporter protein for pDNA as well as for mRNA. Our results indicated that for pDNA containing paCDs, cellular uptake was significantly lower in a serum-containing environment. It was hypothesized that the CDplexes need interactions with the cellular cholesterol to result in a successful transfection. Therefore, the most efficient pDNA CDplexes were saturated with cholesterol before they were added to the cells in serum-free conditions. Cellular uptake was significantly decreased, indicating a connection between the uptake mechanism of CDplexes and interactions with cellular membrane cholesterol. Our hypothesis is that also serum proteins block the interactions between CDplexes and the cellular membrane by the formation of a protein corona, leading to a loss of uptake and consequently a loss of transfection. Further optimization of the paCDs is thus required to result in complexes than remain efficient in protein-rich environments such as cell culture medium.

INTRODUCTION

Already four decades ago, the use of nucleic acids (NAs) in gene replacement therapy was proposed as a method to alleviate genetic disease. [1] Gene replacement therapy can be described as the introduction of a healthy gene into a patient to replace the function of a defective gene. This healthy gene is provided by plasmid DNA (pDNA) or mRNA. The lack of a broad range of gene-based pharmaceuticals on the market indicates that no general approach has been found yet to translate the, relatively simple, concept of gene therapy into practice.

Intensive research has been done to increase the efficiency of the transfer of NAs into cells. NAs are degraded by nucleases (see **Chapter 4**), or cleared from the body due to their physical properties (size and charge), which prevent the diffusion through cellular membranes. After reaching the target cells, the NAs still need to reach their intracellular location which is the nucleus for pDNA or the cytoplasm for mRNA. To help NAs with stability, improve their physical properties, and facilitate cellular entry, mechanic and physical methods (e.g. injections, electric field, etc.), recombinant viral vectors, non-viral vectors, and combinations of the above (e.g., ultrasound-mediated gene delivery by microbubbles) were developed. Mechanical and physical methods prove to be interesting for target cells and tissues that are easily accessible. [2, 3] For harder to reach tissues and cells, vector-based approaches could be more promising. To ensure an efficient NA delivery, the vector needs to display the following characteristics: (i) protection of the NAs from enzymatic degradation by systemic nucleases, (ii) avoid being cleared by the innate immune system, (iii) enable the therapeutic NAs to reach the target cells, (iv) induce NA release in the desired cell compartment (e.g., mRNA to the cytoplasm, pDNA to the cell nucleus) and (v) don't induce toxicity, inflammation or mutagenic effects.

The two types of vectors that can be used as gene carrier are viral and non-viral vectors. The use of recombinant viral vectors hijacks the natural ability of viruses to enter the cell and use the cell's machinery to replicate their NA. These properties, that in normal circumstances induce illness, are used to transfect (transient expression of a protein in the cell) or transduce (the introduction of foreign DNA into the host its genomic DNA) cells with a therapeutic gene. This is accomplished by replacing the viral genes, that lead to replication and toxicity by therapeutic genes.

These attenuated viruses are therefore called recombinant viral vectors and are very efficient. Several hundreds of clinical trials have therefore been performed with these type of vectors, [4] but there is one big drawback: safety. [5] The transduction of the therapeutic genes happens in a random manner, but with a preference for actively transcribed genes, which can lead to insertional mutagenesis. This means that the disruption of the host genome will induce uncontrolled cell proliferation. [6] Furthermore, the presence of high concentrations of viral particles, can still induce a strong and even lethal immunogenic response, identical to the reaction on natural occurring viruses, as was observed in clinical trials with adenoviruses. [7, 8] Additionally, the production of these recombinant viral particles proves to be costly and hard to scale-up. [5] Not surprisingly, these vectors have found, and still find, strong opposition when attempts are made to translate them to the clinic.

Under the title of non-viral vectors, a diverse group of synthetic nanocarriers that support the transfection of cells is grouped. Opposed to the viral carriers, the non-viral counterparts, in general, are candidates for large scale production, while having lower toxicity, oncogenicity and immunogenicity. This is achieved by using lipid – or polymer-based particles that allow for a broad range of modifications. These modifications lead to a near endless range of possibilities. [9] However, when the efficiency of NA transfer and transgene expression is compared to their viral counterpart, non-viral carriers cannot compete. Two types of non-viral vectors are mainly used: liposomal NA carriers (lipoplexes) and polymeric NA carriers (polyplexes). As the name indicates, lipoplexes are complexes formed by (a combination of) lipids and NAs. To generate an electrostatic interaction between the negatively charged NAs with the liposome, positively charged (cationic) lipids (e.g., DOTAP is the most widely used cationic lipid [10]) are combined with helper lipids (e.g., cholesterol) in a formulation. During complexation, NAs are adsorbed to the surface or bound between the different phospholipid layers. [11, 12] Polyplexes are another important category of non-viral carriers, and most relevant for this chapter. They are constructed by the complexation of NAs with a cationic polymer. A large amount of possible polymers has been described that show promise in providing good protection of the NA, efficient transfection, and low immunogenicity and toxicity. [13] In this chapter, a specific type of polymers is used, namely cyclodextrins.

Cyclodextrins (CDs) are cyclic (α-1,4)-linked oligosaccharides of α-D-glucopyranose. The number of α-D-glucopyranose units determines the type of CD that is encountered. α-CDs consist of six, β-CDs of seven and γ-CDs of eight α-D-glucopyranose units (Figure 1 A-C). This structure results in molecules that are shaped in a torus-like manner (see Figure 1 D). X-ray experiments revealed that in CDs the primary hydroxyl groups (C6) are located on the small edge of the ring, the secondary hydroxyl groups (C2 and C3) are located on the wide edge of the ring, and the apolar (C3 and C5) hydrogens and ether-like oxygens are at the interior of the molecule. [14] The result is an amphiphilic molecule that has both a hydrophilic cavity at the exteriors and an apolar hydrophobic cavity at the interior (see Figure 1 D). This provides a unique micro-environment that is perfect for the encapsulation and solubilization of hydrophobic molecules in water. [15-17] Besides being used for the encapsulation of small hydrophobic drugs, CDs gained interest in gene delivery. [18-20] Initially, CDs were used as an addition to other gene carriers since β-CDs were seen to lower the cytotoxicity of the gene carriers and increase the cellular entry. [21] Although the evidence on the CD-mediated absorption is still obscure and further study is required, it was hypothesized that cholesterol depletion (by CDs) improves membrane permeability. [17, 22, 23]

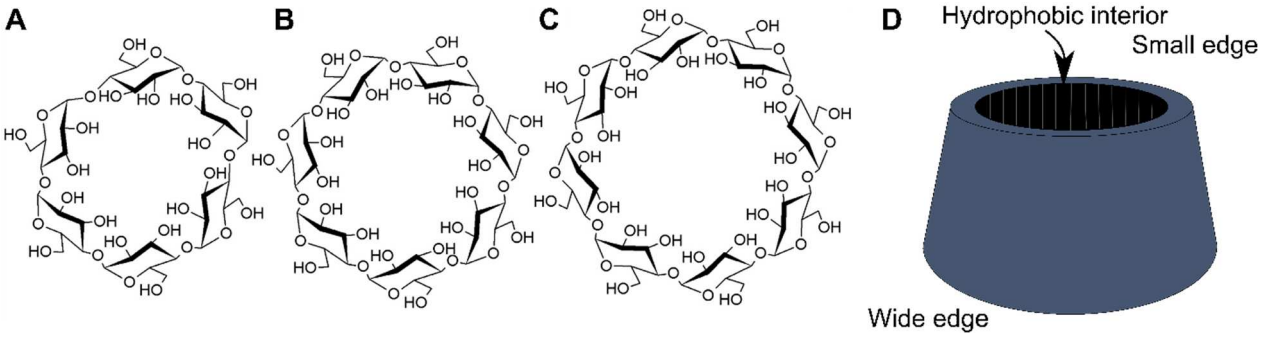

Figure 1 Structure of (A) α-CD, (B) β-CD, and (C) γ–CD. (D) Schematic representation of a CD. Structure adapted from Lai (2014)[17].

It should be noted that the standard, non-modified CD molecules carry no net positive charge and therefore do not complex NAs. Therefore, derivatives were synthesized with the aim to induce the potential of NA binding. Polycationic amphiphilic CDs (paCDs) gained the most interest. By the adjustment of the ratio and type of cationic and hydrophobic elements, the size, charge, and affinity for NAs can be controlled. This allowed for the synthesis of a large group of possible paCD-based

gene carriers. Three of these derivatives were evaluated in this chapter, namely ADM-65, ADM-70 and IP202-libre. Their structure is given in Figure 2 C-E and consists of 14 hexanoyl chains at the secondary hydroxyl face (wide edge) and respectively 21, 14 and 21 protonable amino groups at the primary face (small edge). This conformation is represented schematically in Figure 2 A. ADM-65 and IP202-libre have polycationic side chains at their small edge with a virtually identical composition. The main difference is that the side chain of ADM-65 is branched, while that of IP202-libre is linear. ADM-70 on the other hand eliminates one amino group in each side chain, compared to ADM-65, resulting in a shorter branched polycationic side chain. These paCDs can be complexed with negatively charged NAs and will be called CDplexes from now on. In their most simple form, these CDplexes are organized in a bilayer structure with the lipophilic tails facing each other and the positive charges facing the aqueous environment and cavity as schematically depicted in Figure 2 B for a pDNA - CDplex. One of the hypotheses is that these CDplexes can interact with the negatively charged proteoglycans on the cell surface. From there on, endocytosis would be the main pathway of cellular uptake. [24-27]. Díaz-Moscoso et al. (2010)[28] determined via inhibition experiments that clathrin-dependent and clathrin-independent cellular internalization were both mechanisms by which CDplexes are taken up by Vero cells. When cholesterol was depleted from the cellular membranes by the addition of a methyl β-CD, a drop in transfection efficiency was observed. These results, combined with the reports that indicate a connection between the membrane permeability and the interactions between CDs and cellular cholesterol, indicate that interactions of the paCDs with cholesterol highly likely are crucial for the efficient delivery of NAs. These interactions would likely involve the interaction of cellular cholesterol with the hydrophobic interior.

In this chapter, the use of the three paβ-CDs, as delivery vehicles for pDNA and mRNA, was evaluated in buffer, optimized transfection medium, and in serum-containing cell culture medium. The CDplexes were characterized in each medium, as well as evaluated in cell experiments. In these cell experiments, the transfection efficiency, cytotoxicity, and cellular uptake were evaluated. Additionally, we looked deeper into the necessity of the CDplexes to interact with cellular cholesterol to succeed in an efficient cellular uptake.

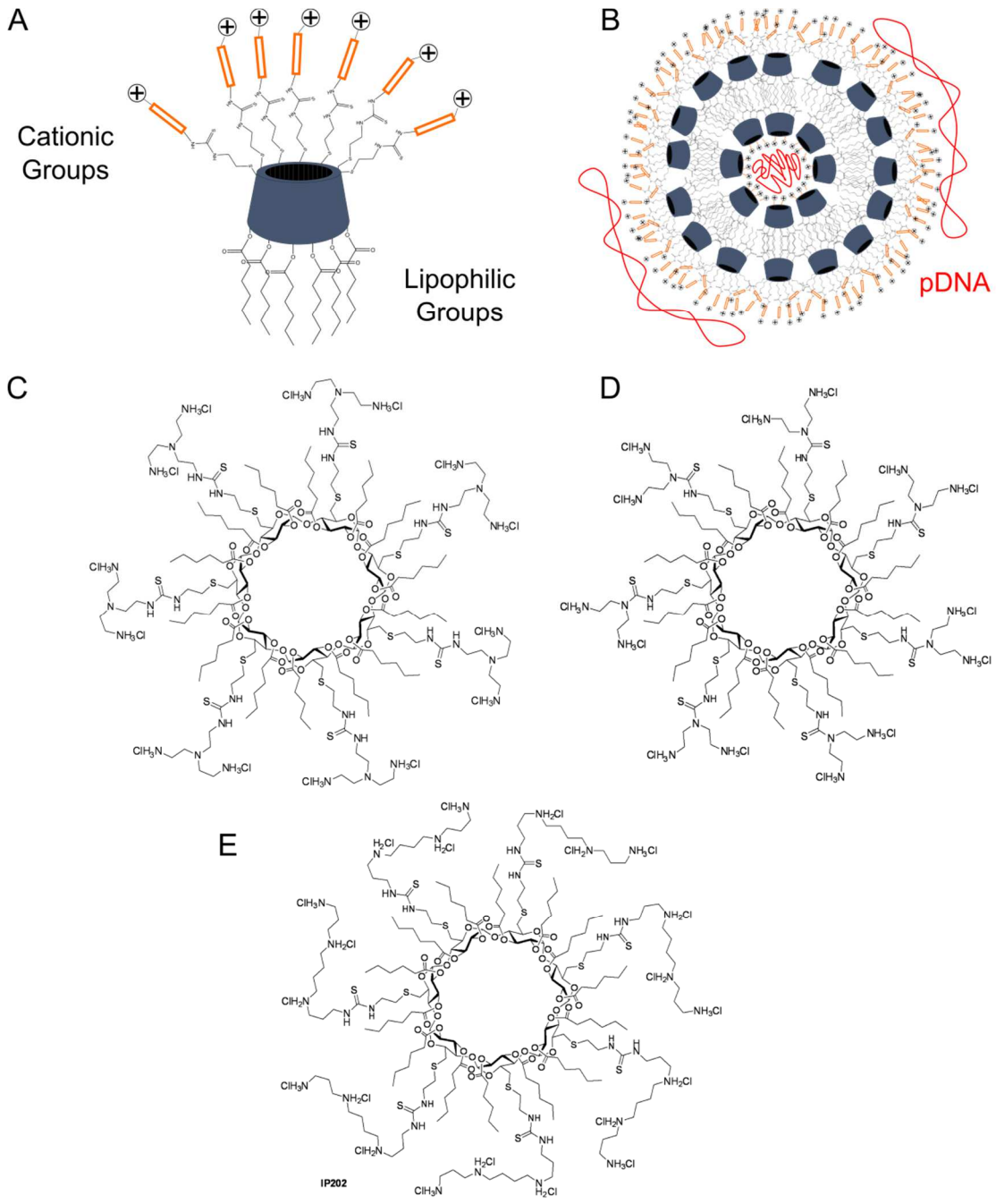

Figure 2 Schematic presentation and structures of the polycationic amphiphilic β-CDs and CDplex used in this chapter. (A) Schematic presentation of the CDs with hydrophobic lipid tails at the wide edge and polycationic side chains at the smaller edge. (B) Schematic presentation of the possible organization of a pDNA (in red) - CDplex. (C) Structure of ADM-65. (D) Structure of ADM-70. (E) Structure of IP202-libre. Encircled + signs stand for positively charged groups. Orange rectangles indicate spacer elements.

MATERIALS AND METHODS

Cell Culture

A HeLa cell line was maintained at 37 °C (5% CO_2) in Dulbecco's modified Eagle's medium supplemented with growth factor F12 (1:1 DMEM/F12), 10% heat inactivated fetal bovine serum, 2 mM L-glutamine, and 100 µg/mL penicillin/streptomycin. All cell culture reagents were purchased from GibcoBRL (Merelbeke, Belgium).

pDNA and mRNA

gWIZ-GFP plasmids were purchased from Genlantis (San Diego, CA, U.S.A.). The plasmids, expressing green fluorescent protein (GFP), were amplified in *Escherichia coli* and isolated from a bacteria suspension using a Plasmid Gigaprep Kit (Qiagen, Thermo Fisher Scientific, Merelbeke, Belgium). Plasmid concentration measurements at a wavelength of 260 nm were performed on a NanoDrop 2000c (Thermo Fisher Scientific, Rockford, IL, USA) . Purity was assessed via the A260/A280 and a 1 µg/µl stock solution was prepared in 20 mM HEPES buffer (pH 7.2) and stored at −20 °C.

pDNA and mRNA were labeled with Cy5 using the Label IT® nucleic acid labeling kit (Mirus Bio LLC, Madison, WI, U.S.A.) at a NA to Cy5 Label IT reagent ratio of 10:1 (w:v). Free fluorescent reagent was removed with ethanol precipitation and labeled NAs were resuspended in 20 mM HEPES buffer (pH 7.2). NA concentration, purity and labeling density were checked respectively at wavelengths 260 nm, 260 nm/280 nm and 647 nm.

Nucleic Acid Complexation

β-cyclodextrins, named ADM-65, ADM-70 and IP202-libre were synthesized at the laboratory of Professor J.M. García Fernández. The freeze dried products were resuspended in a Dimethyl Sulfoxide (Sigma Aldrich, Diegem, Belgium):ddH_2O (1:3 v:v) mixture resulting in a concentration of positive charges of 300 mM. A working solution (3 mM positive charges) is obtained through a 1:100 dilution of the stock solution with ddH_2O. CDplexes were prepared by mixing the CDs with pDNA or mRNA at the desired concentration to obtain Nitrogen/Phosphate (N/P) ratios of 4, 6 and 8.

Agarose Gel Electrophoresis

1% agarose gel was prepared in 1× TBE buffer (90 mM Tris base/90 mM borate/2 mM EDTA) and prestained with the GelRed stain (Biotum, Hayward, CA, U.S.A.). Samples were mixed with gel loading buffer II (Ambion, Merelbeke, Belgium) and loaded onto the gel which was ran for 45' at 100 V and visualized under UV.

Physical Characterization of Complexes

Hydrodynamic diameter and zeta potential were determined using dynamic light scattering (DLS). Complexes were prepared as described above, diluted in 20 mM HEPES buffer (pH 7.2), optiMEM, or cell culture medium and measured in triplicate on a NanoZS Zetasizer (Malvern Instruments, Hoeilaart, Belgium).

Cellular Uptake and Transfection Efficiency

HeLa cells were plated in 24 well plates at 50,000 cells/well and were allowed to grow overnight. For uptake experiments, complexes were prepared with Cy5-pDNA or Cy5-mRNA in 20 mM HEPES buffer (pH 7.2), as described above, and diluted in optiMEM or regular growth medium. The complexes were added to the cells at a concentration of 500 ng pDNA/50,000 cells and the plates were incubated at 37°C for 4 hours. As a negative control, plates were pre-incubated on ice for 1 hour and incubated with the particles on ice for 4 hours. To obtain information on the uptake, cells were washed and trypsinized after the 4 hours incubation. Cells were collected from the neutralized cell suspension by centrifugation and resuspended in flow buffer (1% bovine serum albumine (Sigma Aldrich, Bornem, Belgium) in PBS Ca^{2+}/Mg^{2+} -/-). Red fluorescence from the pDNA or mRNA inside the cells was measured using flow cytometry (FACSCalibur™, BD Biosciences Benelux N.V., Erembodegem, Belgium). For transfection experiments, CDplexes were prepared with non-labeled pDNA or mRNA. Cells were incubated with the CDplexes for 4 hours, after which the cells were washed to remove free CDplexes, supplied with fresh growth medium, and allowed to grow in the incubator. 24 hours after the transfection, the cells were prepared for flow cytometry, as described above. Green fluorescence from GFP expression inside the cell was measured with flow cytometry and used as a measure for a successful transfection. All samples were prepared and measured in triplicate.

Toxicity

Cytotoxicity of the CDplexes was evaluated with the MTT assay. HeLa cells were plated in 24 well plates at 50,000 cells per well. Identical to the transfection protocol, complexes, prepared as previously described, were added to the cells in optiMEM or growth medium and incubated for 4 hours at 37 °C. After removal of the polyplexes, fresh growth medium was added to the cells. 24 h after addition of the complexes, MTT reagent was added to the medium for 4 hours at 37 °C. Afterwards, cells were washed and lysed with cell lysis buffer (0.04 N HCl and 1% Triton-X in isopropanol) for 1 hour on a shaker. Then, absorbance at 590 nm and 690 nm was measured on a plate spectrophotometer (PerkinElmer 2104 EnVision). The absorbance at 590 nm relates to the metabolic activity, while the absorbance at 690 nm is used as a baseline reference.

Pre-Incubation with Cholesterol

The effect of pre-incubation of the pDNA – CDplexes with free cholesterol on uptake and transfection was tested. Cholesterol (Sigma Aldrich, Bornem, Belgium) was dissolved in absolute ethanol to a concentration of 0.1 M. Cholesterol was added to the CDplexes at a mol:mol ratio of 20:1 (CD:Chol).[29] After 15' of pre-incubation, the Chol:Cy5-pDNA:CDplexes were incubated in optiMEM with HeLa cells plated in 24 well plates at 50,000 cells/well. After 4 hours, cells were washed and harvested. All measurements were conducted on the FACS, as described above for cellular uptake and transfection.

RESULTS

Complexation

Complexation properties were checked on agarose gel for CDplexes with N/P 4, 6, and 8 in HEPES buffer, optiMEM and full cell growth medium. Free NAs will be mobile on the gel and migrate like the free NA control, while complexes will be stationary in the loading well. For pDNA (Figure 3) in HEPES buffer, complexation is complete for N/P ratios 6 and 8 for all CDs. IP202-libre complexes pDNA completely at all N/P ratios. When CDplexes are exposed to the serum-free medium optiMEM, complete complexation shifts to higher N/P ratio's when compared to the HEPES buffer conditions. In full cell culture medium, again, IP202-libre shows the best complexation efficiency, with no free pDNA detectable in the gel at N/P ratios 6 and

8. For ADM-70, a fraction of free pDNA remains visible on the gel, demonstrating ADM-70 is not able to fully complex all pDNA at the studied N/P ratios.

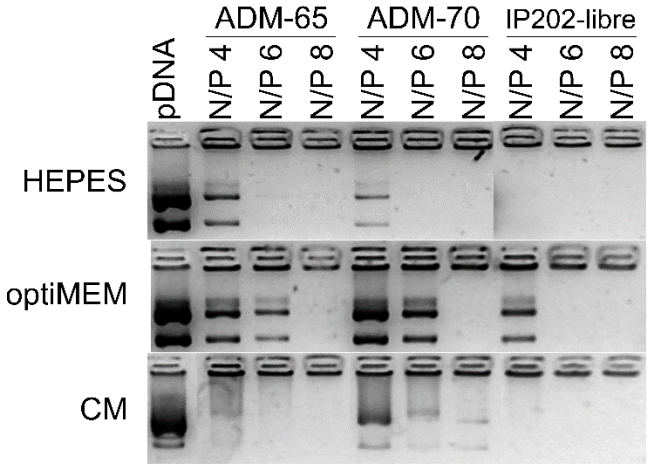

Figure 3 Complexation of pDNA by ADM-65, ADM-70 and IP202-libre. pDNA: free pDNA control. N/P: Nitrogen/Phosphate ratio. HEPES: 20 mM HEPES buffer (pH 7.2). CM: Cell Culture Medium. Gel is representative for the results seen in three independent experiments and was edited to delete empty lanes.

For mRNA (Figure 4), the complexation efficiency seems less dependent on the biological environment the complexes are in. All studied CDs complex mRNA completely at all studied N/P ratios and all incubation fluids.

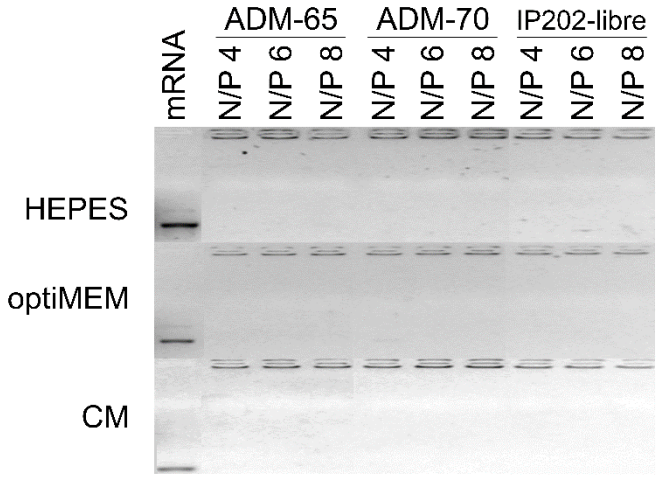

Figure 4 Complexation of mRNA by ADM-65, ADM-70 and IP202-libre. mRNA: free mRNA control. N/P: Nitrogen/Phosphate ratio. HEPES: 20 mM HEPES buffer (pH 7.2). CM: Cell Medium. Gel is representative for the results seen in three independent experiments and was edited to delete empty lanes.

Physical Characterization: Size and Charge

After the NA complexing potential of the different CDs was established on agarose gel, the size and zeta potential were checked with DLS for both pDNA and mRNA complexes. The change in size and zeta potential of a particle over the different N/P ratios and in the three different media is a good representation of the stability of a complex. A positive zeta potential is essential to avoid electrostatic repulsion by the negative charged cell membrane, while a small size is believed to enhance cellular uptake. In Table 1, the average hydrodynamic diameter and the zeta-potential of the CDplexes are shown in HEPES buffer, optiMEM and cell culture medium for different N/P ratios.

In general, the zeta-potential dropped from positive (HEPES buffer) to neutral (optiMEM) and negative values (culture medium) due the presence of a higher amount of ions in the optiMEM and cell medium compared to the HEPES buffer and the presence of serum proteins in culture medium which all interact with the surface of the particles. This was represented in the size of the CDplexes which formed large aggregates for the more neutral absolute values of the zeta potential as seen in optiMEM. These larger sizes were also observed for the N/P ratios of 4 of both pDNA and mRNA with ADM 65 and ADM 70 in HEPES buffer, which indicated incomplete complexation as seen on the agarose gel (Figure 3). In cell culture medium the size of all particles dropped to very small sizes, due to interactions with the serum proteins. Based on these results, IP202-libre with both pDNA and mRNA seemed to be the most stable in all three media with a decrease in size when the N/P ratio went up.

Table 1 Size ($d_{hydr.}$) and zeta-potential (ξ) for all CDplexes complexed with pDNA and mRNA in HEPES buffer, optiMEM and cell culture medium. All values are averages of three independent experiments with three repetitions and errors are the standard deviation on the average.

		HEPES buffer		optiMEM		Cell Culture Medium	
Carrier	**N/P**	$d_{hydr.}$ (nm)	ξ (mV)	$d_{hydr.}$ (nm)	ξ (mV)	$d_{hydr.}$ (nm)	ξ (mV)
pDNA							
ADM-65	4	565 ± 744	35 ± 1	1706 ± 110	-20 ± 2	68 ± 4	-12 ± 1
	6	147 ± 30	38 ± 3	1829 ± 11	-4 ± 1	68 ± 1	-10 ± 1
	8	152 ± 23	35 ± 1	2135 ± 50	6 ± 1	78 ± 1	-10 ± 1
ADM-70	4	1167 ± 1483	34 ± 1	676 ± 28	-30 ± 1	98 ± 28	-14 ± 1
	6	144 ± 21	40 ± 1	1473 ± 62	-23 ± 1	91 ± 17	-14 ± 1
	8	137 ± 14	42 ± 1	2128 ± 28	-7 ± 2	53 ± 14	-14 ± 1
IP202-libre	4	156 ± 20	35 ± 3	340 ± 17	12 ± 1	88 ± 12	-10 ± 1
	6	154 ± 24	35 ± 2	1205 ± 57	10 ± 1	129 ± 25	-9 ± 1
	8	128 ± 30	34 ± 3	469 ± 14	14 ± 1	134 ± 15	-8 ± 1
mRNA							
ADM-65	4	1586 ± 218	-2 ± 1	2095 ± 548	-8 ± 1	25 ± 1	-10 ± 2
	6	292 ± 9	17 ± 1	1079 ± 73	4 ± 1	22 ± 1	-8 ± 1
	8	141 ± 1	32 ± 4	1412 ± 23	15 ± 2	22 ± 1	-7 ± 1
ADM-70	4	1054 ± 107	14 ± 1	1976 ± 107	-25 ± 2	189 ± 70	-12 ± 1
	6	174 ± 2	34 ± 2	1529 ± 338	-8 ± 1	425 ± 120	-11 ± 1
	8	162 ± 3	34 ± 1	2050 ± 408	-5 ± 1	892 ± 394	-13 ± 1
IP202-libre	4	131 ± 1	21 ± 1	145 ± 1	16 ± 1	28 ± 1	-10 ± 1
	6	128 ± 7	13 ± 2	116 ± 1	16 ± 1	27 ± 1	-11 ± 1
	8	109 ± 24	16 ± 2	114 ± 1	16 ± 1	34 ± 1	-9 ± 1

.

Transfection Efficiency

GFP expressing pDNA and mRNA were complexed with CDs at N/P ratios 4, 6, and 8 and incubated on HeLa cells. Flow cytometry was used to measure the transfection efficiency by determining the percentage of cells that express GFP. A cell was deemed positive for green fluorescence when the signal exceeded a threshold, which was determined by the negative control. The commercially available Lipofectamine 2000 was used as a positive control. Transfections were carried out in optiMEM, which is a protein-free transfection medium, while cell culture medium containing serum proteins was used as the transfection medium which is more representative for the *in vivo* situation. In Figure 5 A, the transfection with pDNA in optiMEM is depicted together with the mean fluorescence intensity (MFI) of green fluorescence from GFP per cell. It can be seen that the transfection efficiency increases with increasing N/P ratio's for each type of cyclodextrin. Percentages of transfections with ADM-70 show the highest level of GFP positive cells, but remain lower than those seen with the commercially available lipid-based Lipofectamine. The ADM-65 CDplexes and IP202-libre N/P 4 and N/P 6 reach very low efficiencies. IP202-libre N/P 8 on the other hand is as efficient as the ADM-70 CDplexes. Also, the trend for the MFIs over the different CDplexes seemed to follow the transfection efficiency closely. When the transfections are carried out in serum-containing cell culture medium, transfections drop for all samples to nearly 0%. ADM-70 at N/P 8 is the only sample that could still transfect a small percentage of cells, but the MFI suggests this is also very limited (Figure 5 B). The protein rich conditions in cell culture medium thus clearly interfere with the potential of the CDs to transfect the HeLa cells.

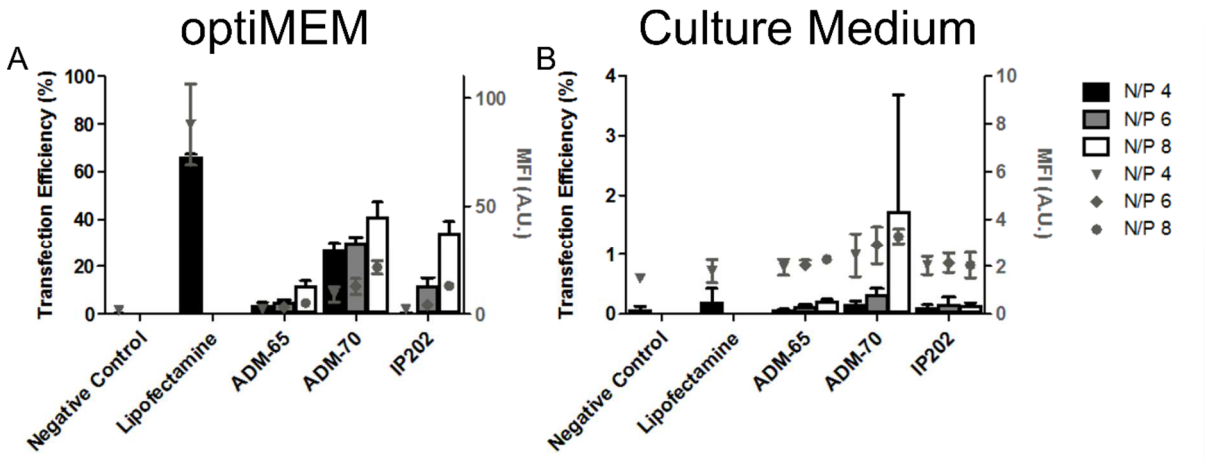

Figure 5 Percentages GFP positive cells after transfection with pDNA-Lipofectamine and pDNA-CDplexes and mean fluorescence intensity (MFI) of GFP fluorescence. Averages obtained from three independent experiments with three repetitions. Error bars depict the standard deviation on the average. (A) Transfections performed in optiMEM, (B) Transfections performed in full cell culture medium. N/P: Nitrogen/Phosphate ratio. Black bars: N/P 4, grey bars: N/P 6, white bars: N/P 8. ▼: N/P 4, ♦: N/P 6, ●: N/P 8.

mRNA transfections are depicted in Figure 6. Also here, transfection efficiency increases with increasing N/P ratio's. In optiMEM (Figure 6 A), ADM-70 again reaches the highest level of GFP positive cells, while ADM-65 and IP202-libre perform less. MFI values again follow this trend closely. When compared to transfections with pDNA, however, it is clear that all CDs containing mRNA reach a higher percentage of GFP positive cells with a higher MFI per cell. This is most likely attributed to the fact that, unlike pDNA, mRNA does not have to cross the nuclear membrane to result in GFP expression. In serum-containing cell culture medium, however, all transfection values again drop to less than 1%, confirming the negative influence of the protein-rich culture medium on the transfection efficiency of the CD complexes.

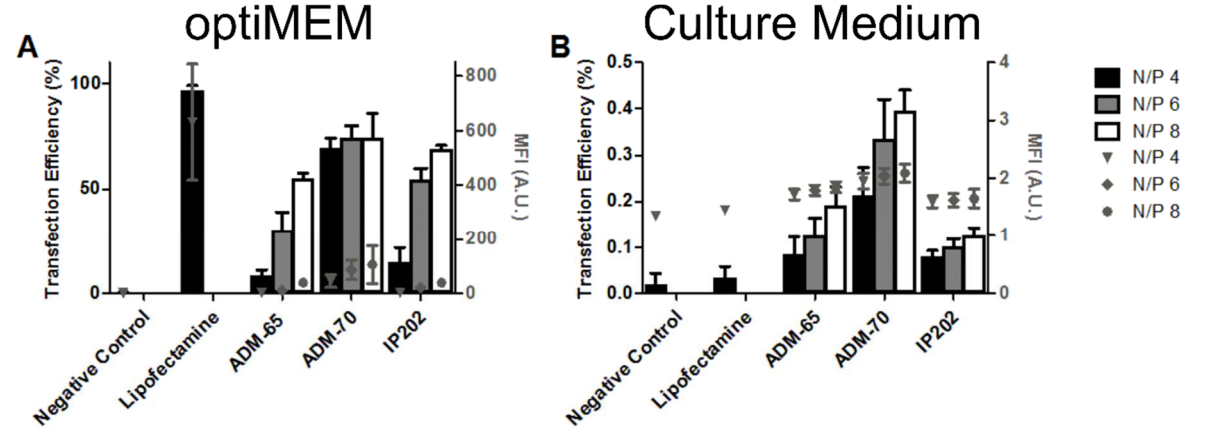

Figure 6 Percentages GFP positive cells after transfection with mRNA-Lipofectamine and mRNA-CDplexes and mean fluorescence intensity (MFI) of GFP fluorescence. Averages obtained from three independent experiments with three repetitions. Error bars depict the standard deviation on the average. (A) Transfections performed in optiMEM. (B) Transfections performed in full cell culture medium. N/P: Nitrogen:Phosphate ratio. Black bars: N/P 4, grey bars: N/P 6, white bars: N/P 8. ▼: N/P 4, ♦: N/P 6, ●: N/P 8.

Toxicity

Toxicity of the CDplexes on the HeLa cells was assessed via an MTT assay. Viability of the cells 24 hours after addition of the pDNA-CDplexes is depicted in Figure 7 A. In general, toxicity of the CDplexes increases with higher N/P ratios, with ADM-70 being the most toxic one. In fact ADM-70 pDNA complexes were statistically significantly more toxic than the Lipofectamine-based pDNA complexes, which were used as positive control ($p < 0.05$). Also for mRNA-CDplexes (Figure 7 B) this trend can be observed. Toxicity of all samples was statistically not different from that of Lipofectamine-based mRNA complexes, except for the mRNA - ADM-70 complex at N/P 8, which was significantly ($p < 0.05$) more toxic than the Lipofectamine complexes, and the mRNA - IP202-libre complex at N/P 4, which was significant less toxic than Lipofectamine complexes ($p < 0.05$).

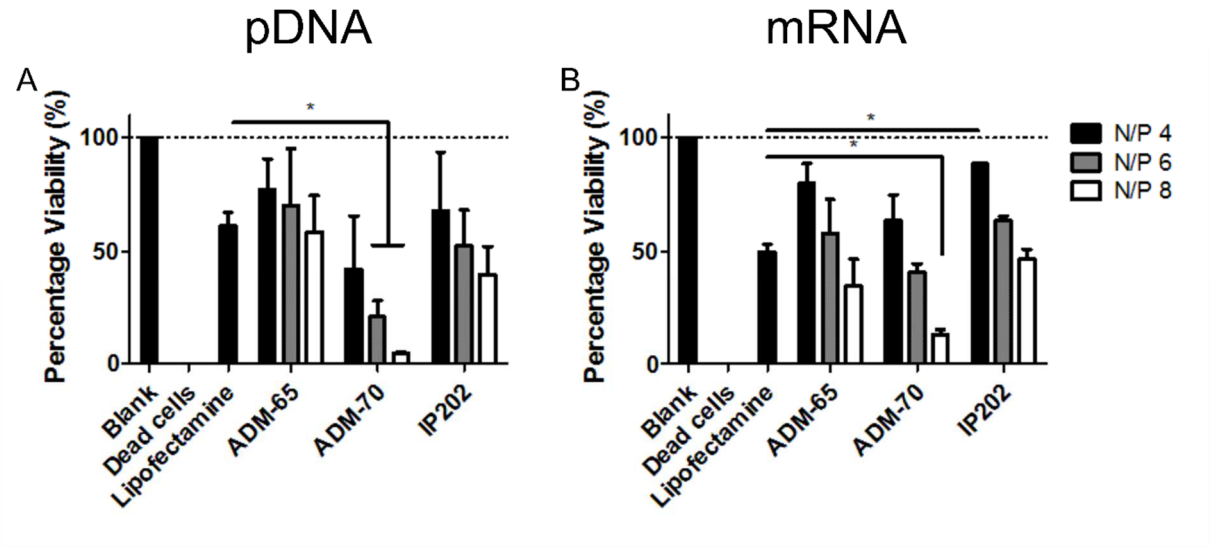

Figure 7 MTT assay for (A) pDNA-CDplexes and (B) mRNA-CDplexes in optiMEM. Blank were non-treated cells. Dead cells were treated with ethanol. *: $p < 0.05$. Averages in each graph obtained from three independent experiments with three repetitions. Error bars depict standard deviation on this average.

Cellular Uptake

The transfection efficiency of the CDplexes clearly dropped whenever the transfections were carried out in serum-containing cell culture medium. Therefore, we were interested to know whether a difference in cellular uptake of the CDplexes in optiMEM, when compared to cell culture medium, could present an explanation for this observation. To determine the cellular uptake of CDplexes, complexes were prepared containing red fluorescent pDNA and the amount of red fluorescence inside the cell was determined using flow cytometry. [30] Figure 8 demonstrates that in optiMEM, all complexes are taken up in the cells, with ADM70 N/P 4 showing the highest amount of red fluorescence per cell (black bars). In cell culture medium, however, all CDplexes except for ADM-70 N/P 4, show a lower value for the red fluorescence per cell, indicating cellular uptake has indeed decreased (white bars). Most likely, the proteins in the cell culture medium interfere with the interaction of the CDplexes with the cell membrane, thereby limiting their cellular uptake. The fact that ADM70 N/P 4 is most efficiently taken up in the cells could potentially result from the formation of larger complexes, which sediment onto the cell surface. The higher uptake, however, did not result in good transfection of the ADM70 complexes at N/P 4, suggesting there is also no direct correlation between the amount of red fluorescence detected in the cells and the obtained GFP expression efficiency.

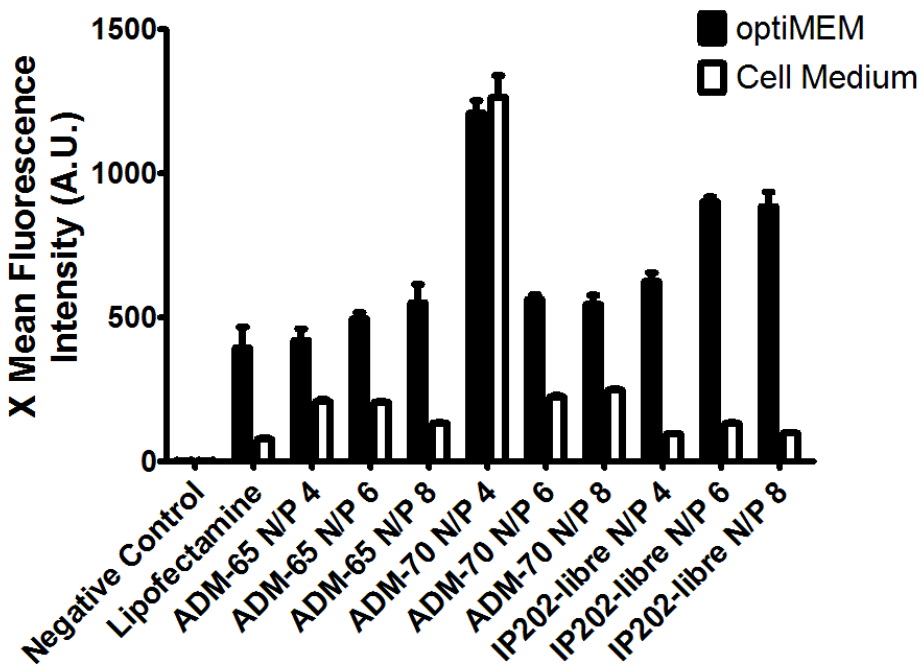

Figure 8 Cellular uptake of pDNA complexes determined by the quantification of red fluorescence inside the cell in function of the used CDplexes after 4 hours of incubation. Negative control was optiMEM or cell medium. Averages obtained from three independent experiments with three repetitions. Error bars depict the standard deviation on the average.

Pre-incubation with Cholesterol

It has been hypothesized that the extraction of cholesterol from the cell membrane, induced by the specific CD structure, is essential for membrane permeability and thus cellular entry and transfection potential of the CDplexes. A possible explanation for the lower transfection efficiency of the CDplexes in cell culture medium could be that the presence of serum proteins blocks this cholesterol depletion from the cell membrane. To mimic the effect of the cell culture proteins, the CDplexes were saturated with free cholesterol by pre-incubation, to prevent the extraction of cellular cholesterol from the cell membrane and to assess the effect on the cellular uptake of the CDplexes.

Figure 9 shows the uptake of ADM-70 CDplexes at N/P 8 in optiMEM, cell culture medium or after pre-incubation of the CDplexes with cholesterol. Uptake was measured by determination of the red fluorescence intensity inside cells, as an indication for the amount of Cy5-pDNA inside each cell. Again, it can be seen that less particles were taken up in the cells when the CDplexes were administered in cell culture medium, when compared to optiMEM ($p < 0.05$). Also, pre-incubation of the

CDplexes with cholesterol resulted in a decrease in cellular uptake, similar as to what was seen for the incubation of complexes in the serum proteins containing cell culture medium. Therefore, it seems that interfering with the potential of the CDplexes to deplete cholesterol from the cellular membrane, either by incubating in cell culture medium or by pre-incubation with cholesterol, indeed results in less efficient uptake of the CDplexes.

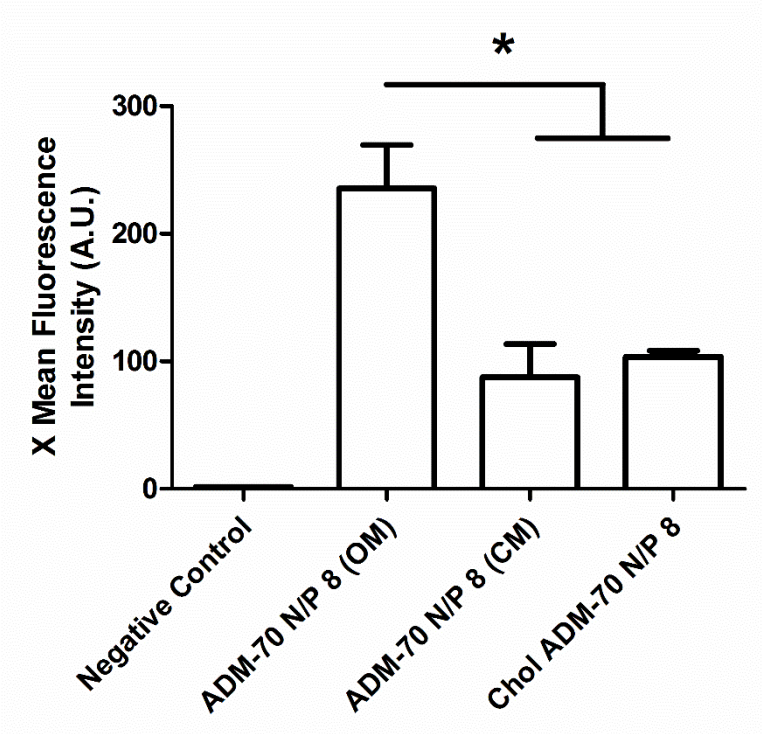

Figure 9 Cellular uptake of pDNA - ADM-70 complexes at N/P ratio 8 in optiMEM (OM), cell medium (CM) or in optiMEM after pre-incubation of the CDplexes with cholesterol (chol) in HeLa cells. Negative control is optiMEM alone. *: $p < 0.05$. Averages obtained from one experiment with three repetitions. Error bars depict the standard deviation on the average.

DISCUSSION

Three different polycationic amphiphilic β-cyclodextrins: ADM-65, ADM-70 and IP202-libre (see Figure 2 B-D), were characterized and evaluated as non-viral carrier for NAs in gene therapy. Several reports already showed that paCDs are a potential carrier for the cellular delivery of NAs. [27, 28] A potent NA carrier should form stable complexes with the NAs and transfect cells in an efficient way, especially in protein-rich media, which more closely resemble the *in vivo* situation. The stability of the CDplexes is determined using three parameters: complexation, size, and zeta potential.

In HEPES buffer, the stability and complexation behavior of the pDNA and mRNA CDplexes showed stable complexes (Figure 3, Figure 4, and Table 1), starting from N/P ratio 6. N/P ratio 4 mostly gave rise to large particles, indicating incomplete complexation and aggregation. Generally, the charge of the CDplexes became more neutral to negatively charged when incubating them in optiMEM or cell culture medium. In optiMEM, CDplexes aggregated to larger particles, except for IP202-libre-mRNA. In cell culture medium, most particles became smaller than 100 nm, a size that is considered interesting for cellular internalization. [31] IP202-libre complexes seemed to be most stable, when complexation, size and zeta potential were considered, for both pDNA and mRNA (Figure 3, Figure 4, and Table 1), but this stability was not represented in the transfection efficiency of the CDplexes. All CDplexes become more efficient with increasing N/P ratio, but both the pDNA and mRNA ADM-70 CDplexes transfected HeLa cells the best, although the efficiency remained lower than that of the Lipofectamine-based complexes (Figure 5 A and Figure 6 A). Unfortunately, these ADM-70 CDplexes also induced the highest cytotoxicity (Figure 7). For mRNA, the transfection efficiencies in optiMEM were higher than those of pDNA, most likely because mRNA has to reach the cytoplasm to be translated, while pDNA needs to overcome the extra barrier of the nuclear membrane to be transcribed into mRNA.

In a serum protein-containing environment, no transfection was seen for both pDNA and mRNA CDplexes. Only pDNA complexed with ADM-70 at N/P 8 had more than 1% transfection, which is still very low. Zeta potentials for both pDNA and mRNA CDplexes were slightly negative, which is known to have a negative influence on cellular internalization. This change was most likely induced by the binding of negatively charged serum proteins to the positively charged surface of the CDplexes. [30, 32] At low absolute values for the zeta potential, electrostatic repulsion is low, leading to aggregation. Nonetheless, a big decrease in size was observed for all CDplexes in culture medium (Table 1). This indicates that very small particles were formed, stabilized by a protein corona in the protein-rich culture medium. Alternatively, large aggregates could sediment in the DLS cuvette, preventing their detection during the size measurements and biasing the results toward smaller particles. Taken together, size and zeta potential measurements alone do not explain

the observed differences in transfection efficiency between the CDplexes and in the different cell culture media.

A prerequisite for good transfection efficiency is the uptake of the CDplexes in the cells. Internalization of Cy5 - pDNA CDplexes, confirmed a decrease in cellular uptake for all CDplexes in cell culture medium with the exception of ADM-70 at N/P 4 (Figure 8). The high uptake values for ADM-70 at N/P 4 in both optiMEM and cell culture medium are puzzling since both complexation efficiency, size and zeta potential and transfection efficiency of these CDplexes is not optimal. Why complexes that are taken up in a good way do not lead to transfection efficiency is not clear. In general, we can conclude that cellular uptake is clearly limited in the presence of serum proteins, but that the amount of internalized CDplexes cannot be directly correlated to transfection efficiency, since the CDplexes with the highest transfection (ADM70 N/P 8), did not have a higher uptake compared to the other CDplexes.

To explain the drop in cellular uptake in the presence of culture medium, an exploratory experiment was performed with the pDNA - CDplex with the highest transfection efficiency to test if blocking the interactions between cellular cholesterol and the CDplex had a negative effect on the cellular uptake. Therefore, Cy5 pDNA – ADM-70 at N/P ratio 8 was pre-incubated with cholesterol, forming a Cy5 pDNA – cholesterol – ADM-70 CDplex. Figure 9 shows that the uptake of the cholesterol-saturated complexes in optiMEM dropped to the level of the pDNA - ADM-70 complexes in cell culture medium. This suggests that the cholesterol interactions which normally occur between non-saturated CDplexes and the cell membrane are essential for the cellular uptake. It should be noted that this hypothesis can only be made, however, when cholesterol does not induce a displacement of the pDNA from the CDplex. Several reports were published describing the connection between the uptake mechanism of the CDplexes and cell membrane cholesterol. [17, 22, 23, 28] Díaz-Moscoso et al. (2010)[28] also observed a drop in uptake and transfection efficiency of pDNA paCDs when cholesterol was depleted from the cell membrane by the addition of methyl β CDs. We therefore hypothesize that blocking the interaction between the hydrophobic moieties of CDs, by serum proteins, saturation with free cholesterol, or the depletion of cholesterol from the cellular membrane, is responsible for the disruption of the cellular uptake and consequently the lack of transfection efficiency.

Facilitating these interactions in serum-containing conditions could potentially retain the full functionality. Further experiments are certainly necessary to find a correlation between the presence of serum proteins and the loss of interactions with cellular cholesterol, but this preliminary result indicates that this is a possible explanation worth investigating.

CONCLUSION

Three cationic amphiphilic β-cyclodextrins were evaluated in their potential to act as non-viral vectors for the delivery of pDNA and mRNA, as a gene replacement therapy. The complexation behavior, as well as the physical characteristics (size and charge), were in a good range for a non-viral vector in HEPES buffer. CDplexes showed acceptable transfection efficiencies in a protein-reduced medium, in which mRNA gave higher transfection efficiency than pDNA. The more efficient formulations, however, also showed the highest toxicity toward the HeLa cells. When transfections were performed in protein-rich cell culture medium, no transfection could be detected. Cellular uptake seems to be hampered, which most likely explains the drop in transfection efficiency. A preliminary experiment indicates that there might be a disruption of the interactions between the CDs and cellular cholesterol by the presence of serum proteins. Further experiments should be performed to test this hypothesis.

REFERENCES

(1) Friedmann, T., and Roblin, R. (1972) Gene Therapy for Human Genetic Disease? *Science 175*, 949-955.

(2) Wells, D. J. (2004) Gene Therapy Progress and Prospects: Electroporation and other physical methods. *Gene therapy 11*, 1363-1369.

(3) Mehier-Humbert, S., and Guy, R. H. (2005) Physical methods for gene transfer: Improving the kinetics of gene delivery into cells. *Advanced Drug Delivery Reviews 57*, 733-753.

(4) Kotterman, M. A., Chalberg, T. W., and Schaffer, D. V. (2015) Viral Vectors for Gene Therapy: Translational and Clinical Outlook. *Annual Review of Biomedical Engineering 17*, 63-89.

(5) Thomas, C. E., Ehrhardt, A., and Kay, M. A. (2003) Progress and problems with the use of viral vectors for gene therapy. *Nature Reviews Genetics 4*, 346-358.

(6) Baum, C., Kustikova, O., Modlich, U., Li, Z., and Fehse, B. (2006) Mutagenesis and oncogenesis by chromosomal insertion of gene transfer vectors. *Human gene therapy 17*, 253-263.

(7) Marshall, E. (1999) Gene therapy death prompts review of adenovirus vector. *Science 286*, 2244-2245.

(8) Raper, S. E., Chirmule, N., Lee, F. S., Wivel, N. A., Bagg, A., Gao, G.-p., Wilson, J. M., and Batshaw, M. L. (2003) Fatal systemic inflammatory response syndrome in a ornithine transcarbamylase deficient patient following adenoviral gene transfer. *Molecular genetics and metabolism 80*, 148-158.

(9) Mintzer, M. A., and Simanek, E. E. (2008) Nonviral vectors for gene delivery. *Chemical reviews 109*, 259-302.

(10) Simberg, D., Weisman, S., Talmon, Y., and Barenholz, Y. (2004) DOTAP (and Other Cationic Lipids): Chemistry, Biophysics, and Transfection. *Critical Reviews in Therapeutic Drug Carrier Systems 21*, 62.

(11) Tarahovsky, Y. S. (2010) Cell transfection by DNA-lipid complexes — Lipoplexes. *Biochemistry (Moscow) 74*, 1293-1304.

(12) Li, W., and Szoka, F. C. (2007) Lipid-based Nanoparticles for Nucleic Acid Delivery. *Pharmaceutical Research 24*, 438-449.

(13) Elfinger, M., Uzgun, S., and Rudolph, C. (2008) Nanocarriers for Gene Delivery - Polymer Structure, Targeting Ligands and Controlled-Release Devices. *Current Nanoscience 4*, 322-353.

(14) Del Valle, E. M. M. (2004) Cyclodextrins and their uses: a review. *Process Biochemistry 39*, 1033-1046.

(15) Loftsson, T., Brewster, M. E., and Másson, M. (2012) Role of cyclodextrins in improving oral drug delivery. *American Journal of Drug Delivery 2*, 261-275.

(16) Szejtli, J. (2004) Past, present and futute of cyclodextrin research. *Pure and Applied Chemistry 76*, 1825-1845.

(17) Lai, W.-F. (2014) Cyclodextrins in non-viral gene delivery. *Biomaterials 35*, 401-411.

(18) Habus, I., Zhao, Q., and Agrawal, S. (1995) Synthesis, Hybridization Properties, Nuclease Stability, and Cellular Uptake of the Oligonucleotide-Amino-.beta.-cyclodextrins and Adamantane Conjugates. *Bioconjugate Chemistry 6*, 327-331.

(19) Gonzalez, H., Hwang, S. J., and Davis, M. E. (1999) New Class of Polymers for the Delivery of Macromolecular Therapeutics. *Bioconjugate Chemistry 10*, 1068-1074.
(20) Pun, S. H., Bellocq, N. C., Liu, A., Jensen, G., Machemer, T., Quijano, E., Schluep, T., Wen, S., Engler, H., Heidel, J., et al. (2004) Cyclodextrin-Modified Polyethylenimine Polymers for Gene Delivery. *Bioconjugate Chemistry 15*, 831-840.
(21) Hwang, S. J., Bellocq, N. C., and Davis, M. E. (2001) Effects of Structure of β-Cyclodextrin-Containing Polymers on Gene Delivery. *Bioconjugate Chemistry 12*, 280-290.
(22) Grunze, M., and Deuticke, B. (1974) Changes of membrane permeability due to extensive cholesterol depletion in mammalian erythrocytes. *Biochimica et Biophysica Acta - Biomembranes 356*, 125-130.
(23) Zidovetzki, R., and Levitan, I. (2007) Use of cyclodextrins to manipulate plasma membrane cholesterol content: Evidence, misconceptions and control strategies. *Biochimica et Biophysica Acta - Biomembranes 1768*, 1311-1324.
(24) Mislick, K. A., and Baldeschwieler, J. D. (1996) Evidence for the role of proteoglycans in cation-mediated gene transfer. *Proceedings of the National Academy of Sciences 93*, 12349-12354.
(25) Baeuerle, P. A., and Huttner, W. B. (1986) Chlorate—a potent inhibitor of protein sulfation in intact cells. *Biochemical and biophysical research communications 141*, 870-877.
(26) Mounkes, L. C., Zhong, W., Cipres-Palacin, G., Heath, T. D., and Debs, R. J. (1998) Proteoglycans mediate cationic liposome-DNA complex-based gene delivery in vitro and in vivo. *Journal of Biological Chemistry 273*, 26164-26170.
(27) Symens, N., Méndez-Ardoy, A., Díaz-Moscoso, A., Sánchez-Fernández, E., Remaut, K., Demeester, J., Fernández, J. M. G., De Smedt, S. C., and Rejman, J. (2012) Efficient transfection of hepatocytes mediated by mRNA complexed to galactosylated cyclodextrins. *Bioconjugate Chemistry 23*, 1276-1289.
(28) Díaz-Moscoso, A., Vercauteren, D., Rejman, J., Benito, J. M., Mellet, C. O., De Smedt, S. C., and Fernández, J. M. G. (2010) Insights in cellular uptake mechanisms of pDNA–polycationic amphiphilic cyclodextrin nanoparticles (CDplexes). *Journal of Controlled Release 143*, 318-325.
(29) Christian, A., Haynes, M., Phillips, M., and Rothblat, G. (1997) Use of cyclodextrins for manipulating cellular cholesterol content. *Journal of lipid research 38*, 2264-2272.
(30) Dakwar, G. R., Braeckmans, K., Demeester, J., Ceelen, W., Smedt, S. C. D., and Remaut, K. (2015) Disregarded Effect of Biological Fluids in siRNA Delivery: Human Ascites Fluid Severely Restricts Cellular Uptake of Nanoparticles. *ACS applied materials & interfaces 7*, 24322-24329.
(31) Rejman, J., Oberle, V., Zuhorn, I. S., and Hoekstra, D. (2004) Size-dependent internalization of particles via the pathways of clathrin-and caveolae-mediated endocytosis. *Biochemical Journal 377*, 159-169.
(32) Lesniak, A., Fenaroli, F., Monopoli, M. P., Åberg, C., Dawson, K. A., and Salvati, A. (2012) Effects of the Presence or Absence of a Protein Corona on Silica Nanoparticle Uptake and Impact on Cells. *ACS Nano 6*, 5845-5857.

CHAPTER 7 |

Broader International Context, Relevance and Future Perspectives

Since the beginning of 2015, Science Direct reports around 6.000 scientific articles when a query is performed with the words “non-viral”, “gene”, and “therapy”. This comes down to a daily average of 15 papers within this field of research. Yearly, these numbers are steadily increasing since the beginning of the 21st century. The articles dealing with non-viral gene therapy can roughly be divided into two categories. In the first category, new gene delivery methods are introduced or evaluated, while in the second category the mechanisms behind the barriers encountered during gene delivery are investigated. Ultimately, both papers in the first and second category aim to contribute to the development of a non-viral gene therapy approved for use in the clinic.

Nucleic acid-based non-viral therapy mostly involves one of the following three possible nucleic acids: small interfering RNA (siRNA), messenger RNA (mRNA), or plasmid DNA. siRNA is a small double stranded RNA molecule of 20-25 bp that silences the expression of a target gene via RNA interference. [1] To achieve this, the siRNA needs to be delivered into the cytoplasm of the cell. This is also the case for mRNA, which is a single stranded RNA molecule that can be translated into a functional protein in the cytoplasm of the cell. Plasmid DNA (pDNA) is a double stranded circular DNA molecule that can be transcribed in the cell’s nucleus into mRNA. This mRNA will migrate back to the cytoplasm where it will be translated into a functional protein. The delivery of nucleic acids to respectively the cytoplasm or the nucleus of the cell is one of the biggest challenges in this field. Not only does the therapeutic nucleic acids need to be protected from the harsh extracellular environment, it also needs to be taken up and be transported to the right intracellular compartment. For viral gene therapy recombinant viruses are used to achieve this. In early clinical trials, however, problems with deadly immunogenic responses and insertional mutagenicity occurred. Additionally, the viral particles are difficult and expensive to produce in a controlled manufacturing process. In the non-viral alternative, the nucleic acids are complexed with lipids or polymers, which are easier to synthesize on a large scale and can be modified in many ways. Additionally, they are less immunogenic and allow for the use of larger constructs that are necessary for the production of some larger proteins. Unfortunately the delivery efficiency is lower when compared to viral carriers, which have naturally evolved to accomplish efficient nucleic acid delivery into a variety of cell types.

A broad range of papers typically evaluate newly synthesized lipid or polymer particles, [2-4] follow-up on particles after a (pre-) clinical trial, [5-7] or deal with the evaluation of a new delivery technique to address the delivery challenge. [8, 9] Although the amount of newly described carriers for nucleic acids is high, the translation to further *in vivo* (human) studies is limited. The reason behind this discrepancy lies in the observation that high transfection efficiencies *in vitro* are predominantly obtained in optimized transfection media, or so-called serum reduced media, which contain the bare minimum of serum proteins that are necessary for cell growth and survival during the (limited) incubation period of cells with the carriers. When transfections are performed in cell culture medium or *in vivo* in an animal model, the carriers encounter a more complex environment with a whole range of (serum) proteins and the efficiency often decreases. [10] It is believed that the interactions with the serum proteins change the surface properties of the carefully synthesized particles, which disturbs uptake, leads to aggregation or to dissociation. [11] Therefore, when a drop in transfection efficiency is already seen *in vitro* in serum-containing media, further *in vivo* attempts seem premature and carriers should be optimized first before the *in vitro* evaluation process is started again. [12] Particles that do obtain high efficiencies in animal studies, however, are interesting to translate to the clinic, but from the hundreds of particles that show promise in animal studies, a very small amount makes it to clinical trials. Up until 2012, only 456 clinical trials with a non-viral approach (of which 75% are naked nucleic acids) have been started worldwide, [13] leading to 1 approved non-viral therapy in Russia: Neovasculgen. This formulation treats peripheral arterial disease by intraneural injection of a naked plasmid, containing the vascular endothelial growth factor. Globally, three other gene therapy products with viral vectors are approved: 1) Glybera, which restores the patients lipoprotein lipase deficiency by the introduction of the gene for a functional lipase by an adeno-associated virus 1, 2) Gendicine, which treats head and neck cancer via a recombinant adenovirus engineered to contain the gene that expresses the wildtype-p53, and 3) T-VEC, which is a melanoma immunotherapy that introduces an oncolytic granulocyte macrophage colony-stimulating factor gene carried by a herpes simplex virus type 1. [14] Despite this apparently discouraging number, especially for non-viral gene therapy, the results of some early phase (I/II) trials show great promise. [15] This optimism is represented by the renewed interest of major players in the pharmaceutical development, indicating that non-viral gene therapy is a realistic

option for the future of gene therapy. [14] Yet it is clear that more and better concepts need to be explored, guided by a better fundamental insight into the (cell) biology of nucleic acid delivery.

Most research papers dealing with fundamental aspects of non-viral gene delivery focus on unravelling the mechanisms of the extra and intracellular barriers, [16, 17] or try to understand the effect modifications have on the interaction of the non-viral particles with the extra and intracellular environment. [18, 19] The knowledge that is obtained in this research field, aids in understanding the challenges that non-viral particles encounter during gene delivery. Based on this, the design of particles can be adapted to anticipate the efficiency limiting steps posed by these barriers.

Both in the *in vitro* research toward the synthesis and evaluation of new particles, as well as in the studies on the mechanisms involved in gene delivery, a very diverse collection of experiments and technologies are used. Nonetheless, some techniques recur throughout the articles. For example, fluorescent microscopy techniques have proven useful to study intracellular barriers to gene therapy. Live-cell colocalization microscopy was, for example, used to study the different modes of cellular uptake and endocytosis, [20] endosomal escape, [21-23] and nuclear entry, [24] while advanced microscopy techniques like fluorescence correlation spectroscopy (FCS) and raster image correlation spectroscopy (RICS) were used, for example, to measure nuclear concentration and mobility of different sizes of pDNA. [25] All these experiments give more information on the intracellular barrier or determine the mechanism behind the cellular process, which shows that fluorescence microscopy is a powerful tool in the field of non-viral nucleic acid delivery.

The work in this thesis should be situated within the same category of research, since the main goal is to increase the understanding of the degradation of pDNA as a potential barrier to non-viral gene delivery. As there are currently no straightforward techniques available for the determination of pDNA degradation in complex biological environments or in living cells, we made use of advanced microscopy methods and in particular FCS and SPT for that purpose. These fluorescence microscopy methods both use fluorescence to obtain information on the level of the individual molecule. Therefore, this fluorescence needs to be introduced into the system under investigation. A variety of fluorescent dyes, probes, and stains to label the carrier, the nucleic acids, or particular cellular components are available

for these applications. We focused on the evaluation and application of fluorescent labeling techniques for nucleic acids to investigate their functionality after delivery by non-viral carriers. When we look at the attachment of fluorescent labels to nucleic acids, a diverse range of labeling methods is available. All these options have interesting properties (versatility, broad range of dyes, sequence specificity, etc.) that in some cases could provide additional information on the studied intracellular process, but could also alter the properties of the nucleic acid, inducing artefacts. For that reason, we felt the need for a clear and concise description and evaluation of a broad spectrum of labeling techniques that are of interest for live-cell imaging experiments. Special attention was given to the effect of random covalent labeling on transfection efficiency. The results indicated that labeling in itself has an influence on the performance of pDNA after transfection with Lipofectamine. This is important, since the labeling method has an influence on the process under investigation. For this reason, this work gives important information on which processes exactly are affected at a high labeling density. To put it differently, our work offers the possibility to choose a labeling density that is low enough to have no or a low effect on the performance of the nucleic acid, while still being high enough to be detectable by the microscopy techniques used. Brighter labels and more sensitive detection technology may in the future also further reduce the number of labels needed. In microscopy, this more sensitive detection is obtained by using advanced methods like FCS-based methods and SPT, which provide the tools to use very low concentrations of fluorescent labels, while delivering detailed information on the diffusion coefficient and concentrations of the molecules of interest. We evaluated different analysis methods for FCS and SPT for their potential to measure the concentrations of large pDNA molecules in buffer and in a biological environment to quantify DNA degradation. SPT, after imaging with a swept field confocal microscope, proved to be a suitable technique to follow degradation of pDNA in cell lysate obtained 4, 8, and 24 hour after lipofection. These results indicated that degradation over this period is significant, since a large portion of the pDNA that is taken up by the cells (4 hour mark) is lost for protein expression. This again illustrates the difficulties non-viral nucleic acid therapy has to overcome, to reach a high transfection efficiency. In the future, this type of experiment could be used to asses if intracellular degradation is dependent on the delivery method or that it is a logical consequence of the presence of pDNA in the cytoplasm before nuclear entry.

Furthermore, this experiment shows the total loss of pDNA over the complete cellular pathway, but it would be interesting to identify the losses induced by each barrier. This could be done by colocalization or FRET microscopy. It was, for example, already shown that the combination of colocalization microscopy and double labeled pDNA could be used to follow degradation, [26] but information of the cell compartment was lacking. With the knowledge obtained through these experiments, not only the carriers' chemical composition or surface chemistry could be optimized, but also better estimations for the total dose that needs to be administered to have a sufficient therapeutic effect can be derived. This dose optimization cannot only be advantageous with regard to obtaining a higher efficiency, but is also important to avoid the administration of too much therapeutic product for a number of reasons. First, too high doses might induce high levels of cytotoxicity and secondly production of non-viral vectors is expensive, so knowledge of the right dose is also beneficial for the manufacturer and for the patient.

When we now focus on the future of fluorescent labeling, it is our belief that the labeling methods, that are used at this moment for the labeling of exogenous DNA, are sufficient for the live-cell imaging applications. The opportunities lie in the smart use of these techniques for the study of certain cell barriers. An easy example of this is that when transcription is studied, a method needs to be used that does not label the DNA in the coding region. The option of a sequence-specific labeling method with an affinity for a recognition array outside of the coding region would in this case be a logic choice. If we think one step further, designing the nucleic acids with a particular research question in mind can also increase the information that can be obtained from the experiment. Jude et al. (2013)[27], for example, designed their own so-called cruciform DNA, which enabled them to look at DNA topology in real time. A fluorescent dye and a quencher were attached to opposing sites of an inverted repeat sequence. A conformational change, due to the presence of a topoisomerase or gyrase, resulted in the gain or loss of fluorescence, detected by a plate reader. For our research designing our own type of double labeled pDNA would be one of the next steps which were already initiated at the end of my PhD period. pDNA, labeled at two recognition arrays with spectrally different labels would then be used to follow the intracellular degradation. Live-cell imaging as well as SPT could be used in this case to visualize this. Since we don't expect much mobility of the pDNA

inside the cell, FCS would be less suitable here. The cruciform pDNA, that is described before, would also be an interesting alternative since a change in topology is also induced by endonuclease activity and has been seen to lower transfection efficiency, [28] this type of plasmid could be introduced into a living cell to monitor DNA degradation in real time by sensitive live-cell microscopy.

Another interesting development is the increasing amount of in situ labeling methods which enable visualization of nucleic acids directly inside the cell. Therefore, target cells express nucleic acid-binding proteins that are fused to fluorescent proteins (GFP, for example) [29-32] or –alternatively- nucleic acid-binding small molecules, [33] or detection probes [34] are introduced into the cell via microinjection, electroporation, bioballistics, chemical cell permeation, or via photoporation after which they can bind to their target sequence. The binding of multiple labels on each target nucleic acid allows for their detection the moment they reach a cell compartment or are transcribed in the nucleus, while the unbound molecules are not visible. [35] This would for example allow for the detection of endosomal escape or nuclear entry in real time, since binding of the fluorescent moiety can only occur respectively in the cytoplasm or in the nucleus.

Label-free detection of polynucleotides is another promising development. The biggest advantage is that the use of bulky fluorophores or haptens is avoided by employing the molecule's own chemical fingerprint for visualization. Additionally, the lack of the disadvantages of fluorescent labels, like photobleaching and phototoxicity, should allow for longer acquisition periods, eliminating a bottleneck for fluorescence live-cell imaging. One of the most promising techniques to achieve the visualization of nucleic acids *in vitro* and *in vivo* is stimulated Raman spectroscopy. [36-38]

All these new techniques and labeling options should ultimately be used to obtain a better knowledge of the cellular environment. It is in our opinion of importance that this information is translated into the development of new particles. A direct collaboration between an imaging specialist and a cell biologist is a first step to incorporate the most recent advances in imaging with the research questions posed in cell biology. These new fundamental insights into the cellular mechanisms should in turn lead to chemical modification of particles by chemical synthesis experts to obtain favorable properties. The evaluation of these particles can then again benefit of the developed microscopy techniques. In this way, the synthesis of new particles

could be steered by fundamental observations. This type of multidisciplinary approach offers, in our opinion, the best possibility for non-viral gene therapy products to reach the clinic.

In summary, non-viral gene delivery is a field that is investing much effort in the synthesis and evaluation of new carriers. Despite all these efforts in the last two decades, the clinical translation is still lagging behind. A more directed design of the carriers seems to be the key to unlock the gateway to efficient non-viral nucleic acid delivery. Multidisciplinary research facilities could aid in this regard. The association of fundamental research with fast and adaptive chemical synthesis, backed up by the most advanced evaluation techniques, should create an atmosphere were progress in the field of non-viral drug development can be made. To move forward from such a successful research drug to a clinical used medicine, collaboration with the pharmaceutical industry will also be necessary. For this reason, an optimistic view toward the future of non-viral gene therapy is justifiable. The newly found interest and investments of major pharmaceutical companies in gene therapy, can be the boost that is needed to get non-viral nucleic acid therapy from bench to the bedside.

REFERENCES

(1) Fire, A., Xu, S., Montgomery, M. K., Kostas, S. A., Driver, S. E., and Mello, C. C. (1998) Potent and specific genetic interference by double-stranded RNA in Caenorhabditis elegans. *Nature 391*, 806-811.

(2) Torrecilla, J., del Pozo-Rodríguez, A., Apaolaza, P. S., Solinís, M. Á., and Rodríguez-Gascón, A. (2015) Solid lipid nanoparticles as non-viral vector for the treatment of chronic hepatitis C by RNA interference. *International Journal of Pharmaceutics 479*, 181-188.

(3) Cutlar, L., Gao, Y., Aied, A., Greiser, U., Murauer, E. M., Zhou, D., and Wang, W. (2016) A knot polymer mediated non-viral gene transfection for skin cells. *Biomaterials Science 4*, 92-95.

(4) Javed, H., Menon, S. A., Al-Mansoori, K. M., Al-Wandi, A., Majbour, N. K., Ardah, M. T., Varghese, S., Vaikath, N. N., Haque, M. E., Azzouz, M., et al. (2016) Development of Nonviral Vectors Targeting the Brain as a Therapeutic Approach For Parkinson/'s Disease and Other Brain Disorders. *Molecular Therapy*.

(5) Slobodianski, A., Schmalix, S., Rosch, V., Hildebrandt, M., Machens, H.-G., and Perisic, T. (2015) Non-viral gene-transfer medicinal product - design and results of GLP pre-clinical study. *Cytotherapy 17*, S53.

(6) Chung, E. S., Miller, L., Patel, A. N., Anderson, R. D., Mendelsohn, F. O., Traverse, J., Silver, K. H., Shin, J., Ewald, G., and Farr, M. J. (2015) Changes in ventricular remodelling and clinical status during the year following a single administration of stromal cell-derived factor-1 non-viral gene therapy in chronic

ischaemic heart failure patients: the STOP-HF randomized Phase II trial. *European heart journal*, ehv254.

(7) Alton, E. W., Armstrong, D. K., Ashby, D., Bayfield, K. J., Bilton, D., Bloomfield, E. V., Boyd, A. C., Brand, J., Buchan, R., and Calcedo, R. (2015) Repeated nebulisation of non-viral CFTR gene therapy in patients with cystic fibrosis: a randomised, double-blind, placebo-controlled, phase 2b trial. *The Lancet Respiratory Medicine 3*, 684-691.

(8) Siene Ng, W., Binley, K., Song, B., and Morgan, J. E. (2015) Use of magnetic nanoparticles and oscillating magnetic field for non-viral gene transfer into mouse cornea. *The Lancet 385, Supplement 1*, S75.

(9) Prosen, L., Čemažar, M., and Sersa, G. (2016) in *1st World Congress on Electroporation and Pulsed Electric Fields in Biology, Medicine and Food & Environmental Technologies* pp 335-338, Springer.

(10) Dakwar, G. R., Braeckmans, K., Demeester, J., Ceelen, W., Smedt, S. C. D., and Remaut, K. (2015) Disregarded Effect of Biological Fluids in siRNA Delivery: Human Ascites Fluid Severely Restricts Cellular Uptake of Nanoparticles. *ACS applied materials & interfaces 7*, 24322-24329.

(11) Tenzer, S., Docter, D., Kuharev, J., Musyanovych, A., Fetz, V., Hecht, R., Schlenk, F., Fischer, D., Kiouptsi, K., Reinhardt, C., et al. (2013) Rapid formation of plasma protein corona critically affects nanoparticle pathophysiology. *Nature Nanotechnology 8*, 772-781.

(12) Lechardeur, D., Sohn, K., Haardt, M., Joshi, P., Monck, M., Graham, R., Beatty, B., Squire, J., O'brodovich, H., and Lukacs, G. (1999) Metabolic instability of plasmid DNA in the cytosol: a potential barrier to gene transfer. *Gene Therapy 6*, 482-497.

(13) Ginn, S. L., Alexander, I. E., Edelstein, M. L., Abedi, M. R., and Wixon, J. (2013) Gene therapy clinical trials worldwide to 2012 – an update. *The Journal of Gene Medicine 15*, 65-77.

(14) Foldvari, M., Chen, D. W., Nafissi, N., Calderon, D., Narsineni, L., and Rafiee, A. (2016) Non-viral gene therapy: Gains and challenges of non-invasive administration methods. *Journal of Controlled Release*.

(15) Naldini, L. (2015) Gene therapy returns to centre stage. *Nature 526*, 351-360.

(16) Di Gioia, S., Trapani, A., Castellani, S., Carbone, A., Belgiovine, G., Craparo, E. F., Puglisi, G., Cavallaro, G., Trapani, G., and Conese, M. (2015) Nanocomplexes for gene therapy of respiratory diseases: Targeting and overcoming the mucus barrier. *Pulmonary Pharmacology & Therapeutics 34*, 8-24.

(17) Avital, Y. Y., Gronbech-Jensen, N., and Farago, O. (2016) The thermodynamics of endosomal escape and DNA release from lipoplexes. *Physical Chemistry Chemical Physics 18*, 2591-2596.

(18) Baumhover, N. J., Duskey, J. T., Khargharia, S., White, C. W., Crowley, S. T., Allen, R. J., and Rice, K. G. (2015) Structure–Activity Relationship of PEGylated Polylysine Peptides as Scavenger Receptor Inhibitors for Non-Viral Gene Delivery. *Molecular Pharmaceutics 12*, 4321-4328.

(19) Martens, T. F., Remaut, K., Deschout, H., Engbersen, J. F., Hennink, W. E., Van Steenbergen, M. J., Demeester, J., De Smedt, S. C., and Braeckmans, K. (2015) Coating nanocarriers with hyaluronic acid facilitates intravitreal drug delivery for retinal gene therapy. *Journal of Controlled Release 202*, 83-92.

(20) Vercauteren, D., Piest, M., van der Aa, L. J., Al Soraj, M., Jones, A. T., Engbersen, J. F., De Smedt, S. C., and Braeckmans, K. (2011) Flotillin-

dependent endocytosis and a phagocytosis-like mechanism for cellular internalization of disulfide-based poly(amido amine)/DNA polyplexes. *Biomaterials 32*, 3072-3084.

(21) Martens, T. F., Remaut, K., Demeester, J., De Smedt, S. C., and Braeckmans, K. (2014) Intracellular delivery of nanomaterials: How to catch endosomal escape in the act. *Nano Today 9*, 344-364.

(22) Rehman, Z. u., Hoekstra, D., and Zuhorn, I. S. (2013) Mechanism of Polyplex- and Lipoplex-Mediated Delivery of Nucleic Acids: Real-Time Visualization of Transient Membrane Destabilization without Endosomal Lysis. *ACS Nano 7*, 3767-3777.

(23) Wittrup, A., Ai, A., Liu, X., Hamar, P., Trifonova, R., Charisse, K., Manoharan, M., Kirchhausen, T., and Lieberman, J. (2015) Visualizing lipid-formulated siRNA release from endosomes and target gene knockdown. *Nature Biotechnology 33*, 870-876.

(24) Breuzard, G., Tertil, M., Goncalves, C., Cheradame, H., Geguan, P., Pichon, C., and Midoux, P. (2008) Nuclear delivery of NFκB-assisted DNA/polymer complexes: plasmid DNA quantitation by confocal laser scanning microscopy and evidence of nuclear polyplexes by FRET imaging. *Nucleic acids research 36*, e71-e71.

(25) Mieruszynski, S., Digman, M. A., Gratton, E., and Jones, M. R. (2015) Characterization of exogenous DNA mobility in live cells through fluctuation correlation spectroscopy. *Scientific Reports 5*, 13848.

(26) Srinivasan, C., Siddiqui, S., Silbart, L. K., Papadimitrakopoulos, F., and Burgess, D. J. (2008) Dual fluorescent labeling method to visualize plasmid DNA degradation. *Bioconjugate Chemistry 20*, 163-169.

(27) Jude, K. M., Hartland, A., and Berger, J. M. (2013) Real-time detection of DNA topological changes with a fluorescently labeled cruciform. *Nucleic acids research*, gkt413.

(28) Remaut, K., Sanders, N. N., Fayazpour, F., Demeester, J., and De Smedt, S. C. (2006) Influence of plasmid DNA topology on the transfection properties of DOTAP/DOPE lipoplexes. *Journal of Controlled Release 115*, 335-343.

(29) Robinett, C. C., Straight, A., Li, G., Willhelm, C., Sudlow, G., Murray, A., and Belmont, A. S. (1996) In vivo localization of DNA sequences and visualization of large-scale chromatin organization using lac operator/repressor recognition. *The Journal of Cell Biology 135*, 1685-1700.

(30) Keppler, A., Gendreizig, S., Gronemeyer, T., Pick, H., Vogel, H., and Johnsson, K. (2003) A general method for the covalent labeling of fusion proteins with small molecules in vivo. *Nature Biotechnology 21*, 86-89.

(31) Los, G. V., Encell, L. P., McDougall, M. G., Hartzell, D. D., Karassina, N., Zimprich, C., Wood, M. G., Learish, R., Ohana, R. F., Urh, M., et al. (2008) HaloTag: A Novel Protein Labeling Technology for Cell Imaging and Protein Analysis. *ACS Chemical Biology 3*, 373-382.

(32) Tyagi, S. (2009) Imaging intracellular RNA distribution and dynamics in living cells. *Nature Methods 6*, 331-338.

(33) Dervan, P. B. (2001) Molecular recognition of DNA by small molecules. *Bioorganic & Medicinal Chemistry 9*, 2215-2235.

(34) Santangelo, P. J. (2010) Molecular beacons and related probes for intracellular RNA imaging. *Wiley Interdisciplinary Reviews: Nanomedicine and Nanobiotechnology 2*, 11-19.

(35) Campbell, P. D., Chao, J. A., Singer, R. H., and Marlow, F. L. (2015) Dynamic visualization of transcription and RNA subcellular localization in zebrafish. *Development 142*, 1368-1374.
(36) Freudiger, C. W., Min, W., Saar, B. G., Lu, S., Holtom, G. R., He, C., Tsai, J. C., Kang, J. X., and Xie, X. S. (2008) Label-free biomedical imaging with high sensitivity by stimulated Raman scattering microscopy. *Science 322*, 1857-1861.
(37) Zhang, X., Roeffaers, M. B., Basu, S., Daniele, J. R., Fu, D., Freudiger, C. W., Holtom, G. R., and Xie, X. S. (2012) Label-Free Live-Cell Imaging of Nucleic Acids Using Stimulated Raman Scattering Microscopy. *ChemPhysChem 13*, 1054-1059.
(38) Wei, L., Hu, F., Shen, Y., Chen, Z., Yu, Y., Lin, C.-C., Wang, M. C., and Min, W. (2014) Live-cell imaging of alkyne-tagged small biomolecules by stimulated Raman scattering. *Nature Methods 11*, 410-412.

SUMMARY AND GENERAL CONCLUSIONS

Gene replacement therapy is a field of research in which the scientific community has spent a tremendous amount of effort over the last two decades. The idea of not only treating the symptoms of a disease, but foremost treating the cause, is indeed promising. To that end, a correct therapeutic gene needs to be introduced into the cell in the right cellular compartment (cytoplasm for mRNA and nucleus for plasmid DNA (pDNA)). Different strategies to achieve this have been developed over the years. Originally, the main delivery strategy consisted of inserting unprotected nucleic acids into the body close to their target and hoping that they spontaneously reach and internalize into the cells. Low efficiency was obtained with this approach, with instability of the nucleic acids in the body as one of the major reasons. Nucleases, for example, that are present in the extra and intracellular environment, not only act as a defense mechanism toward foreign genetic material from viral or bacterial origin, but also function as a clearing mechanism for endogenous nucleic acids that originate from the normal regeneration cycle of cells. To protect the therapeutic gene vectors from degradation, protective vehicles were adapted from nature, in the form of recombinant viral particles, or developed by chemical synthesis. The viral vectors have the advantage that evolution has adapted them to hijack the cellular machinery of organisms for the expression of viral genes, needed for their own reproduction. This leads to highly efficient gene carriers, but next to being limited in their therapeutic cargo and requiring a challenging production process, the main concern for clinical use is immunogenicity. Clinical trials have shown that these concerns were not idle.

Non-viral nucleic acid carriers are in this regard a safer choice. Two main types of non-viral vectors can be distinguished. On one hand we have the cationic lipid-based carriers and on the other hand we have the cationic polymer-based gene carriers. The addition of negatively charged nucleic acids leads to nucleic acid – carrier complexes with low immunogenicity coupled to a controllable chemical production process. However, the efficiency of gene expression cannot compete with their viral counterparts, as they are less adapted to overcome the biological barriers that are encountered during the delivery process. First of all, after intravenous injection, nucleases as well as immune cells in blood try to eliminate circulating exogenous materials. Also, blood proteins may lead to aggregation of the nanocarrier, dissociation of the nucleic acid – nanocarrier, or loss of targeting functionality. Therefore, protective and stabilizing characteristics of the carrier are required. While protecting the nucleic

acids, the complexes need to extravasate out of the circulation into the surrounding tissues to avoid clearance by, among others, the liver, spleen or kidneys and to reach the target cells. Following extravasation and transport across the extracellular space, the nanocarrier finally reaches its target cell where it can commence its intracellular journey. The cellular uptake poses a first barrier. In general uptake happens through endocytosis, leading to particles that are located in early and sorting endosomes at first. From there on the endosomes mature into late endosomes and finally fuse with lysosomal vesicles to become endolysosomes. Due to the low pH and presence of degradation enzymes in endolysosomes, nanocarriers should preferably escape to the cytoplasm while being in early to late endosomes. Successful endosomal escape is, however, currently recognized as one of the major bottlenecks on the intracellular level to successful gene therapy. Those carriers that successfully reach the cytoplasm need to be able to release their nucleic acid cargo in order to produce a biological effect. In case of mRNA the cytoplasm is the suitable end location. Plasmid DNA, however, needs to overcome one additional barrier, namely the nuclear envelope, as it should be transcribed into mRNA in the nucleus before being ultimately translated into the therapeutic protein. For pDNA it is well-known that nuclear translocation only happens efficiently after cell division. This means that the pDNA might reside a relatively long time in the cytoplasm before cell division occurs. During that time, degradation can again occur due to the presence of nucleases. Considering all those barriers, it comes as no surprise that successful delivery of therapeutic nucleic acids is a major challenge with ample room for improvement. Rational development of gene therapy nanocarriers requires thorough understanding of how they interact with each of those barriers. Fluorescence microscopy, and especially live-cell fluorescence imaging, has proven to be a particularly powerful tool to investigate the interactions of gene therapy carriers with the biological barriers. It offers detailed insight in the cellular processing of nanocarriers, especially on the intracellular level.

The general aim of this thesis was to investigate the barrier posed by enzymatic degradation encountered by pDNA during the different steps of the transfection. As currently there are only limited methods available to follow pDNA degradation in more complex biological environments, we evaluated the use of two advanced fluorescence microscopy methods for this purpose, namely fluorescence correlations spectroscopy (FCS) and single particle tracking (SPT). To be able to measure the pDNA with these

techniques, evidently they need to be labeled with a fluorescent tag. In the design of microscopy experiments, however, attention to the labeling method that best suits the eventual application is often lacking. In **Chapter 1**, we therefore presented an overview of the full range of methods to attach fluorescent molecules to pDNA and mRNA. This detailed overview lists the advantages and disadvantages encountered when working with the different labeling methods. It is clear that there is more than one method that is ideal for every fluorescence microscopy experiment. For this reason, considerations like ease of use and cost can play an important role while choosing a labeling method. With the information included, a researcher designing a live-cell imaging experiment that follows nucleic acids during intracellular trafficking should be able to make an informed decision on which labeling methods suit the experiments best. Special attention is given to the effect of the nucleic acid labeling methods on the intracellular processes that lead to the induction of protein expression in the cell, a process also called transfection.

In **Chapter 2**, the theory and methodology behind the two advanced fluorescence microscopy techniques, that are used throughout this thesis, are presented. This should improve the understanding of the terms and the analysis methods that are used further on in the thesis.

Building onto **Chapter 1**, a deeper look into the effect the fluorescent labeling methods have on the intracellular processing and transfection is presented in **Chapter 3**. Different amounts of fluorescent labels were attached to pDNA with a frequently used commercial labeling kit. This covalent attachment couples a fluorophore directly to the nucleobase, with a preference for the guanine nucleotides, but without any sequence specificity. This results in random labeling of nucleotides in plasmids. Using Lipofectamine as a transfection agent, it was seen that a maximum of on average 10 labels could be attached per plasmid without inducing a problematic drop in transfection efficiency. We then investigated the reasons behind this observation. Our experimental data showed that, while cellular uptake was not affected, the dissociation of the pDNA from the lipoplex, the endosomal escape, and the transcription of the pDNA by the cell were altered. We hypothesize that the presence of hydrophobic fluorescent labels induces a higher affinity towards the lipophilic transfection agent and endosomal membranes, thus leading to problems with pDNA release and endosomal escape. In addition, attachment of fluorescent labels to the nucleobase also might

induce steric hindrance to the cellular machinery for transcription, leading to reduced protein expression. Our results show that plasmid labeling density should not be too high in order not to disturb the normal pDNA intracellular processing.

One of the intracellular barriers to gene therapy is the potential degradation of nucleic acids after being delivered in the cell's cytoplasm. In **Chapter 4**, we evaluated two advanced microscopy techniques which might have the capacity to measure the degradation of (fluorescently labeled) pDNA. FCS and SPT are both microscopy techniques that have been reported to be able to measure the concentration of fluorescently labeled compounds. In this chapter we compared both of them to see which one is better fit to the task of measuring degradation of pDNA. It was found that FCS could not reliably retrieve the ratio of intact and degraded pDNA in well-defined mixtures. Likely this is due to the fact that intact plasmids contribute more strongly to the intensity-based autocorrelation curve. SPT measurements performed on a swept-field confocal microscope (SFC), in combination with an in-house developed and previously published concentration analysis method, could very well retrieve the expected ratios between intact and degraded pDNA. FCS and SPT were subsequently applied to measure the degradation of pDNA subjected to DNase I degradation. SPT was the only technique that could successfully retrieve a profile that represented the degradation pattern as observed on the control agarose gel. SPT was finally applied to follow plasmid degradation in a biologic medium. Cell lysate was obtained at different time points after lipofection with fluorescent labeled pDNA. The results showed that pDNA is significantly degraded already 8 hour after lipofection and almost fully degraded after 24 hour, demonstrating that SPT is suited to investigate the degradation of pDNA in biologic media.

In both **Chapter 3** and **4**, the random covalent attachment of fluorophores to pDNA was used. In **Chapter 5** we explored a selection of alternative pDNA labeling strategies, namely the intercalating cyanine dimeric nucleic acid stains, hybridization of fluorescent labeled peptide nucleic acid (PNA) probes, methyltransferase-mediated enzymatic labeling, and a label-free method. Building forth on the results of **Chapter 3**, a change in transfection efficiency was taken as a hallmark of the potential negative influence of the labels on the intracellular pDNA processing. None of the tested labeling strategies influenced the transfection efficiency of pDNA, except to the label-free labeling method. The sequence-specific methods (PNA hybridization and enzymatic

labeling) have the advantage that plasmids can be designed with special arrays of recognition sequences. This allows for plasmid designs that minimize the interference of the fluorophores with the coding sequence. Also double labeling and the attachment of interesting non-fluorescent molecules is possible, enabling a wide range of modifications. These custom designs are on the other hand very specific and decrease the interchangeability of the labeling method for other plasmids of interest. In the label-free approach, a modified nucleotide with an alkyne group was incorporated in the pDNA to enable visualization by stimulated Raman spectroscopy. Our data showed that this modification resulted in the loss of functionality of the pDNA. In this regard, the random Mirus nucleic acid labeling kit, might still be the best choice when used at the right fluorophore density (cf. **Chapter 3** and **4**).

Finally, the potential of three new non-viral carriers was evaluated in **Chapter 6**. Three polycationic amphiphilic β-cyclodextrins (paCDs) were complexed with pDNA and mRNA and stability and transfection efficiency were assessed. Transfection experiments in an optimized serum-free transfection medium showed efficiencies slightly lower than Lipofectamine for one of the paCDs, while the others were slightly less efficient. When the transfections were carried out in serum-containing cell culture medium, the efficiencies decreased over the whole line. Cellular uptake was found to be significantly lower for most paCDs when the transfections were carried out in the presence of serum. Further experiments indicate that the interaction between paCDs and cellular cholesterol might play an important role in the cellular uptake of the complexes. The pre-incubation of the paCD-pDNA complexes with cholesterol before addition to cells, resulted in a drop in cellular uptake. This indicates that the saturation of the hydrophobic cavity of the paCDs, disturbs the interactions with the cellular cholesterol and subsequently the cellular uptake. Our hypothesis is that serum proteins also block these interactions by adsorption to the paCD complexes.

Taken together, we conclude that the use of microscopy methods is highly valuable in the study and evaluation of barriers for non-viral nanoparticles. SPT on the images obtained by fast SFC microscopy is a suitable technique to study degradation of pDNA in a biological environment. It is, however, important that, next to the microscopy technique and the biologic parameters of the experiment, attention is given to the used fluorescent labeling method, since it might influence the cellular processes under investigation when a non-optimal labeling method was used. Also, one should

take into account that apart from the enzymatic degradation of nucleic acids, many other extracellular and intracellular barriers exist that might limit the transfection efficiency. Therefore, we recommend to always study the transfection efficiency of newly developed carriers in conditions that are as close as possible to the eventual *in vivo* situation in which the carriers are expected to be used. The tremendous efforts to optimize new delivery systems and to understand the hurdles nucleic acids have to overcome before successful transfection will continue to shape the future of non-viral gene delivery.

SAMENVATTING EN CONCLUSIES

Gentherapie is een onderzoeksgebied waarin de wetenschappelijke wereld de laatste twee decennia sterk heeft geïnvesteerd. Het idee dat niet enkel de symptomen, maar in de eerste plaats de oorzaak wordt behandeld is veelbelovend. Om dit te verwezenlijken moet een correct therapeutisch gen afgeleverd worden in het juiste cel compartiment (cytoplasma voor mRNA en de nucleus voor plasmide DNA (pDNA)). Over de jaren werden verschillende strategieën ontwikkeld om dit doel te bereiken. Oorspronkelijk bestond de belangrijkste afleveringsstrategie uit het injecteren van onbeschermde nucleïnezuren rechtstreeks in de nabijheid van de te behandelen cellen, waarna verwacht werd dat ze spontaan hun doelcellen bereikten en werden opgenomen. Dit resulteerde echter in een lage efficiëntie, die grotendeels te wijten was aan de instabiliteit van de nucleïnezuren in het lichaam. Eén van de oorzaken is de aanwezigheid van nucleasen in de extra- en intracellulaire omgeving. Deze familie van eiwitten doet niet enkel dienst als afweermechanisme tegen vreemd genetisch materiaal afkomstig van virale of bacteriële afkomst, maar is ook verantwoordelijk voor de vernietiging van nucleïnezuren afkomstig van de normale vernieuwingscyclus van lichaamseigen cellen. Om de toegediende therapeutische genen te beschermen werden dragers uitgezocht die gebaseerd zijn op de natuur, in de vorm van recombinante virale partikels, of aangemaakt via chemische synthese. De virale dragers hebben het voordeel dat ze door genetische evolutie aangepast zijn om de processen in cellen over te nemen om hun eigen genen tot expressie te brengen, wat leidt tot hun vermenigvuldiging. Ondanks dat deze aanpak aanleiding geeft tot zeer efficiënte genetische dragers, hebben deze virale dragers als nadeel dat ze beperkt zijn in de grootte van de therapeutische cargo en dat ze een zeer veeleisend productieproces hebben. Het grootste struikelblok om deze dragers toe te passen in de praktijk is echter dat ze een sterke immuunrespons kunnen opwekken, wat reeds werd aangetoond in klinische tests.

Met deze kennis indachtig zijn niet-virale dragers voor nucleïnezuren een veiligere keuze. Twee belangrijke types van niet-virale dragers worden onderscheiden. In de eerste plaats hebben we de kationische dragers die bestaan uit polymeren. Wanneer hier negatief geladen nucleïnezuren aan worden toegevoegd ontstaan er nucleïnezuur- drager complexen die een lage immuunrespons verenigen met een eenvoudig te controleren chemisch productieproces. De efficiëntie om genexpressie op te wekken kan echter niet tippen aan hun virale tegenhangers doordat ze minder

aangepast zijn om de verschillende biologische barrières, die ze tijdens de aflevering van de therapeutische genen tegenkomen, te overwinnen. Wanneer deze dragers via intraveneuze weg worden toegediend, denken we hierbij in de eerste plaats aan de aanwezigheid van nucleasen en immuuncellen die aanwezig zijn in het bloed om lichaamsvreemd materiaal te verwijderen. Ook de aanwezigheid van eiwitten in het bloed kan leiden tot aggregatie van de dragers, loskomen van de nucleïnezuren van de drager, of het verlies van de werking van de complexen. Daarom worden dragers ontworpen zodat ze beschermende en stabiliserende eigenschappen tentoonspreiden. Dit is noodzakelijk aangezien de complexen vanuit het bloed naar de omliggende weefsels moet migreren om te ontsnappen aan de verwijdering uit de bloedbaan door, onder andere, de lever, milt, of nieren en om vervolgens de doelcellen te bereiken. Nadat ze de extracellulaire ruimte hebben bereikt moeten de complexen naar de doelcellen migreren waar de uiteindelijke intracellulaire aflevering zal plaatsvinden. Allereerst moeten de complexen opgenomen worden door de cellen, wat meestal gebeurt via het proces van endocytose. Dit leidt initieel tot complexen die zich in vroege en sorterende endosomen bevinden, waarna deze vesikels zich ontwikkelen tot late endosomen. Dit type endosoom zal zich uiteindelijk samenvoegen met lysosomale vesikels wat resulteert in endolysosomen die gekenmerkt worden door een lage pH en de aanwezigheid van enzymen verantwoordelijk voor de afbraak van biomoleculen. Om afbraak te vermijden moeten de complexen ontsnappen uit deze endosomen. Deze stap wordt over het algemeen beschouwd als één van de belangrijkste knelpunten voor de aflevering van producten voor gentherapie op het niveau van de cel. Wanneer de complexen hierin slagen moeten de nucleïnezuren loskomen van de drager om hun therapeutisch effect te hebben. Voor mRNA vindt dit plaats in het cytoplasma, maar in het geval van pDNA moet er nog een extra barrière overwonnen worden, namelijk de nucleaire envelop, waarna het pDNA wordt omgezet in mRNA dat uiteindelijk zal zorgen voor de expressie van het therapeutische eiwit. Het is reeds beschreven dat het nucleaire transport enkel plaatsvindt na de celdeling. Dit betekent echter dat het pDNA een relatief lange tijd moet doorbrengen in het cytoplasma voor er celdeling plaatsvindt. Gedurende deze tijd wordt het pDNA opnieuw blootgesteld aan nucleasen die zorgen voor afbraak. Met al deze barrières in het achterhoofd, mag het geen verrassing zijn dat het afleveren van nucleïnezuren allesbehalve een eenvoudige taak is waarbinnen verscheidene stappen ruimte bieden tot verbeteringen. Het op een rationele manier ontwikkelen van dragers voor gentherapie producten vergt

echter een vergaand begrip van de interacties die plaatsvinden tussen de betrokken componenten tijdens elke stap van de aflevering. Fluorescentiemicroscopie, en in het bijzonder het in beeld brengen van levende cellen, vormt hierbij een bijzonder krachtig wapen om deze interacties in kaart te brengen, vooral op het niveau van de cel.

Het algemene doel van deze thesis was het onderzoeken van de enzymatische afbraak van pDNA die tijdens verschillende stappen van een transfectie plaatsvindt. Aangezien er momenteel slechts een beperkt aantal methoden beschikbaar zijn om afbraak van pDNA op te volgen in een complexe biologische omgeving, hebben we hiervoor twee geavanceerde fluorescentiemicroscopietechnieken geëvalueerd. Deze twee technieken zijn fluorescentie correlatie spectroscopie (FCS) en 'single particle tracking' (SPT). Om met deze technieken experimenten uit te voeren met pDNA is het noodzakelijk dat een fluorescent label wordt toegevoegd. Tijdens het ontwerpen van microscopie-experimenten wordt er echter weinig aandacht besteed aan het type labelingsmethode dat het meest geschikt is voor de gekozen toepassing. In **Hoofdstuk 1** is om deze reden een overzicht gegeven van het volledige assortiment van methoden die gebruikt worden om fluorescente labels te bevestigen aan pDNA en aan mRNA. Zowel de voor – als de nadelen van elke techniek werden opgelijst. Hieruit blijkt dat er vaak meer dan één methode is die, technisch gezien, het beste past bij elk fluorescentiemicroscopie-experiment. Om deze reden werd er ook rekening gehouden met het gebruiksgemak en de kostprijs van elke methode. Met de informatie die aangereikt werd in dit hoofdstuk zou een onderzoeker die nucleïnezuren wil visualiseren tijdens hun weg door de cel, gebruik makend van fluorescentiemicroscopie, voldoende moeten weten om een onderbouwde keuze te maken tussen de verschillende labelingsstrategieën. Extra aandacht is besteed aan het effect dat deze verschillende technieken hebben op de intracellulaire processen die leiden tot een succesvolle eiwitexpressie, ook wel transfectie genoemd.

Vervolgens werd in **Hoofdstuk 2** de theorie en methodologie achter beide geavanceerde fluorescentiemicroscopietechnieken (FCS en SPT) uitgediept. Hierdoor zou alle terminologie en de analysemethoden die doorheen de thesis gebruikt worden, duidelijk moeten zijn, zodat de experimenten in de volgende hoofdstukken makkelijker te interpreteren zijn.

Op het effect van de fluorescente labeling op de intracellulaire verwerking en transfectie werd dieper ingegaan in **Hoofdstuk 3**. Verschillende hoeveelheden van het

fluorescente label werden op het pDNA aangebracht gebruikmakend van een veelgebruikte commerciële kit. Hierbij worden fluorescente moleculen covalent gekoppeld aan een nucleobase en bij voorkeur op de guanine nucleotiden zonder enige voorkeur voor de rest van de sequentie. Het resultaat van deze reactie zijn plasmiden met willekeurig verspreide fluorescent gemerkte nucleotiden. Door gebruik te maken van het transfectiereagens Lipofectamine 2000, werd vastgesteld dat een gemiddelde van 10 labels het maximale aantal fluorescente labels is dat bevestigd kan worden aan één plasmide zonder een problematisch negatief effect te hebben op de transfectie-efficiëntie. We toonden aan dat de opname door de cel niet beïnvloed werd door de labels, maar dat het loskomen van het pDNA van de drager, de ontsnapping uit de endosomen, en de transcriptie van het pDNA naar mRNA in de celkern negatief werden beïnvloed. Onze hypothese stelde dat de aanwezigheid van hydrofobe fluorescente labels de affiniteit van het pDNA ten opzichte van zowel het lipofiele transfectiereagens alsook de endosomale membranen verhoogt. Dit leidt vervolgens tot problemen met de vrijgave van het pDNA van het complex en de ontsnapping uit de endosomen. Bijkomend zorgen de labels op de nucleobasen voor sterische hindering voor de enzymen in de celkern verantwoordelijk voor de transcriptie, wat leidt tot een lagere eiwitexpressie. Al deze resultaten geven aan dat de hoeveelheid labels per plasmide niet te hoog mag zijn om de normale werking van de intracellulaire processen te verzekeren.

Eén van de intracellulaire barrières die nucleïnezuren tegenkomen nadat ze het cytoplasma van de cel bereiken, is enzymatische afbraak. In **Hoofdstuk 4** werden twee geavanceerde microscopietechnieken vergeleken die mogelijk de afbraak van fluorescent gemerkte pDNA moleculen kunnen volgen. FCS en SPT zijn allebei microscopietechnieken waarvan reeds werd aangetoond dat ze in staat zijn om de concentratie te meten van fluorescent gemerkte moleculen. In dit hoofdstuk werd gekeken welke techniek beter geschikt was om de afbraak van pDNA te volgen. Onze bevindingen toonden aan dat diffusiemetingen via FCS de verhoudingen tussen intact en afgebroken plasmiden op onvoldoende wijze kon onderscheiden in vooraf samengestelde mengsels van beide varianten van pDNA. Dit was waarschijnlijk te wijten aan de grotere invloed die door de intacte plasmiden werd uitgeoefend op de intensiteit-gebaseerde correlatiecurve. De SPT metingen die werden uitgevoerd op een swept-field confocal (SFC) microscoop, gecombineerd met een

concentratieanalyse die binnen onze onderzoeksgroep werd ontwikkeld, slaagden er wel in om de verwachte verhouding tussen intact en afgebroken pDNA te achterhalen. FCS met piekanalyse en SPT werden vervolgens ingezet om de afbraak van pDNA met het endonuclease DNase I op te volgen over de tijd. SPT was de enige techniek die het afbraakprofiel kon achterhalen dat via de controle op agarosegel bepaald werd. Uiteindelijk werd SPT gebruikt om de afbraak van plasmiden te volgen in een biologische omgeving. De concentratie aan intact pDNA werd, op verschillende tijdstippen na lipofectie met fluorescent gemerkte plasmiden, gemeten in cellysaat. De resultaten toonden aan dat pDNA reeds 8 uur na de lipofectie significant afgebroken werd en zelfs bijna volledig afgebroken was na 24 uur. Dit resultaat toont aan dat SPT geschikt is om de afbraak van fluorescent gelabeld pDNA in een biologische omgeving te volgen.

In zowel **Hoofdstuk 3** als **4** werd de willekeurige covalente labeling van pDNA met fluorescente merkers gebruikt. In **Hoofdstuk 5** werd een selectie gemaakt van alternatieve labelingstechnieken. 'Cyanic dimeric nucleic acid stains', hybridisatieprobes gebaseerd op fluorescente peptide nucleïnezuren (PNA), methyltransferase-gebaseerde enzymatische labeling en een niet-fluorescente 'label-free' methode waren de technieken die geëvalueerd werden op basis van hun transfectie-efficiëntie (cf. **Hoofdstuk 3**). Aangezien deze parameter kan gezien worden als de lakmoesproef voor de invloed van de fluorescente labels op de intracellulaire verwerking van pDNA. Geen enkele fluorescente labelingstechniek beïnvloedde de transfectie-efficiëntie van pDNA ingrijpend. Wanneer de niet-fluorescente "label-free" methode werd gebruikt was er echter geen transfectie meer te detecteren. De sequentiespecifieke technieken (PNA hybridisatie en enzymatische labeling) hebben als bijkomend voordeel dat plasmiden zo ontworpen kunnen worden dat ze afgelijnde regio's bevatten met meerdere herkenningssequenties. Hierdoor wordt de invloed van de fluorescente merkers op de coderende pDNA sequentie geminimaliseerd. Bijkomend kunnen ook plasmiden worden ontworpen met de mogelijkheid voor een dubbele labeling met twee kleuren of het bevestigen van niet-fluorescente moleculen die de aflevering positief beïnvloeden. Deze ontwerpen zijn echter zeer specifiek wat uitwisseling van de labelingsmethode over verschillende types plasmiden minder praktisch maakt. Wanneer de niet-fluorescente "label-free" techniek werd gebruikt, werd een alkyne-gemodificeerd nucleotide ingevoegd. Dit

alkyne maakt visualisatie met gestimuleerde Raman spectroscopie mogelijk. Onze resultaten met deze techniek toonden echter aan dat alle functionaliteit verdwijnt na de toevoeging van het gemodificeerd nucleotide aan pDNA. Met de voorgaande informatie in het achterhoofd, kunnen we besluiten dat Mirus nucleïnezuur labelingskit waarschijnlijk de beste keuze blijft, wanneer de juiste hoeveelheid fluorescente merker gebruikt wordt (cf. **Hoofdstuk 3** en **4**).

In **Hoofdstuk 6** werd het potentieel van drie nieuwe niet-virale dragers geëvalueerd. Deze drie polykationische amfifiele β-cyclodextrins (paCDs) werden gecomplexeerd met pDNA en mRNA waarna de stabiliteit en de transfectie-efficiëntie werden bestudeerd. De transfectie-experimenten in een geoptimaliseerd serumvrij transfectiemedium toonde aan dat de efficiëntie slechts marginaal lager lag dan bij de transfecties met Lipofectamine. Wanneer ze werden uitgevoerd in celcultuurmedium dat serum bevat, viel de efficiëntie terug voor alle complexen tot een verwaarloosbare hoeveelheid. De daaropvolgende experimenten toonden aan dat de interactie tussen cellulaire cholesterol en de paCDs een belangrijke rol zou kunnen spelen met betrekking tot de opname in de cel. Er werd namelijk gezien dat het toevoegen van vrij cholesterol aan de paCD complexen de opname in de cel verhinderde. Dit toont aan dat de saturatie van de hydrofobe holte van de paCDs de interacties met cellulair cholesterol bemoeilijken. Om deze reden luidde onze hypothese dat bij het uitvoeren van een transfectie in de aanwezigheid van serumproteïnen deze interacties eveneens verhinderd worden, wat leidt tot een verlaagde opname in de cel.

Kortom, we kunnen concluderen dat het gebruik van microscopietechnieken zeer waardevol is in de studie en de evaluatie van niet-virale nanopartikels. SPT, dat wordt uitgevoerd op de beelden opgenomen met een snelle SFC microscoop, is een geschikte methode voor het bestuderen van afbraak van pDNA in een biologische omgeving. Naast de microscopietechniek en de biologische parameters van het experiment is het echter belangrijk dat aandacht wordt besteed aan de techniek waarmee fluorescente labels aan de nucleïnezuren worden bevestigd. De keuze voor een suboptimale techniek zou namelijk een invloed kunnen hebben op het cel proces dat bestudeerd wordt. Naast de enzymatische afbraak van pDNA, moet men ook altijd rekening houden met de vele andere extra-en intracellulaire barrières die aanwezig zijn tijdens een transfectie. Daarom zijn wij ervan overtuigd dat de transfectie-efficiëntie van nieuwe dragers altijd bestudeerd moet worden in een situatie die nauw aansluit bij

de *in vivo* situatie waarin de dragers gebruikt gaan worden. Al deze inspanningen om nieuwe afleveringsmethoden te optimaliseren en om de knelpunten te bestuderen die nucleïnezuren moeten overwinnen om een transfectie te veroorzaken, zullen in de nabije toekomst van het onderzoeksveld van de niet-virale dragers, de grootste uitdaging blijven vormen.

CURRICULUM VITAE

PERSONALIA

Name	**Koen Rombouts**
Date of Birth	04/04/1988
Place of Birth	Mortsel
Nationality	Belgian
Address	Langemunt 49/101, 9000 Gent
E-mail	KoenRombouts@gmail.com
Phone	+32 (0)478 59 43 72

EDUCATION

Master Degree 2009 - 2011

Master in Bioscience Engineering: Cel and Gene Biotechnology,

Ghent University

Master Thesis

Possibilities of Systemic RNAi by Feeding Experiments in Colorado Potato Beetle

Bachelor Degree 2006 – 2009

Bachelor in Bioscience Engineering: Cell and Gene Biotechnology

University of Antwerp

INTERNATIONAL PEER REVIEWED PUBLICATIONS

S. Heras, K. Forier, K. Rombouts, K. Braeckmans, and A. Van Soom, DNA counterstaining for methylation and hydroxymethylation immunostaining in bovine zygotes, *Analytical Biochemistry* **2014**, 454, 14–16

K. Rombouts, T. F. Martens, E. Zagato, J. Demeester, S. C. De Smedt, K. Braeckmans, and K. Remaut, Effect of Covalent Fluorescence Labeling of Plasmid DNA on Its Intracellular Processing and Transfection with Lipid-Based Carriers, *Molecular Pharmaceutics*, **2014**, 11 (5), 1359–68

A. C. N. Oliveira, K. Raemdonck, T. F. Martens, K. Rombouts, R. Simón-Vázquez, C. Botelho, I. Lopes, M. Lúcio, Á. González-Fernández, M. E. C. D. Real Oliveira, A. C. Gomes, and K. Braeckmans, Stealth monoolein-based nanocarriers for delivery of siRNA to cancer cells, *Acta Biomaterialia*, **2015**, 25, 216–29

K. Remaut, E. De Clercq, O. Andries, K. Rombouts, M. Van Gils, L. Cicchelero, I. Vandenbussche, S. Van Praet, J. M. Benito, J. M. Garcia Fernandéz, N. Sanders, and D. Vanrompay, Aerosolized Non-Viral Nucleic Acid Delivery in the Vaginal Tract of Pigs, *Pharmaceutical Research*, **2015**, 33(2), 384-94

K. Rombouts, K. Braeckmans, and K. Remaut, Fluorescent Labeling of Plasmid DNA and Messenger RNA: Gains and Losses of Current Labeling Strategies, *Bioconjugate Chemistry*, **2016**, 27(2), 280-97

ORAL PRESENTATIONS

K. Rombouts, K. Remaut, and K. Braeckmans, The Effect of the Labeling of Plasmid DNA on Transfection Efficiency, *16th Forum of Pharmaceutical Sciences*, Blankenberge (Belgium), May 7-8, 2012

K. Rombouts, T. F. Martens, J. Demeester, S. C. De Smedt, K. Braeckmans, and K. Remaut, The Effect of Fluorescence Labeling on the Intracellular Procesing of Nanoparticles for Gene Therapy, *Bio-Nano-Photonics Symposium*, Cardiff (U.K.), September 16-17, 2013

K. Rombouts, T. F. Martens, J. Demeester, S. C. De Smedt, K. Braeckmans, and K. Remaut, The Effect of Fluorescence Labeling on the Intracellular Procesing of

Nanoparticles for Gene Therapy, *3rd MC & DNA Vector Conference*, Bielefeld (Germany), May 30, 2014

K. Rombouts, T. F. Martens, J. Demeester, S. C. De Smedt, K. Braeckmans, and K. Remaut, The Effect of Fluorescence Labeling on the Intracellular Procesing of Nanoparticles for Gene Therapy, *Biopharmacy Day*, Vlaardingen (The Netherlands), December 12, 2014

K. Rombouts, E. Zagato, T. F. Martens, J. Demeester, S. C. De Smedt, K. Braeckmans, and K. Remaut, The Effect of Covalent Fluorescence labeling of Plasmid DNA on the Intracellular Processing of Lipid-based Nanoparticles for Gene Therapy, *Annual Meeting of the Belgian Society of Microscopy: When Materials Meet Biology*, Mons (Belgium), September 11, 2015

POSTER PRESENTATIONS

K. Rombouts, K. Remaut, and K. Braeckmans, The Effect of the Labeling of Plasmid DNA on Transfection Efficiency, *European Society of Gene and Cell Therapy French Society of Cell and Gene Therapy Collaborative Congress*, Versailles (France) October 25-29, 2012

K. Rombouts, T. F. Martens, J. Demeester, S. C. De Smedt, K. Braeckmans, and K. Remaut, The Effect of Fluorescence Labeling on the Intracellular Processing of Nanoparticles for Gene Therapy,

- *Focus on Microscopy*, Maastricht (The Netherlands), March 24-27, 2013
- *Knowledge for Growth*, Ghent (Belgium), May 30, 2013
- *Annual Meeting NB Photonics*, Ghent (Belgium), September 20, 2013
- *Biopharmacy Day*, Ghent (Belgium), December 18, 2013
- *13th Edition of the European Symposium on Controlled Drug Delivery*, Egmond-aan-Zee (The Netherlands), April 16-18, 2014
- *Knowledge for Growth*, Ghent (Belgium), May 8, 2014

K. Rombouts, T. F. Martens, J. Demeester, S. C. De Smedt, K. Braeckmans, and K. Remaut, The Effect of Covalent Fluorescence labeling of Plasmid DNA on the Intracellular Processing of Lipid-based Nanoparticles for Gene Therapy, *μFiBR*, Hasselt (Belgium), October 3, 2014

EDUCATION

Practical Courses

2012 – 2016

Biochemistry and Biophysics II and Physicochemistry of Drugs

Classes

2014

Biochemistry and Biophysics I: Theory and Excercises Excel 2010

2015

Biochemistry and Biophysics I: Theory and Excercises Excel 2013

Students

2013

Erasmus student: Rui Ferreira. Faculty of Pharmacy of the University of Porto.

> The Effect of Fluorescent Covalent Labeling of mRNA on the Transfection Efficiency with Lipid-Based Nanoparticles.

2014

Master student: Justin Claesens, Faculty of Pharmaceutical Sciences, Ghent University

> Evaluation of β-cyclodextrins for the complexation and transfection of pDNA

2015

Erasmus Plus student: Cristiana Costa, University of Minho, Guimarães

> Evaluation of -cyclodextrins for the complexation and transfection of pDNA and mRNA in optimized transfection medium and serum-containing medium.

SPECIALIST COURSE

4th European Short Course on “Time-resolved Microscopy and Correlation Spectroscopy

DANKWOORD | ACKNOWLEDGEMENTS

Vier en een half jaar werken in het labo voor algemene biochemie en fysische farmacie (vanaf nu kortweg hét labo), maanden schrijven aan deze thesis, weken voorbereiden op de verdediging(en), dagen stressen om alle last-minute correcties uit te voeren…en dan rest me enkel nog het schrijven van het dankwoord. Het, zeer waarschijnlijk, vaakst gelezen stukje tekst uit de meeste doctoraatsthesissen. Ondanks de zware last op mijn schouders om er dan ook iets leuks van te maken, doet het ook ongelooflijk veel plezier om dit te mogen schrijven. Net zoals iedereen heb ik namelijk een hele waslijst aan mensen die ervoor hebben gezorgd dat ik sta waar ik nu sta en naar mijn gevoel is dat op alle vlak op een heel andere (en betere!) plaats dan waar ik gestart ben. Ik zou jullie dan ook graag snel willen meenemen in een beknopte “highlight reel” van de periode tussen aankomst op het labo en het heden.

Voor ik daarmee van start ga wil ik eerst de mensen bedanken die mij hebben begeleid in elke stap van het wetenschappelijke parcours dat ik heb afgelegd. **Katrien**, als mijn principal investigator/begeleidster heb je veel tijd en moeite besteed aan mijn werk en veel geduld met mij gehad. Het zou een leugen zijn om te zeggen dat alles van een leien dakje liep, maar ik denk dat we er uiteindelijk in zijn geslaagd om dingen te creëren die de moeite waard zijn. Meer nog dan het wetenschappelijke zal ik echter vooral je eerlijkheid en directheid onthouden. In mijn ogen is dat een kwaliteit die zorgt voor een betere verstandhouding en samenwerking. Ik wil je dan ook bedanken voor alle ideeën, verbeteringen, discussies, vertrouwen en vooral voor de eerlijke gesprekken over waarom dingen soms niet vlot liepen!

Naast Katrien kon ik ook rekenen op mijn tweede promotor **Kevin**. Ondanks dat we de laatste twee jaar iets minder samenzaten om de wetenschappelijke ideeën en resultaten te bespreken, slaagde je er altijd in om zeer snel de problemen te detecteren en oplossingen aan te reiken wanneer we elkaar spraken. Verder ben je onwaarschijnlijk sterk in het aanscherpen van een tekst. Met soms kleine, en vaak grote, ingrepen kan je een tekst meer dan één niveau hoger tillen. Dit vakmanschap (want hoe zou je dat anders kunnen benoemen?) heeft zonder twijfel enorm bijgedragen aan het welslagen van mijn doctoraat en daar wil ik je graag voor bedanken!

Behalve mijn promotoren is het labo nog twee andere professoren rijk. In de eerste plaats Prof. (Emeritus) Demeester, kortweg **Jo**, die mij vooral zal bijblijven als de persoon die het labo deed “draaien” als director en de prof die zeer begaan was

met het goede verloop van de practica. Prof. De Smedt, kortweg **Stefaan**, is tenslotte de man die als geen ander de juiste vragen kan stellen. Deze wetenschappelijke, maar ook vaak filosofische, interpellaties zorgden vaak voor verwarring en soms tot hilariteit, maar mondden uiteindelijk altijd uit in een aha-erlebnis. Ook jullie wil ik dan ook graag bedanken voor de kansen die ik via het labo heb gekregen.

Zoals eerder gezegd zou ik jullie als lezer even snel meenemen door een korte tocht door mijn periode op het labo.

Op mijn eerste dag op het labo voor algemene biochemie en fysische farmacie kwam ik, met een bang hartje, onder de hoede van Prof. Braeckmans en -toen nog- Post-doc Katrien terecht. Zoals gebruikelijk begint die eerste dag met een rondleiding langs alle bureaus. Onmiddellijk werd ik voorgesteld aan waarschijnlijk de drie belangrijkste personen die het labo rijk is: onze secretaresses **Katharine** en **Ilse** en onze rots in de branding/manusje van alles/practicumgoeroe **Bart L.**. **Katharine** en **Ilse**, bij jullie kan je altijd terecht voor alle administratieve zorgen, organisatorische vragen, maar evengoed leven jullie mee met de stress die bijvoorbeeld het printen van een thesis met zich meebrengt of hebben jullie nog een motiverend woordje over vlak voor de interne verdediging. Dankjewel om er altijd voor te zorgen dat alles op wieltjes loopt! Voor eender welke andere vraag kan je altijd terecht bij **Bart**. Zo'n multi-getalenteerde kerel als jou heb ik nog ~~niet vaak~~ nooit ontmoet. Hoe jij er elke keer in slaagt om iets, al dan niet op de conventionele methode, te fixen daar doe ik mijn petje voor af. Daarnaast ben je een wandelende encyclopedie van het practicum, waar ik met veel plezier 5 keer aan heb mogen meewerken. Ik kan mij inbeelden dat je de woorden: "Ah Bart, 't is Koen hier ee. Is er nog … " wel kotsbeu bent gehoord. Ondanks al die straffe toeren die ik hier net heb opgesomd, ga ik je toch vooral missen als enorm wijze kerel (zowel in de Nederlandse als in de Gentse betekenis) die altijd wel zin heeft in een pintje en een feestje. Hopelijk mogen we nog vaak klinken!

Op weg naar mijn nieuwe bureau werd ik voorgesteld aan allemaal nieuwe collega's om uiteindelijk aan te belanden bij **Dries**. Dit Duracell-konijn was bezig aan zijn laatste maanden op het lab en wilde onmiddellijk alles weten over mijn toekomstige onderzoek. Een binnenkomer van jewelste! Naast zijn tomeloze enthousiasme verdient hij nog een eervolle vermelding als inspiratiebron voor de lay-out van deze thesis. Merci!

Toen ik uiteindelijk plaatsnam aan mijn plekje voor de volgende 4.5 jaar, merkte ik al snel dat ik terecht kwam in een iets kalmere bureau. Met **Bart Geers**, **Koen Ra.** en **Nathalie** kwam ik terecht bij drie totaal verschillende karakters, waar ik graag de bureau mee deelde. Ik vond er ook snel gelijkgestemden over “de laatste kms” van de tour of de finale van de 100m op het wk atletiek snel meepikken. **Bart G.,** ook wel gekend als **den Barry** kwam ik daarnaast, samen met **Marie-luce** ook tegen in het practicum. Tijdens dat eerste jaar kon ik dat geen onverdeeld succes noemen, maar ik pikte heel veel op van de geboren onderwijzer die **Bart** is. Dankzij dat stichtende voorbeeld, werd het practicum vanaf het tweede jaar iets om naar uit te kijken. Samen met **Katrien F.**, **Rein**, **Joke** en **Karen** heb ik daar veel topmomenten (en ook veel oersaaie momenten) mogen beleven.

Naarmate de tijd vorderde verminderde mijn initiële schuchterheid dankzij de altijd gezellige lunchpauzes, die toen collectief van 12u30 tot 13u30 werden gehouden, burgerevents onder de mannen en andere festiviteiten. Meer en meer dingen werden georganiseerd en wanneer er het volgende jaar enkele toptoevoegingen werden gedaan aan het labo, begon er een periode die ik tussen pot en pint de “golden years” durf te noemen. De perfecte mix tussen karakters, maar vooral het gedeelde enthousiasme voor **TGIF**-drinks, pizza en een pintje in het park en een ongepland stapje in het Gentse uitgaansleven zorgden voor een fantastische tijd. Het labweekend kreeg een nieuw leven, mede doordat er een cultureel verantwoord brouwerijbezoek werd ingevoerd en er vervolgens **Gangnam Style**-gewijs moest worden aangetreden voor het filmpje voor de PhD verdediging van Bart G..

Meer en meer activiteiten werden de volgende tijd georganiseerd en volgens sommigen moest het “social committee” daardoor een nieuw leven worden ingeblazen. Er werd beslist dat ik mij vanaf dat moment tot die taak zou kwijten. Ik vond dat dit wel een titel verdiende, dus bedachten we de titel **CPO** (Chief Party Operations/Officer). Veel verder dan de permanentie verwittigen wanneer we bleven plakken na het werk, het vastleggen van de Sioux/Apache voor onze, ondertussen legendarische, labofeestjes en het organiseren van enkele lab events ging deze functie gelukkig niet.

Door het afleggen van het doctoraat van **Nathalie** en door de “promotie” van **Koen Ra** naar de “Post-Doc bureau” werd mijn bureau ondertussen een beetje drukker. Het Italiaanse temperament en vrolijkheid (wat soms gepaard gaat met

gezang) van **Elisa** en de iets rustigere, gezellige babbeltjes met **Freya** vulden met glans het vertrek van hun voorgangers op en doordat ook Bart aflegde, kwam de plek recht tegenover mij vrij. Ondanks de diepe voetsporen die moesten gevuld worden vulde **Lotte** die met verve en af en toe met een tragikomische noot. Haar problemen met de SFC zorgden vaak voor hilarische (voor ons, minder voor jou) gesprekken.

Zoals dat gaat met PhD's verlieten er nog meer mensen het labo. Eerst gingen onze minzame SPT wizard **Hendrik**, en onze Limburgse practical joker **Katrien F.** andere oorden opzoeken. Daarna volgde **Thomas** -qui est-tu?- Mertens, euh, Martens. Naast een topwetenschapper – en gitarist ben jij ook gewoon een fantastische kerel! Een drukke periode met doctoraatsverdedigingen bood zich daarna aan met de flamboyante Poolse Mad Dog-queen **Oliwia** en de doctoraten van de twee toppers **Heleen** en **Lynn** die allebei op een compleet andere manier zorgden voor enorm veel humor tijdens de middagpauze. **Heleen** jouw scherpe opmerkingen en **Lynn** jouw gave om gênante opmerkingen enkel maar erger te maken ga ik ongetwijfeld missen. Het lab mag blij zijn met twee zo'n top-Post-Docs! De laatste die vertrok voor het mijn beurt is, was **Ine D.C.**, die haar mannetje makkelijk stond wanneer er Keizer Karels van de tap te krijgen waren en daarbuiten altijd wel in was voor gezelligheid. Naast de verste zendeling is zij ook direct de eerste van "mijn" generatie PhD studenten die hebben afgelegd. De derde van deze topgeneratie die binnenkort zal afleggen is **Laura**. Waarschijnlijk ben jij de liefste en meest empathische persoon die ik ooit tegenkwam. Succes met jouw laatste loodjes en diegenen waarbij je hierna gaat werken, mogen hun pollekes kussen met zo'n topper!

Zo'n verloop betekent dat er ook nieuwe mensen moeten bijkomen en op één of andere manier slaagden de proffen er telkens opnieuw in om mensen aan te trekken die perfect binnen het plaatje pasten. Not long after my arrival, the always thirst **Ranhua** arrived at the lab. I'll never forget how you mistakenly thought that the bottle with vanilla jenever was milk during a short hike at the lab weekend. Your face was precious (and again sorry for not telling you clearly). Rond dezelfde tijd kwam ook **George** erbij. George, my man, naast de manier waarop jij het Nederlands zo snel hebt opgepikt, wil ik toch ook even zeggen dat ik respect heb en jaloers ben op jouw werkethiek. Ook jij binnenkort veel succes met het vervolg van je carrière!

Nog zo'n knaller is **Stephan**. Het voorbije anderhalf jaar hebben wij 's middags veel arbeid verricht op de 14^{e} verdieping van het UZ of langs de Schelde om een

beetje aan die torso's te werken en ik kan niet ontkennen dat ik je daardoor nog meer als een echte maat beschouw (en dat was daarvoor ook al niet lief ;-)). Ondanks een drukke planning in jouw volgende maanden, hoop ik dat we toch een paar keer met de boys ouderwets een receptie'ke kunnen doen op de verdediging van **Laura**, maar ook daarna. In dezelfde periode dat **Stephan** erbij kwam, kregen we er met **Karen** een sprankelende persoonlijkheid bij. Jouw weetjes over zeezoogdieren, jouw tomeloos (en ja, soms is dat een beetje vermoeiend) enthousiasme en jouw bereidheid om altijd iedereen te helpen, maken jou één uit de duizend. Ook **Freya** kwam er in die periode bij en kwam zoals reeds gezegd in dezelfde bureau als ik terecht. Al snel bleek dat we qua smaak in muziek, reizen en andere zaken best wel op één lijn zaten. Ik ben er zeker van dat ik onze korte gesprekjes ga missen, waar ik hierna ook terecht kom. **Elisa**, although you already spent some time at the lab during your master thesis, at your "real" start at the lab, you also became an office-buddy. Thank you for making my messy desk looking "tidy" next to yours ;-), but foremost thank you for always being your happy self!

De derde vrouw die ik office-buddy mocht noemen is **Lotte**. Het zou al te makkelijk zijn om jou enkel te beschrijven met jouw pech met de SFC, want jouw talent om een situatie met één nuchtere, droge én daarenboven grappige opmerking te fileren zijn ongetwijfeld wat ik zal onthouden. Die andere generatiegenoten **Rein**tje en **Joke**tje, zijn allebei opgeklommen van masterthesisstudent in het lab tot PhD student en hebben daar een speciale plek voor mij veroverd. **Rein**, zoals al eerder gezegd, door een droom mede-assistent te zijn. Jouw al dan niet aangebrande moppen maakten de saaie momenten véél aangenamer. Daarnaast ben je de auteur van legendarische uitspraken waarvan: "Omer obeter" één is waar ik zelf al mee heb gescoord bij maten op café. **Joke**, jij verdient een speciale plek in dit dankwoord omdat ik de eer had jouw peter te zijn. Daarnaast was je ook mijn **vice-CPO** en is het duidelijk dat je die fakkel met glans hebt overgenomen. Ik kan mezelf dus zeker een trotse peter noemen. Ik hoop dat je jezelf zonder mijn fantastische begeleiding kan behelpen ;-).

Another ravishing lady in the lab is **Rita**, who joined us in two times. Looking back on things, I regret not running together sooner, since I have the feeling we only really got to know each other during those moments. Our last lunch run will be probably a sad one, since I will sincerely miss those 25-30 mins and already look

forward to be “running through barriers” with you, **Stephan**, **PJ**, **Joke**, and **Rein** if he feels like it ;-).

Dat **Stephan** ook in goed gezelschap verkeert in zijn bureau laat geen twijfel, want naast **Karen** en **Rita**, heeft hij ook **Eline** naast zijn zijde. Jij bracht ons een hele nieuwe woordenschat bij van “hippe” jongerentaal en daarnaast heb ik nog nooit zo’n fantastische banaan het beste van zichzelf zien geven. Jammer dat er soms obstakels in de weg hingen! **Sangram**, you were always the definition of calm and friendliness. I wish you the best of luck in your new job in India.

Dan resten mij enkel nog onze groentjes van de lichting 2015. **Pieterjan**, jij hebt nu al de harten veroverd van zowel de mannelijke als de vrouwelijke kant van het labo. Voor een man die de weetjes zo los uit zijn mouw schudt is dat niet verwonderlijk! **Silke**, jij hebt de zware opdracht gekregen om Ine D.C. te vervangen bij “the bubble girls from Ghent”, maar dat kan met jouw spontaniteit geen probleem zijn. **Molood**, **Jing** and **Heyang**, unfortunately I didn’t have the pleasure to really get to know you well, but I wish you all a great time at the lab.

Naast de PhD studenten wil ik ook even de andere Post-Docs bedanken. **Ine**, jouw manier van werken vind ik heerlijk. In mijn ogen een beetje dwars op de gangbare methoden bij de rest van ons labo, probeer jij connecties te leggen met andere labs om vooruitgang te boeken. Volgens mij de enige goeie manier om wetenschappelijke vooruitgang te boeken! **Koen**, jou zal ik naast een vat vol wetenschappelijke ideeën toch vooral onthouden als de man die een gerecht kan beschrijven op een manier dat je het bijna kan ruiken en proeven. Last but not least, **Toon**, ik denk oprecht dat je op de korte tijd dat je nu op het labo werkt enorm veel mensen hebt geholpen. Daarnaast blijkt dat je bijdrage niet stopt bij het wetenschappelijke, want je hebt bewezen dat je ook op gezelligheid hoog scoort.

Tot slot wil ik nog enkele mensen in het bijzonder extra bedanken: **Rein**, **Joke**, **Karen**, **Bart L.** en **Hilde**, jullie zijn in het bijzonder toppers aangezien ik mij dit jaar enkel kon toeleggen op schrijven van deze thesis en amper in het practicum moest staan, nog eens bedankt daarvoor. Daarbuiten heb ik ook het genoegen gehad om enkele thesisstudenten te begeleiden. **Rui**, **Justin** and **Cristiana**, I had a good time “supervising” you guys and I hope you felt the same way about your time in the lab!

Naast de collega’s op het labo, wil ik ook mijn vrienden en familie bedanken. **BuB** ook wel de google 2.0 van Antwerpen of de boyz, jullie zorgen altijd voor de

ontspanning in het weekend wanneer die nodig is. **Team Antwerp**, ik zie jullie veel te weinig tegenwoordig, hopelijk kunnen we die schade binnenkort een beetje inhalen!

Tot slot resten er mij nog drie heel belangrijke mensen om te bedanken. Eerst en vooral **Suus**. Schat, jij bent van onschatbare waarde geweest voor mij de laatste –bijna- drie jaar. Jouw spontaniteit, enthousiasme, drive en zin om op ontdekkingstochten te gaan, ga ik nooit beu geraken! Verder slaag je er ook als geen ander in om mijn cheerleader te zijn wanneer het nodig is. Een beetje tough love is je daarbij niet vreemd. De laatste weken waren vaak stressy en mijn humeur had daar zeker onder te lijden, dankjewel om op die momenten mijn rots in de branding te zijn. Ik kijk er nu al reikhalzend naar uit om met jou onze plannen voor volgende jaren waar te maken. (En ja, ik beloof plechtig dat ik vanaf nu volop tijd ga steken in de voorbereiding!)

De twee andere enorm belangrijke mensen die ik nog absoluut moet bedanken zijn mijn geweldige ouders. Mama, papa, bedankt om al die jaren mee te leven, naar mijn gezaag te luisteren als ik in het weekend thuis kwam na een frustrerende week en mij al die jaren te steunen. Zonder jullie was dit zonder enige twijfel nooit gelukt. Dankjewel!

Koen